

UNIVERSITY OF CINCINNATI

Date: 28th February, 2008

I, Shashank Chauhan,

hereby submit this work as part of the requirements for the degree of:
Doctor of Philosophy

in:

Mechanical Engineering

It is entitled:

Parameter Estimation and Signal Processing Techniques
for Operational Modal Analysis

This work and its defense approved by:

Chair: Dr. Randall J. Allemang

Dr. David L. Brown

Dr. Allyn W. Phillips

Parameter Estimation and Signal Processing Techniques for Operational Modal Analysis

A dissertation submitted to the

Department of Research and Advanced Studies
of the University of Cincinnati

in the partial fulfillment of the
requirements for the degree of

DOCTORATE OF PHILOSOPHY (Ph.D.)

In the Department of Mechanical Engineering

March, 2008

by

Shashank Chauhan

B.E., Bhilai Institute of Technology, Bhilai, India
M.Tech., Indian Institute of Technology, New Delhi, India

Committee Chair: Randall J. Allemang, Ph.D.

February 28th, 2008

Abstract

Operational Modal Analysis (OMA) is a technique that characterizes a structure/system on the basis of output responses only. It is an emerging field in structural dynamics and has been applied to complex structures that are often difficult to analyze using traditional Experimental Modal Analysis (EMA) techniques. However, the unavailability of input force information, in the case of OMA, makes the overall process significantly more complex as it affects every stage of modal analysis including data acquisition, data processing, parameter estimation, etc. Factors such as these have been responsible for the lack of frequency domain OMA algorithms, inconsistent damping estimation, etc.

This research provides useful insights into the OMA techniques by in-depth exploration of the various assumptions under which OMA works and suggests some new signal processing approaches and algorithms to aid in modal parameter estimation using OMA techniques. The dissertation starts with a general literature review of OMA which is followed by presentation of the Unified Matrix Polynomial Approach (UMPA) to the OMA problem. In subsequent chapters, a frequency domain, lower order algorithm and a spatial domain algorithm are presented. Next, new signal processing techniques like Blind Source Separation / Independent Component Analysis (BSS/ICA) are adapted for OMA purposes. The performance of these algorithms is verified by conducting studies on analytical and experimental systems. Intense analytical studies are conducted to understand the effect of the violation of OMA assumptions on OMA modal parameter estimation, especially in view of inconsistent damping estimation. The algorithms developed in this dissertation are then applied to two newly built cable-stayed bridges for assessing their performance in real-life situations. Finally, the research conclusions are presented and recommendations for the future research in this area are given.

Acknowledgements

“Teachers mold the lives that they influence and the lessons learned from the teachers remain with their students throughout life”.

I dedicate this work to Prof. B.C. Nakra, my guru at Indian Institute of Technology, Delhi.

Thanks a lot Sir for being my inspiration and for initiating the desire to work in the area of vibrations and structural dynamics.

The time spent at SDRL is very memorable and I will treasure the associations formed here all my life. I would like to thank my advisor, Dr. Allemang, for not only providing the technical expertise but also the personal support during the course of this work. Dear Sir, it's been a pleasure and privilege to be your student. There is so much to learn from you and four years are not sufficient for that. I hope future will continue to provide me with opportunities to interact and learn more from you.

I would also like to express my gratitude to Dr. Brown and Dr. Phillips for their time, constructive advice and guidance. I will always cherish talking to them, be it on any technical issue or their interesting observations on anything under the sun. I would also like to acknowledge Dr. Helmicki and others at UCII for providing me support and opportunity for the work at US Grant and MRC bridges.

Big thanks to the whole Cincy Friends group (my family away from India). You people mean a lot to me, great friends are hard to come by and I know how lucky I am to have you all as someone to fall back on in times of need. Thanks a lot for all that you have done for me (and you have done a lot). A word of thanks won't be complete without the mention of the delicious food and the never ending, fun-filled discussions, I have had on numerous occasions at your places; I never felt like missing my family and home.

I would like to thank all my friends from my days at BIT and IIT for being the constant source of motivation and happiness; Mitesh, Shirish, Lavish, Tushar, Abhishek, Shashvat, Sanket, Alok, Rishi, Anshul, Naved and the whole Vibrant 2K gang. I also extend my thanks to my good friends at SDRL and University of Cincinnati, Amit Sharma, Jassi Paaji, Raghav, Hemant, Sushant, Shrikant, Goutham and Ananta, Balakumar, Balaji, Wancheng, Steve, Ray, Matt, Dave and several others. The twice-a-day coffee break at TUC with you guys was as much a part of the research as battling with cables and data acquisition.

I thank my parents and my lovely sister, Arpan, for giving me all the support, love and encouragement and for being my strength throughout my life. I know this means to you just as much as it means to me. If there's a sense of achievement attached to the completion of this work I undertook, its essence lies in the happiness that it has brought for you. I would also like to thank all my relatives for their love and care and their words of encouragement.

Finally, a word of special thanks to Ekta, I would not have even dreamt of this, but for you. Thanks for instilling that self-confidence in me and, in many a ways, making it all possible. I hope you are doing fine and having best of time and life ☺

Be kind, my friend.

Hold on, in times of pain and strife;

Until death comes, all is life....

(A Little Night Music, Ruskin Bond)

Contents

Abstract	i
Acknowledgements	iii
List of Figures	ix
List of Tables	xviii
Symbols Used	xxii
Abbreviations Used	xxvi
1. Introduction	1
1.1 Operational Modal Analysis	1
1.2 Motivation and Problem Definition	6
1.3 Research Goals and Contributions	8
1.4 Thesis Outline	12
2. Literature Survey	14
2.1 OMA Algorithms	15
2.1.1 Time Domain Algorithms	15
2.1.2 Spatial Domain Algorithms	22
2.1.3 Frequency Domain Algorithms	25
2.1.4 Maximum Likelihood (ML) Estimator Based Algorithms	27
2.2 Issues with OMA	28
2.3 OMA Applications	31

2.4	Conclusions	33
3.	Unified Matrix Polynomial Approach for Operational Modal Analysis	35
3.1	Modal Parameter Estimation and UMPA	36
3.2	OMA Basics and Associated Signal Processing	43
3.3	UMPA Formulation of OMA Algorithms	49
3.3.1	Time Domain Algorithms	50
3.3.2	Frequency Domain Algorithms	52
3.3.3	Spatial Domain Algorithms	54
3.4	Case Study: Lightly Damped Circular Plate	55
3.5	Conclusions	56
4.	UMPA-LOFD: A Low Order Frequency Domain Algorithm for OMA	58
4.1	UMPA-LOFD	60
4.2	Numerical Conditioning Issues and Generalized Frequency	61
4.3	Case Studies: UMPA-LOFD Performance	65
4.3.1	Analytical 15 Degrees of Freedom System	65
4.3.2	Lightly Damped Circular Plate	73
4.4	Case Studies: Effect of Complex Z Mapping on UMPA-LOFD	79
4.4.1	Analytical 15 Degrees of Freedom System	79
4.4.2	Lightly Damped Circular Plate	83
4.5	Conclusions	86

5.	OMA-EMIF: A Spatial Domain OMA Algorithm	88
5.1	CMIF and FDD/eFDD	89
5.2	OMA-EMIF: Enhanced Mode Indicator Function for OMA	91
5.3	Singular Value Percentage Contribution (SVPC) Plot	94
5.4	Experimental Validation	95
5.4.1	15 DOF Analytical System	95
5.4.2	Lightly Damped Circular Plate	101
5.4.3	H-Frame Structure	107
5.5	Conclusions	111
6.	Application of ICA/BSS Techniques to OMA	113
6.1	Independent Component Analysis	114
6.1.1	ICA/BSS Algorithms	115
6.2	ICA and BSS in Vibrations	120
6.2.1	ICA/BSS Techniques for Operational Modal Analysis	121
6.3	Analytical 15 Degree of Freedom System	123
6.4	Conclusions	130
7.	Damping Estimation Using OMA Techniques	131
7.1	Analytical 5 DOF System	132
7.2	Cyclic Averaging	135
7.2.1	Cyclic Averaging Theory	136
7.2.2	Effect of Cyclic Averaging	138
7.2.3	Effect of More RMS Averages (Use of Longer Time Histories)	142

7.3	Correlated Input Forces and OMA Parameter Estimation	148
7.4	Conclusions	159
8.	Application to Civil Structures	162
8.1	US Grant Cable-Stayed Bridge	162
8.1.1	Design of Experiments	164
8.1.2	Final Superstructure Test: Test Set-Up and Data Acquisition	170
8.1.3	Operational Modal Analysis	173
8.2	Maumee River Crossing Cable-Stayed Bridge	183
8.2.1	OMA Test Set-Up	184
8.2.2	Operational Modal Analysis	186
8.3	Conclusions	190
9.	Conclusions and Recommendations for Future Work	191
9.1	Summary and Conclusions	191
9.2	Recommendations for Future Work	194
	References	198

List of Figures

Figure No.	Title	Page No.
1.1	Experimental Modal Analysis	2
1.2	Operational Modal Analysis	3
3.1	Auto-correlation function of a typical output response	45
3.2	Generation of positive power spectrum from output time responses	47
3.3	Experimental set up for the lightly damped circular plate	55
4.1	Analytical 15 Degree of Freedom System	66
4.2	Auto power spectrum and positive power spectrum for the first degree of freedom (15 DOF analytical system)	67
4.3	Complex Mode Indicator Function (CMIF) based on power spectrum (15 DOF analytical system)	67
4.4	Complex Mode Indicator Function (CMIF) based on positive power spectrum (15 DOF analytical system)	68
4.5	Consistency diagram for Polyreference Time Domain (PTD) algorithm (15 DOF analytical system)	70

4.6	Consistency diagram for Eigensystem Realization Algorithm (ERA) (15 DOF analytical system)	71
4.7	Consistency diagram for Low Order Frequency Domain (UMPA-LOFD) algorithm (15 DOF analytical system)	71
4.8	Consistency diagram for Rational Fraction Polynomial (RFP) algorithm (15 DOF analytical system)	72
4.9	Consistency diagram for Low Order Frequency Domain (UMPA-LOFD) algorithm based on complete power spectrum (Analytical system)	72
4.10	Experimental set up for the lightly damped circular plate	73
4.11	CMIF plot based on complete power spectrums obtained when plate is excited sufficiently over its surface	74
4.12	Consistency diagram for Polyreference Time Domain (PTD) algorithm (Circular plate)	75
4.13	Consistency diagram for Eigensystem Realization Algorithm (ERA) algorithm (Circular plate)	76
4.14	Consistency diagram for Lower Order Frequency Domain (UMPA-LOFD) algorithm (Circular plate)	76
4.15	Consistency diagram for Rational Fraction Polynomial (RFP) algorithm (Circular plate)	77
4.16	MAC plot for UMPA-LOFD algorithm (Circular plate)	78
4.17	Selected mode shapes of the circular plate	78

4.18	Consistency diagram for Rational Fraction Polynomial (RFP) algorithm (Analytical system)	81
4.19	Consistency diagram for Rational Fraction Polynomial (RFP-z) algorithm (Analytical system)	82
4.20	Consistency diagram for Low Order Frequency Domain (UMPA-LOFD) algorithm (Analytical system)	82
4.21	Consistency diagram for UMPA-LOFD with algorithm Complex Z mapping (Analytical system)	83
4.22	Consistency diagram for Rational Fraction Polynomial (RFP) algorithm (Circular plate)	84
4.23	Consistency diagram for RFP-z algorithm (Circular plate)	85
4.24	Consistency diagram for UMPA-LOFD algorithm (Circular plate)	85
4.25	Consistency diagram for UMPA-LOFD with algorithm Complex Z mapping (Circular plate)	86
5.1	eFDD estimation of modal frequency and damping	91
5.2	Analytical 15 DOF system	96
5.3	CMIF of spatially well excited 15 DOF analytical system	96
5.4	CMIF of analytical system excited at three locations (Cross-Power based)	98

5.5	CMIF of analytical system excited at three locations (FRF based)	99
5.6	SVPC plot for spatially insufficient excitation case (Analytical system)	100
5.7	Experimental set up for the lightly damped circular plate	101
5.8	CMIF of circular plate excited over the entire surface (Spatially well excited)	102
5.9	SVPC plot for circular plate (Spatially well excited)	103
5.10	CMIF of circular plate based on FRFs	103
5.11	CMIF of circular plate excited over one quarter of the surface	104
5.12	SVPC plot for circular plate excited in one quarter	104
5.13	CMIF of circular plate excited at two points	105
5.14	SVPC plot for circular plate excited at two points	105
5.15	H-Frame structure	108
5.16	CMIF of the spatially well excited H-Frame structure	108

5.17	SVPC plot for spatially well excited H-Frame	109
5.18	CMIF of the H-Frame structure excited at two locations	109
5.19	SVPC plot for H-Frame excited at two points	110
6.1	Analytical 15 degree of freedom system	125
6.2	Power spectrum of modal coordinate responses obtained using AMUSE	125
6.3	Power spectrum of modal coordinate responses obtained using SOBI	126
6.4	Power spectrum of modal coordinate responses obtained using FOBI	126
6.5	Power spectrum of modal coordinate responses obtained using JADE	127
6.6	MAC comparison plot - AMUSE / SOBI	128
6.7	MAC comparison plot - AMUSE / OMA-EMIF	128
6.8	MAC comparison plot - AMUSE / True Modes	129
6.9	MAC comparison plot - True Modes / OMA-EMIF	129

7.1	Input force power spectra comparison (5 DOF analytical system)	133
7.2	Virtual forces (Principal components of the force power spectra matrix)	134
7.3	Theoretical frequency response functions (5 DOF analytical system)	134
7.4	Effect of cyclic averaging (Power spectrum comparison 1-1)	139
7.5	Effect of cyclic averaging (Power spectrum comparison 1-2)	139
7.6	Effect of cyclic averaging (Percentage error in modal frequency estimates)	141
7.7	Effect of cyclic averaging (Percentage error in modal damping estimates)	142
7.8	Effect of longer time histories $N_C = 5$ (Percentage error in modal frequency estimates)	144
7.9	Effect of longer time histories $N_C = 5$ (Percentage error in modal damping estimates)	144
7.10	Effect of longer time histories $N_C = 10$ (Percentage error in modal frequency estimates)	146
7.11	Effect of longer time histories $N_C = 10$ (Percentage error in modal damping estimates)	147
7.12	Effect of correlated input forces Case A (Percentage error in modal frequency estimates)	152

7.13	Effect of correlated input forces Case A (Percentage error in modal damping estimates)	152
7.14	Comparison of auto and cross power spectrum of input forces (Case B)	153
7.15	Virtual forces (Case B)	154
7.16	Effect of correlated input forces Case B (Percentage error in modal frequency estimates)	156
7.17	Effect of correlated input forces Case B (Percentage error in modal damping estimates)	156
7.18	Effect of correlated input forces Case C (Percentage error in modal damping estimates)	159
8.1	US Grant Cable-Stayed Bridge	163
8.2	Typical plan and elevation of the US Grant Bridge	164
8.3	Response comparison measured using a capacitive and a piezoelectric accelerometer	166
8.4	Comparative bridge response in X, Y and Z directions (US Grant Bridge)	167
8.5	Sensor layout for first preliminary test (US Grant Bridge)	168
8.6	Sensor layout for second preliminary test (US Grant Bridge)	169

8.7	Sensor layout for final superstructure test (US Grant Bridge)	171
8.8	OMA test with van excitation along with ambient sources (Second dataset)	172
8.9	Typical auto-power spectrum of a measured response	174
8.10	Typical Short Time Fourier Transform (STFT) plot of response data for a chosen location	174
8.11	CMIF plot of second dataset (Final superstructure test of the US Grant Bridge)	175
8.12	Mode shapes (OMA vs. FEM) (US Grant Bridge)	176
8.13	MAC plot between the various modes obtained using OMA of the US Grant Bridge	177
8.14	AutoMAC for RFP-z estimates (US Grant Bridge)	181
8.15	AutoMAC for PTD estimates (US Grant Bridge)	181
8.16	Maumee River Crossing Bridge, Toledo, OH	183
8.17	OMA Test Set-Up Layout for the MRC Bridge	185
8.18	Typical accelerometer set up for the MRC Bridge OMA test	185

8.19	Autopower spectrum of individual channels (MRC Bridge)	186
8.20	Complex Mode Indicator Function Plot (MRC Bridge)	186
8.21	AutoMAC plot for the various modes obtained by OMA of the MRC Bridge	188
8.22	Mode shapes (MRC Bridge)	189

List of Tables

Table No.	Title	Page No.
3.1	UMPA representations of various EMA algorithms	42
3.2	Modal parameters estimated using various UMPA formulated OMA algorithms	56
4.1	UMPA-LOFD modal parameter comparison for 15 DOF analytical system	70
4.2	UMPA-LOFD modal parameter comparison for lightly damped circular plate	75
4.3	Effect of complex Z mapping - Modal parameter comparison for 15 DOF analytical system	79
4.4	Effect of complex Z mapping - Modal parameter comparison for lightly damped circular plate	84
5.1	Comparison of true modes and OMA-EMIF modes for 15 DOF analytical system	97
5.2	FRF and G_{xx} based results comparison for spatially insufficient excitation case	100
5.3	Modal parameters estimated using OMA-EMIF for lightly damped circular plate	106
5.4	Modal parameters estimated using OMA-EMIF for the H-Frame structure	110

6.1	Comparison of modal parameter estimates using ICA techniques and OMA-EMIF	127
7.1	Modal frequencies and damping of the 15 DOF analytical system	132
7.2	Modal Matrix of the 15 DOF analytical system	133
7.3	Effect of cyclic averaging ($N_C = 0$, RMS Averages = 3997)	140
7.4	Effect of cyclic averaging ($N_C = 5$, RMS Averages = 797)	140
7.5	Effect of cyclic averaging ($N_C = 10$, RMS Averages = 397)	140
7.6	Effect of longer time histories ($N_C = 5$, Time points = 102400, RMS Averages = 77)	143
7.7	Effect of longer time histories ($N_C = 5$, Time points = 1024000, RMS Averages = 797)	143
7.8	Effect of longer time histories ($N_C = 5$, Time points = 1536000, RMS Averages = 1197)	143
7.9	Effect of longer time histories ($N_C = 10$, Time points = 102400, RMS Averages = 37)	145
7.10	Effect of longer time histories ($N_C = 10$, Time points = 1024000, RMS Averages = 397)	145
7.11	Effect of longer time histories ($N_C = 10$, Time points = 1536000, RMS Averages = 597)	145

7.12	Damping estimation by frequency domain OMA algorithms utilizing PPS ($N_C = 5$, RMS Averages = 797)	147
7.13	Damping estimation by frequency domain OMA algorithms utilizing PPS ($N_C = 10$, RMS Averages = 397)	148
7.14	H_{Gen} - Effect of Correlated Forces (Case A)	150
7.15	$(H^*H^H)_{Gen}$ - Effect of Correlated Forces (Case A)	150
7.16	$(H^*GFF_{diag}^*H^H)_{Gen}$ - Effect of Correlated Forces (Case A)	150
7.17	$(H^*GFF_{comp}^*H^H)_{Gen}$ - Effect of Correlated Forces (Case A)	151
7.18	G_{XX} - Effect of Correlated Forces (Case A)	151
7.19	$(H^*GFF_{diag}^*H^H)_{Gen}$ - Effect of Correlated Forces (Case B)	154
7.20	$(H^*GFF_{comp}^*H^H)_{Gen}$ - Effect of Correlated Forces (Case B)	154
7.21	G_{XX} - Effect of Correlated Forces (Case B)	155
7.22	H_{Gen} - Effect of Correlated Forces (Case C)	157
7.23	$(H^*H^H)_{Gen}$ - Effect of Correlated Forces (Case C)	157

7.24	$(H^*GFF_{diag}^*H^H)_{Gen}$ - Effect of Correlated Forces (Case C)	158
7.25	$(H^*GFF_{comp}^*H^H)_{Gen}$ - Effect of Correlated Forces (Case C)	158
7.26	G_{xx} - Effect of Correlated Forces (Case C)	158
8.1	Results of the finite element analysis of the US Grant Bridge	165
8.2	Sensor locations on the US Grant Bridge (Second Preliminary Test)	169
8.3	Sensor locations on the US Grant Bridge (Final Superstructure Test)	171
8.4	Estimated modal parameters for the US Grant Bridge using OMA-EMIF	175
8.5	Comparison of FEM and OMA modes for the US Grant Bridge	179
8.6	Cross MAC between OMA and FEM Bending Modes for the US Grant Bridge	179
8.7	Comparison between RFP-z, PTD and OMA-EMIF estimates for the US Grant Bridge	180
8.8	Cross MAC comparison between various OMA algorithms for the US Grant Bridge	182
8.9	Estimated modal parameters for MRC Bridge using OMA-EMIF	187

Symbols Used

$\{x(t)\}, \{X(\omega)\}, \{X(s)\}$	Measured response vector in time, frequency and Laplace domain
$[H(\omega)]$	Frequency response function matrix
$\{f(t)\}, \{F(\omega)\}, \{F(z)\}$	Input force vector in time, frequency and Z domain
ψ_k	Mode shape for the k^{th} mode, Also used for modal filter vector
Q_k	Modal scaling factor for the k^{th} mode
λ_k	Modal frequency for the k^{th} mode
$[]^H$	Hermitian of a matrix
$[G_{XX}(\omega)]$	Output response power spectra matrix
$[G_{FF}(\omega)]$	Input force power spectra matrix
$[I]$	Identity matrix
R_{pqk}, S_{pqk}	Mathematical residues for a particular response location p and reference location q for the k^{th} mode
*	Complex conjugate
$\{x_k\}$	Measured output vector in a state-space model

$\{u_k\}$	Measured input vector in a state-space model
$\{y_k\}$	Discrete state vector in a state-space model
[A]	State transition matrix in a state-space model, Also used for Mixing matrix
[B]	Input matrix in a state-space model
[C]	Output matrix in a state-space model that describes how the internal state is being transferred by means of output measurements $\{y_k\}$. Also used for companion matrix
[D]	Direct transmission matrix in a state-space model
$\{w_k\}$	Process noise vector in a state-space model
$\{v_k\}$	Measurement noise vector in a state-space model
[Φ]	Eigenvector matrix, Mode shape matrix
[R], $R_{xx}(t)$	Block Hankel matrix of output response correlation / covariance data, and Output response correlation data
N_o	Number of outputs
N_i	Number of inputs
$U(\omega_k)$	Left singular matrix at any frequency ω_k
$V(\omega_k)$	Right singular matrix at any frequency ω_k

$\Sigma(\omega_k), [S]$	Singular value matrix at any frequency ω_k
$[L]$	Modal participation factor matrix
$[Q]$	Diagonal scaling factor matrix
$[\Lambda]$	Diagonal matrix with system poles
α_k, β_k	Denominator and Numerator polynomial coefficients of the common-denominator model
$[\alpha_k], [\beta_k]$	Denominator and Numerator matrix polynomial coefficients of the UMPA model
$[M], [C], [K]$	Mass, damping and stiffness matrices
$h(t)$	Impulse response function
$[G_{xx}^+(\omega)]$	Output response positive power spectrum
$H[]$	Hilbert transform of a matrix
$\hat{H}(\omega)$	Biased FRF
m	Modal order
$[\bar{G}(\omega)]$	Enhanced positive power spectra matrix
$\{\psi_{physical}\}$	Eigenvectors of the original physical system
$\{\psi_{enhanced}\}$	Eigenvectors of the enhanced system

$s(t)$	Source signal
η_r	Modal coordinates corresponding to r^{th} mode
T	Observation time period
Δf	Frequency resolution
N_c	Number of cyclic averages
$\bar{x}(t)$	Averaged time history
C_k	Fourier coefficients of the averaged time history
$U_x U_y U_z R_x R_y R_z$	Modal participation factors in translational and rotational directions

Abbreviations Used

FEA	Finite element analysis
EMA	Experimental modal analysis
OMA	Operational modal analysis
FRF	Frequency response function
UMPA	Unified matrix polynomial approach
RFP	Rational fraction polynomial algorithm
EMIF	Enhanced mode indicator function
CMIF	Complex mode indicator function
FDD	Frequency domain decomposition
eFDD	Enhanced frequency domain decomposition
OMA-EMIF	Enhanced mode indicator function algorithm for OMA
SVPC	Singular value percentage contribution plot
BSS	Blind source separation

ICA	Independent component analysis
RMS	Root mean square averaging
MRC	Maumee River Crossing bridge
SDOF	Single degree of freedom
PP	Peak picking method
NExT	Natural excitation technique
LSCE	Least square complex exponential algorithm
ITD	Ibrahim time domain algorithm
PTD	Polyreference time domain algorithm
ERA	Eigensystem realization algorithm
PEM	Prediction error method
IV	Instrument variable method
ARMA	Auto-Regressive Moving Average
MIMO	Multiple input multiple output
SSI-COV	Covariance driven stochastic subspace iteration algorithm

SVD	Singular value decomposition
IRF	Impulse response function
PC	Principal component
CVA	Canonical variant analysis
UPC	Unweighted principal component
BR	Balanced realization algorithm
SSI-DATA	Data driven stochastic subspace iteration algorithm
FFT	Fast Fourier Transform
LSCF	Least square complex frequency algorithm
ML	Maximum likelihood estimator
pLSCE	Polyreference least square complex exponential algorithm
IMAC	International modal analysis conference
IOMAC	International operational modal analysis conference
ISMA	International seminar on modal analysis
pdf	Probability density function

ARX	AutoRegressive model with eXogenous inputs
CEA	Complex exponential algorithm
PFD	Polyreference frequency domain algorithm
MRITD	Multiple Reference Ibrahim Time Domain
PPS	Positive power spectrum
SISO	Single input single output
SIMO	Single input multiple output
pLSCF	Polyreference least square complex frequency
UMPA-LOFD	UMPA based lower order frequency domain algorithm for OMA
DOF	Degrees of freedom
RFP-z	Rational fractional polynomial algorithm in z domain (PolyMAX)
MAC	Modal assurance criterion
ePPS	Enhanced positive power spectrum
eFRF	Enhanced frequency response functions
BSE	Blind signal extraction

MBD	Multichannel blind deconvolution
SOBI	Second order blind identification algorithm
FOBI	Fourth order blind identification algorithm
JADE	Joint approximate diagonalization of eigen matrices algorithm
AMUSE	Algorithm for multiple unknown signals extraction
PCA	Principal component analysis
HOS	Higher order statistics
SOS	Second order statistics
EVD	Eigenvalue decomposition
JAD	Joint approximate diagonalization
NU	North upstream
SU	South upstream
SUI	South upstream inner girder
ND	North downstream
SD	South downstream

STFT

Short time Fourier transform

Chapter One

Introduction

1.1 Operational Modal Analysis

In today's world, lots of emphasis is laid on designing safe and reliable engineering structures. Introduction of improved materials has also made it imperative for these structures to be light and yet capable of withstanding heavy loads while in operation. These requirements make it important for the design community to understand the dynamic characteristics of structures while designing them for safety, reliability and quality points of view.

Dynamic characterization of structures is of significant importance in a wide variety of industries including aerospace, automotive, rotating machinery, civil structures such as buildings and bridges, etc. Generally, the dynamic behavior of structures is characterized in terms of their modal parameters (modal frequencies, modal damping and scaled mode shapes). Availability of technologies like *Finite Element Analysis* (FEA) has aided in this regard however there are serious limitations which restrict the use of these techniques to complex, real life structures. These problems arise on account of the inability of FEA to correctly model structural properties like damping, nonlinearity, boundary conditions, etc. Thus these methodologies are complemented by experiments for accurately determining the dynamic characteristics of the structure.

Experimental Modal Analysis (EMA) is a popular technique for determining the modal parameters of a structure. The extracted modal parameters are then used for formulating a mathematical model that is representative of the system/structure dynamics. This model is called the *modal model*. The term experimental modal analysis involves both the data acquisition stage (*Modal Testing*) and subsequent analysis to come up with the modal model (*Modal Parameter Estimation*). EMA results are used for a variety of applications such as troubleshooting dynamics related problems, correlating and updating finite element model, simulation and prediction of structural modifications, to analyze sensitivity of modal parameters to system physical parameter changes (Sensitivity analysis), force identification, structural damage detection and health monitoring, active vibration control, etc. EMA is a relatively well understood technique and is well described in a number of texts [Ewins, 2000; Maia, Silva et al., 1997; Allemang, 1999; Heylen et al., 1995; He, Fu, 2001].

Experimental modal analysis (Figure 1.1) involves exciting the structure by means of known forces (either using shakers or impact hammers) and measuring the response to these forces over the structure (usually by means of accelerometers). The system/structure is then characterized (estimation of unknown modal parameters) on the basis of both the known input forces and output responses.

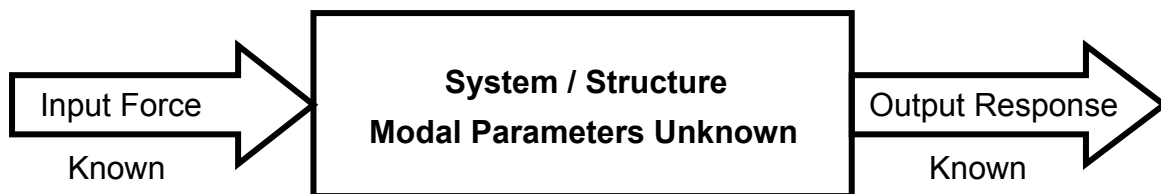


Figure 1.1 Experimental Modal Analysis

Over the last ten years researchers across the globe have worked on various techniques that utilize only the output response data to determine the modal parameters (Figure 1.2). To distinguish these techniques from traditional frequency response function (FRF)

based experimental modal analysis (EMA), the response data based modal parameter identification process became popular as Operational Modal Analysis (OMA) or Output-Only modal analysis. One of the prime motives for researchers to shift from the traditional and more established experimental modal analysis to operational modal analysis is the problems faced while studying and characterizing large, complex systems such as civil structures like bridges, buildings, etc and simulating exact operating conditions (such as those encountered by vehicles on road). It is not only difficult but sometimes impossible to provide sufficient artificial forced excitation to such huge structures. Even under circumstances when it's possible to excite the structure artificially, the associated costs are often too high to be justified. Thus, difficulties involved in exciting the structure sufficiently and simulating the operational conditions proves to be a major setback in application of traditional EMA techniques that require the structure to be excited by a known artificial force.

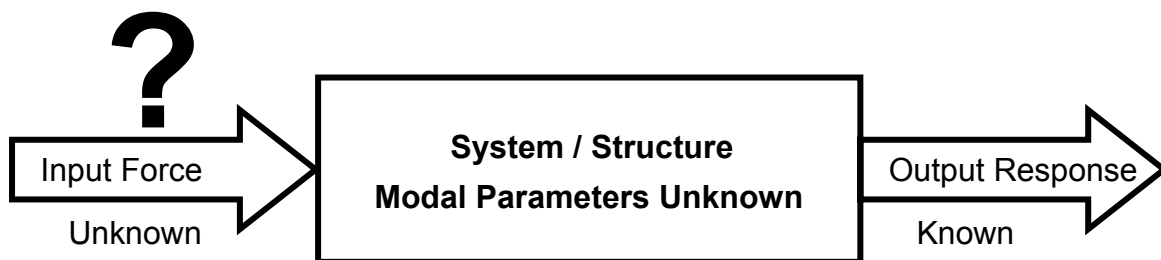


Figure 1.2 Operational Modal Analysis

To understand the OMA identification process further, the input-output model of Figure 1.1 can be expressed mathematically. If $\{X(\omega)\}$ is the measured response or the output and $\{F(\omega)\}$ is the input force, the relationship between them in terms of frequency response function (FRF) $[H(\omega)]$ is given as follows [Bendat, Piersol, 1986]:

$$\{X(\omega)\} = [H(\omega)]\{F(\omega)\} \quad 1.1)$$

This equation forms the basis of Experimental Modal Analysis where the frequency response functions $[H(\omega)]$ are formed from the measured input forces $\{F(\omega)\}$ and output responses $\{X(\omega)\}$. The FRFs contains all the necessary information required to obtain the modal parameters that characterize a system. This can be observed by expressing the frequency response functions in terms of modal parameters as

$$H_{pq}(\omega) = \sum_{r=1}^N \frac{Q_r \{\psi\}_r \{\psi\}_r^T}{j\omega - \lambda_r} + \frac{Q_r^* \{\psi\}_r^* \{\psi\}_r^{*T}}{j\omega - \lambda_r^*} \quad 1.2)$$

Eq. (1.2) shows the frequency response function $H(\omega)$ for a particular input location q and output location p being expressed in terms of the modal parameters; mode shape ψ , modal scaling factor Q and modal frequency λ . This model is referred to as the **modal model**. The goal of EMA modal parameter estimation is to extract this modal model from the measured FRF data.

Now Eq. (1.1) can be written as

$$\{X(\omega)\}^H = \{F(\omega)\}^H [H(\omega)]^H \quad 1.3)$$

Multiplying Eq. (1.1) and Eq. (1.3)

$$\{X(\omega)\}\{X(\omega)\}^H = [H(\omega)]\{F(\omega)\}\{F(\omega)\}^H [H(\omega)]^H$$

or with averaging,

$$[G_{XX}(\omega)] = [H(\omega)] [G_{FF}(\omega)] [H(\omega)]^H \quad 1.4)$$

where $[G_{XX}(\omega)]$ is the output response power spectra matrix and $[G_{FF}(\omega)]$ is the input force power spectra matrix.

Eq. (1.4) forms the basis of Operational Modal Analysis. Since the input force is not measured in the case of OMA, the OMA procedure only works under certain assumptions. Two key assumptions in this regard are

1. **The nature of the input force is assumed to be random, broadband and smooth. This means that the input power spectra is constant and has no poles or zeroes in the frequency range of interest.**
2. **The forcing is further assumed to be uniformly distributed spatially (i.e. number of inputs N_i approaching number of outputs N_o , considering the response is being measured all over the structure).**

Since $[G_{FF}(\omega)]$ is constant, $[G_{XX}(\omega)]$ can be expressed in terms of frequency response functions as

$$[G_{XX}(\omega)] \propto [H(\omega)][I][H(\omega)]^H \quad 1.5)$$

The partial fraction model of G_{XX} for a particular response location p and reference location q is given by

$$G_{pq}(\omega) = \sum_{k=1}^N \frac{R_{pqk}}{j\omega - \lambda_k} + \frac{R_{pqk}^*}{j\omega - \lambda_k^*} + \frac{S_{pqk}}{j\omega^* - \lambda_k} + \frac{S_{pqk}^*}{j\omega^* - \lambda_k^*} \quad 1.6a)$$

and can be more conveniently written as [Peeters, Auweraer, 2005]

$$G_{pq}(\omega) = \sum_{k=1}^N \frac{R_{pqk}}{j\omega - \lambda_k} + \frac{R_{pqk}^*}{j\omega - \lambda_k^*} + \frac{S_{pqk}}{-j\omega - \lambda_k} + \frac{S_{pqk}^*}{-j\omega - \lambda_k^*} \quad 1.6b)$$

$$G_{pq}(\omega) = \sum_{k=1}^N \frac{R_{pqk}}{j\omega - \lambda_k} + \frac{R_{pqk}^*}{j\omega - \lambda_k^*} + \frac{S_{pqk}}{j\omega - (-\lambda_k)} + \frac{S_{pqk}^*}{j\omega - (-\lambda_k^*)} \quad 1.6c)$$

where S_{pqk} and S_{pqk}^* are redefined to incorporate (-1).

Note that λ_k is the pole and R_{pqk} and S_{pqk} are the k^{th} mathematical residues. These residues are different from the residue obtained using a frequency response function based partial fraction model since they do not contain the modal scaling factor (as no force is measured). The form of Eq. (1.6c) clearly indicates that the roots that will be found from the power spectrum data will be $\lambda_k, \lambda_k^*, -\lambda_k$ and $-\lambda_k^*$ for each model order 1 to N.

1.2 Motivation and Problem Definition

Due to its usefulness in situations where application of EMA techniques is not possible or is difficult, OMA has found application in a number of areas including large civil structures such as bridges, stadiums, high rise buildings etc, automotive and aerospace industry etc.

Operational modal analysis possesses several advantages. Since the OMA tests are performed in-situ, they are expected to better represent the real world systems in comparison to the laboratory based EMA tests. The environmental effects of, for example mass loading or aero-elastic interaction, etc on system behavior can be taken into account while performing in-operation tests. Since OMA is an output-only technique, the cost involved in providing artificial excitation is avoided. Further, OMA tests are also better suited for the continuous monitoring of large structures [Peeters, 2000].

However, OMA techniques are still evolving and there are number of issues which remain to be understood more completely. Despite all the above stated advantages,

OMA suffers from serious limitations on account of unavailability of input force measurement. Normally system identification techniques are based on the knowledge of both the input and the output. In structural dynamics, the lack of input force information in OMA methods means that the mode shapes are unscaled. The modal scaling factor is an important modal parameter which is required in addition to modal frequency, damping and mode shape for completion of the modal model. This becomes necessary for further use of modal parameters for procedures such as modal updating, etc.

Yet another limitation of OMA is the assumption about the nature of the input force. In OMA it is assumed that the input force is random white noise. This assumption though applicable in many a situations (wind and rain on a bridge) is not always true. Presence of harmonic input ends up appearing as a peak in the output response power spectra and is difficult to distinguish from the genuine modes of the structure especially when signal to noise ratio is not very high (which is often the case in OMA).

This dissertation focuses on the following issues associated with OMA methods which define the problem and scope of the dissertation and also underlines the motivation for this work.

1. The primary data on which the OMA parameter estimation algorithms work is output power spectra (G_{xx}) (or correlation functions in time domain). This affects the modal analysis process considerably including the data acquisition, data processing and parameter estimation stages. In OMA, the forcing is ambient or natural and hence is not under control. Thus it is very possible that these forces are not able to excite all the modes of interest. There can also be cases where forcing is not sufficient, hence resulting in low signal-to-noise ratio. This means that in comparison to EMA, OMA requires much more data processing which creates a need for better data processing techniques [Chauhan et al., 2006].

2. Power spectra contain the same information twice in terms of, positive and negative modes (see Eq. 1.6c). In other words, the order of power spectrum is twice that of frequency response functions (this is further explored in Chapter 3). This makes the parameter estimation in the case of OMA more complex in comparison to EMA, especially for the frequency domain algorithms as higher order and presence of duplicate information in terms of negative modes affect the numerical conditioning aspects of frequency domain algorithms [Chauhan et al., 2006].
3. The second assumption stated in the previous section concerns the spatial distribution of input forcing excitation and states that the excitation is considered to be distributed uniformly all over the structure. In other words the structure is excited completely in spatial sense. However, this assumption is not true for several conventional EMA situations where excitation might be localized in nature [Chauhan et al., 2006].
4. It has also been noticed that damping values are often over estimated using OMA techniques [Chauhan, Phillips, Allemang, 2008]. The opinions on this aspect of OMA are widely varying and no consensus or definite answers are available.

1.3 Research Goals and Contributions

The issues stated in the previous section and, additionally, the algorithmic aspects of the modal parameter estimation stage of OMA form the basis of the research goals which are listed as follows

1. **Development of frequency domain parameter estimation algorithms and associated signal processing techniques for OMA,**

2. **Understand the effect of spatial distribution of excitation on OMA and how they affect the performance of OMA spatial domain algorithms,**
3. **Accurate estimation of damping using OMA techniques,**
4. **Extend Unified Matrix Polynomial Approach [Allemang, Brown, Fladung, 1994; Allemang, Brown, 1998; Allemang, Phillips, 2004] concept to OMA for the purpose of utilizing the advantages of UMPA for better understanding and development of various parameter estimation algorithms,**
5. **Use of advanced techniques such as Independent Component Analysis and other methods based on Higher Order Statistics [Hyvarinen, Karhunen, Oja, 2001; Chichoki, Amari, 2002] for the purpose of Operational Modal Analysis, and**
6. **Application of OMA techniques to real life structures (Cable-stayed bridges).**

With respect to these goals, the significant contributions of the research work carried out towards the field of OMA are

- The Unified Matrix Polynomial Approach is extended to OMA. The UMPA concept is recognized as a very good methodology for understanding and developing various modal analysis algorithms. In light of various differences with conventional input measurement based EMA and assumptions that are made in the case of OMA, the UMPA concept is extended to OMA. Emphasis is placed on understanding the basic difference between traditional Experimental Modal Analysis and output-only Operational Modal Analysis, the various assumptions made in the case of OMA and how the fundamental data (correlation functions and power spectrums) should be used in order to utilize the UMPA model for the purpose of parameter estimation in the case of OMA. It is revealed that understanding the underlying basic polynomial model not only helps in theoretical

development of various algorithms but also provides a common framework which makes it much easier and simpler to understand these algorithms. [Chauhan et al., 2007]

- As stated in the previous section, the lack of frequency domain algorithms in the field of Operational Modal Analysis can be attributed to numerical conditioning problems associated with them. In this research this aspect is studied in detail and reasons for poor numerical conditions in case of OMA are identified. A signal processing technique based on multiplying the power spectrum with a step function and utilizing only its positive lags portion is suggested to overcome the higher order of the power spectrums. A low order frequency domain algorithm based on the UMPA formulation was proposed and shown to have good numerical conditioning properties in comparison to high order frequency domain algorithms such as Rational Fraction Polynomial (RFP). [Chauhan et al., 2006].
- A new spatial domain OMA algorithm based on the previously introduced *Enhanced Mode Indicator Function* (EMIF) [Fladung, Phillips, Brown, 1997; Fladung, 2001; Allemang, Brown, 2006], is developed. This algorithm, referred as OMA-EMIF algorithm, is an alternative to the popular OMA algorithm, Frequency Domain Decomposition and enhanced Frequency Domain Decomposition (FDD/eFDD) and works entirely in the frequency domain. One of the major advantages of estimating the modes in the frequency domain is the ability to utilize the residuals which helps in improving the results by taking into account the contribution of the out-of-band modes. The algorithm is shown to give good results by implementing it on analytical and experimental systems. [Chauhan et al., 2006]
- Critical issues and limitations associated with the application of spatial domain algorithms to the OMA framework under different excitation scenarios are

studied. It is shown how the ability of *Complex Mode indicator Function* (CMIF) based methods is limited when the system is not adequately excited spatially. Though such problems are not encountered while analyzing structures such as bridges and buildings (where forcing is more uniform), in situations like automobiles on the road having narrow band point excitations (such as engine unbalance or other rotating unbalance), this can be a major problem as the resulting CMIF plot might not indicate the modes correctly. A tool based on contribution of singular values to total variance, *Singular Value Percentage Contribution* (SVPC) plot, is devised which helps in determining whether the system is being excited locally or spatially uniformly. This tool makes it possible to use the CMIF plot even in cases where the system is not spatially well excited. [Chauhan et al., 2006]

- Emerging concepts of Independent Component Analysis (ICA) and Blind Source Separation (BSS) are utilized for the purpose of OMA. Four popular ICA / BSS techniques are evaluated for their performance on an analytical system. It is shown how these techniques can be utilized for output-only modal parameter estimation purposes by relating them to the concepts of modal filtering and the modal expansion theorem. These algorithms are found to be relatively simple and less time consuming. [Chauhan et al., 2007]
- Issues related to the estimation of damping using OMA techniques are studied in more depth. By means of this study, it is shown how it is considerably difficult to get good, leakage free estimates of the power spectrums in comparison to the FRFs. It is further shown that cyclic averaging together with RMS averaging deals with leakage much more effectively in comparison to regular RMS signal processing that involves overlapping and windowing. It is noted that damping estimates are affected if the most basic OMA assumption (input forces being

random and uncorrelated) is not entirely true. The error in damping estimates is shown to be considerably increased if the input forces are not entirely uncorrelated. The results of this study indicate that for accurate estimation of damping, it is necessary to have good estimates (leakage free) of the output response power spectrum and that the input forces should be as uncorrelated as possible. While the first issue can be improved by using signal processing techniques like cyclic averaging, the second factor is often beyond one's control, especially in real-life scenarios. [Chauhan et al., 2008]

- Suggested OMA algorithms have been applied to complex real life structures like cable-stay bridges. This not only helped in evaluating the performance of these algorithms to practical scenarios but also provided valuable insight into designing and executing OMA tests of such huge and complex structures. [Chauhan, Saini et al., 2007, Chauhan, Saini et al., 2008]

1.4 Dissertation Outline

The research work presented in the dissertation is organized in the following manner

Chapter One introduces the dissertation. The motivation and merits of the dissertation are listed in this chapter along with a brief outline of how the dissertation is organized.

Chapter Two gives a comprehensive literature survey about OMA. It aims at providing the reader with the state of art about the various aspects of OMA including the need and development of the field of OMA, OMA algorithms, advantages and limitations of OMA and its application to various real life structures.

Chapter Three deals with *Unified Matrix Polynomial Approach* (UMPA) and its extension to OMA in this chapter. Various OMA algorithms developed using UMPA methodology are applied to an analytical system to show how UMPA can help in understanding and developing various algorithms.

In **Chapter Four** a frequency domain OMA algorithm is developed and is shown to perform satisfactorily by means of application to an analytical and an experimental (Circular plate) structure. The performance of this algorithm is also compared with its z-domain variant.

Chapter Five presents a spatial domain algorithm, OMA-EMIF. This algorithm is an alternative to the popular OMA algorithm FDD-eFDD and is based on reformulation of the EMIF algorithm. It also explores the issues related to application of spatial domain OMA algorithms in light of OMA assumptions.

Chapter Six focuses on utilizing advance signal processing techniques like Independent Component Analysis and Blind Source Separation for the purpose of OMA.

Chapter Seven emphasizes on exploring and deeper understanding of the OMA assumptions. The effect of violation of these assumptions on OMA parameter estimation process is studied. Signal processing techniques such as use of cyclic averaging, positive power spectrum and difficulties associated with use of frequency domain algorithms is also illustrated. This chapter also includes the work related to damping estimation using OMA algorithms.

Chapter Eight discusses the results of application of OMA algorithms to the US Grant and MRC cable stayed bridges, thus highlighting the performance of these algorithms in real life situations.

Chapter Nine concludes the thesis with the recapitulation of the salient points of the research and recommendations for the future work in the field of OMA.

Chapter Two

Literature Survey

It was in the 1990's that researchers started to work in the field that later developed into Operational Modal Analysis (OMA). As the work progressed, it came to be referred by several other names including Output-Only Modal Analysis, Ambient Modal Analysis and Natural Input Modal Analysis. The need for OMA was first realized by the civil engineering community due to the problems faced while studying and characterizing complex systems such as bridges, buildings, stadiums, offshore platforms, etc. Such structures were not only complex but also huge in size and thus finding dynamic properties of these structures using conventional Experimental Modal Analysis techniques posed several difficulties. Conventional EMA requires artificial excitation to excite the structure in order to obtain the modal parameters by means of measured output responses to the known input excitation forces. However, due to the immense size of civil structures it is often difficult and sometimes even impossible to excite these structures artificially. Even under circumstances when it's possible to excite the structure artificially, the associated costs are too high to be justified. Thus difficulties involved in exciting the structure sufficiently and simulating the operational conditions proves to be a major setback in application of traditional EMA techniques that require the structure to be excited by a known artificial force. This need initiated the work in the area of OMA with the objective of developing techniques that will enable engineers to find dynamic characteristics of a structure without the need to measure the input excitation forces.

Subsequently, other applications of OMA also emerged in traditional modal analysis areas of automotive, aerospace and other mechanical industries. These included applications where the modal parameters are required to be obtained in-situ. Simulating actual loading conditions artificially still remains a challenge and thus OMA, which can be performed in-situ, provided an alternative.

This chapter reviews the relevant literature available in the area of OMA including a survey of various OMA algorithms (**Section 2.1**), OMA application case studies (**Section 2.2**) and the work that has been carried out to identify and overcome the limitations of OMA (**Section 2.3**).

2.1 OMA Algorithms

Most OMA algorithms are essentially extensions of the traditional EMA algorithms. In this section the most common and popularly used OMA sections are reviewed.

2.1.1 Time Domain Algorithms

SDOF Peak Picking (PP) Method

The earliest OMA algorithms utilized the classical single degree of freedom based peak picking method [Allemang, 1999; Phillips, Allemang, 1996; Heylen et al., 1995], a simple technique that can be applied fairly successfully to modes that are well separated and have low damping. In EMA, this method identifies the modal frequencies as the peaks of an FRF plot. The damping ratios are obtained using the half-power bandwidth method and mode shapes are identified as the value of the frequency response function for all the response points at the modal frequency.

This method is extended to OMA by applying it to output response power spectrum instead of frequency response functions [Felber, 1993; Bendat, Piersol, 1993]. However,

this method does not work for situations where modes are not well separated and damping is moderate to heavy. Thus identification of closely spaced modes is not possible using this method. Insufficient frequency resolution can also hamper the effectiveness of this method.

NExT – Natural Excitation Technique and Other Similar Algorithms

The utilization of Autoregressive Moving Average (ARMA) procedure for estimating modal parameters using response data only was first suggested in 1970s [Gersch, Luo, 1972; Gersch, Fouth, 1974; Pandit, 1977; Pandit, Suzuki, 1979]. These methods assumed input force to be white random and the technique was applied to estimate the characteristics of the buildings excited by wind forces.

However, it was not till early 1990s that researchers started taking note of these output response only based techniques. The Natural Excitation Technique (NExT) [James, Carne, Lauffer, 1995] emerged during this time and was developed while modal testing the vertical-axis wind turbines and is one of the earliest OMA algorithms. The basis of the NExT algorithm is the auto and cross-correlation functions calculated between the measured output response time histories. This method then uses the traditional EMA time domain modal parameter estimation algorithms such as Least Square Complex Exponential (LSCE) [Brown et al., 1979], Ibrahim Time Domain (ITD) [Ibrahim, Mikulcik, 1977; Fukuzono, 1986] or their multiple input multiple output (MIMO) equivalents; Polyreference Time Domain (PTD) [Vold, Kundrat, et al., 1982; Vold, Rocklin, 1982] and Eigensystem Realization Algorithm (ERA) [Juang, Pappa, 1985; Longman, Juang, 1989].

Theoretical basis of NExT is that the correlation functions between output responses to a random white-noise input can be expressed as the sum of decaying sinusoids which

have same characteristics as the impulse response function, thus possessing the same modal parameters information.

Prediction Error Method (PEM) and Instrument Variable (IV) Method

These algorithms utilized the Auto-Regressive Moving Average (ARMA) model for identifying modal parameters. Ljung [Ljung, 1999] described a Prediction-Error method (PEM) approach in which the modal parameters are obtained by minimizing the prediction error. This algorithm results in a highly nonlinear optimization problem due to which its utility is severely affected. The algorithm is sensitive to initial values, is computationally intensive, convergence not guaranteed; all of which makes it unsuitable for OMA purposes, especially for analyzing large structures. A MIMO version of this algorithm, PEM-ARMAV (Vector ARMA), was proposed by Andersen (Andersen, 1997).

The nonlinear nature of the ARMA based PEM arises due to the MA polynomial coefficients. For the purpose of modal parameters though, only AR polynomial coefficients are needed. The Instrument Variable (IV) method [Peeters, De Roeck, 2001] uses this approach for system parameter identification purposes, thus avoiding the limitations of PEM. The IV method thus utilizes an AR model based on output covariance. It is to be noted that IV method yields equations similar to NExT and PTD, though it is derived in a different manner. As is the case with PTD, the model order in these algorithms is typically over specified and the spurious (mathematical) modes are filtered using tools such as stabilization diagrams [Allemang, 1999; Maia, Silva et al., 1997; Heylen et al., 1995].

State-Space Model Based Approaches

The OMA algorithms developed using the state-space approach can be further classified as either covariance-driven (realization based) and data-driven methods (subspace based).

Covariance-driven Stochastic Realization-based algorithms (SSI-COV)

Covariance driven stochastic realization based algorithms derive inspiration from the classical realization theory as explained by Ho and Kalman [Ho, Kalman, 1966]. The deterministic system realization method was subsequently refined by use of Singular Value Decomposition (SVD) to reduce the effect of noise [Zeiger, McEwen, 1974; Kung, 1974]. The eigensystem realization algorithm (ERA) [Juang, Pappa, 1985; Longman, Juang, 1989; Juang, 1994] belongs to this category of algorithms and is a popular EMA algorithm.

The discrete-time deterministic state-space model is given as

$$\begin{aligned}\{y_{k+1}\} &= [A]\{y_k\} + [B]\{u_k\} \\ \{x_k\} &= [C]\{y_k\} + [D]\{u_k\}\end{aligned}\tag{2.1}$$

where $\{x_k\}$ is the measured output vector, $\{u_k\}$ is the measured input vector and $\{y_k\}$ is the discrete state vector. $[A]$ is the state transition matrix describing the dynamics of the system (in terms of its eigenvalues), $[B]$ is the input matrix, $[C]$ is the output matrix that describes how the internal state is being transferred by means of output measurements $\{y_k\}$ and $[D]$ is the direct transmission matrix.

This model can be extended to discrete time combined deterministic-stochastic state space model by including the stochastic noise terms, the process noise $\{w_k\}$ and the measurement noise $\{v_k\}$, as shown in Eq. (2.2).

$$\begin{aligned}\{y_{k+1}\} &= [A]\{y_k\} + [B]\{u_k\} + \{w_k\} \\ \{x_k\} &= [C]\{y_k\} + [D]\{u_k\} + \{v_k\}\end{aligned}\tag{2.2}$$

For stochastic or the output-only case, the above state space model can be used without including the terms involving measured input vector $\{u_k\}$. The stochastic noise terms, $\{w_k\}$ and $\{v_k\}$, are considered zero mean, white noise vectors. Thus a discrete time stochastic state space model is given as

$$\begin{aligned}\{y_{k+1}\} &= [A]\{y_k\} + \{w_k\} \\ \{x_k\} &= [C]\{y_k\} + \{v_k\}\end{aligned}\tag{2.3}$$

As mentioned earlier, the dynamics of the system is described by the eigenvalues and eigenvectors of $[A]$ which can be obtained by its eigenvalue decomposition,

$$[A] = [\Phi] [\Lambda] [\Phi]^{-1}\tag{2.4}$$

System modes λ_r can be obtained by transforming the discrete eigenvalues z_r (Diagonal values of $[\Lambda]$) into continuous eigenvalues λ_r and the mode shape are obtained from the observed part of the eigenvectors $[\Phi]$. It should be noted that the mode shapes cannot be scaled as the input force information is not available.

$$z_r = e^{\lambda_r \Delta t}, \quad \lambda_r = \sigma_r + j\omega_r = \frac{1}{\Delta t} \ln(z_r)\tag{2.5}$$

$$\{\psi_r\} = [C]\{\phi_r\}$$

The covariance driven stochastic realization algorithm involves the formation of block-Hankel matrix [R] with correlation data (or covariance data as for a zero mean process covariance is equal to correlation) instead of impulse response functions (IRF) as in case of traditional EMA algorithms like ERA. The Hankel matrix can then be decomposed in the similar manner as explained by Ho and Kalman. This is shown in [Akaike, 1974; Aoki, 1987].

$$[R] = [C] \begin{bmatrix} A^{i-1} \\ \vdots \\ A \\ I \end{bmatrix} [G] \quad 2.6)$$

where [G] is the output covariance matrix of the next state

$$[G] = E[y_{k+1} x_k^T] \quad 2.7)$$

Formulation of OMA algorithms based on this model is shown in several papers including [Beveniste, Fuchs, 1985; Hermans, Van der Auweraer, 1999; Peeters, 2000; Peeters, De Roeck, 2001]. The SSI-COV algorithm is generally implemented in three different methods:

- 1). Principal Component (PC) method
- 2). Canonical Variant Analysis (CVA) method
- 3). Unweighted Principal Component (UPC) method

All these methods differ in the way the covariance Hankel matrix [R] is weighted before applying the Singular Value Decomposition (SVD) procedure to them. The UPC method is also called the Balanced Realization (BR) method and is equivalent of the popular

EMA algorithm, ERA. The implementation of these methods can be found in [Arun, Kung, 1990; Van Overschee, De Moor, 1996]. It is observed that in practical scenarios all three implementations have similar accuracy in terms of identified modal parameters [Peeters, De Roeck, 2001; Zhang, Brincker, Andersen, 2005].

Data-driven Stochastic Realization-based algorithms (SSI-DATA)

SSI-DATA [Van Overschee, De Moor, 1996; Peeters, De Roeck, 1999; Zhang, Brincker, Andersen, 2005] algorithm involves projecting the row space of the future outputs into row space of the past outputs by means of QR decomposition of the data Hankel matrix. This step is different from the SSI-COV method as, in this case, the data reduction is achieved by means of QR decomposition step rather than the covariance calculation step, as is the case with SSI-COV method. Finally the system parameters are obtained by performing an SVD of the projection matrix. In this case as well, one has the option of implementing the algorithm using PC, CVA or UPC methods as discussed previously.

The SSI-DATA algorithm works directly on the raw output response time histories instead of covariance data as in case of SSI-COV. In case of SSI-DATA, the data reduction is obtained in terms of a projection matrix computed by projecting the row space of the future outputs on row space of the past outputs, unlike SSI-COV where this data reduction is obtained by means of calculating covariance functions. This data reduction step is done by using QR decomposition. This is followed by application of SVD to the computed projection matrix to obtain its Kalman filter state. Finally least square approach is used to get the modal parameters. This algorithm is numerically more robust as it uses a square root algorithm, where as in SSI-COV matrices are squared in order to find covariance functions. It also avoids the leakage effect and other issues associated with calculation of covariance. The SSI-DATA method can also yield prediction errors and modal contributions which is not always the case with SSI-COV.

The computation times are however more in comparison, as covariance functions in case of SSI-COV can also be computed by inverse Fourier transforming power spectra which can be computed using faster discrete Fourier transform techniques.

2.1.2 Spatial Domain Algorithms

Spatial domain algorithms in OMA derive inspiration from the popular EMA algorithm, Complex Mode Indicator Function (CMIF) [Shih, Tsuei et al., 1989; Phillips, Allemang, Fladung, 1998; Allemang, Brown, 2006]. CMIF involves a frequency by frequency singular value decomposition of the frequency response function matrix.

$$[H(\omega_k)]_{N_o \times N_i} = [U(\omega_k)]_{N_o \times N_i} [\Sigma(\omega_k)]_{N_i \times N_i} [V(\omega_k)]_{N_i \times N_i}^H \quad 2.8)$$

where

N_o is number of outputs,

N_i is number of inputs,

$H(\omega_k)$ is the FRF matrix at any frequency ω_k ,

$U(\omega_k)$ is the left singular matrix at any frequency ω_k , which is a unitary matrix,

$V(\omega_k)$ is the right singular matrix at any frequency ω_k , which is also a unitary matrix,

$\Sigma(\omega_k)$ is the singular value matrix at any frequency ω_k , which is a diagonal matrix.

The frequency response function matrix is commonly expressed in matrix form as

$$[H(\omega)]_{N_o \times N_i} = [\Phi]_{N_o \times 2N_m} [j\omega[I] - [\Lambda]]_{2N_m \times 2N_m}^{-1} [L]_{2N_m \times N_i} \quad 2.9)$$

where

N_{2m} is number of modes being identified,

$[\Phi]$ is mode shape matrix,

$[L] = [Q][\Phi]^t$ is modal participation factor matrix,

$[Q]$ is the diagonal scaling factor matrix,

$[\Lambda]$ is the diagonal matrix with system poles.

Thus the SVD of the FRF matrix as given by Eq. (2.8) corresponds to its modal model as represented by Eq. (2.9). The procedure for estimating the modal parameters using this technique involves the realization that local maximum in a CMIF plot occurs near resonance and thus gives an estimate of the location of the system pole on the frequency line. In general, the response of a system at any given frequency is linear combination of the modal vectors. However, at the resonance, the response is primarily due to the modal vector corresponding to that mode. The estimate of the mode shape or the modal vector corresponding to this mode is given by the left singular vector associated with the peak singular value (generally the highest) at that frequency.

It should be noted that unlike other EMA algorithms that estimate modal frequency and damping in the first stage and the mode shapes later, the CMIF method does the reverse. It estimates the mode shapes in the first stage and, though it gives an estimate of the modal frequency, for more accurate estimates of the modal frequency and damping (which is not estimated in the first step), the CMIF routine is followed by the enhanced FRF based approach, referred commonly as Enhanced Mode Indicator Function (EMIF) [Allemang, 1980; Fladung, Philips, Brown, 1997; Phillips, Allemang, Fladung, 1998; Fladung, 2001; Allemang, Brown, 2006].

Frequency Domain Decomposition (FDD) and enhanced Frequency Domain Decomposition (eFDD)

As explained in Chapter 1, under certain assumptions about the input excitation forces, the output response power spectra $[G_{xx}]$ is proportional to multiplication of the FRF matrix with its hermitian $[H][H]^H$. Eq. (1.6-c) is recalled here to reiterate that the power spectrum matrix contains all the necessary information pertaining to the modal parameters, under these assumptions.

$$G_{pq}(\omega) = \sum_{k=1}^N \frac{R_{pqk}}{j\omega - \lambda_k} + \frac{R_{pqk}^*}{j\omega - \lambda_k^*} + \frac{S_{pqk}}{j\omega - (-\lambda_k)} + \frac{S_{pqk}^*}{j\omega - (-\lambda_k^*)}$$

Frequency Domain Decomposition [Brincker, Zhang, Andersen, 2000] and enhanced Frequency Domain Decomposition algorithm [Brincker, Ventura, Andersen, 2000] are one of the most popular OMA algorithms. They are similar in principle to the CMIF algorithm. The Frequency Domain Decomposition technique also involves the singular value decomposition (SVD), but it applies the SVD on the output response power spectra matrix, instead of the FRF matrix. Thus at any particular frequency ω_k the singular value decomposition of $[G_{xx}]$ results in

$$[G_{xx}(\omega_k)] = [U][S][V]^H \quad 2.10)$$

where $[S]$ is the singular value diagonal matrix and $[U]$, $[V]$ are singular vector matrices which are orthogonal. For the case where the where all response locations are considered as references to form the square $[G_{xx}]$ matrix, $[U]$ and $[V]$ are theoretically equal. The singular vectors near a resonance are good estimates of the mode shapes and the modal frequency is obtained by the simple, single degree of freedom peak-

picking method [Phillips, Allemang, 1996; Brincker, Zhang, Andersen, 2000; Gade, Moller et al., 2005].

FDD algorithm gives the frequency and mode shapes but for damping estimation (and also for more accurate estimation of modal frequency) one has to utilize the eFDD algorithm. In the eFDD algorithm [Brincker, Ventura, Andersen, 2000; Gade, Moller et al., 2005], power spectra of a SDOF system is identified around a peak of resonance (A peak in the SVD plot). A user defined Modal Assurance Criterion (MAC) [Allemang, 1980; Heylen, Lammens, Sas, 1995] rejection level is set to compare the singular vectors around the peak and corresponding singular values are retained as those belonging to the SDOF power spectrum. This SDOF power spectrum is transformed back to the time domain by inverse FFT. The natural frequency and damping are then estimated for this SDOF system by determining zero crossing time and logarithmic decrement methods respectively.

2.1.3 Frequency Domain Algorithms

PolyMAX – Polyreference LSCF Algorithm

The use of frequency domain algorithms for OMA purposes is not very common due to the numerical conditioning issues as discussed briefly in Chapter 1. The PolyMAX algorithm [Verboven, 2002; Guillaume, Verboven et al., 2003; Peeters, Van der Auweraer et al., 2004; Peeters, Van der Auweraer, 2005] is perhaps the only commercially available frequency domain OMA algorithm. This algorithm is the polyreference variant of the Least Square Complex Exponential algorithm in frequency domain.

The PolyMAX algorithm is based upon to the historical Rational Fractional Polynomial (RFP) [Richardson, Formenti, 1982] algorithm. The RFP algorithm uses the rational

fraction form of the FRF, which for a particular output location p and excitation location q is given by Eq. (2.11)

$$H_{pq}(\omega) = \frac{X_p(\omega)}{F_q(\omega)} = \frac{\sum_{k=0}^n \beta_k (j\omega)^k}{\sum_{k=0}^m \alpha_k (j\omega)^k} \quad (2.11)$$

The rational fraction form of the frequency response function is also referred to as the Common-Denominator model. To obtain the system modes or poles, one has to utilize the FRF data as per the model in Eq. (2.11) and then solve for the roots of the denominator characteristic polynomial after finding the polynomial coefficients α_k . The roots of the numerator characteristic polynomial gives the zeros of transfer function which can be used to estimate the residues (Note that the estimation of zeros is not necessary from modal analysis point of view, though both poles and zeros are needed to characterize the dynamics of a system represented by the transfer function as in case of electrical networks). This algorithm can also be extended to the MIMO case by including the measurements corresponding to other input points. This follows from the understanding that since the system characteristics do not depend on the measurement locations but are inherent in the system poles (roots of the denominator polynomial), the characteristic polynomial for all the measurements should be the same. This generally results in more equations than unknowns and thus a least squared based solution is used to obtain the polynomial coefficients. The same equations also happen to be the basis of the PolyMAX method [Guillaume, Verboven et al., 2003]. In the mentioned reference, the model is referred to as the Right-Matrix Fraction model which is essentially the same model as that used for RFP algorithm. The key difference between the PolyMAX and the RFP method is that the PolyMAX method uses z-domain mapping

to improve the numerical conditioning, i.e. formulation of the problem is done in the discrete time model instead of a continuous time model as is the case with RFP which uses a different form of generalized frequency mapping [Peeters, Van der Auweraer et al., 2004]. This is explained further in Chapter 4.

2.1.4 Maximum Likelihood (ML) Estimator Based Algorithms

In addition to above mentioned algorithms, most of which utilize a least squares approach to estimate the modal parameters, researchers have also tried to utilize Maximum Likelihood (ML) estimator based optimization technique to estimate the modal parameters [Scoukens, Pintelon, 1991; Pintelon, Guillaume et al., 1994].

This algorithm involves estimation of the same model as represented by Eq. (2.11) by Gauss-Newton optimization of the negative log-likelihood function given as

$$l_{ML}(\theta) = \sum_{o=1}^{N_o} \sum_{i=1}^{N_i} \sum_{f=1}^{N_f} \frac{|\hat{H}_{oi}(\theta, \omega_f) - H_{oi}(\omega_f)|^2}{\text{var}\{H_{oi}(\omega_f)\}} \quad (2.12)$$

where θ are the coefficients of the polynomial (α_k and β_k), N_o and N_i are number of outputs and inputs and $H(\omega)$ is the measured FRF. However, for more robust and faster implementation, a logarithmic estimator, as shown in Eq. (2.13) is minimized instead of the above mentioned function [Guillaume, Verboven, Vanlanduit, 1998].

$$l_{LOG}(\theta) = \sum_{o=1}^{N_o} \sum_{i=1}^{N_i} \sum_{f=1}^{N_f} \frac{|\log(\hat{H}_{oi}(\theta, \omega_f)) / H_{oi}(\omega_f)|^2}{\text{var}\{\hat{H}_{oi}(\theta, \omega_f)\} / |H_{oi}(\omega_f)|^2} \quad (2.13)$$

The ML estimator approach is extended to OMA in similar manner as other popular EMA algorithms by applying the method to response power spectrum data instead of FRFs [Hermans, Van der Auweraer, Guillaume, 1998].

Since the ML estimator algorithm uses an optimization scheme, it is iterative and requires a good starting values. It is interesting to note that a least squares approach as in RFP or PolyMAX is used to get good initial values and it is observed that these values are themselves good estimates of the modal parameters and further iterations doesn't result in any considerable improvement [Verboven, 2002; Zhang, Brincker, Andersen, 2005].

2.2 Issues with OMA

The very assumptions that make the OMA procedure possible are also the cause of its limitations. The unavailability of input excitation force information leads to hindrances at various modal analysis stages which are interrelated. These issues are briefly listed in the following points.

1. *Data Acquisition:* Since the excitation force to the structure is provided by natural means, quality of acquired data now depends on uncontrolled factors. For example, while analyzing a building, it is important to have sufficient excitation being provided by natural sources like the wind in order to get a good signal-to-noise ratio. In addition to this, longer time histories are required in order to compute better and more accurate estimates of the response power spectrums (or correlation in time domain), in comparison to that required for computing FRFs as in EMA. This aspect will be discussed further in Chapter 7. Yet another aspect of dependence on natural excitation is that one can't be sure whether all the modes of interest are being excited or not. This is also the basis of the

second assumption listed in Chapter 1, which states that the excitation should be spatially complete, which will ensure that it excites all the modes of interest.

2. *Data Processing:* Output power spectrum has twice the order of a FRF and contains the same system related information twice, in slightly different form. In order to estimate the modal parameters accurately, special data processing techniques, such as calculation of positive power spectrum (Chapter 3), is needed to make modal parameter estimation algorithms work satisfactorily.
3. *Parameter Estimation:* Issues associated with output power spectra as mentioned in the previous point also make the parameter estimation process more complicated. Further, unavailability of input excitation forces means that the obtained mode shapes are not scaled.

These issues also affect the application of modal parameters for other purposes such as sensitivity analysis, structural modification, modal updating, force identification, structural health monitoring, etc. as these require a complete modal model which is not obtained using OMA (the scaling factor cannot be directly determined). This problem also makes it difficult to analyze huge structures such as a bridge because the number of sensors available are often limited and a number of different setups are required to analyze the structure completely. This causes a problem while stitching the mode shapes, obtained from the various setups, together since it is very possible that excitation levels are different while acquiring data for various setups. In absence of the force information there is no simple way to normalize the mode shapes.

The scaling factor needed for completing the modal model can be obtained by employing a mass change method [Parloo, Verboven, et al., 2002; Brincker, Andersen, 2003; Aenlle, Brincker, Canteli, 2005]. These methods are based on the fact that if a small mass modification is made in such a manner that the mode shape practically remains the same but natural frequency of the system changes only slightly. These

methods are simple but tedious. Sometimes, it is required to perform several mass changes to obtain good estimates. This is called the extrapolation approach. Also, theoretically if mass changes are distributed in such a manner that the resulting mass change matrix is proportional to original mass matrix of the system, then the error in scaling factor is diminished. However, this is not practically possible and thus estimated scaling factors tend to be error prone. Thus, in cases where scaling factor estimation is must, conventional FRF based Experimental Modal Analysis techniques are preferred. Yet another major issue with application of OMA to systems with rotating and reciprocating parts is how to distinguish between the system modes and the harmonic excitation. The prime assumption on which OMA works states that the input excitation force is considered random and thus the input power spectra is broadband and smooth. This means that the input power spectra is constant and has no poles or zeroes in the frequency range of interest. This is however not true for systems with rotating and reciprocating parts. The presence of harmonic excitation is common in systems like ventilation systems, turbines, generators, and several automotive and aerospace applications, and thus, in such systems, the excitation is a combination of random stochastic excitation and harmonic excitation. The detection of harmonic components is not only difficult, as there aren't any straight forward ways to distinguish them from system modes, but also important from the point of view of bias errors that they might introduce in the estimated modal parameters.

The following are some of the ways to distinguish between the structural modes and the harmonic response content:

1. One of the simple ways to distinguish between a structural mode and harmonic excitation is that modes appearing due to harmonic excitation will have very low (near zero) damping (though this might not be true if the frequency is not constant) [Jacobsen, 2006]. A method was suggested by Mohanty and Rixen to

- distinguish the harmonic excitation but it required that the frequency of harmonic excitation is known apriori. This information might be available in few cases but that might not always be the case and thus this significantly reduces the effectiveness of this method [Mohanty, Rixen, 2004].
2. Yet another way of detecting harmonics is based on the fact that the probability distribution function (PDF) of a harmonic response is different from that of a stochastic structural response [Brincker, Andersen, Moller, 2000]. The PDF of a harmonic response is a distribution having two peaks where as that of a structural response due to stochastic excitation is a Gaussian distribution having single peak. This method is, however, not very successful if frequency of the harmonic excitation is close to a structural mode as in such a scenario the pdf will be a combination of the two unique PDF shapes.

2.3 OMA Applications

As stated earlier, the problems encountered during attempts at EMA of large complex structures such as buildings, stadiums and bridges that caused OMA to be developed. Thus civil structures were the first applications to which the OMA techniques were applied. Civil structures still remain the most popular OMA application area. In current literature, there are several real life cases of application of OMA techniques to civil structures for parameter estimation. The Swiss Z24 highway bridge was tested considerably and data was collected under various excitation scenarios including under ambient conditions. Several OMA parameter estimation methods were applied and evaluated for comparison and performance basis. These methods included from simplest peak picking to more involved SSI and polyreference LSCE methods. The methods yielded comparable modal parameters [Andersen, Brincker, Peeters et al., 1999]. In a follow up to this paper, the performance of OMA techniques was compared

with EMA methods. This study provided insights to various OMA methods from a practical application point of view and the results showed that SSI method gave the most complete and consistent modal parameters. It was also suggested that if the structure has low natural frequencies, below 1 Hz, then they are best excited by ambient sources or by drop weight excitation. In such cases use of a shaker might not be advantageous. Further, the high frequency modes are not always well excited by ambient sources. Importantly, if continuous health monitoring is one of the intended purposes then only ambient excitation can be used [Peeters, Ventura, 2003].

Ambient vibration based studies were conducted on the Heritage Court Tower 2 in Vancouver, Canada. Several papers were presented in the proceedings of International Modal Analysis Conference (IMAC) in 2000 in relation to this study. The summarized results of this study are presented by Horyna and Ventura [Horyna, Ventura, 2000]. As with Z24 bridge study, this study also concludes that there is a good agreement between results obtained through the various techniques and, though SSI is bit more elaborate procedure, it results in consistent estimation of modal parameters.

OMA algorithms have been very popular in application to civil engineering structures, since, they have found application in automotive and aerospace applications as well. FDD and SSI algorithms were applied to a car body subjected to engine excitation [Brincker, Andersen, Moller, 2000] and also to a diesel engine [Moller, Brincker, Andersen, 2000]. In [Hermans, Van der Auweraer, 1999] pLSCE and CVA and BR variants of SSI-COV algorithm were applied to rear suspension system of a passenger car to identify the modal parameters. The operational data in this case was collected by running the vehicle on a rough asphalt road at a speed on 50 km/hour. The main purpose of this study was to identify the source of a booming interior noise at around 80 Hz. With the help of OMA tests, the first bending mode of the rear suspension twist beam was identified around 70-80 Hz which was the potential cause of the problem. The

study suggested that the mode was more easily identified by CVA and BR algorithms in comparison to pLSCE.

This paper also presents a case study where OMA is applied to flight flutter test data. The aim of the study was to find out the robustness and suitability of these techniques to non-stationary conditions as those encountered in flight flutter testing. In this example the SSI-COV also methods gave better results than the pLSCE results. In yet another study, flight flutter data was analyzed using least squares time and frequency domain algorithms as well as maximum likelihood based approach [Vecchio, Peeters, Van der Auweraer, 2002]. It was observed that time domain LSCE does not perform as well as the other methods.

The performance of subspace based OMA methods was evaluated for time varying structures by applying these methods to Ariane 5 launcher [Goursat, Basseville et al., 2001]. The data was collected over the commercial flight of the space launcher under unknown natural excitation. It was observed that, more important than the varying nature of the structure, it is the location and number of the sensors that poses more challenges while analyzing such a complex structure.

2.4 Conclusions

This chapter provides the theoretical background and past research carried out in the area of the Operational Modal Analysis, thus laying the foundation for the work to be presented in the coming chapters. Various popular OMA algorithms have been discussed in terms of their development and limitations. The major issues associated with OMA have been highlighted and significant OMA case studies in the various application areas have been listed. OMA is still a growing area and has shown tremendous promise as a useful tool for analyzing structural dynamics related problems. OMA research studies are presented frequently at the International Modal Analysis

Conference (IMAC) and at the International Seminar on Modal Analysis (ISMA) and more details on the state-of-art research in OMA can be obtained in the proceedings of these conferences. Recently a new conference, International Operational Modal Analysis Conference (IOMAC), dedicated to the field of OMA has started. This conference is organized once in every two years and was organized for the first time in 2005. This is another excellent source for OMA related research.

Chapter Three

Unified Matrix Polynomial Approach for Operational Modal Analysis

One of the significant contributions of the Unified Matrix Polynomial Approach (UMPA) [Allemang, Brown, Fladung, 1994; Allemang, Brown, 1998; Allemang, Phillips, 2004] concept to the field of the experimental modal analysis (EMA) was to present the various modal parameter estimation algorithms using a consistent mathematical formulation. This approach not only helped in better understanding of the underlying similarities and differences of the various algorithms, it also provided a common framework to develop these same algorithms which over the years had been developed in isolation.

The basic difference between the OMA based modal parameter estimation algorithms and the more common EMA parameter estimation algorithms is the fundamental data used. While EMA based algorithms use frequency response functions or impulse response functions (normalized input-output functions in the frequency or time domain), OMA based algorithms use output response power spectrum or correlation functions.

With so many obvious advantages both in terms of developing or understanding the various parameter estimation algorithms and also in understanding the overall parameter estimation process, it is very relevant to extend the concept of UMPA to Operational Modal Analysis. This forms the motivation of this chapter where a unified matrix polynomial approach based formulation is reviewed for various OMA algorithms. Section 3.1 discusses the general modal parameter estimation process and introduces the

UMPA model. In Section 3.2, basics of OMA are discussed and UMPA is extended to OMA framework. Section 3.3 provides the UMPA based mathematical equations of the various time, frequency and spatial domain algorithms and finally a simple case study is provided to show the effectiveness of the UMPA methodology in OMA domain.

3.1 Modal Parameter Estimation and UMPA

The matrix equation of motion for a general multi degree of freedom system is given by

$$[M]\{\ddot{x}(t)\} + [C]\{\dot{x}(t)\} + [K]\{x(t)\} = \{f(t)\} \quad 3.1)$$

where:

[M] is mass matrix,

[C] is damping matrix,

[K] is stiffness matrix,

{x(t)} is response vector and

{f(t)} is force vector.

The above equation represents the physical M-C-K model of the system. It is a second order differential equation that can be solved either in time, frequency or Laplace domain. This second order model can be converted into higher order model to handle the case where spatial information is truncated to a size smaller than the number of eigenvalues in the measured data. One way to develop this concept is to obtain the characteristic equation by Laplace transforming Eq. (3.1).

Thus

$$[[M]s^2 + [C]s + [K]]\{X(s)\} = \{F(s)\} \quad 3.2)$$

and the characteristic equation becomes

$$[M]s^2 + [C]s + [K] = 0 \quad (3.3)$$

The partitioned form of above equation can be written as

$$\begin{bmatrix} [M_{11}] & [M_{12}] & \dots & [M_{1m}] \\ [M_{21}] & [M_{22}] & \dots & [M_{2m}] \\ \dots & \dots & \dots & \dots \\ [M_{m1}] & [M_{m2}] & \dots & [M_{mm}] \end{bmatrix} s^2 + \begin{bmatrix} [C_{11}] & [C_{12}] & \dots & [C_{1m}] \\ [C_{21}] & [C_{22}] & \dots & [C_{2m}] \\ \dots & \dots & \dots & \dots \\ [C_{m1}] & [C_{m2}] & \dots & [C_{mm}] \end{bmatrix} s + \begin{bmatrix} [K_{11}] & [K_{12}] & \dots & [K_{1m}] \\ [K_{21}] & [K_{22}] & \dots & [K_{2m}] \\ \dots & \dots & \dots & \dots \\ [K_{m1}] & [K_{m2}] & \dots & [K_{mm}] \end{bmatrix} = [0] \quad (3.4)$$

This equation can be expanded to a higher order matrix polynomial and put in a generic form as

$$[\alpha_{2m}]s^{2m} + [\alpha_{2m-1}]s^{2m-1} + \dots + [\alpha_0] = 0 \quad (3.5)$$

Note that size of $[a]$ is same as the size of the portioned sub matrices and each $[a]$ matrix involves a matrix product and summation of several $[M_{ij}]$, $[C_{ij}]$ and $[K_{ij}]$ sub matrices.

The higher order equation Eq. (3.5) has the same eigenvalues as the original second order differential equation Eq. (3.1). The general matrix polynomial formulation of the differential equations in the time, frequency and Laplace domain is given by

Time Domain (Continuous)

$$\left\{ [\alpha_m] \frac{d^m x(t)}{dt^m} + [\alpha_{m-1}] \frac{d^{m-1} x(t)}{dt^{m-1}} + \dots + [\alpha_0] \right\} \{x(t)\} = \left\{ [\beta_n] \frac{d^n f(t)}{dt^n} + [\beta_{n-1}] \frac{d^{n-1} f(t)}{dt^{n-1}} + \dots + [\beta_0] \right\} \{f(t)\} \quad 3.6)$$

Time Domain (Discrete)

$$\left\{ [\alpha_m] \{x(t_{i+m})\} + [\alpha_{m-1}] \{x(t_{i+m-1})\} + \dots + [\alpha_0] \{x(t_i)\} \right\} = \left\{ [\beta_n] \{f(t_{i+n})\} + [\beta_{n-1}] \{f(t_{i+n-1})\} + \dots + [\beta_0] \{f(t_i)\} \right\} \quad 3.6a)$$

Frequency Domain

$$\left\{ [\alpha_m] (j\omega)^m + [\alpha_{m-1}] (j\omega)^{m-1} + \dots + [\alpha_0] \right\} \{X(\omega)\} = \left\{ [\beta_n] (j\omega)^n + [\beta_{n-1}] (j\omega)^{n-1} + \dots + [\beta_0] \right\} \{F(\omega)\} \quad 3.7)$$

Laplace Domain

$$\left\{ [\alpha_m] (s)^m + [\alpha_{m-1}] (s)^{m-1} + \dots + [\alpha_0] \right\} \{X(s)\} = \left\{ [\beta_n] (s)^n + [\beta_{n-1}] (s)^{n-1} + \dots + [\beta_0] \right\} \{F(s)\} \quad 3.8)$$

The above described matrix coefficient polynomial forms a good basis to understand the common characteristics of different modal parameter estimation algorithms.

To understand the model further, Eq. (3.7) is considered. This is the historically used polynomial model for frequency response function ($H(\omega)$). If p and q are response and excitation degree of freedoms respectively, Eq. (3.7) can be written as

$$H_{pq}(\omega_i) = \frac{X_p(\omega_i)}{F_q(\omega_i)} = \frac{\beta_n (j\omega)^n + \beta_{n-1} (j\omega)^{n-1} + \dots + \beta_0 (j\omega)^0}{\alpha_m (j\omega)^m + \alpha_{m-1} (j\omega)^{m-1} + \dots + \alpha_0 (j\omega)^0} \quad 3.9)$$

This can be rewritten as

$$H_{pq}(\omega_i) = \frac{X_p(\omega_i)}{F_q(\omega_i)} = \frac{\sum_{k=0}^n \beta_k (j\omega)^k}{\sum_{k=0}^m \alpha_k (j\omega)^k} \quad 3.10)$$

or for a general multiple input, multiple output case

$$\left[\sum_{k=0}^m (j\omega)^k [\alpha_k] \right] [H(\omega_i)] = \left[\sum_{k=0}^n (j\omega)^k [\beta_k] \right] [I] \quad 3.11)$$

The size of coefficient matrices is normally $N_i \times N_i$ or $N_o \times N_o$ for $[\alpha_k]$ and $N_i \times N_o$ or $N_o \times N_i$ for $[\beta_k]$ where N_i and N_o are number of input and output degrees of freedom respectively .

This general model corresponds to an AutoRegressive – Moving Average (ARMA(n,m)) model developed from a set of discrete time equations in the time domain. The model, more appropriately, is an AutoRegressive with eXogenous inputs (ARX(n,m)) model. The general matrix polynomial model concept recognizes that both time and frequency domain models generate functionally similar matrix polynomial models. This model which describes both domains is thus termed as **Unified Matrix Polynomial Approach (UMPA)** [Allemang, Brown, Fladung, 1994; Allemang, Brown, 1998; Allemang, Phillips, 2004]. Note that Eq. (3.11) can be repeated at many frequencies (ω_j) until the system is sufficiently over determined.

Parallel to above formulation, a time domain model can be developed. For a general multiple input, multiple output case, from Eq. (3.6a)

$$\sum_{k=0}^m [\alpha_k] \{x(t_{i+k})\} = \sum_{k=0}^n [\beta_k] \{f(t_{i+k})\} \quad 3.12)$$

For impulse response or free decay data the above equation will reduce to

$$\sum_{k=0}^m [\alpha_k] \{h(t_{i+k})\} = 0 \quad 3.13)$$

as forcing can be assumed to be zero for all times greater than zero. Note that $h(t)$ is impulse response function.

The characteristic matrix polynomial equation, for the time and frequency domain are given by Eq. (3.14) and Eq. (3.15) respectively.

$$\left| \begin{matrix} [\alpha_m] & z^m + [\alpha_{m-1}] & z^{m-1} + [\alpha_{m-2}] & z^{m-2} + \dots + [\alpha_0] \end{matrix} \right| = 0 \quad 3.14)$$

$$\left| \begin{matrix} [\alpha_m] & s^m + [\alpha_{m-1}] & s^{m-1} + [\alpha_{m-2}] & s^{m-2} + \dots + [\alpha_0] \end{matrix} \right| = 0 \quad 3.15)$$

Once the matrix coefficients $[\alpha]$ are found, the modal parameters can be obtained in a number of ways, the most common being the companion matrix approach. Eq. (3.16) shows one of the ways in which the companion matrix $[C]$ can be formulated.

$$[C] = \begin{bmatrix} -[\alpha]_{m-1} & -[\alpha]_{m-2} & \cdots & \cdots & \cdots & -[\alpha]_1 & -[\alpha]_0 \\ [I] & [0] & \cdots & \cdots & \cdots & [0] & [0] \\ [0] & [I] & \cdots & \cdots & \cdots & [0] & [0] \\ \cdots & \cdots & \cdots & \cdots & \cdots & \cdots & \cdots \\ \cdots & \cdots & \cdots & \cdots & \cdots & \cdots & \cdots \\ [0] & [0] & \cdots & \cdots & \cdots & [0] & [0] \\ [0] & [0] & \cdots & \cdots & \cdots & [I] & [0] \end{bmatrix} \quad 3.16)$$

The roots of the characteristic equation can be obtained by using the companion matrix to solve the eigenvalue problem, as in Eq. (3.17).

$$[C]\{X\} = \lambda[I]\{X\} \quad 3.17)$$

It is important to note that the eigenvectors are of length model order m multiplied by the matrix coefficient size, N_i or N_o . The useful portion of the eigenvector is of the length of the coefficient matrix, i.e. N_i or N_o and is repeated in the eigenvector $m+1$ times, each repetition being multiplied by integer power of the associated modal frequency. This can be understood more easily through Eq. (3.18).

$$\{\phi\}_r = \begin{Bmatrix} \lambda_r^m \{\psi\}_r \\ \cdot \\ \cdot \\ \lambda_r^1 \{\psi\}_r \\ \lambda_r^0 \{\psi\}_r \end{Bmatrix}_r \quad 3.18)$$

The Unified Matrix Polynomial Approach as explained above provides common framework to most commonly used modal parameter estimation algorithms. This unified perspective provides for easy understanding of the various algorithms such as *Complex*

Exponential Algorithm (CEA) [Spitznogle, 1971; Brown Allemang, et al., 1979], *Least Squares Complex Exponential (LSCE)* [Brown Allemang, et al., 1979], *Ibrahim Time Domain (ITD)* [Ibrahim, Mikulcik, 1977; Pappa, 1982], *Polyreference Time Domain (PTD)* [Vold, Kundrat, et al., 1982; Vold, Rocklin, 1982], *Polyreference Frequency Domain (PFD)* [Zhang, Kanda et al., 1984; Lembregts, Leuridan et al., 1986; Lembregts, Leuridan, Van Brussel, 1989], *Eigensystem Realization Algorithm (ERA)* [Juang, Pappa, 1985; Longman, Juang, 1989], *Multiple Reference Ibrahim Time Domain (MRITD)* [Fukuzono, 1986], *Rational Fractional Polynomial (RFP)* [Richardson, Formenti, 1982] etc. which over the years have been developed in isolation. Table 3.1 shows how various commercial modal parameter estimation algorithms fit into UMPA framework. Thus UMPA model helps in understanding the similarities, differences and numerical characteristics of the various modal parameter estimation algorithms by providing a common mathematical structure. [Allemang, Brown, Fladung, 1994; Allemang, Brown, 1998; Allemang, Phillips, 2004] provide more insights and details of the modal parameter estimation using the unified matrix polynomial approach.

The goal of modal parameter estimation is to obtain the modal model of the system which is defined in terms of complex valued modal frequencies (λ_r), modal vectors ($\{\psi_r\}$) and modal scaling (modal mass or modal A). However, in case of OMA the modal scaling is not estimated due to lack of input force data. Thus the mode shapes are unscaled mode shapes.

Table 3.1 - UMPA representations of various EMA algorithms

	High Order	Low Order	Zero Order
Time Domain	PTD, LSCE, CEA	ITD, ERA, MRITD	-
Frequency Domain	RFP, PolyMAX, AF POLY, Orthogonal Polynomial	PFD	-
Spatial Domain	-	-	CMIF

3.2 OMA Basics and Associated Signal Processing

To reformulate UMPA equations in OMA framework, the Eq. (1.4) is reconsidered.

$$[G_{XX}(\omega)] = [H(\omega)] [G_{FF}(\omega)] [H(\omega)]^H$$

where $[G_{XX}(\omega)]$ is the output response power spectra and $[G_{FF}(\omega)]$ is the input force power spectra.

Recalling that in case of OMA the input force spectrum is assumed to be constant, it is easy to note that the output response power spectra $[G_{XX}(\omega)]$ is proportional to the product $[H(\omega)][H(\omega)]^H$ and the order of output response power spectrum is twice that of frequency response functions. Since $[G_{FF}(\omega)]$ is constant, $[G_{XX}(\omega)]$ can be expressed in terms of frequency response functions as

$$[G_{XX}(\omega)] \propto [H(\omega)] [I] [H(\omega)]^H$$

In terms of the UMPA model of $[H(\omega)]$ this can be expanded as

$$G_{XX}(\omega_i) = \left[\frac{\sum_{k=0}^n [\beta_k] (j\omega)^k}{\sum_{k=0}^m [\alpha_k] (j\omega)^k} \right] \times \left[\frac{\sum_{k=0}^n [\beta_k] (j\omega)^k}{\sum_{k=0}^m [\alpha_k] (j\omega)^k} \right]^H \quad 3.19)$$

Further, since $(n < m)$, a partial fraction form of the modal model can be formed for the output power spectrum which was shown in Chapter 1 by Eq. (1.6-c). This partial fraction model for a particular response location p and reference location q is given by

$$G_{pq}(\omega) = \sum_{k=1}^N \frac{R_{pqk}}{j\omega - \lambda_k} + \frac{R_{pqk}^*}{j\omega - \lambda_k^*} + \frac{S_{pqk}}{j\omega - (-\lambda_k)} + \frac{S_{pqk}^*}{j\omega - (-\lambda_k^*)} \quad 3.20)$$

where S_{pqk} and S_{pqk}^* are redefined to incorporate (-1).

Note that λ_k is the pole and R_{pqk} and S_{pqk} are the k^{th} mathematical residues. These residues are different from the residue obtained using a frequency response function based partial fraction model since they do not contain modal scaling factor (as no force is measured). The form of Eq. (20-c) clearly indicates that the roots that will be found from the power spectrum data will be $\lambda_k, \lambda_k^*, -\lambda_k$ and $-\lambda_k^*$ for each model order 1 to N . To formulate a unified matrix polynomial approach for Operational Modal Analysis, Eq. (3.19) can be rewritten as

$$\left[\sum_{k=0}^{2m} (j\omega)^k [\alpha'_k] \right] [G_{XX}(\omega_i)] = \left[\sum_{k=0}^{2n} (j\omega)^k [\beta'_k] \right] [I] \quad 3.21)$$

Note that the power spectrum UMPA model is twice the order of the FRF based UMPA model. Further, the coefficient matrices α' and β' , contains the same system parameter related information twice. This explains Eqs. (3.20-c) which shows that power spectrum data contains the positive and negative poles.

The presence of negative poles can also be explained by means of correlation functions, which are time domain equivalent of power spectrums. Figure 3.1 shows auto-correlation function of a typical structural response obtained when the structure is randomly excited. The correlation function is a symmetric function. Further, the positive lags give rise to the decaying exponential portion of the correlation function and the negative lags results in the growing exponential portion. There is essentially the same information in both the

decaying and growing exponential portions of the correlation function. This again explains the presence of the positive (stable) and negative (unstable) poles as indicated by Eq. (3.20-c) through the use of power spectrums. The positive and negative poles are obtained from the decaying exponential and growing exponential portion of the correlation function respectively.

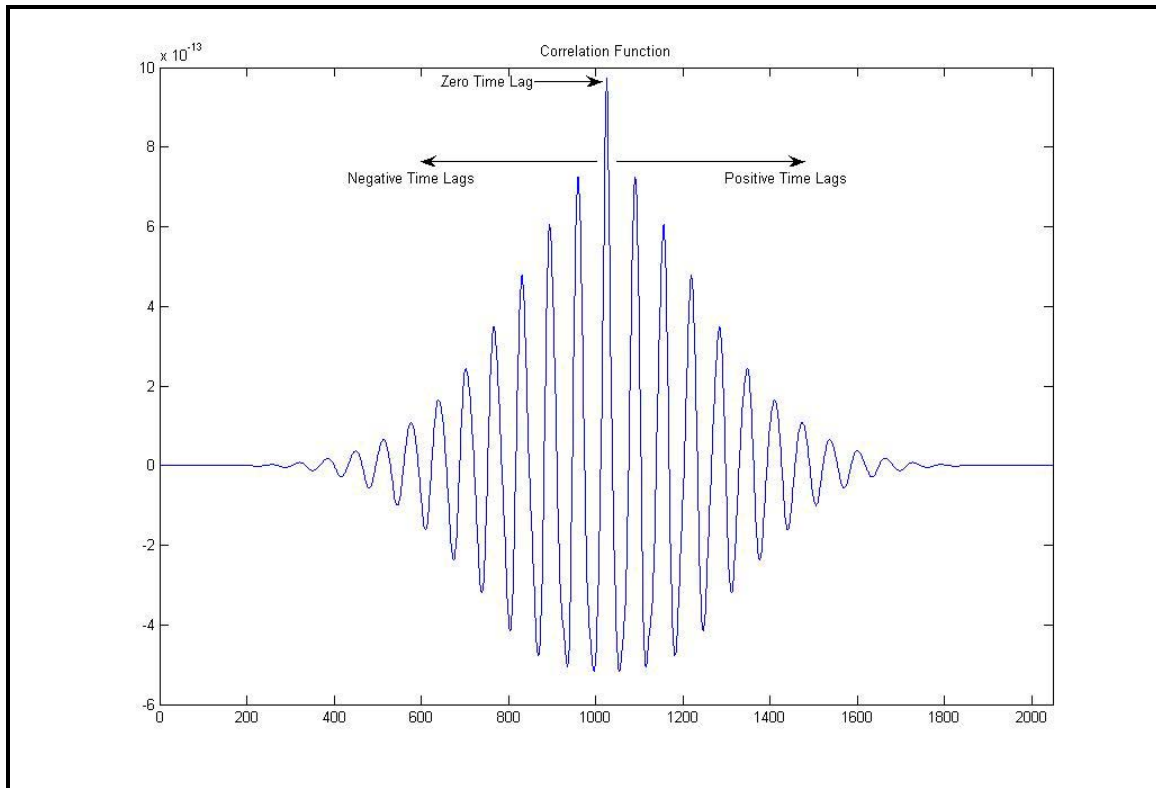


Figure 3.1 – Auto-correlation function of a typical output response

The high order of the power spectrum based model in comparison to FRF based model causes various disadvantages which makes it more difficult for the frequency domain based algorithms to give good results as they inherently suffer from numerical conditioning problems [Peeters, Van Der Auweraer et al., 2004; Phillips, Allemang, 2004, Chauhan, Martell, et al., 2006]. This problem is not as severe in the case of time domain algorithms. Most time domain OMA methods use information from the positive lag part of the correlation functions only and thus estimate only the stable poles. Thus in case of

time domain based methods the numerical problems resulting due to higher order of power spectrum matrix can be avoided.

Positive Power Spectrum (PPS)

This problem of dealing with the higher order model and presence of positive and negative poles forms the basis of the positive power spectrum which is defined in the frequency domain by the following equation.

$$G_{pq}^+(\omega) = \sum_{k=1}^N \frac{R_{pqk}}{j\omega - \lambda_k} + \frac{R_{pqk}^*}{j\omega - \lambda_k^*} \quad 3.22)$$

The positive power spectrum is calculated by first inverse Fourier transforming the power spectrum to obtain the circular correlation functions and then removing the negative lag portion of the correlation function. This is equivalent to multiplying the correlation function with the unit step function in the time domain. The resultant function is then Fourier transformed back to obtain the positive power spectrum. Figure 3.2 illustrates the process of obtaining the positive power spectrum from the output response data. The advantage of positive power spectrum is that it has the same order as the frequency response functions and also contains all the necessary system information (poles and vectors). Thus UMPA equations can now be applied to positive power spectrum data to perform operational modal analysis of the given system.

The UMPA equivalent equations of Eqs. (3.12) and (3.13) for the operational modal analysis can thus be written in terms of positive power spectrum G_{XX}^+ (in frequency domain) and Correlation function R_{XX} (in time domain) as

$$\left[\sum_{k=0}^m (j\omega)^k [\alpha_k] \right] [G_{XX}^+(\omega_i)] = \left[\sum_{k=0}^n (j\omega)^k [\beta_k] \right] [I] \quad 3.23)$$

$$\sum_{k=0}^m [\alpha_k] \{R_{XX}(t_{i+k})\} = 0 \quad 3.24)$$

Note that only positive lags of the correlation function are used for the above formulation. In the next section the various algorithms in terms of their UMPA formulation are described.

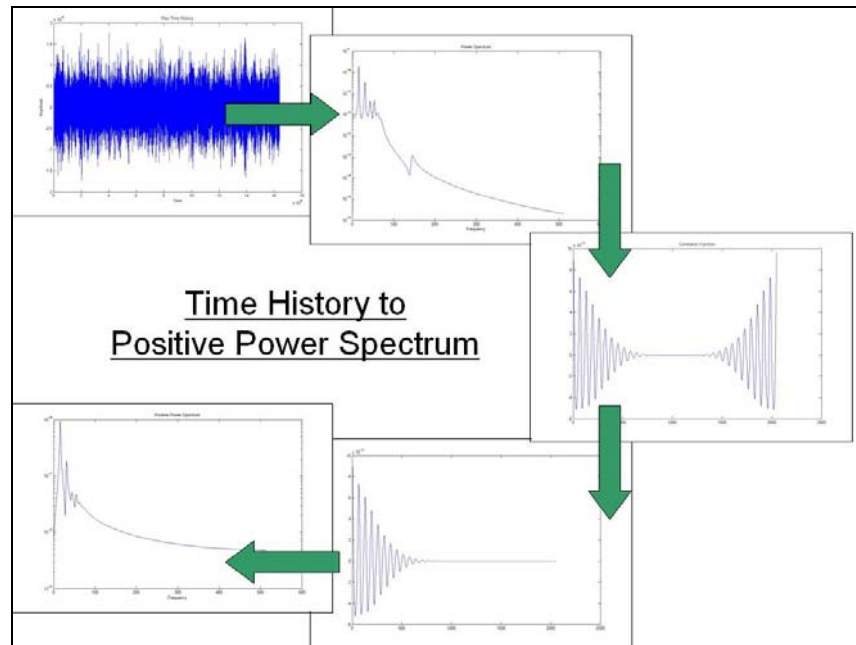


Figure 3.2 – Generation of positive power spectrum from output time responses

Hilbert Transform Technique

In [Agneni, Brincker, Coppotelli, 2004; Agneni, Coppotelli, 2006] a method based on Hilbert Transform technique is suggested to achieve an estimate of biased FRFs that serve the same purpose as PPS in terms of avoiding the numerical conditioning issues associated with power spectra while applying the frequency domain OMA algorithms.

The autopower spectrum $G_{XX}(\omega)$ for a response point p due to input excitation force at the point p can be written by modifying Eq. (1.4) as

$$G_{XX}(\omega) = G_{FF}(\omega) |H_{pp}(\omega)|^2 \quad 3.25)$$

where $G_{FF}(\omega)$ is input force spectra and $H_{pp}(\omega)$ is driving point FRF at point p . Thus the magnitude of $H_{pp}(\omega)$ can be obtained as

$$|H_{pp}(\omega)| = \frac{\sqrt{G_{XX}(\omega)}}{\sqrt{G_{FF}(\omega)}} \quad 3.26)$$

It should be noted that since the input force is considered random, the power spectrum will be constant, smooth in the frequency range of interest, which means that the $G_{FF}(\omega)$ term will only influence the estimation of $H_{pp}(\omega)$ by scaling it with an unknown term $\sqrt{G_{FF}(\omega)}$. $H_{pp}(\omega)$ is however a complex quantity and for its complete estimation, one needs to estimate the phase, which can be obtained by means of the Hilbert Transform. This is possible because of the fact that the output responses are causal in nature.

$$phase(H_{pp}(\omega)) = -H[\ln|H_{pp}(\omega)|] \quad 3.27)$$

or

$$phase(H_{pp}(\omega)) = -\frac{1}{2} H[\ln(G_{XX}(\omega))] \quad 3.28)$$

Thus the biased driving point FRF, $\hat{H}_{pp}(\omega)$, can be expressed in terms of the response power spectrum $G_{XX}(\omega)$ as

$$\hat{H}_{pp}(\omega) = \frac{1}{K} \sqrt{G_{XX}(\omega)} e^{-\frac{1}{2} jH[\ln(G_{XX}(\omega))]} \quad 3.29)$$

where $K = \sqrt{G_{FF}(\omega)}$. The other FRFs (biased estimate) can be obtained by means of the following relationship between non-driving point FRF $\hat{H}_{pq}(\omega)$, output response cross power spectrum $[G_{XX}(\omega)]_{pq}$ and the driving point biased FRF $\hat{H}_{pp}(\omega)$ as calculated earlier.

$$\hat{H}_{pq}(\omega) = \frac{G_{X_p X_q}(\omega)}{\sqrt{G_{F_q F_q}(\omega)} \hat{H}_{pp}^*(\omega)} \quad 3.30)$$

The UMPA equations can now be modeled on $\hat{H}(\omega)$ just like correlation and power spectrum based models of Eq. (3.23) and (3.24).

Recently a Cepstrum based signal processing approach was also suggested to obtain modal parameters from output responses [Hanson, Randall, et al., 2007]. This approach is developed for systems excited by at least one cyclostationary (A signal whose statistical properties vary cyclically with time) input with a unique cyclic frequency, which limits the performance of the approach in very low-frequency region.

3.3 UMPA Formulation of OMA Algorithms

Before discussing the various algorithms, it is important to note that in the case of Operational Modal Analysis only output responses are measured, thus the measured data does not have any typical reference location as is typical of traditional experimental modal analysis where reference locations are often the degrees of freedom where input force is provided. In other words there's no such thing as a driving point FRF in case of OMA. However, for the purpose of parameter estimation, certain response locations are chosen as reference locations. These locations are chosen keeping the same considerations as those while choosing the driving point FRFs, i.e. reference locations

should be the degrees of freedom which excite most modes (or in case of OMA the locations from where most modes can be observed, node points should be avoided, etc.). Unlike the EMA case, though, the reference locations for the OMA case do not mean that an independent excitation has been applied at these degrees of freedom. Therefore, the independent information associated with the reference in the EMA case does not extend to the OMA case. In the discussion that follows, N_{ref} refers to the response locations chosen as reference locations and N_o refers to the output response locations. Also the starting equation in case of time domain algorithms is Eq. (3.24) and in case of frequency domain algorithms is Eq. (3.23).

3.3.1 Time Domain Algorithms

Higher Order UMPA Model

Typically higher order UMPA algorithms utilize more temporal information in comparison to the spatial information. In case of OMA this essentially translates to the number of response locations being comparatively much higher than the number of reference responses, i.e. $N_o \gg N_{ref}$. The matrix coefficients in this case have the dimension $N_{ref} \times N_{ref}$. Further, if m is model order, the total number of system modes that will be estimated by the model is mN_{ref} which is much higher than the required $2N$ modes of the system. Since N_{ref} is a small number, typically 2 or 3, the order m has to be high; thus such algorithms are referred to as high order algorithms. The basic equation for this algorithm is given as

$$\begin{bmatrix} [\alpha_1] & [\alpha_2] & \dots & [\alpha_m] \end{bmatrix}_{N_{ref} \times mN_{ref}} \begin{bmatrix} [R_{xx}(t_{i+1})] \\ [R_{xx}(t_{i+2})] \\ \dots \\ [R_{xx}(t_{i+m})] \end{bmatrix}_{mN_{ref} \times N_o} = -[R_{xx}(t_{i+0})]_{N_{ref} \times N_o} \quad 3.31)$$

Note that the above equation utilizes zero order coefficient $[\alpha_0]$ normalization. Similar equations can be developed by normalizing other coefficients to come up with different set of solutions. This normalization is very important with respect to where the unwanted poles, associated with the noise in the data, are found [Allemang, 1999]. This aspect of the coefficient normalization affects all model solutions (high and low order, time and frequency domain). Every solution will comprise of mN_{ref} number of modes out of which $2N$ will be genuine system modes and rest will be computational modes. One of the ways to filter out these computational modes is to compare the solution obtained by normalizing various coefficients. The true modes of the system will be retained in each solution but computational modes will differ and can thus be filtered. Once the coefficient matrices are obtained, the roots of the matrix characteristic equation can be found as the eigenvalues of the associated companion matrix. As mentioned earlier, while working with correlation functions, care should be taken to utilize only the positive lag portion of the correlation function.

The popular Polyreference Time Domain (PTD) [Vold, Kundrat, et al., 1982; Vold, Rocklin, 1982] algorithm is a multi-input, multi-output version of a high order UMPA model based algorithm. Similarly, the Complex Exponential [Spitznogle, 1971] and Least Squares Complex Exponential algorithms [Brown Allemang, et al., 1979] are SISO and SIMO versions of this model.

Lower Order UMPA Model

Lower order algorithms use more spatial information in comparison to temporal information. The matrix coefficients α have a dimension $2N_o \times 2N_o$ (or $N_o \times N_o$) and model order m is 1 (or 2). Thus, the total number of modes obtained through the algorithm is $2N_o$ which is more than the required $2N$ number of system modes. Ibrahim

Time Domain (ITD) [Ibrahim, Mikulcik, 1977; Pappa, 1982], Eigensystem Realization Algorithm (ERA) [Juang, Pappa, 1985; Longman, Juang, 1989] and Multiple Reference Time Domain (MRITD) [Fukuzono, 1986] algorithms belong to this category of UMPA formulation. In the OMA domain, this lower order UMPA formulation is equivalent to the Stochastic Subspace Identification (SSI) algorithm [Hermans, Van der Auweraer, 1999; Peeters, 2000] that uses a state space model based on output response correlation functions. The process of obtaining the modes once the coefficient matrices have been found is same as explained in previous section. Eq. (3.32) shows the zero order coefficient $[\alpha_0]$ normalization with $m = 1$.

$$\begin{bmatrix} [\alpha_1] \end{bmatrix}_{2N_o \times 2N_{oi}} \begin{bmatrix} [R_{xx}(t_{i+1})] \\ [R_{xx}(t_{i+2})] \end{bmatrix}_{2N_o \times N_{ref}} = - \begin{bmatrix} [R_{xx}(t_{i+0})] \\ [R_{xx}(t_{i+1})] \end{bmatrix}_{2N_o \times N_{ref}} \quad 3.32)$$

3.3.2 Frequency Domain Algorithms

Higher Order UMPA Model

The frequency domain equivalent of higher order time domain algorithms can be formulated using the UMPA model in the following manner as the time domain algorithm.

This formulation utilizes the positive power spectrum data rather than power spectrum.

$$\begin{bmatrix} [\alpha_1] & [\alpha_2] & \dots & [\alpha_m] & [\beta_1] & [\beta_2] & \dots & [\beta_n] \end{bmatrix}_{N_{ref} \times mN_{ref} + (n+1)N_o} \begin{bmatrix} (js_i)^0 [G_{XX}^+(\omega_i)] \\ (js_i)^1 [G_{XX}^+(\omega_i)] \\ \dots \\ (js_i)^m [G_{XX}^+(\omega_i)] \\ -(js_i)^1 [I] \\ -(js_i)^2 [I] \\ \dots \\ -(js_i)^n [I] \end{bmatrix}_{mN_{ref} + (n+1)N_o \times N_o} = -(js_i)^0 [G_{XX}^+(\omega_i)]_{N_{ref} \times N_o} \quad 3.33)$$

Note that in Eq. (3.33) the zero order coefficient $[\alpha_0]$ is normalized and this equation can be repeated for other frequencies. This model is the UMPA equivalent of the Rational

Fraction Polynomial (RFP) ($s_i = j\omega_i$) [Richardson, Formenti, 1982] and polyreference least square complex frequency (PLSCF or PolyMAX) ($s_i = z_i = e^{j \times \omega_i \times \Delta t}$) [Guillaume, Verboven et al., 2003; Peeters, Van der Auweraer et al., 2004; Peeters, Van der Auweraer, 2005] algorithms. One of the disadvantages of high order frequency domain algorithms like RFP is that these algorithms involve power polynomials with increasing powers of the frequency. These matrices have Van der Monde form and suffer from poor numerical conditioning problems for wide frequency range and high orders. This obviously hinders the modal parameter estimation process. Along with limiting the frequency range and reducing the order of the model, normalizing the frequency range and using orthogonal polynomials are some of the methods to reduce this ill-conditioning problem [Phillips, Allemang, 2004]. The polyreference least square complex frequency (PolyMAX) algorithm proposed the use of complex z mapping and has been shown to have much superior numerical conditioning than other prevalent RFP methods. These aspects are discussed further in Chapter 4 while discussing the formulation of a low-order frequency domain OMA algorithm.

Lower Order UMPA Model

Lower order, frequency domain algorithms are basically UMPA based models that generate first or second order matrix coefficient polynomials. In Chapter 4 the UMPA-LOFD algorithm [23] is proposed for OMA which is a second order ($m=2$) UMPA model based algorithm. It is shown that the UMPA-LOFD algorithm has good numerical characteristics in comparison to high order frequency domain algorithm. The matrix coefficients in this case have $N_o \times N_o$ dimensions and thus the total number of modes found is $2N_o$. Similar to high order frequency domain algorithms this basic equation can be repeated for several frequencies and the matrix polynomial coefficients can be

obtained using either $[\alpha_2]$ or $[\alpha_j]$ normalization The normalized zero order coefficient $[\alpha_0]$ version of this algorithm is shown below

$$[[\alpha_1] \ [\alpha_2] \ [\beta_0] \ [\beta_1]]_{N_0 \times 4N_i} \begin{bmatrix} (js_i)^1 [G_{XX}^+(\omega_i)] \\ (js_i)^2 [G_{XX}^+(\omega_i)] \\ -(j\omega_i)^0 [I] \\ -(j\omega_i)^1 [I] \end{bmatrix}_{4N_0 \times N_i} = -(j\omega_i)^0 [G_{XX}^+(\omega_i)]_{N_0 \times N_i} \quad 3.34)$$

3.3.3 Spatial Domain Algorithms

Spatial domain algorithms like the Complex Mode Indicator Function (CMIF) [Shih, Tsuei et al., 1989; Phillips, Allemang, Fladung, 1998; Allemang, Brown, 2006] and its extension Enhanced Mode Indicator Function (EMIF) [Fladung, Philips, Brown, 1997; Phillips, Allemang, Fladung, 1998; Fladung, 2001] can be treated as a special case of the UMPA model where coefficient matrix has an order zero ($m = 0$). These algorithms rely only on spatial information and essentially neglect temporal information (spatial information is compared between different temporal solutions). These algorithms utilize the singular value decomposition of the frequency response function matrix at each frequency line to estimate the modal parameters of the system (See Chapter 2, section 2.1.2 for details). The Frequency Domain Decomposition (FDD) [Brincker, Zhang, Andersen, 2000] technique is an extension of CMIF technique in the operational modal analysis domain. This technique performs the singular value decomposition on the power spectrum matrix instead of frequency response function matrix. The FDD technique is followed by enhanced Frequency Domain Decomposition (eFDD) [Brincker, Ventura, Andersen, 2000; Gade, Moller et al., 2005] technique to estimate the damping and complete the parameter estimation procedure. In Chapter 5, an alternative to eFDD algorithm is proposed which extends the EMIF algorithm to operational modal analysis [Chauhan, Martel et al., 2006]. This algorithm differs from the eFDD approach in the

sense that the parameter estimation is carried out in the frequency domain unlike eFDD where the parameter estimation is done in the time domain.

3.4 Case Study: Lightly Damped Circular Plate

Having developed various OMA algorithms using the UMPA formulation, these algorithms are now applied to a simple lightly damped circular plate. A circular plate, due to its peculiar geometry, is a good experimental structure to test these algorithms as a lot of closely spaced modes are present. The plate is excited randomly all over its surface by means of an impact hammer. A total of 30 accelerometers are placed over the plate to measure the output response (Figure 3.3).

The modal parameters obtained using various OMA algorithms are shown in the Table 3.2. The modal parameters obtained using the various UMPA formulated OMA algorithms show very good agreement. The purpose of this case study is not to comment on the performance of the individual algorithms but the fact these algorithms can be developed very easily if the underlying unified concept is understood. UMPA methodology aid greatly in this regard and this underlines its utility and effectiveness.



Figure 3.3: Experimental set up for the lightly damped circular plate

Table 3.2: Modal parameters estimated using various UMPA formulated OMA algorithms

System modes using EMA		UMPA Higher Order Time Domain (PTD)		UMPA Lower Order Time Domain (ERA)		UMPA Higher Order Frequency Domain (RFP or PLSCE)		UMPA Lower Order Frequency Domain (PFD or LOFD)		UMPA Higher Order Frequency Domain with complex z mapping (RFP-z or PolyMAX)		UMPA Lower Order Frequency Domain with complex z mapping (PFD-z or LOFD z)		UMPA Zero Order Spatial Domain (CMIF-EMIF)	
Damp	Freq	Damp	Freq	Damp	Freq	Damp	Freq	Damp	Freq	Damp	Freq	Damp	Freq	Damp	Freq
0.258	56.591	0.611	56.439	0.611	56.436	0.663	56.462	0.612	56.478	0.762	56.504	0.578	56.542	0.671	56.461
0.285	57.194	0.632	57.191	0.619	57.197	0.669	57.214	0.621	57.253	0.717	57.24	0.66	57.252	0.669	57.211
0.312	96.577	0.636	96.571	0.631	96.561	0.638	96.663	0.636	96.665	0.637	96.662	0.626	96.653	0.647	96.664
0.412	132.101	0.351	131.702	0.338	131.705	0.353	131.847	0.342	131.83	0.349	131.84	0.369	131.842	0.359	131.86
0.147	132.65	0.304	132.589	0.31	132.601	0.312	132.743	0.285	132.76	0.302	132.723	0.337	132.735	0.313	132.75
0.243	219.582	0.302	219.094	0.301	219.092	0.299	219.373	0.3	219.375	0.303	219.365	0.292	219.368	0.319	219.37
0.216	220.952	0.371	221.075	0.37	221.088	0.367	221.35	0.364	221.358	0.366	221.344	0.359	221.342	0.393	221.36
0.214	231.172	0.252	230.545	0.26	230.553	0.257	230.855	0.256	230.851	0.257	230.856	0.265	230.843	0.279	230.86
0.137	232.077	0.212	232.102	0.22	232.095	0.227	232.391	0.225	232.394	0.221	232.4	0.218	232.421	0.244	232.39
0.089	352.997	0.152	351.214	0.144	351.18	0.151	351.69	0.147	351.677	0.151	351.715	0.138	351.716	0.161	351.69
0.174	355.509	0.224	355.303	0.222	355.283	0.22	355.78	0.219	355.773	0.219	355.801	0.207	355.801	0.232	355.78
0.18	374.554	0.273	373.424	0.271	373.382	0.27	373.941	0.268	373.933	0.271	373.936	0.269	373.882	0.278	373.92
0.176	377.569	0.239	376.99	0.242	377.013	0.236	377.508	0.236	377.505	0.236	377.506	0.235	377.499	0.243	377.5
0.313	412.414	0.245	411.168	0.238	411.138	0.241	411.729	0.241	411.727	0.242	411.731	0.244	411.734	0.252	411.73
0.209	486.801	0.22	484.72	0.22	484.627	0.221	485.408	0.219	485.405	0.219	485.397	0.225	485.425	0.224	485.38

3.5 Conclusions

In this Chapter, the concept of Unified Matrix Polynomial Approach (UMPA) is extended to Operational Modal Analysis. It is shown how various time, frequency and spatial domain OMA algorithms can be formulated using the UMPA model. Emphasis is placed on understanding the basic difference between traditional Experimental Modal Analysis and output-only Operational Modal Analysis, the various assumptions made in the case of OMA and how the fundamental data (correlation functions and power spectrums) should be used in order to utilize the UMPA model for the purpose of parameter estimation in the case of OMA. It is revealed that understanding the underlying basic polynomial model not only helps in theoretical development of various algorithms but also provides a common framework which makes it much easier and simpler to understand these algorithms. It is important to reiterate that assumptions concerning the

nature of the assumed excitation (smooth and broadband in frequency, spatially well distributed, etc.) are critical to the success of OMA methods.

Chapter Four

UMPA-LOFD: A Low Order Frequency Domain Algorithm for OMA

Most of the algorithms for Operational Modal Analysis work in the time domain and there are very few frequency domain based algorithms. Only FDD and eFDD can be classified as frequency domain algorithms though they too are essentially spatial domain algorithms. One of the reasons for the lack of frequency domain algorithms in OMA framework can be attributed to poor numerical conditioning problems associated with them. Traditional higher order algorithms like Rational Fraction Polynomial (RFP) [Richardson, Formenti, 1982] have been known to suffer from this problem of poor numerical characteristics. Limiting the frequency range, reducing the order of the model, normalizing the frequency range and using orthogonal polynomials are some of the methods used in the past to reduce this ill-conditioning problem in traditional experimental modal analysis set up. However estimating modal parameters in the frequency domain using output-only response data still remains a challenge as the numerical conditioning problem is much more severe in the case of OMA since the order of the power spectrum based model used in OMA is twice that of the frequency response function based model used in EMA. Recently, a new method called Polyreference Least Squares Complex Frequency (PolyMAX) [Guillaume, Verboven et al., 2003; Peeters, Van der Auweraer et al., 2004] was proposed that builds upon the classical least squares complex frequency domain estimator by using a complex Z

mapping (or trigonometric orthogonalization) to improve numerical conditioning. Along with implementing this method in traditional FRF based experimental modal analysis framework, it was also extended to operational modal analysis [Peeters, Van der Auweraer, 2005].

In this chapter the Unified Matrix Polynomial Approach (UMPA) [Allemang, Brown, 1998; Allemang, Phillips, 2004], as discussed in previous chapter, is utilized for developing a low order frequency domain algorithm (UMPA-LOFD) suited for the output response based OMA framework. The algorithm is applied to an analytical 15 degree of freedom system and also a lightly damped circular plate. It is shown to have better numerical characteristics than high order frequency domain algorithms and the results are comparable to time domain based OMA algorithms. Additionally, complex Z mapping is used with a low order frequency domain algorithm for the purpose of operational modal analysis and its performance is evaluated and compared with the low order frequency domain algorithm (UMPA-LOFD) which does not use the complex Z mapping. The complex Z mapping was first used in the polyreference least squares complex frequency (PolyMAX) algorithm and demonstrated another method that gives better numerical characteristics with high order frequency domain based methods. The concept is applied successfully not only to other traditional, frequency domain experimental modal analysis methods but also in the field of operational modal analysis. Thus it is worth exploring if complex Z mapping improves the low order algorithm in the same manner as the high order frequency domain algorithm.

4.1 UMPA-LOFD

The UMPA equivalent equations for the operational modal analysis were shown in Chapter 3, Eq. (3.23) and (3.24). These equations are in terms of positive power spectrum G_{XX}^+ (in frequency domain) and correlation function R_{XX} (in time domain).

$$\left[\sum_{k=0}^m (j\omega)^k [\alpha_k] \right] [G_{XX}^+(\omega_i)] = \left[\sum_{k=0}^n (j\omega)^k [\beta_k] \right] [I] \quad 4.1)$$

$$\sum_{k=0}^m [\alpha_k] \{R_{XX}(t_{i+k})\} = 0 \quad 4.2)$$

Lower order, frequency domain algorithms are basically UMPA based models that generate first or second order matrix coefficient polynomials. To estimate a large number of system poles using a low order algorithm, the long dimension of the PPS matrix (positive power spectra are the primary data on which the algorithm operate) $N_o \times N_i$, must be at least as large as the number of positive modal frequencies desired. The UMPA-LOFD algorithm can be developed by substituting model order $m=2$ in the multiple input, multiple output PPS model of Eq. (4.1).

$$\left[[\alpha_2](j\omega_i)^2 + [\alpha_1](j\omega_i) + [\alpha_0] \right] [G_{XX}^+(\omega_i)] = [\beta_1](j\omega_i) + [\beta_0] \quad 4.3)$$

This basic equation can be repeated for several frequencies and the matrix polynomial coefficients can be obtained using either $[\alpha_2]$ or $[\alpha_0]$ normalization.

[α_2] Normalization

$$\begin{bmatrix} [\alpha_0] & [\alpha_1] & [\beta_0] & [\beta_1] \end{bmatrix}_{N_0 \times 4N_i} \begin{bmatrix} (j\omega_i)^0 [G_{XX}^+(\omega_i)] \\ (j\omega_i)^1 [G_{XX}^+(\omega_i)] \\ -(j\omega_i)^0 [I] \\ -(j\omega_i)^1 [I] \end{bmatrix}_{4N_0 \times N_i} = -(j\omega_i)^2 [G_{XX}^+(\omega_i)]_{N_0 \times N_i} \quad 4.4)$$

[α_0] Normalization

$$\begin{bmatrix} [\alpha_1] & [\alpha_2] & [\beta_0] & [\beta_1] \end{bmatrix}_{N_0 \times 4N_i} \begin{bmatrix} (j\omega_i)^1 [G_{XX}^+(\omega_i)] \\ (j\omega_i)^2 [G_{XX}^+(\omega_i)] \\ -(j\omega_i)^0 [I] \\ -(j\omega_i)^1 [I] \end{bmatrix}_{4N_0 \times N_i} = -(j\omega_i)^0 [G_{XX}^+(\omega_i)]_{N_0 \times N_i} \quad 4.5)$$

Once the matrix polynomial coefficients are obtained, a companion matrix can be formed (as shown in Chapter 3) and eigenvalue decomposition can be applied to estimate the modal parameters i.e. modal frequencies and modal vectors.

4.2 Numerical Conditioning Issues and Generalized Frequency

As discussed previously, frequency domain modal parameter estimation algorithms suffer from poor numerical conditioning characteristics. The data matrix used for estimating the matrix coefficients in the case of frequency domain algorithms are of the Van der Monde form (Eq. (4.6)) and involve power polynomials which are functions of increasing powers of frequency. This data matrix has a high condition number and is ill-conditioned especially for wide frequency range and high orders if the polynomial. The **Condition Number** is measure of the sensitivity of the solution of linear equations to errors, or noise in the data. Condition Number is essentially the ratio of the largest singular value to the smallest singular value of the data matrix. For good numerical conditioning the Condition Number should be close to unity.

$$\begin{bmatrix} (s_1)^0 & (s_1)^1 & (s_1)^2 & \dots & (s_1)^{2N-1} \\ (s_2)^0 & (s_2)^1 & (s_2)^2 & \dots & (s_2)^{2N-1} \\ (s_3)^0 & (s_3)^1 & (s_3)^2 & \dots & (s_3)^{2N-1} \\ \dots & \dots & \dots & \dots & \dots \\ (s_i)^0 & (s_i)^1 & (s_i)^2 & \dots & (s_i)^{2N-1} \end{bmatrix} \quad 4.6)$$

Following are some of the ways to overcome the numerical issues with frequency domain algorithms [Allemang, Phillips, 2004]:

- **Minimizing the frequency range of the data**

This means that while estimating the modal parameters, the algorithm fits the data only within a limited frequency range.

- **Minimizing the order of the model**

This is essentially what lower order algorithms do. By restricting to a low order the power to which the polynomial is raised is not high and thus the numerical issues can be avoided.

- **Normalizing the frequency range of the data**

- **Use of orthogonal polynomials**

- **Complex Z mapping**

Normalization, use of orthogonal polynomials and complex Z mapping methods map the data to a new generalized frequency without alteration in order to reducing the numerical conditioning issues. This concept where the data in the frequency range is mapped to a different frequency mapping is called **Generalized Frequency**.

1. Normalized Frequency

In this method the frequency range is mapped between (-1, 1) in the following manner

$$s_i = j^* (\omega_i / \omega_{\max}) \quad 4.7)$$

This mapping results in comparatively better numerical conditioning in comparison to the original mapping where frequency range was between $(-\omega_{\max}, \omega_{\max})$. After estimation of modal parameters, the correct modal frequencies can be obtained by multiplying them with ω_{\max} .

2. Orthogonal Polynomials

The numerical issues associated with frequency domain algorithms can be also be reduced by converting the power polynomial series into an equivalent orthogonal polynomial series by using the relationship in Eq. (4.8). Some of the commonly used orthogonal polynomials are the Forsythe Polynomials [Richardson, Formenti, 1982] and the Chebychev Polynomials [Vold, 1986; Shih, 1989]. The orthogonal polynomial series can be obtained in following manner.

$$\sum_{k=0}^m (s_i)^k \alpha_k = \sum_{k=0}^n P_k(s_i) \gamma_k \quad 4.8)$$

$$P_0(s_i) = 1.0 \quad 4.9)$$

$$P_j(s_i^*) = P_j^*(s_i) \quad 4.10)$$

$$P_{n+1}(s_i) = a_n s_i P_n(s_i) - \sum_{k=0}^n b_{n,k} P_k(s_i) \quad 4.11)$$

Difference between the various orthogonal polynomials is due to the different weighting coefficients used to generate them and also the range over which they are orthogonal. The Forsythe polynomials are orthogonal over $(-2, 2)$ where as

Chebyshev polynomials are orthogonal over (-1, 1). In the orthogonal polynomial approach, the original unknown matrix coefficients α_k are replaced by γ_k and these are then utilized to find the roots of the equation by forming a companion matrix as explained in the previous chapter. It should be noted that in this case the solution of the modal parameters is found using the following equation.

$$[[C]+[W_b]] \{X\} = \lambda [W_a] \{X\} \quad 4.12)$$

$[W_a]$ and $[W_b]$ are the weighting matrices which differ depending on the orthogonal polynomial used.

3. Complex Z Mapping

The major motivation behind the development of the polyreference least squares complex frequency (PolyMAX) algorithm was to overcome the numerical problems inherent with the high order, RFP frequency domain algorithms [Phillips, Allemang, 2004; Allemang, Phillips, 2004]. The polyreference least squares complex frequency (PolyMAX) algorithm is essentially RFP algorithm with complex Z mapping and will subsequently be referred to in a generic sense as the RFP-Z algorithm. The RFP-Z algorithm replaces the mathematically cumbersome orthogonal polynomial method by a trigonometric mapping function (complex Z mapping) [Peeters, Van der Auweraer et al., 2004; Allemang, Phillips, 2004].

The generalized frequency in case of UMPA-LOFD algorithm is just the normalized power polynomial given by Eq. (4.7)

$$s_i = j * (\omega_i / \omega_{max})$$

Thus the generalized frequency variable is bounded by (-1, 1). The complex Z mapping on the other hand is given by

$$s_i = z_i = e^{j \times \pi \times (\omega_i / \omega_{\max})} = e^{j \times \omega \times \Delta t} \quad 4.13)$$

$$s_i^m = z_i^m = e^{j \times \pi \times m \times (\omega_i / \omega_{\max})} \quad 4.14)$$

Using this mapping the positive and negative frequency ranges are mapped to the positive and negative unit circles in the complex plane respectively. This yields a real part of mapping functions which are cosine terms and an imaginary part which are sine terms. Since sine and cosine functions are mathematically orthogonal, the numerical conditioning of this mapping function is quite good.

4.3 Case Studies: UMPA-LOFD Performance

4.3.1 Analytical 15 Degrees of Freedom System

An analytical 15 degree of freedom system as shown in Figure 4.1 is considered. To simulate a near perfect operational modal analysis situation, the system is excited by a white random uncorrelated input at all 15 degrees of freedom. Power spectrums are calculated using the correlogram method [Stoica, Moses, 1997; Oppenheim, Schaffer, 1989; Kay, 1988]. As explained before, the power spectrums are converted back to time domain to obtain the correlation functions. The positive lags portion of the correlations is retained while zeroing the negative lags portion and then it is Fourier transformed back to frequency domain to obtain the positive power spectrums.

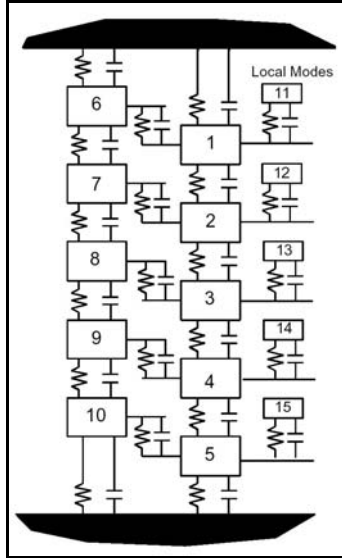


Figure 4.1: Analytical 15 Degree of Freedom System

Figure 4.2 shows the auto power spectrum and positive power spectrum for the degree of freedom number 1 or driving point 1 ($G_{xx_{11}}$ and $G_{xx_{11}}^+$). A complex mode indicator function (CMIF) plot based on power spectrums as shown in Figure 4.3 indicates clearly the presence of all 15 modes including a repeated mode around 53.3 Hz. It is noted that a similar plot based on positive power spectrum does not yield satisfactory results and thus positive power spectra cannot be used for the indication of modes using CMIF method (Figure 4.4). Further it has been observed that in the case of insufficient spatial excitation, the resulting CMIF does not give proper indication of the number of modes in the system. In such cases, spatial domain algorithms like FDD and eFDD which are similar to CMIF are difficult to use [Chauhan, Martell et al, 2006 (a); Chauhan, Martell et al, 2006 (c)]. This is further explained in Chapter 5.

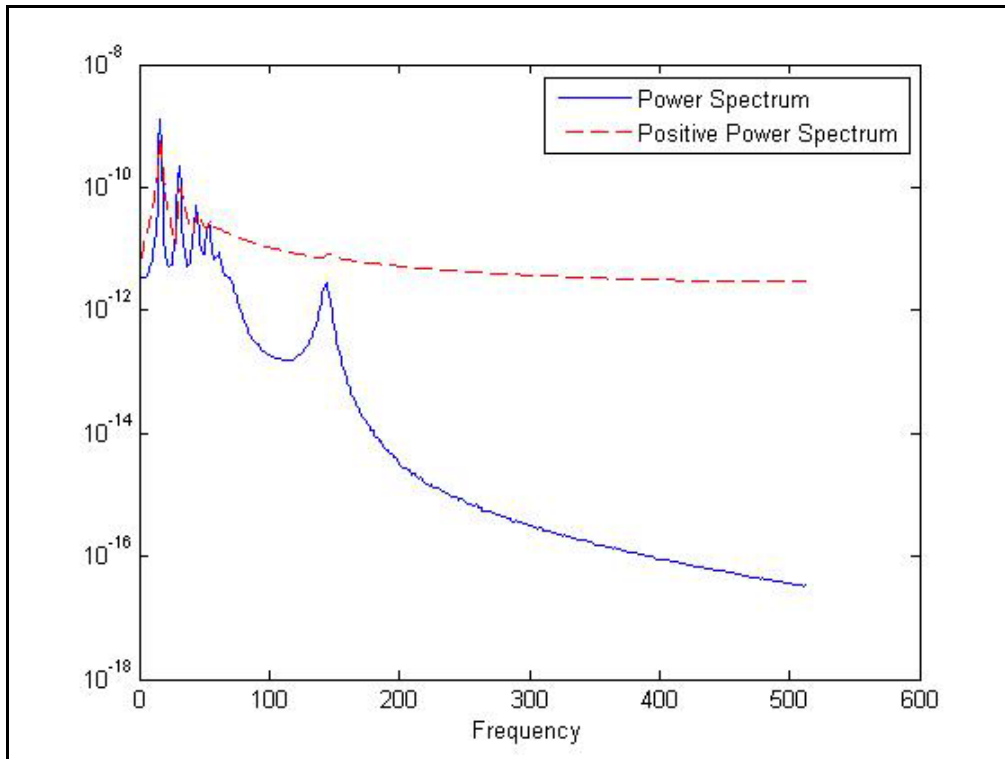


Figure 4.2 – Auto power spectrum and positive power spectrum for the first degree of freedom (15 DOF analytical system)

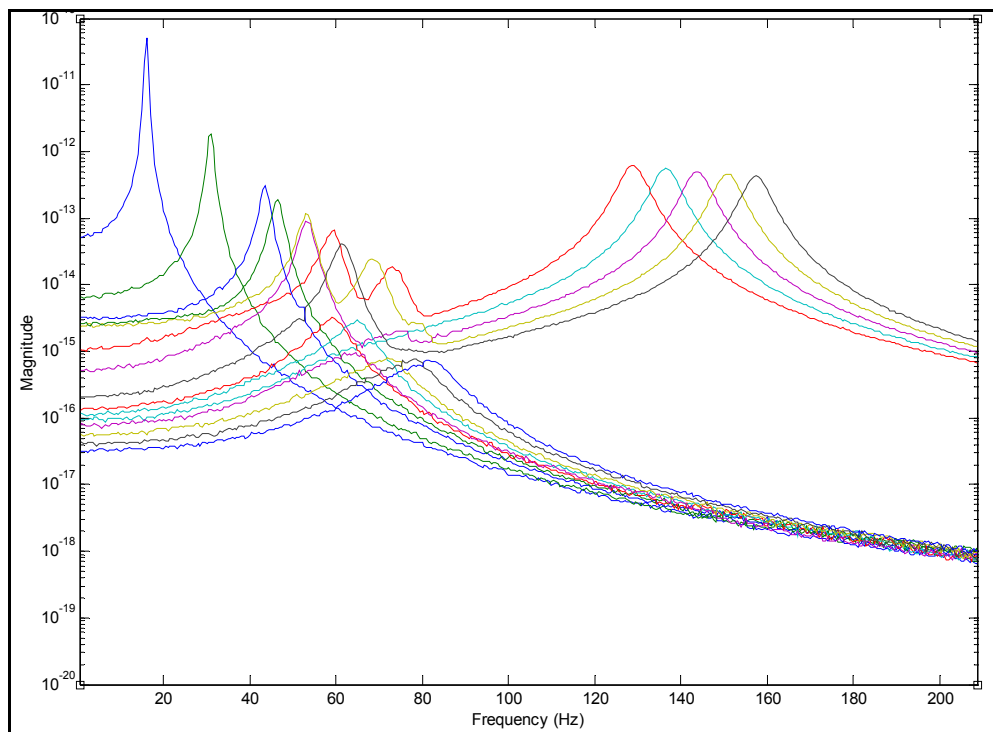


Figure 4.3: Complex Mode Indicator Function (CMIF) based on power spectrum (15 DOF analytical system)

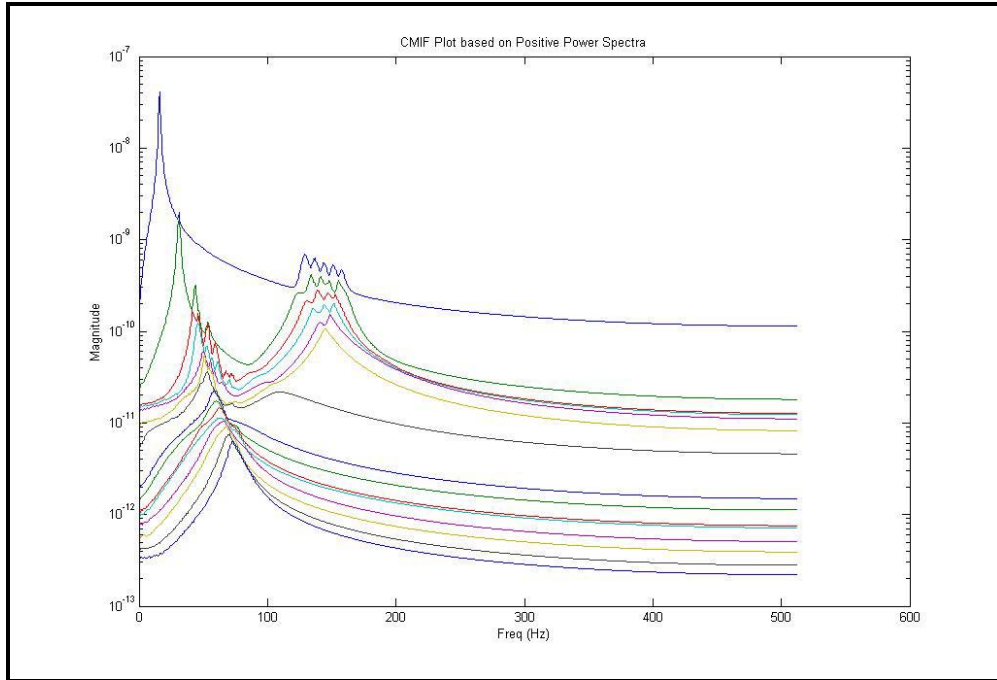


Figure 4.4: Complex Mode Indicator Function (CMIF) based on positive power spectrum (15 DOF analytical system)

Table 4.1 illustrates the modal parameters obtained using the low order frequency domain algorithm. The results obtained are compared to the true modes of the system and also with the results obtained using other time domain algorithms like ERA, PTD. Note that though these algorithms are referred by the name through which they are known popularly in the conventional frequency response function based experimental modal analysis framework, in this study they are essentially operational modal analysis algorithms i.e. working on output-only data. As noted in the previous section, most OMA time domain algorithms estimate modal parameters based on positive lags of the correlation functions and thus it does not make much difference whether positive power spectrums or simply the power spectrums are used for parameter estimation purposes. The results obtained using UMPA-LOFD algorithm compare very well with those obtained by more established time domain methods. The comparison with true modes of the system is also good though damping values are in error. However this behavior is

also shown by time domain methods. Since the damping values are expressed in percent critical, the variation is not very significant for this case.

The consistency diagrams obtained for the ERA and PTD algorithms and the consistency diagrams for the UMPA-LOFD and RFP algorithm are shown in Figures 4.5-4.8. Note that in case of RFP and UMPA-LOFD, positive power spectrums are used. Except for RFP, the consistency diagrams obtained using other algorithms are very clear and show good stability of the modes. Note that the diamonds (\diamond) in the consistency diagram represent stable pole and vector. Thus UMPA-LOFD not only gives comparable results to time domain methods, it provides a frequency domain alternative to modal parameter estimation using output-only data. The poor quality of consistency diagram in case of RFP is due to the numerical conditioning problems and renders the RFP method useless for modal parameter estimation purposes. The advantage of processing the positive power spectrums instead of power spectrums can also be seen in the consistency diagrams. Figure 4.9 shows consistency diagram for UMPA-LOFD based on processing regular power spectrums. It is very evident that using positive power spectrums considerably improves the consistency diagram and aids in stabilizing system modes.

Table 4.1: UMPA-LOFD modal parameter comparison for 15 DOF analytical system

True Modes		UMPA-LOFD (Low Order, Freq Domain)		UMPA-ERA (Low Order, Time Domain)		UMPA-PTD (High Order, Time Domain)	
Damp	Freq	Damp	Freq	Damp	Freq	Damp	Freq
1.0042	15.985	2.338	15.963	2.286	15.904	2.261	15.917
1.9372	30.858	2.517	30.863	2.478	30.691	2.445	30.731
2.7347	43.6	3.043	43.680	3.059	43.435	3.022	43.451
2.9122	46.444	3.431	46.437	3.394	46.179	3.399	46.178
3.3375	53.317	3.932	53.209	3.634	53.015	3.682	52.992
3.3454	53.391	3.296	53.306	3.385	53.148	3.390	53.102
3.7145	59.413	4.430	59.116	4.075	59.058	3.998	59.087
3.858	61.624	4.180	61.133	4.373	61.055	4.469	60.923
4.2978	68.811	4.291	69.237	4.397	68.633	4.800	68.462
4.5925	73.63	4.812	73.253	4.963	73.264	4.753	73.576
2.6093	128.84	2.712	128.848	2.672	128.909	2.432	128.587
2.4548	136.55	2.563	136.547	2.419	136.637	2.531	136.254
2.3288	143.86	2.426	143.869	2.360	143.973	2.591	143.325
2.221	150.83	2.314	150.799	2.390	150.606	2.486	150.576
2.122	157.47	2.216	157.444	2.155	157.510	2.573	157.123

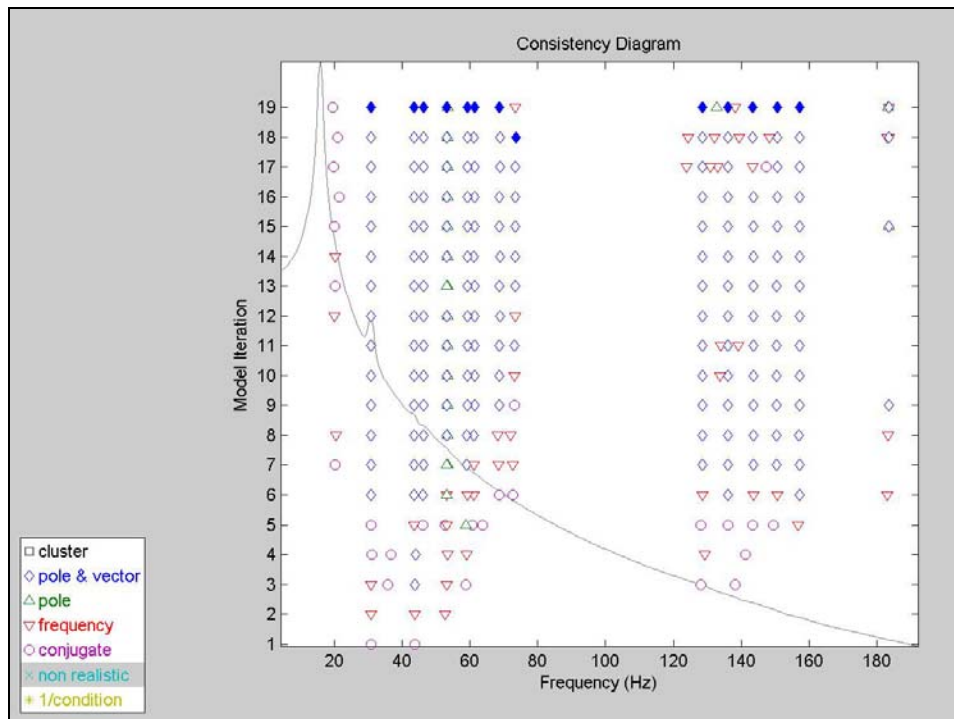


Figure 4.5: Consistency diagram for Polyreference Time Domain (PTD) algorithm (15 DOF analytical system)

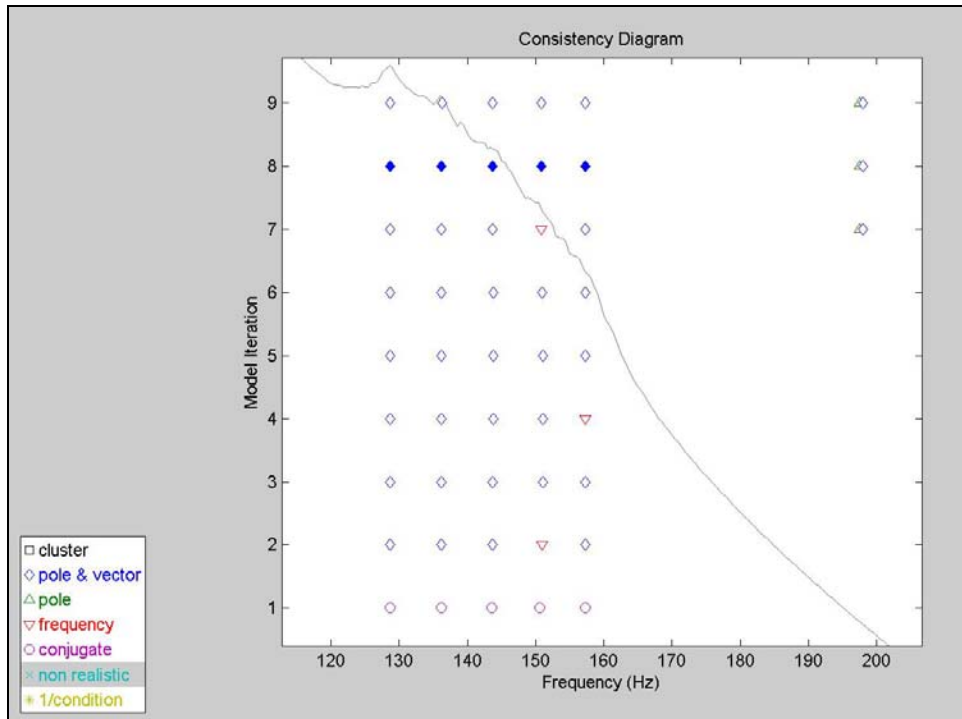


Figure 4.6: Consistency diagram for Eigensystem Realization Algorithm (ERA) (15 DOF analytical system)

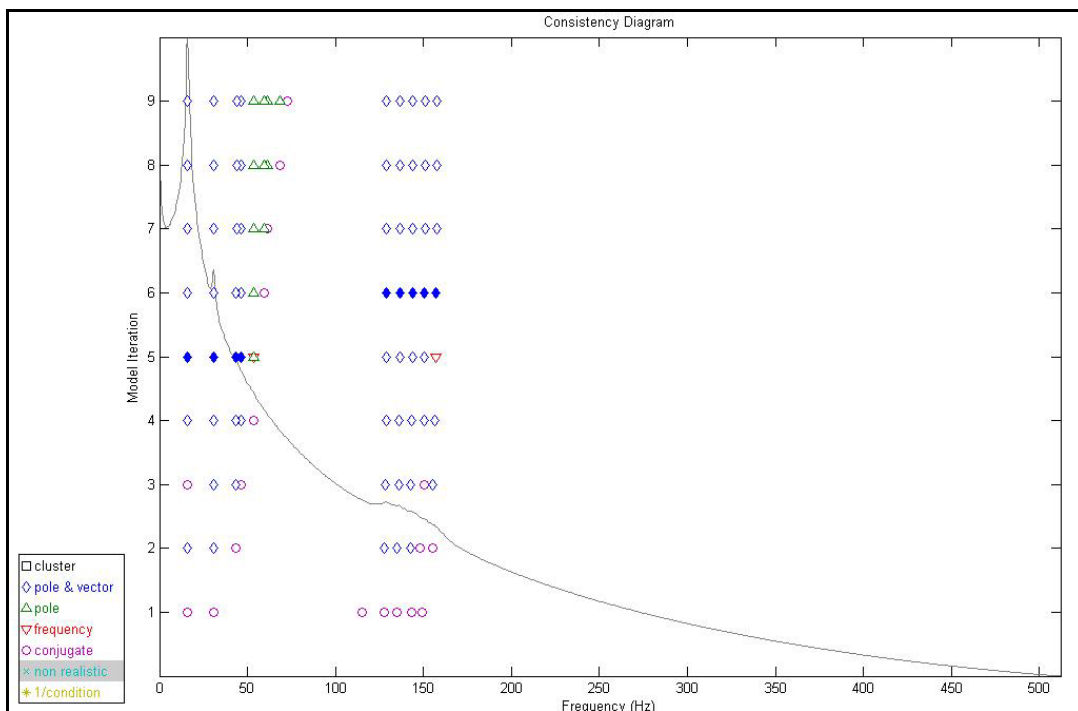


Figure 4.7: Consistency diagram for Low Order Frequency Domain (UMPA-LOFD) algorithm (15 DOF analytical system)

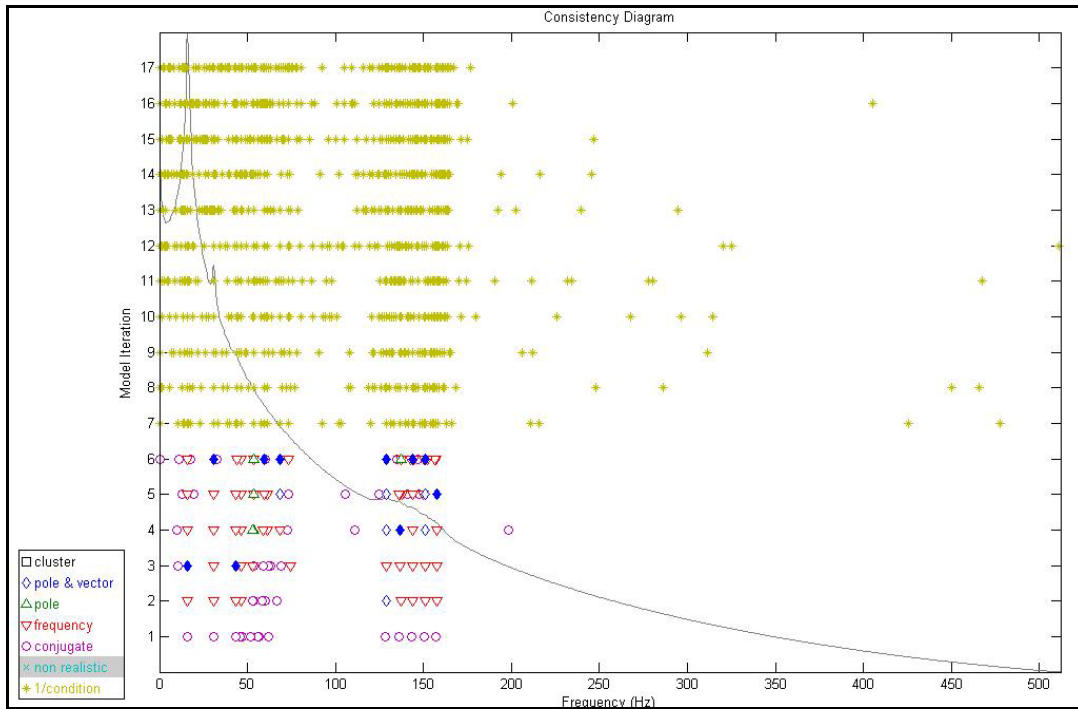


Figure 4.8: Consistency diagram for Rational Fraction Polynomial (RFP) algorithm (15 DOF analytical system)

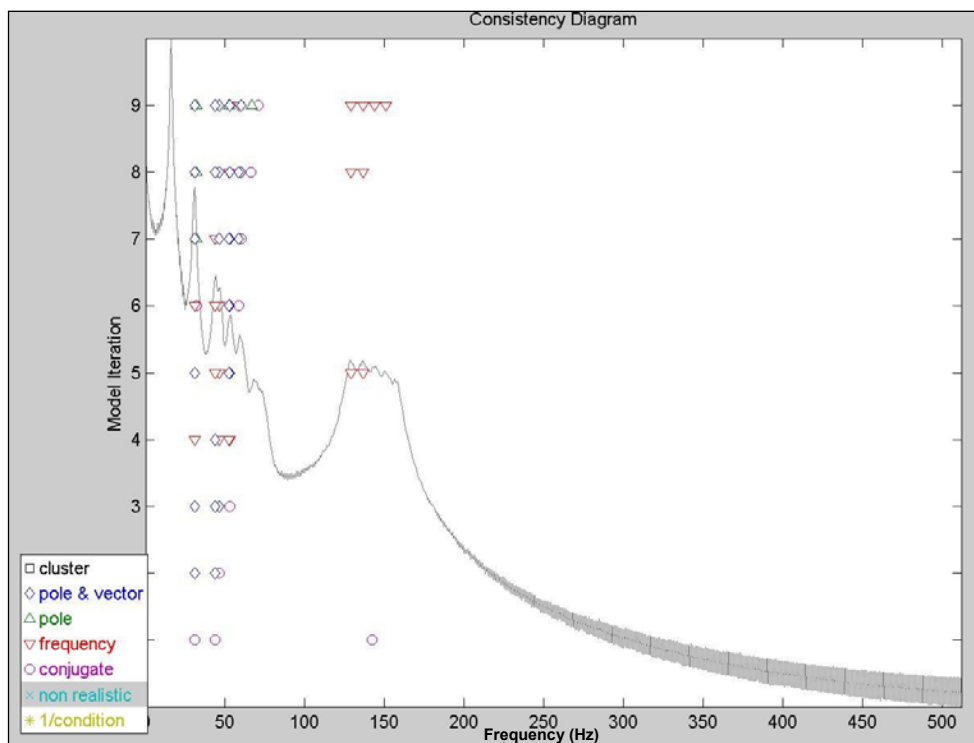


Figure 4.9: Consistency diagram for Low Order Frequency Domain (UMPA-LOFD) algorithm based on complete power spectrum (Analytical system)

4.3.2 Lightly Damped Circular Plate

Experimental studies are conducted on a lightly damped circular plate made of aluminum. The experimental set up is shown in Figure 4.10. The plate is randomly excited all across its surface using an impact hammer. Accelerometers are placed at 30 locations for measuring the output response. For comparing the results obtained using operational modal analysis to those using experimental modal analysis, a separate experiment is conducted where the plate is excited at two locations using an ergodic, stationary, broad-band pure random signal. To measure the input excitation force, two force transducers are also placed at the excitation points. In this configuration the plate is excited only at two locations, thus the plate is not excited uniformly over its surface. In other words, this is the case of insufficient excitation which is a typical (perfectly acceptable) frequency response function based modal analysis test configuration but a non-ideal operational modal analysis configuration.



Figure 4.10: Experimental set up for the lightly damped circular plate

Figure 4.11 shows the CMIF plots based on power spectra when the plate is excited completely over its surface thus abiding completely with the assumptions of OMA.

Table 4.2 lists the modal parameters estimated using various algorithms including the UMPA-LOFD algorithm. There's a good agreement among the results from various algorithms. Figures 4.12-4.15 show the consistency diagrams for the different algorithms. As expected, the consistency diagram for UMPA-LOFD algorithm is very clear and is also comparable to consistency diagrams of the time domain algorithms.

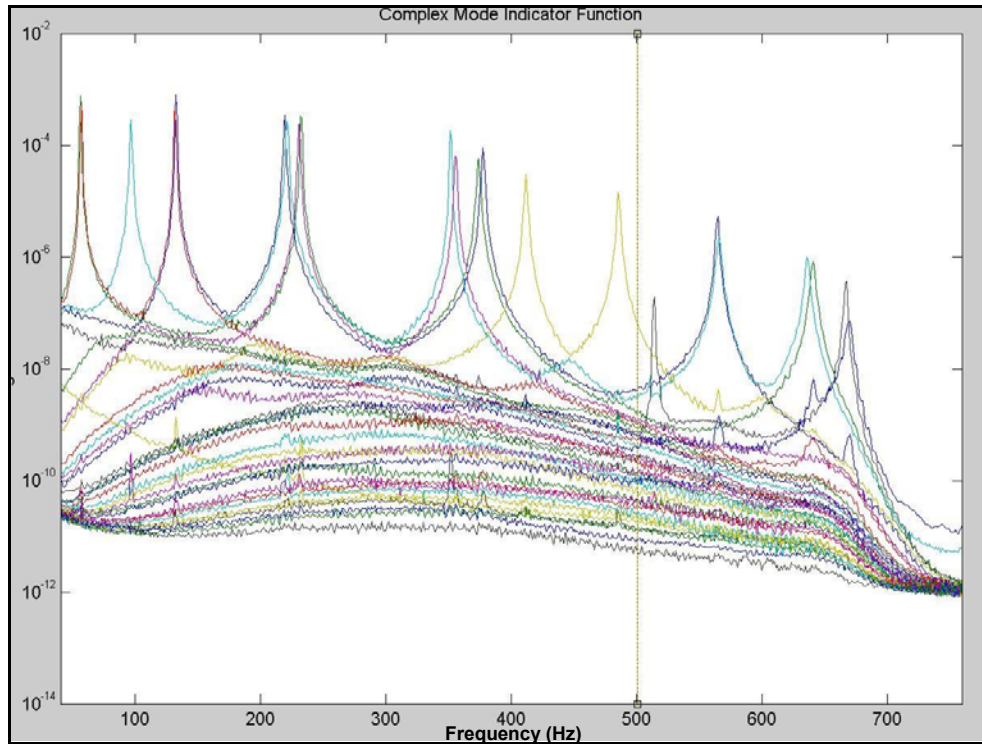


Figure 4.11: CMIF plot based on complete power spectrums obtained when plate is excited sufficiently over its surface

Table 4.2: UMPA-LOFD modal parameter comparison for lightly damped circular plate

System Modes Using EMA		UMPA-LOFD (Low Order, Freq Domain)		UMPA-ERA (Low Order, Time Domain)		UMPA-PTD (High Order, Time Domain)	
Damp	Freq	Damp	Freq	Damp	Freq	Damp	Freq
0.258	56.591	0.612	56.478	0.611	56.436	0.611	56.439
0.285	57.194	0.621	57.253	0.619	57.197	0.632	57.191
0.312	96.577	0.636	96.665	0.631	96.561	0.636	96.571
0.412	132.101	0.342	131.830	0.338	131.705	0.351	131.702
0.147	132.650	0.285	132.760	0.310	132.601	0.304	132.589
0.243	219.582	0.300	219.375	0.301	219.092	0.302	219.094
0.216	220.952	0.364	221.358	0.370	221.088	0.371	221.075
0.214	231.172	0.256	230.851	0.260	230.553	0.252	230.545
0.137	232.077	0.225	232.394	0.220	232.095	0.212	232.102
0.089	352.997	0.147	351.677	0.144	351.180	0.152	351.214
0.174	355.509	0.219	355.773	0.222	355.283	0.224	355.303
0.180	374.554	0.268	373.933	0.271	373.382	0.273	373.424
0.176	377.569	0.236	377.505	0.242	377.013	0.239	376.990
0.313	412.414	0.241	411.727	0.238	411.138	0.245	411.168
0.209	486.801	0.219	485.405	0.220	484.627	0.220	484.720

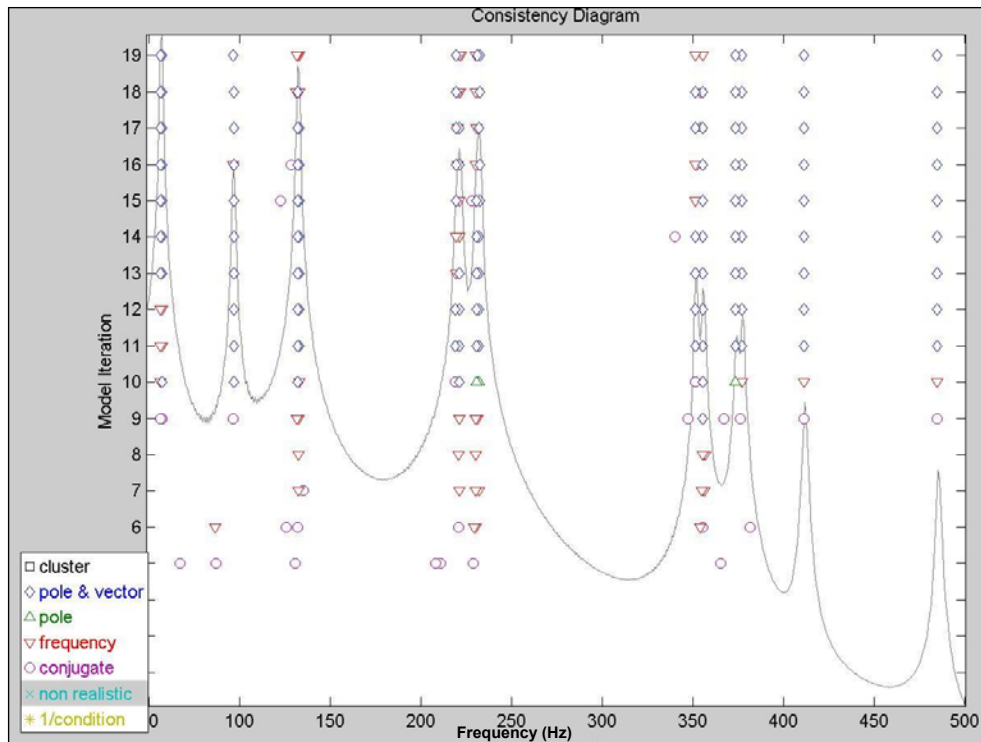


Figure 4.12: Consistency diagram for Polyreference Time Domain (PTD) algorithm (Circular plate)

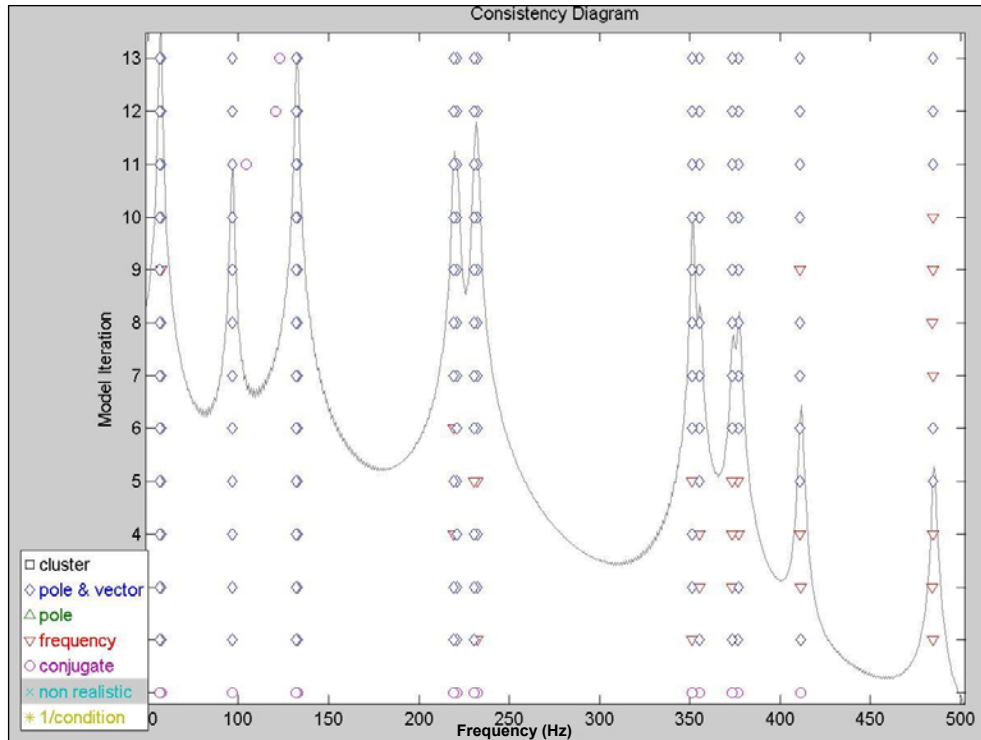


Figure 4.13: Consistency diagram for Eigensystem Realization Algorithm (ERA) algorithm (Circular plate)

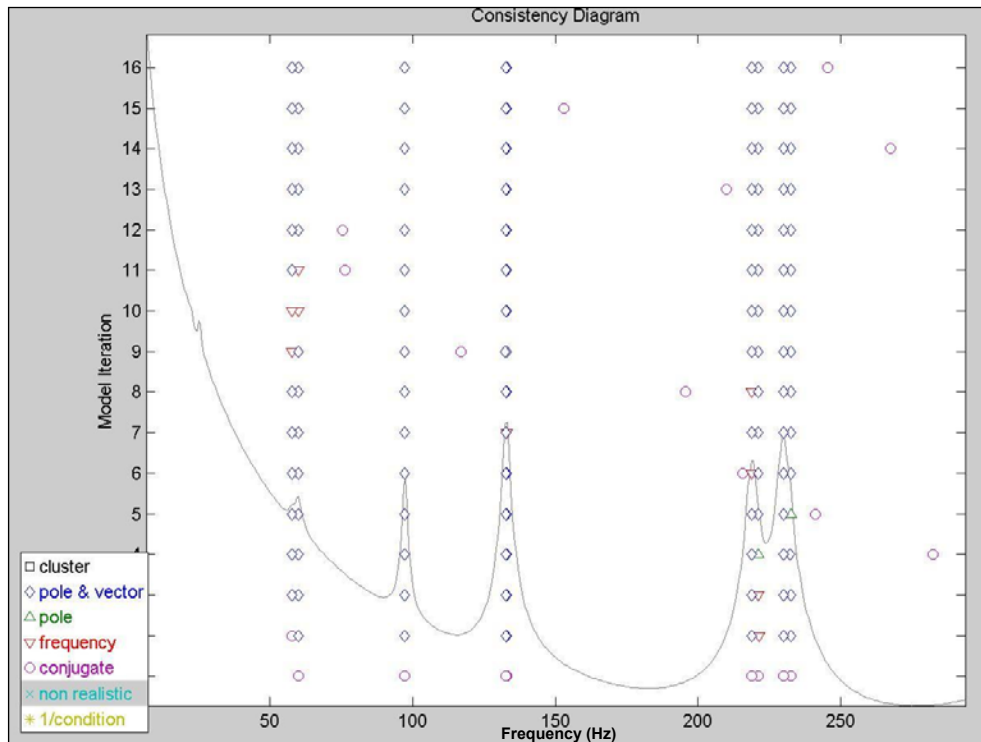


Figure 4.14: Consistency diagram for Lower Order Frequency Domain (UMPA-LOFD) algorithm (Circular plate)

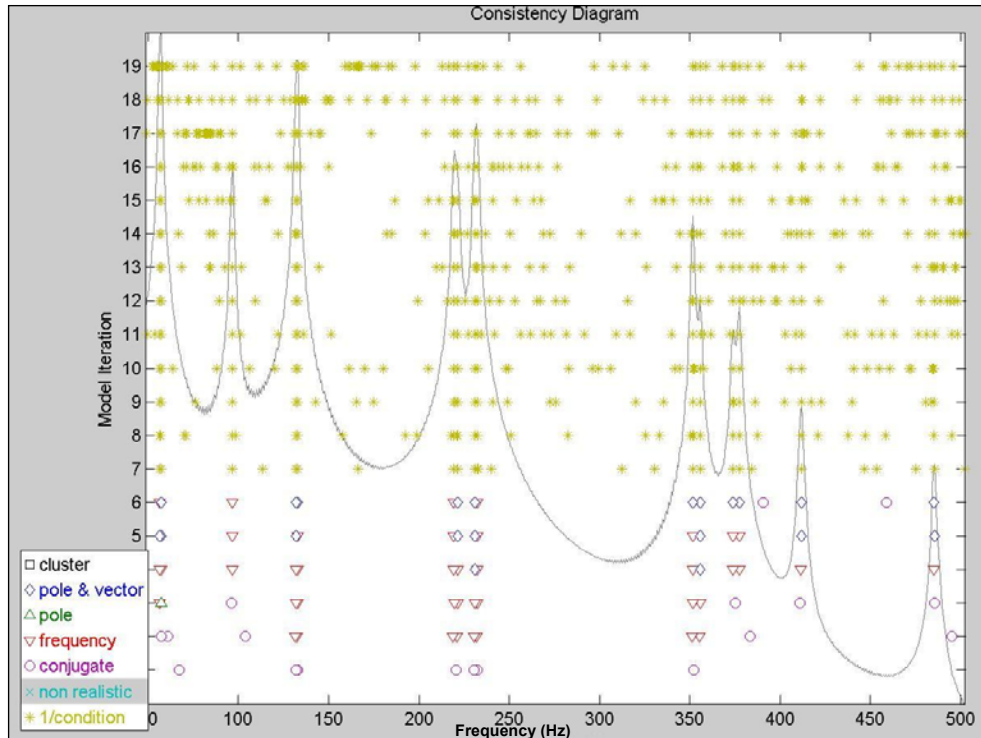


Figure 4.15: Consistency diagram for Rational Fraction Polynomial (RFP) algorithm (Circular plate)

Further the independence of the various estimated modes is checked by the means of modal assurance criterion (MAC) [Allemang, 1980, Heylen, Lammens, Sas, 1995] plot as shown in Figure 4.16. It is evident that all 15 modes, most of which are closely spaced modes, are independent and represent different modes of the system. The mode shapes obtained for the circular plate are shown in Figure 4.17. The mode shapes are of a similar nature to the ones obtained through experimental modal analysis, except that they are not scaled.

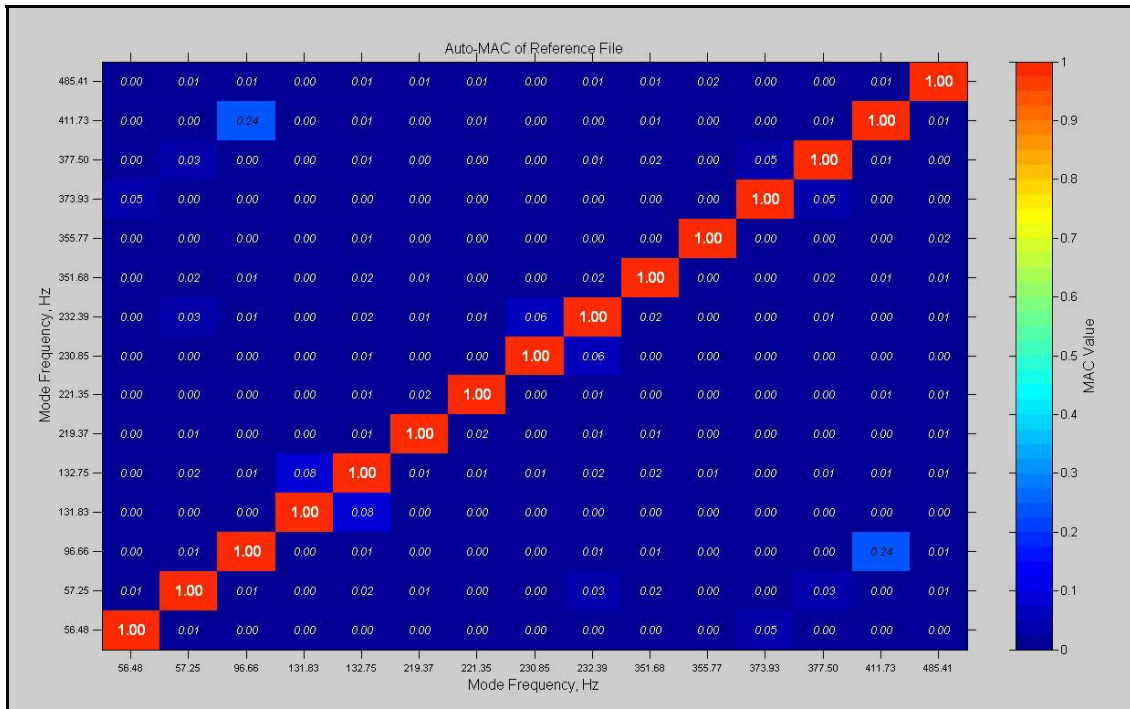


Figure 4.16: MAC plot for UMPA-LOFD algorithm (Circular plate)

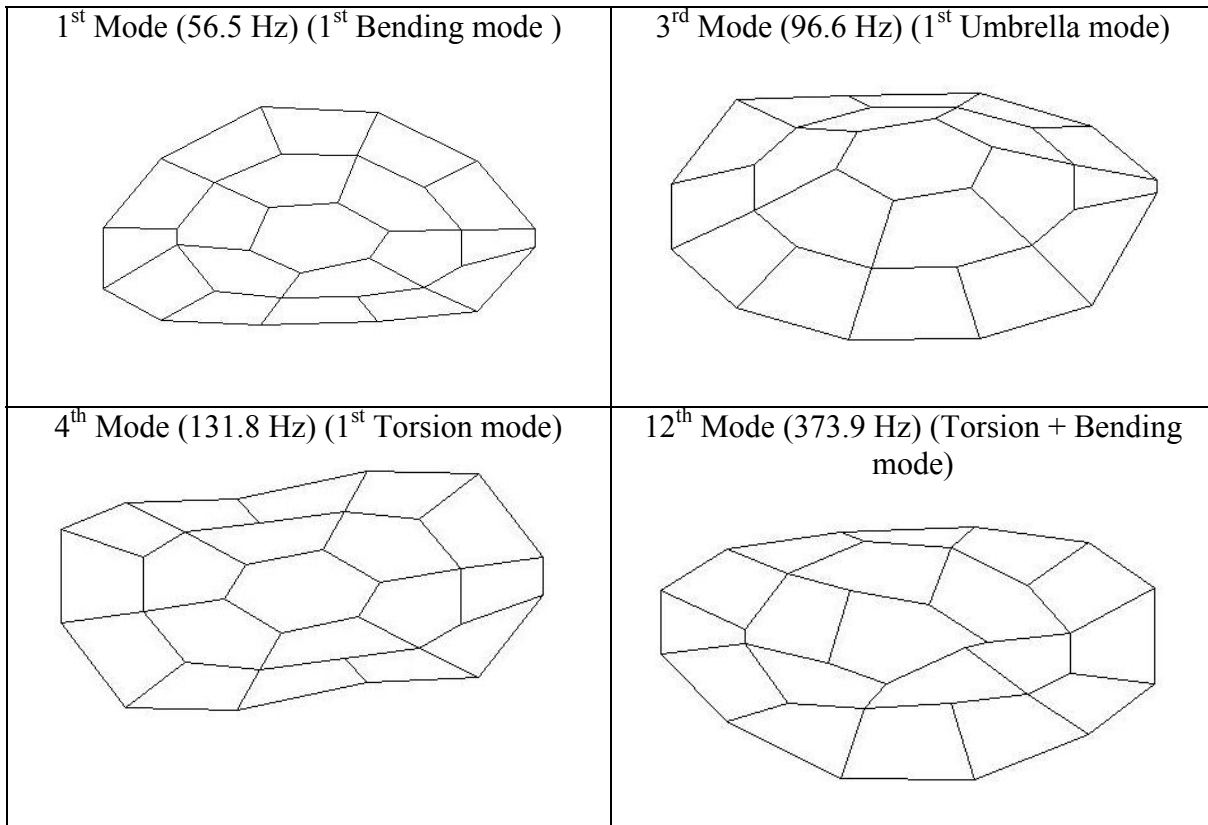


Figure 4.17: Selected mode shapes of the circular plate

4.4 Case Studies: Effect of Complex Z Mapping on UMPA-LOFD

In this section, the previous two case studies are discussed in view of the effect of complex Z mapping on both high and low order frequency domain Operational Modal Analysis algorithms. In addition to analyzing the modal parameter estimates, consistency diagrams are also studied to analyze the performance of the various algorithms.

4.4.1 Analytical 15 Degrees of Freedom System

The 15 degree of freedom system as shown in Figure 4.1 is considered again. The modal parameter estimation process is carried out using RFP, RFP-Z, UMPA-LOFD and its complex Z mapping variation.

Table 4.3: Effect of complex Z mapping - Modal parameter comparison for 15 DOF analytical system

True Modes		UMPA-LOFD (Low Order, Frequency Domain)		UMPA-LOFD with Complex Z Mapping		RFP (High Order, Frequency Domain)		RFP-z (High Order, Complex Z Mapping)	
Damp	Freq	Damp	Freq	Damp	Freq	Damp	Freq	Damp	Freq
1.0042	15.985	2.338	15.963	2.4028	15.9943	2.3531	15.9587	3.1379	15.976
1.9372	30.858	2.517	30.863	2.4530	30.8710	2.53	30.8519	2.8758	30.912
2.7347	43.6	3.043	43.680	2.9028	43.6425	2.9814	43.7026	2.9318	43.762
2.9122	46.444	3.431	46.437	3.3260	46.1123	3.4852	46.3877	3.3806	46.498
3.3375	53.317	3.932	53.209	3.5984	53.2767	3.5670	53.4123	3.0676	53.316
3.3454	53.391	3.296	53.306	3.3930	53.3452	3.3236	53.4890	3.5501	53.370
3.7145	59.413	4.430	59.116	3.9630	59.4063	4.1472	59.3597	3.7389	59.169
3.858	61.624	4.180	61.133	4.1202	61.2957	4.1735	61.4719	3.7502	61.240
4.2978	68.811	4.291	69.237	3.0884	68.9138	4.3943	68.9440	4.8688	68.612
4.5925	73.63	4.812	73.253	4.3108	72.5819	4.4734	73.2355	4.3604	73.220
2.6093	128.84	2.712	128.848	2.6453	128.8716	2.6415	128.9428	2.7789	128.965
2.4548	136.55	2.563	136.547	2.4747	136.5401	2.5578	136.5783	2.4850	136.684
2.3288	143.86	2.426	143.869	2.3172	143.8190	2.3947	143.8762	2.3207	143.919
2.221	150.83	2.314	150.799	2.1831	150.6178	2.2871	150.7683	2.2171	150.866
2.122	157.47	2.216	157.444	2.3106	157.0458	2.2041	157.4022	2.1305	157.408

Table 4.3 shows the modal parameters obtained by the four algorithms and the corresponding consistency diagrams are shown in Figures 4.18-4.21. It is observed that all the algorithms give good results though damping is over estimated for some of the modes. The modal parameter estimation is subject to user experience and depends significantly on parameters such as selected frequency range, choice of reference responses and use of residuals to account for modes out of the frequency range of interest, etc. It can be seen from Figure 4.18 that the higher order frequency domain algorithm, RFP, does not yield a good consistency diagram. The consistency diagram deteriorates severely as the order increases or a wide frequency range is chosen. This can be attributed to the ill-conditioned matrices of the Van der Monde form. The poor consistency diagram adds to the uncertainty of the obtained modal parameters and requires significant user judgment. The application of complex Z mapping improves the RFP-z consistency diagram significantly (Figure 4.19) thus underlining its significance and contribution to the field of parameter estimation. The obtained consistency diagrams are very clear and thus make it easy for the correct modes to be picked.

As shown previously, the numerical issues associated with the RFP algorithm are not apparent in case of UMPA-LOFD algorithm. Unlike RFP which involves power polynomials with increasing powers of the frequency resulting in ill-conditioned matrices, the UMPA-LOFD algorithm being a low order algorithm does not run into these sorts of numerical problems. The modal parameters estimated by UMPA-LOFD algorithm show good agreement with the results obtained using other algorithms. Further the consistency diagram (Figure 4.20) is very clear. One important thing to note with application of UMPA-LOFD algorithm is that since it's a low order algorithm it requires more spatial information than that required by RFP or RFP-Z.

Finally, complex Z mapping is applied to UMPA-LOFD to see if it results in any significant improvement like in case of high order RFP algorithm. The obtained

consistency diagram as shown in Figure 4.21 is very clear but does not provide any prominent improvement over the UMPA-LOFD consistency diagram (Figure 4.20). It is observed that unlike UMPA-LOFD, the complex Z mapping version is not able to pick modes outside the selected frequency range of interest. It is also observed that the complex Z mapping implementation of UMPA-LOFD cannot easily obtain the heavily damped modes in the range 68-74 Hz. Overall it is observed, that complex Z mapping when applied to UMPA-LOFD does not result in any significant advantage unlike its application to the high order RFP algorithm. However no particular further judgment can be made for this case, as both UMPA-LOFD and its complex Z mapping variation are giving equally good results.

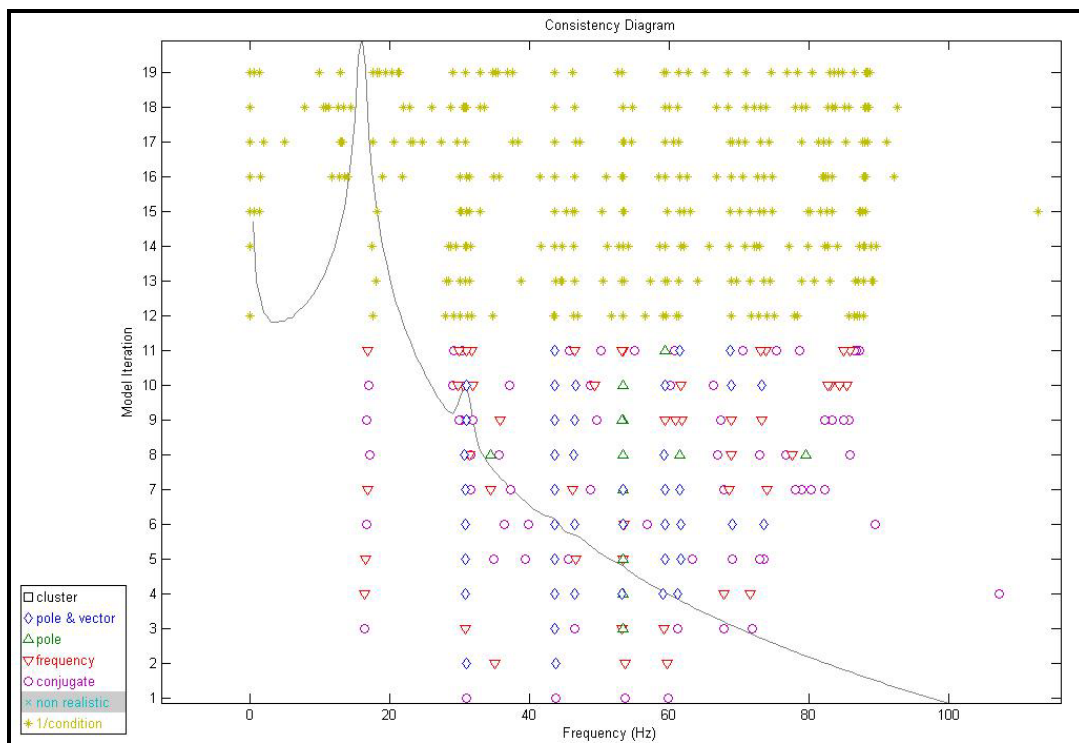


Figure 4.18: Consistency diagram for Rational Fraction Polynomial (RFP) algorithm (Analytical system)

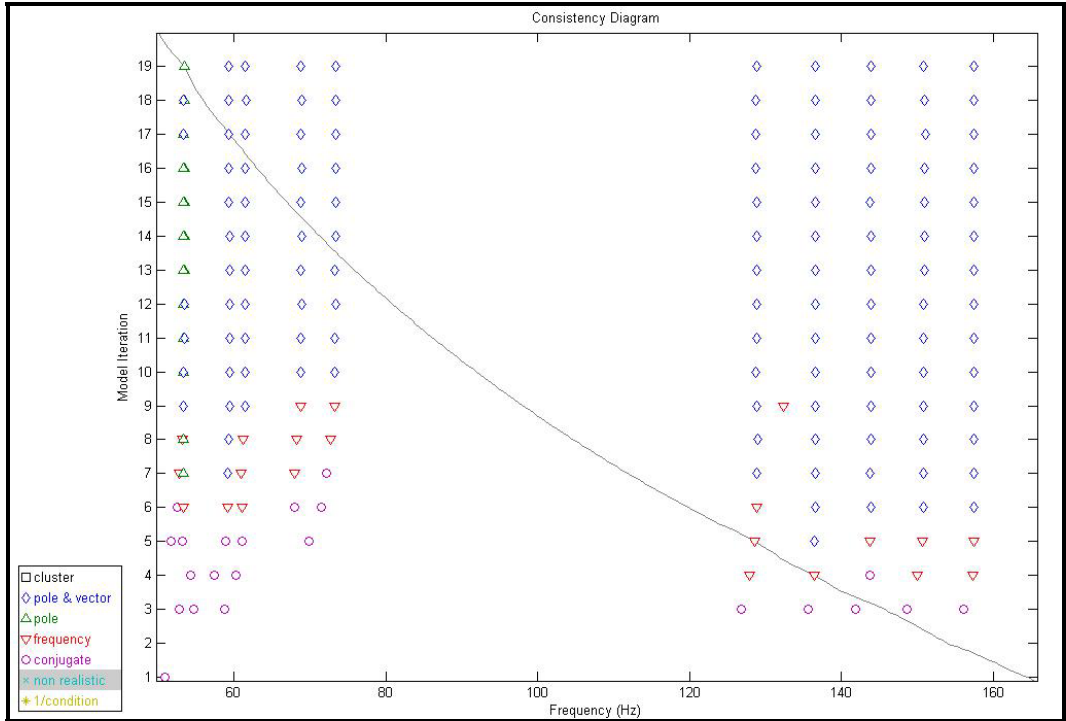


Figure 4.19: Consistency diagram for Rational Fraction Polynomial (RFP-z) algorithm (Analytical system)

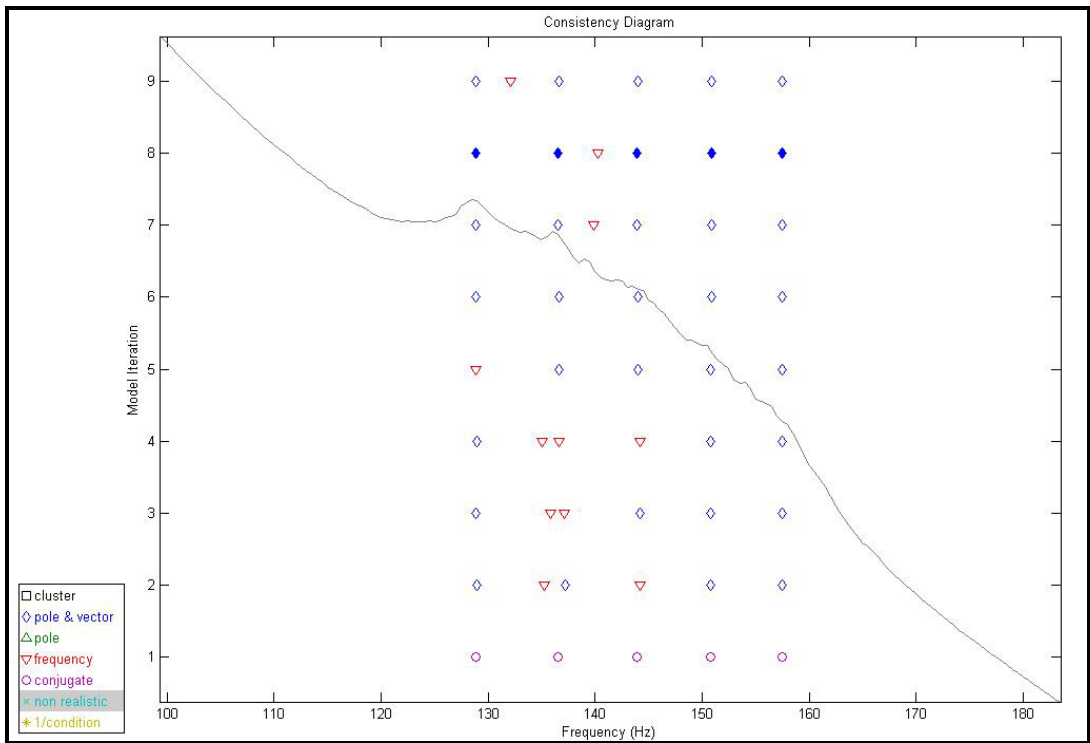


Figure 4.20: Consistency diagram for Low Order Frequency Domain (UMPA-LOFD) algorithm (Analytical system)

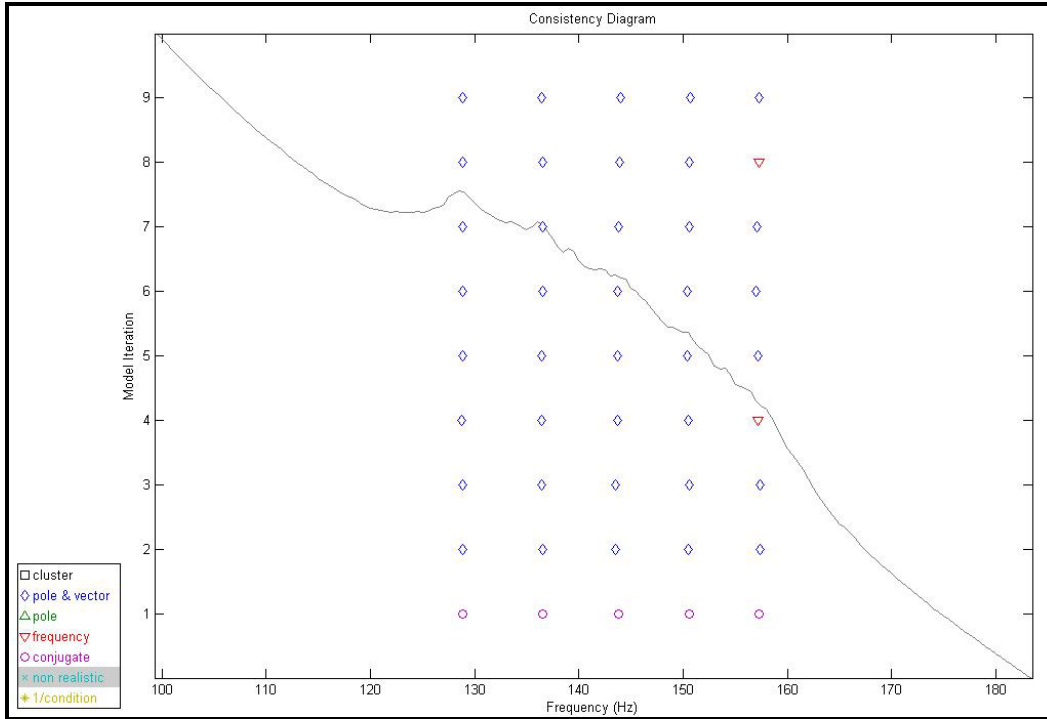


Figure 4.21: Consistency diagram for UMPA-LOFD with algorithm Complex Z mapping (Analytical system)

4.4.2 Lightly Damped Circular Plate

The response data collected over the circular plate is analyzed using various algorithms and the modal parameters are listed in Table 4.4. The estimated modal parameters show good agreement with each other and also with the experimental modal analysis based modal parameters. The consistency diagrams for the various algorithms for the same frequency range are shown in Figures 4.22-4.25. It can be seen that the RFP-Z gives a very clear consistency diagram. Application of complex Z mapping on UMPA-LOFD algorithm also results in improving the consistency diagram but, as in the analytical system, the effect is not as significant.

Table 4.4: Effect of complex Z mapping - Modal parameter comparison for lightly damped circular plate

EMA based modal parameters		UMPA-LOFD (Low Order, Frequency Domain)		UMPA-LOFD (Low Order, Complex Z Mapping)		RFP (High Order, Frequency Domain)		RFP-z (High Order, Complex Z Mapping)	
Damp	Freq	Damp	Freq	Damp	Freq	Damp	Freq	Damp	Freq
0.258	56.591	0.612	56.478	0.578	56.542	0.663	56.462	0.762	56.504
0.285	57.194	0.621	57.253	0.66	57.252	0.669	57.214	0.717	57.24
0.312	96.577	0.636	96.665	0.626	96.653	0.638	96.663	0.637	96.662
0.412	132.101	0.342	131.83	0.369	131.842	0.353	131.847	0.349	131.84
0.147	132.65	0.285	132.76	0.337	132.735	0.312	132.743	0.302	132.723
0.243	219.582	0.3	219.375	0.292	219.368	0.299	219.373	0.303	219.365
0.216	220.952	0.364	221.358	0.359	221.342	0.367	221.35	0.366	221.344
0.214	231.172	0.256	230.851	0.265	230.843	0.257	230.855	0.257	230.856
0.137	232.077	0.225	232.394	0.218	232.421	0.227	232.391	0.221	232.4
0.089	352.997	0.147	351.677	0.138	351.716	0.151	351.69	0.151	351.715
0.174	355.509	0.219	355.773	0.207	355.801	0.22	355.78	0.219	355.801
0.18	374.554	0.268	373.933	0.269	373.882	0.27	373.941	0.271	373.936
0.176	377.569	0.236	377.505	0.235	377.499	0.236	377.508	0.236	377.506
0.313	412.414	0.241	411.727	0.244	411.734	0.241	411.729	0.242	411.731
0.209	486.801	0.219	485.405	0.225	485.425	0.221	485.408	0.219	485.397

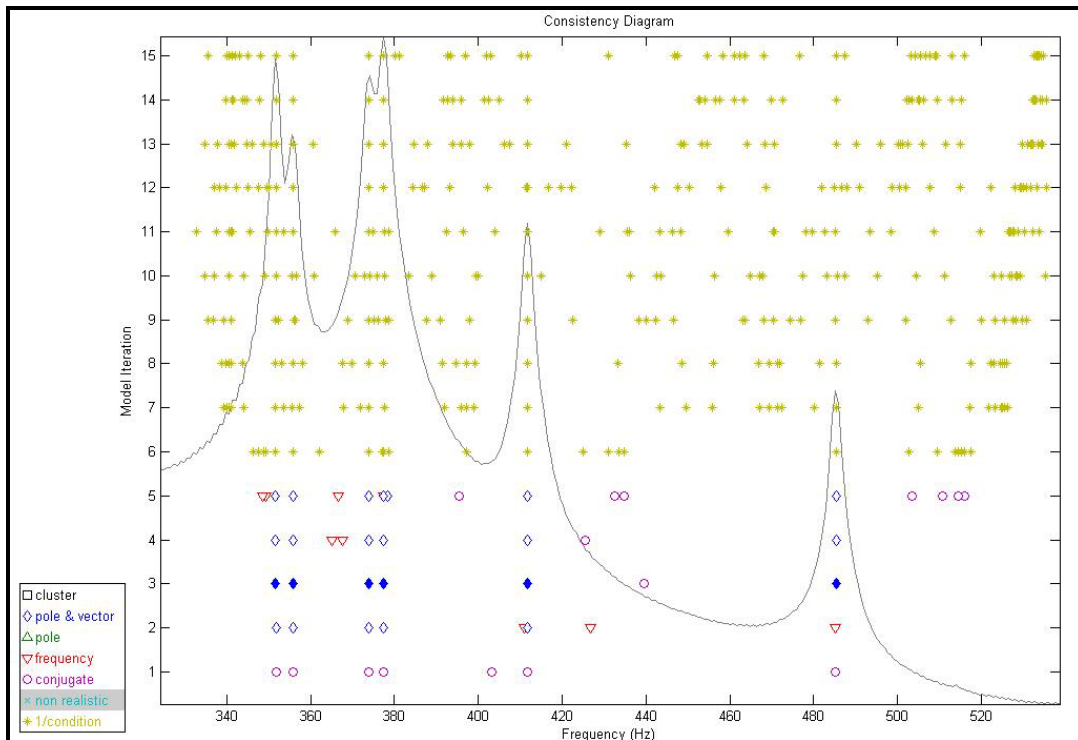


Figure 4.22: Consistency diagram for Rational Fraction Polynomial (RFP) algorithm (Circular plate)

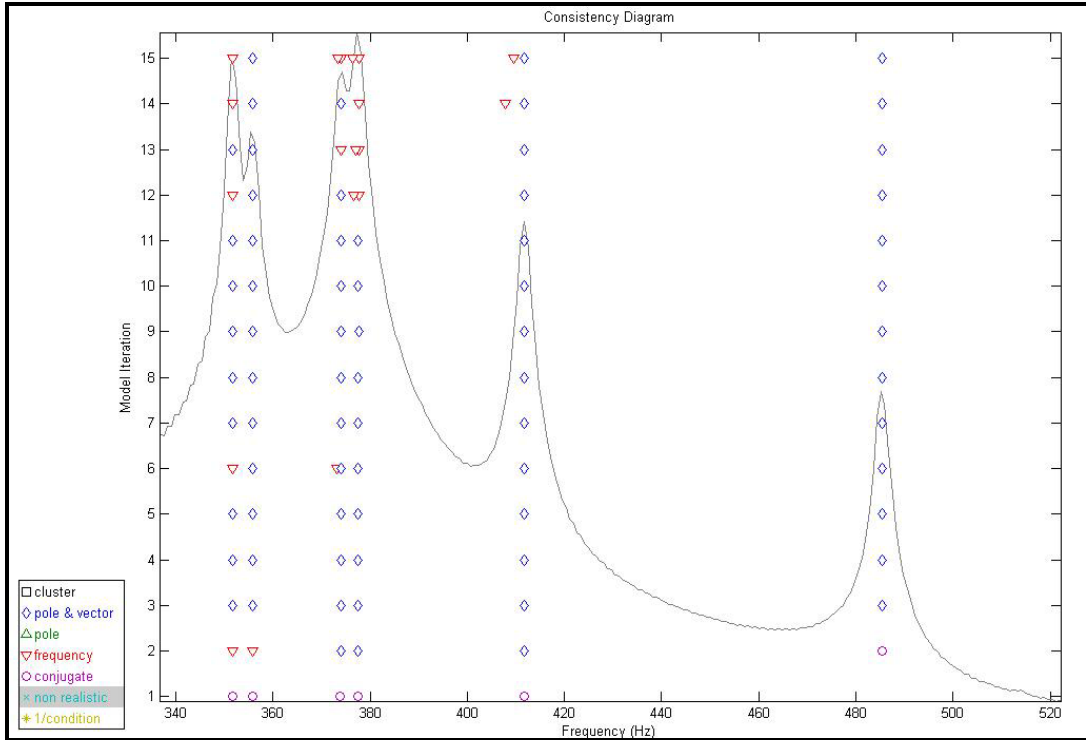


Figure 4.23: Consistency diagram for RFP-z algorithm (Circular plate)

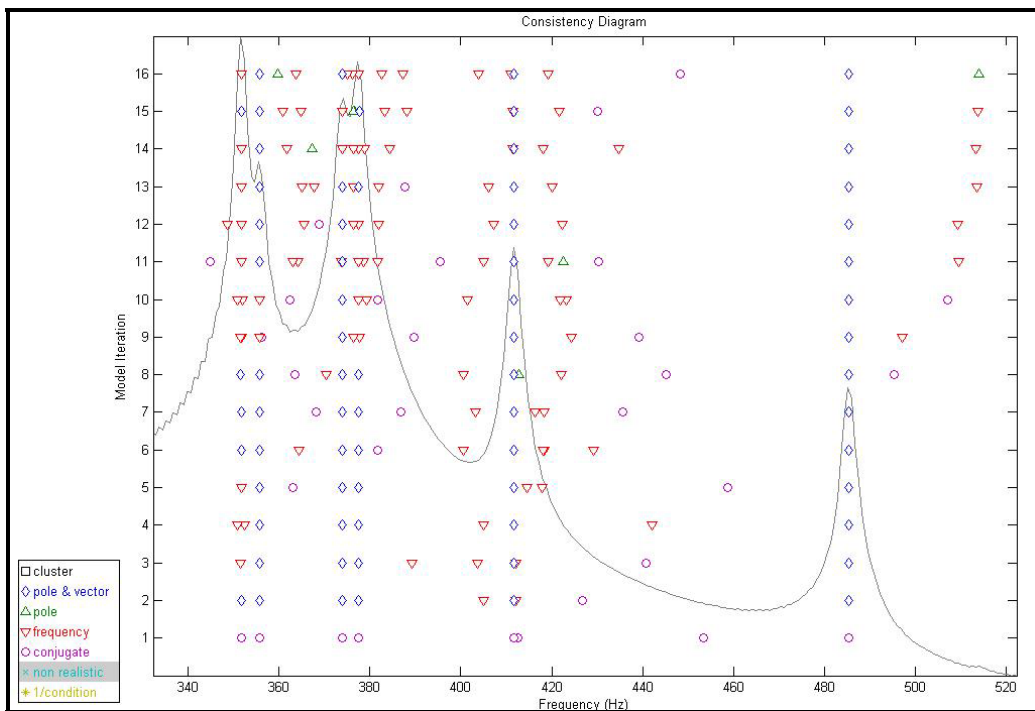


Figure 4.24: Consistency diagram for UMPA-LOFD algorithm (Circular plate)

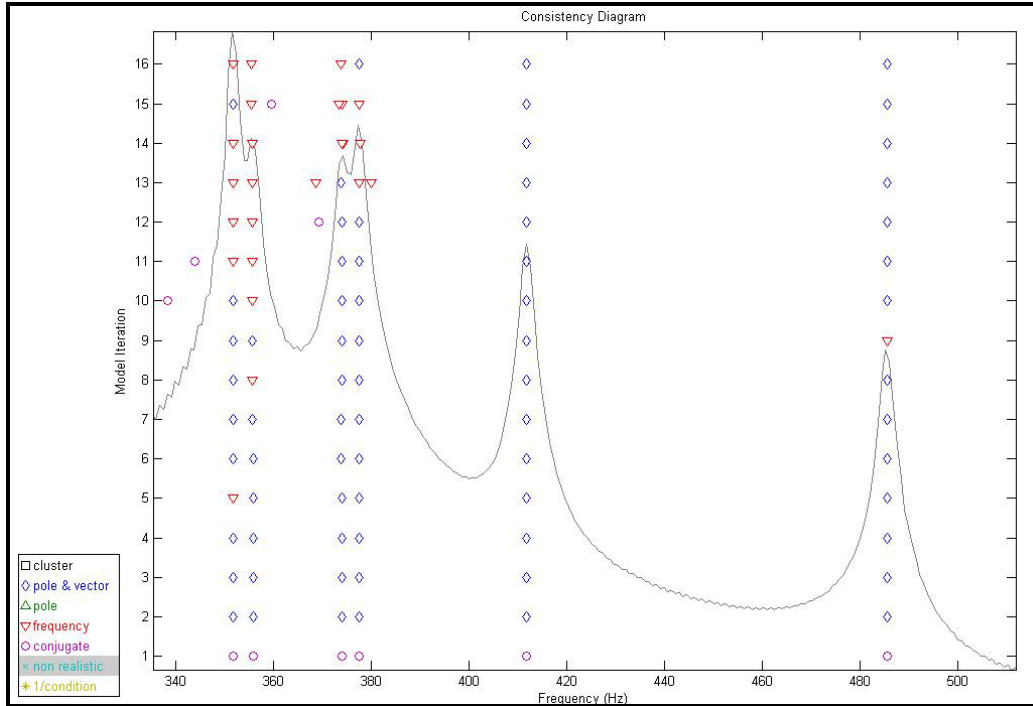


Figure 4.25: Consistency diagram for UMPA-LOFD with algorithm Complex Z mapping (Circular plate)

4.5 Conclusions

Due to its good numerical conditioning properties, the UMPA-LOFD algorithm proposed in this paper offers a frequency domain alternative in the field of operational modal analysis. The problems associated with higher order frequency domain algorithms are not encountered with the use of this algorithm and the obtained results compare well with the established time domain based approaches. Case studies undertaken in the paper, show that the modal parameters closely match the expected values and the consistency diagram is of good quality. Further, the concept of utilizing the complex Z mapping as in the polyreference least squares complex frequency (PolyMAX) algorithm, or generically the RFP-Z algorithm, for the purpose of obtaining better numerical characteristics for frequency domain algorithms is extended to UMPA-LOFD algorithm. It is shown that complex Z mapping significantly improves the performance of the high order frequency domain algorithms like RFP. The effect in the case of low order UMPA-

LOFD is noticeable but not very prominent. However, with no apparent negative issues, application of complex Z mapping to UMPA-LOFD can be considered as another alternative for the purpose of modal parameter estimation using output-only data. Further, this study should also be applied to real life systems which might throw some more light on the effectiveness of complex Z mapping on UMPA-LOFD.

With diverse fields of application such as civil structures, automobile and aerospace structures and complex rotating machinery falling in the domain of operational modal analysis, the low order frequency domain algorithm with its promising results can be considered as a good addition to the family of operational modal analysis algorithms.

Chapter Five

OMA-EMIF: A Spatial Domain OMA Algorithm

The Complex Mode Indicator Function (CMIF) is a popular spatial domain modal parameter estimation technique that utilizes the singular value decomposition of the frequency response function matrix for estimating the modal parameters of the system. Due to several advantages like identification of closely spaced modes, this technique is extremely popular for modal parameter estimation purposes. In recent times, the Frequency Domain Decomposition (FDD) technique [Brincker, Zhang, Andersen, 2000] extends the CMIF algorithm to the operational modal analysis framework. The FDD technique works on the power spectrums unlike working on frequency response functions as in conventional modal analysis. The FDD technique however suffers from a limitation that one cannot estimate damping. Normally the FDD is followed by the Enhanced Frequency Domain Decomposition (eFDD) [Brincker, Ventura, Andersen, 2000] to complete the overall parameter estimation procedure. eFDD is essentially a single degree of freedom system identification approach that works in the time domain. In this chapter an alternative to the eFDD, the previously introduced *Enhanced Mode Indicator Function* (EMIF) [Fladung, Phillips, Brown, 1997; Fladung, 2001; Allemang, Brown, 2006], is reviewed and extended to the operational modal analysis framework. This algorithm differs from the eFDD in that the parameter estimation is carried out in the frequency domain. Further the chapter analyzes the application of spatial domain

algorithms to operational modal analysis framework in more detail. It discusses the critical issues and limitations associated with the application of spatial domain algorithms to the OMA framework under different excitation scenarios. It is shown in [Chauhan, Martell et. al, 2005, Herlufsen, Gade, Moller, 2005; Gade, Moller et al., 2005] that spatial domain algorithms suffer from some limitations when they are applied to conventional EMA situations. When the system isn't completely excited spatially, the resulting power spectrum based singular value decomposition plots (or CMIF plots) differ significantly from the FRF based CMIF and are often confusing. A simple tool, *Singular Value Percentage Contribution (SVPC)* plot, is proposed to deal effectively with this problem. This aspect is studied and explained with the help of an analytical 15 degree of freedom system and experiments conducted on a circular plate and an H-Frame structure.

5.1 CMIF and FDD/eFDD

As previously stated, the FDD algorithm is inspired by the conventional CMIF algorithm. CMIF involves a frequency by frequency singular value decomposition of the frequency response function matrix [Shih, Tsuei, Allemang, Brown, 1989; Heylen, Lammens, Sas, 1997].

$$[H(\omega_k)]_{N_o \times N_i} = [U(\omega_k)]_{N_o \times N_i} [\Sigma(\omega_k)]_{N_i \times N_i} [V(\omega_k)]_{N_i \times N_i}^H \quad 5.1)$$

where

N_o is number of outputs,

N_i is number of inputs,

$H(\omega_k)$ is the FRF matrix at any frequency ω_k ,

$U(\omega_k)$ is the left singular matrix at any frequency ω_k , which is a unitary matrix,

$V(\omega_k)$ is the right singular matrix at any frequency ω_k , which is also a unitary matrix,

$\Sigma(\omega_k)$ is the singular value matrix at any frequency ω_k , which is a diagonal matrix.

As explained in Chapter 2, the Frequency Domain Decomposition technique involves the singular value decomposition (SVD) of this output response power spectra matrix frequency by frequency. Thus at any particular frequency ω_k the singular value decomposition of G_{XX} results in

$$[G_{XX}(\omega_k)] = [U][S][V]^H \quad 5.2)$$

where $[S]$ is the singular value diagonal matrix and $[U]$, $[V]$ are singular vector matrix which are orthogonal. The singular vectors near a resonance are good estimates of the mode shapes and the modal frequency is obtained by the simple single degree of freedom peak-picking method. In this manner, the FDD algorithm gives an estimate of the modal frequencies and the mode shapes and is followed by the enhanced Frequency Domain Decomposition (eFDD) algorithm to determine the damping (ζ) associated with the mode, thus completing the modal parameter estimation process (Figure 5.1).

In the eFDD algorithm, power spectra of a SDOF system is identified around a peak in the SVD plot. A user defined Modal Assurance Criterion (MAC) rejection level is set to compare the singular vectors around the peak and the corresponding singular values are retained as those belonging to the SDOF power spectrum. This SDOF power spectrum is transformed back to the time domain by an inverse FFT. The natural frequency and damping are then estimated for this SDOF system by determining zero crossing times and logarithmic decrement methods, respectively. Thus the parameter estimation in case of eFDD algorithm is carried out in time domain.

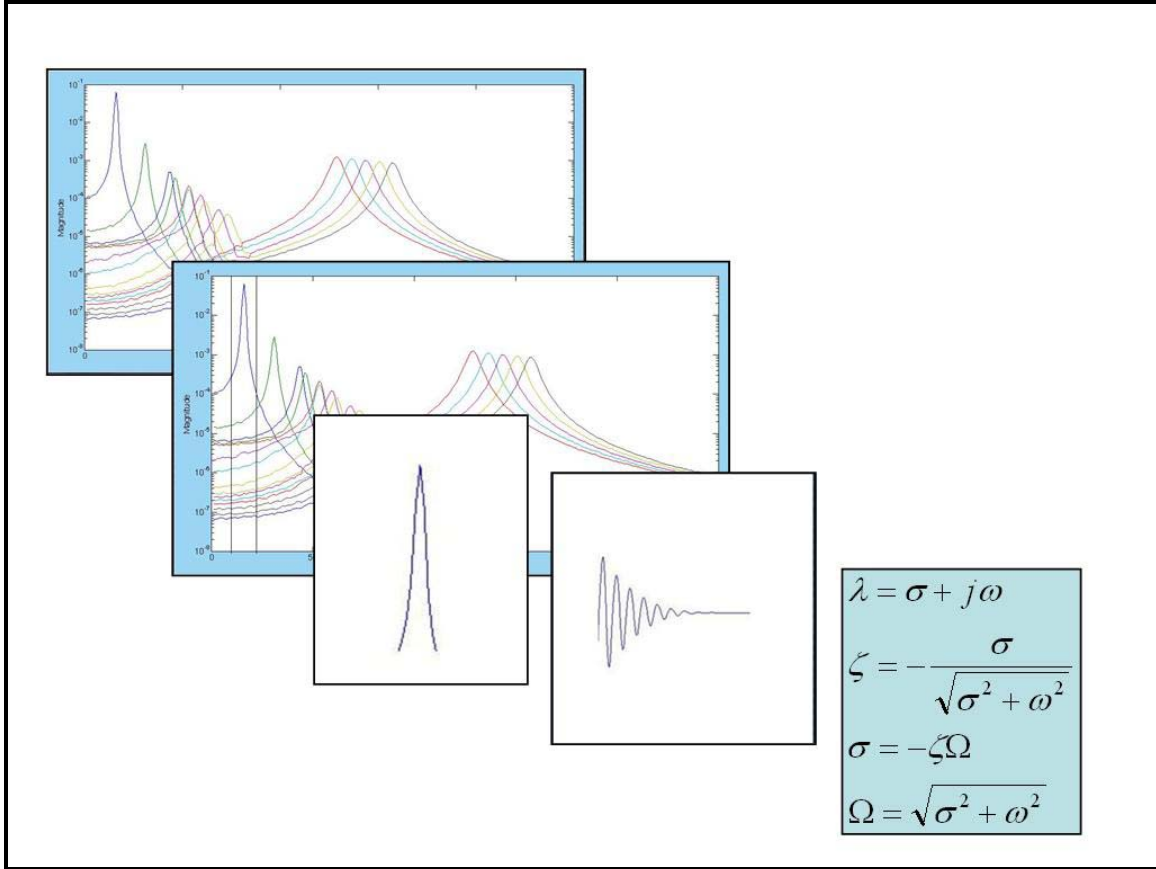


Figure 5.1 – eFDD estimation of modal frequency and damping

5.2 OMA-EMIF: Enhanced Mode Indicator Function for OMA

The algorithm proposed in this chapter differs from the eFDD approach in the sense that the modal frequency and damping estimation is carried out in the frequency domain. This allows the use of residual terms to reduce the effects of out of band modes. However, instead of processing the power spectrums, this algorithm utilizes positive power spectrum which is mathematically represented as

$$G_{pq}^+(\omega) = \sum_{k=1}^n \frac{R_{pqk}}{j\omega - \lambda_k} + \frac{R_{pqk}^*}{j\omega - \lambda_k^*} \quad 5.3)$$

The EMIF algorithm [Fladung, Phillips, Brown, 1997; Fladung, 2001; Allemang, Brown, 2006] is reformulated here for use with positive power spectra. It involves the selection of a frequency range containing a discrete number of frequencies N_f and number of modes N_b to be identified in that range. The number of modes in the frequency band cannot be greater than the number of singular values. When the frequency range to be analyzed and the number of modes within the band have been chosen, the algorithm uses the following process in the frequency domain to determine the modal parameters. The first order model, frequency domain equivalent of the ERA method, is used to form the augmented matrix $[A_0]$ utilizing the cross-spectral matrix.

$$[A_0]_{N_o \times (N_i N_f)} = \begin{bmatrix} G_{11}^+(\omega) & \dots & G_{11}^+(\omega_{i+N_f}) & \dots & G_{21}^+(\omega) & \dots & G_{21}^+(\omega_{i+N_f}) & \dots & G_{p1}^+(\omega) & \dots & G_{p1}^+(\omega_{i+N_f}) \\ \vdots & \vdots \\ G_{pq}^+(\omega) & & G_{pq}^+(\omega_{i+N_f}) & \dots & G_{pq}^+(\omega_{i+N_f}) \end{bmatrix} \quad 5.4)$$

An SVD is then performed on the matrix $[A_0]$. This calculation yields the left and right hand singular vectors as well as the singular values.

$$[A_0(\omega_i)]_{N_o \times (N_i N_f)} = [U] [S] [V]^H \quad 5.5)$$

For the economical SVD, the size of $[S]$ is the lesser dimension of (N_o) or $(N_i N_f)$. The dominant right or left singular vectors $\{U\}$ corresponding to the number of modes N_b in the frequency band are then used as modal filters to reduce the number of effective positive power spectra. This creates an enhanced positive power spectrum (ePPS) in the frequency band of interest that is similar to the enhanced frequency response functions or eFRFs [Fladung, Phillips, Brown, 1997].

$$ePPS(\omega) = [\bar{G}(\omega)]_{N_b \times N_i} = [U]_{N_b \times N_o}^T [G^+(\omega)]_{N_o \times N_i} \quad 5.6)$$

This ePPS matrix is then used as the data matrix in a first order UMPA formulation. This formulation may include N_r residual terms $[\beta_m]$ to account for out of band modes.

$$\left[(j\omega)[\alpha_1]_{N_b \times N_b} + (j\omega)^0 [\alpha_0]_{N_b \times N_b} \right] [\bar{G}(\omega)]_{N_b \times N_i} = \left[\sum_{m=0}^{N_r} (j\omega)^m [\beta_m(\omega)]_{N_b \times N_i} \right] \quad (5.7)$$

When rearranged, the equations yield the following when $[\alpha_0]$ is set equal to $[I]$.

$$\left[[\alpha_1] \quad [\beta_0] \quad \dots \quad [\beta_m] \right] = -[\bar{G}(\omega)] \begin{bmatrix} [j\omega\bar{G}(\omega)] \\ -[I] \\ \vdots \\ -[(j\omega)^m [I]] \end{bmatrix}^+ \quad (5.8)$$

The equations yield the following when $[\alpha_1]$ is set equal to $[I]$.

$$\left[[\alpha_0] \quad [\beta_0] \quad \dots \quad [\beta_m] \right] = -[j\omega\bar{G}(\omega)] \begin{bmatrix} [\bar{G}(\omega)] \\ -[I] \\ \vdots \\ -[(j\omega)^m [I]] \end{bmatrix}^+ \quad (5.9)$$

It should be noted that in Eqn. (5.8) and (5.9) conjugate terms can be included. The equations can then be reformulated in a second order form such that the solution also includes conjugate poles. These equations can then be solved in a least square sense for $[\alpha]$ and $[\beta]$ matrices with either $[\alpha_1]$ or $[\alpha_0]$ assumed to equal $[I]$. The + sign in the above equations represents Moore-Penrose pseudo inverse of a matrix.

The eigenvalues of the system can then be computed as the eigenvalues of the matrix $[\alpha_0]$ or the eigenvalues of the inverse of $[\alpha_1]$. The eigenvectors are the eigenvectors of the enhanced system and therefore have little physical meaning. They must be converted back to the original physical coordinates. This is performed by multiplying the

eigenvectors from the enhanced system by the eigenvectors from the original physical system.

$$\{\psi_{physical}\}_{N_o \times 1} = [U^H]_{N_o \times N_b} \{\psi_{Enhanced}\}_{N_b \times 1} \quad 5.10)$$

5.3 Singular Value Percentage Contribution (SVPC) Plot

It is observed in case the of operational modal analysis that, when the system is uniformly (completely) excited spatially, the resulting power spectra based CMIF plot indicates the modes present in the system in the same manner as a FRF based CMIF plot. However when the system is excited locally, in other words when the excitation is insufficient spatially, the power spectrum based CMIF plot contains extra peaks at the frequencies where modes are expected. The insufficient spatial excitation case for OMA is typical of traditional FRF based experimental modal analysis. An analysis of the FRF based CMIF plot for this case reveals that it is quite similar to the CMIF plot based on power spectrums except that it does not have the extra peaks. Presence of more than one peak around the same frequency in a FRF based CMIF plot usually indicates the presence of a repeated or closely-spaced mode. However, in the case of power spectrum based CMIF, the extra peaks may not be due to other modes but due to insufficient excitation. Thus the presence of extra peaks in the power spectrum based CMIF may act as an indicator of insufficient spatial excitation.

A method based on percentage contribution of singular values is devised to get around this confusion caused by the presence of extra peaks. After singular value decomposition of the G_{xx} matrix at every frequency, the percentage contribution of each singular value to the total variance (Note that the singular values are a measure of variance) can be plotted. The number of significant singular values can be found based

on how many singular values are contributing to a large percentage of the total variance. Any conclusion about the number of modes present in the system can now be made on the basis of these significant singular values. This plot is referred to as *Singular Value Percentage Contribution* plot or SVPC plot. As discussed earlier in this section, a FRF based CMIF plot resembles the power spectrum based CMIF plot if only the significant singular value curves are considered instead of all the singular value curves. Further, the presence of a large number of significant singular values in the SVPC plot means that the system is being excited spatially fairly well. On the other hand if only a few (two or three) singular values are contributing to the total variance, it can be inferred that the system is being excited more locally. In later sections, the utility of the SVPC tool is shown through various examples

5.4 Experimental Validation

5.4.1 15 DOF ANALYTICAL SYSTEM

The fifteen degree-of-freedom analytical system shown in Figure 5.2 was excited by a non-correlated random forcing function at each degree of freedom. The time domain response at each degree-of-freedom was used to calculate the cross-spectral matrix between all inputs and outputs. This cross-spectral matrix was then used to calculate the Complex Mode Indicator Function for the system as shown in Figure 5.3. The CMIF plot clearly indicates all the 15 modes present in the system and closely resembles the CMIF plot obtained from a fully excited FRF based singular value decomposition.

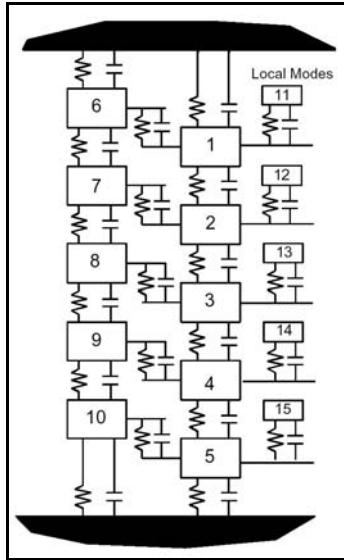


Figure 5.2: Analytical 15 DOF system

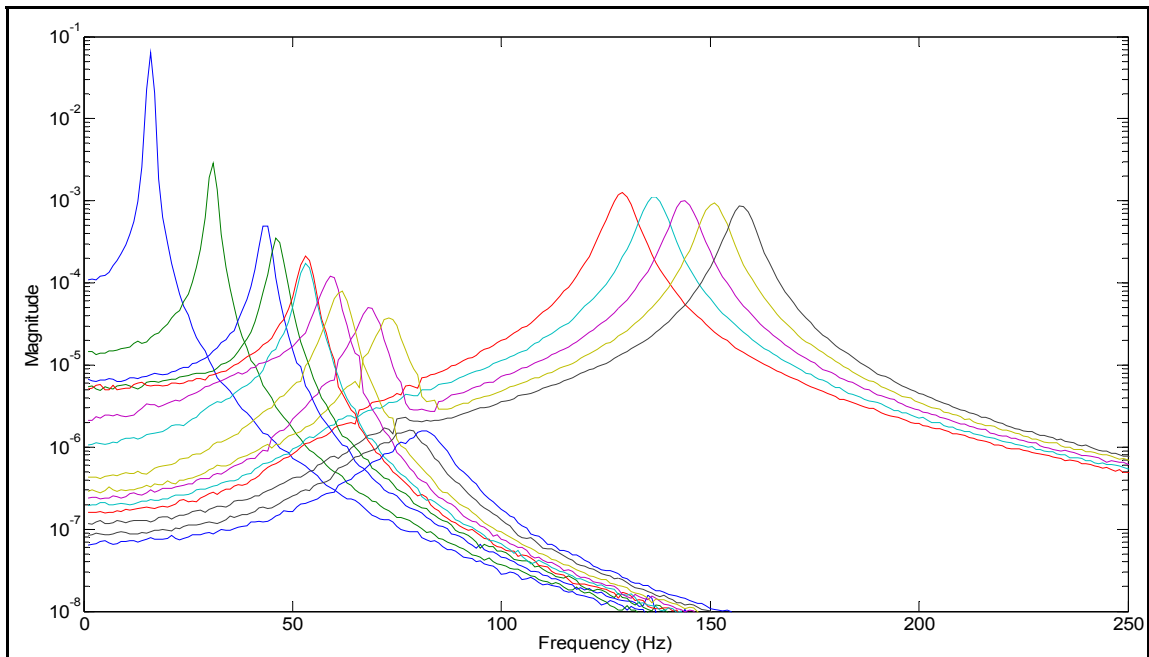


Figure 5.3 – CMIF of spatially well excited 15 DOF analytical system

Table 5.1 - Comparison of true modes and OMA-EMIF modes for 15 DOF analytical system

True Modes		Enhanced Mode Indicator Function (EMIF)	
Damp	Freq	Damp	Freq
1.0042	15.985	4.147	15.92
1.9372	30.858	3.163	30.87
2.7347	43.6	3.475	43.65
2.9122	46.444	3.688	46.69
3.3375	53.317	4.224	53.8
3.3454	53.391	4.857	53.9
3.7145	59.413	3.749	59.13
3.858	61.624	3.647	61.44
4.2978	68.811	4.038	68.29
4.5925	73.63	3.949	73.17
2.6093	128.84	2.51	128.46
2.4548	136.55	2.62	136.45
2.3288	143.86	2.459	143.91
2.221	150.83	2.299	150.9
2.122	157.47	1.773	157.86

Table 5.1 shows the comparison of true modes and the modal parameters obtained using the EMIF algorithm. The modal parameters obtained using the proposed EMIF algorithm are comparable to the true modes of the system which indicates that the algorithm works well. The ability of the EMIF algorithm to identify closely spaced modes and the possible inclusion of residuals makes it an attractive option for operational modal analysis applications.

The system was next excited at limited locations, which is typical of traditional experimental modal analysis where the system is excited by known input forces at a few select locations. The CMIF plot for the case where the system is excited at three locations is shown in Figure 5.4. It should be noted that the CMIF plot shown in Figure 5.5 based on frequency response functions for the same case of 3 point excitation shows that it is quite similar to the CMIF plot based on power spectrums shown in Figure 5.4 (first three singular value curves) except that it does not have the extra peaks. It can be observed that the CMIF plot (Figure 5.4) contains extra peaks at the frequencies

where modes are expected. This makes it difficult to interpret the CMIF; whether the peaks are indicating the presence of closely spaced modes or are just false indications as in this case. This is more troublesome in real life situations where the acquired data will not be as clear as in this analytical case.

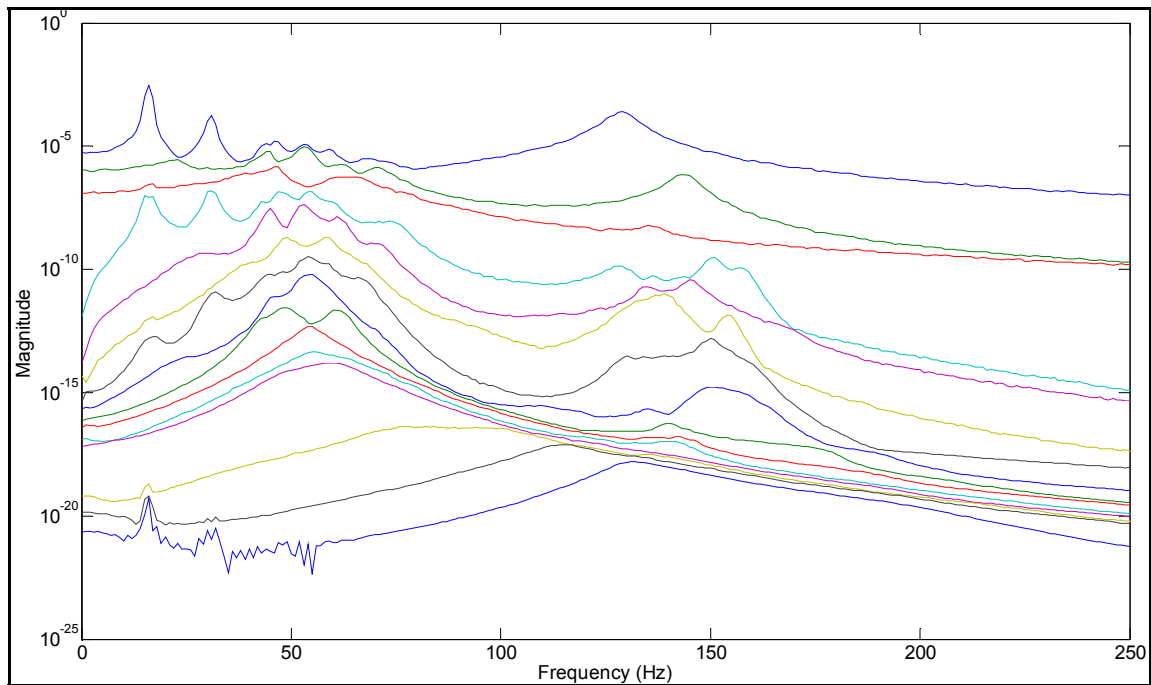


Figure 5.4 – CMIF of analytical system excited at three locations (Cross-Power based)

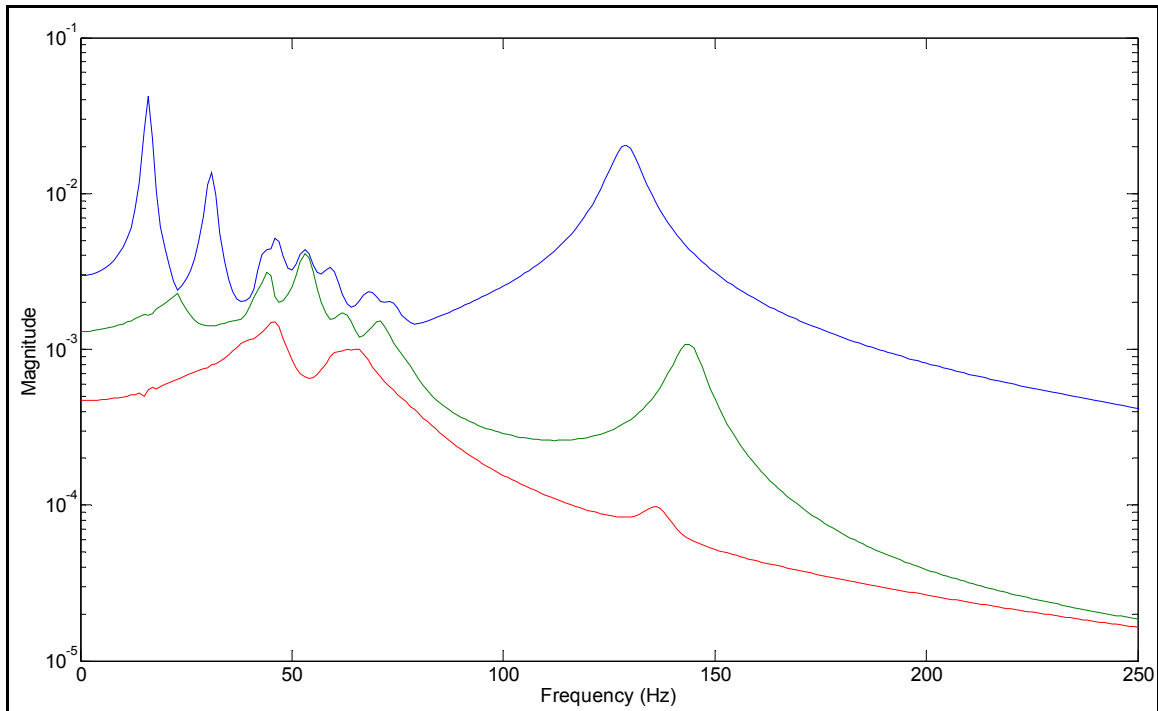


Figure 5.5 - CMIF of analytical system excited at three locations (FRF based)

Figure 5.6 shows the Singular Value Percentage Contribution (SVPC) plot for the case when the system is excited at only three points. It is very clear from this plot that out of fifteen, there are only three significant singular values (3 curves). This means that only three singular values are contributing toward the total variance, or in other words, the system is not being uniformly excited spatially. As stated earlier, any system related conclusion should now be made on the basis of the first three curves from which it can be inferred that there are 13 modes present in the system. Table 5.2 presents the results obtained using the frequency response function and output response power spectrum data for this spatially insufficient excitation case. It should be noted that the EMIF method, due to the inherent nature of enhancing the spectra using the singular vectors does not extract the modal parameters for all modes even when using FRF based methods. However, for all modes that were found, the results matched the true modes quite well.

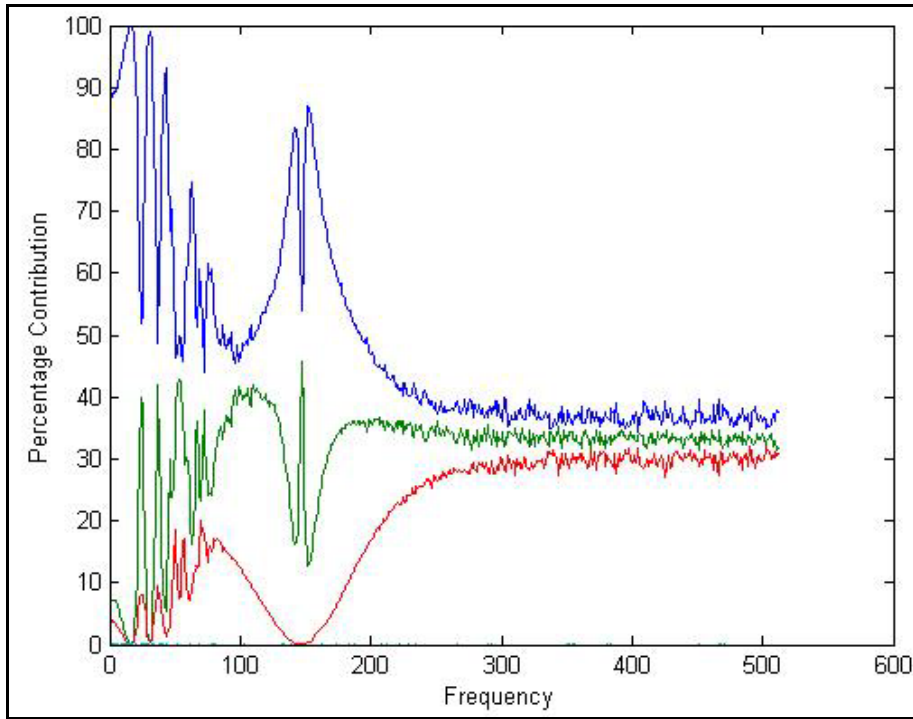


Figure 5.6 - SVPC plot for spatially insufficient excitation case (Analytical system)

Table 5.2 - FRF and G_{xx} based results comparison for spatially insufficient excitation case

EMIF,Insufficient Spatial Excitation (EMA)		EMIF,Insufficient Spatial Excitation (OMA)	
Damp	Freq	Damp	Freq
2.717	15.972	5.024	16.017
2.56	30.834	3.83	30.909
3.08	43.618	3.665	43.551
3.21	46.439	3.664	46.4
3.581	53.341	3.892	53.188
1.752	53.721	4.057	53.66
3.918	59.389	4.057	58.891
3.984	61.666	3.29	61.406
4.435	68.838	3.718	68.445
4.636	73.777	3.589	72.495
2.662	128.855	2.661	128.602
2.509	136.559		
2.388	143.874		

5.4.2 Lightly Damped Circular Plate

A lightly damped aluminum circular plate was instrumented with 30 accelerometers and suspended by soft springs as shown in Figure 5.7. The plate was tested by three excitation techniques. The first test case involved randomly impacting over the entire surface of the plate, the second case involved impacting randomly over one quarter of the surface area of the plate and the third case involved exciting the plate through the use of electro-mechanical shakers at only two points on the structure. The excitation signals for the third case were two uncorrelated random signals.



Figure 5.7 - Experimental set up for the lightly damped circular plate

The CMIF plot for the case where the plate was fully excited is shown in Figure 5.8. The CMIF looks nearly identical to a CMIF obtained through a traditional modal analysis utilizing Frequency Response Functions shown in Figure 5.10. The CMIF plots for other two cases (quarter plate excitation and two point shaker excitation) are shown in Figure 5.11 and Figure 5.13. It is observed that when the plate is not uniformly excited spatially, extra peaks begin to emerge in the CMIF plot. This effect, as explained with the analytical system, tends to reduce the utility of CMIF plots as mode indicators. The more localized the input forcing function, the more severe the effect on CMIF plot. The SVPC

plots for the three cases (shown in Figures 5.9, 5.12 and 5.14) show that the number of significant singular values decrease as the excitation becomes more and more local. As explained earlier, for highly localized excitation, it is advisable to use only the significant singular values in the CMIF plot as potential mode indicators.

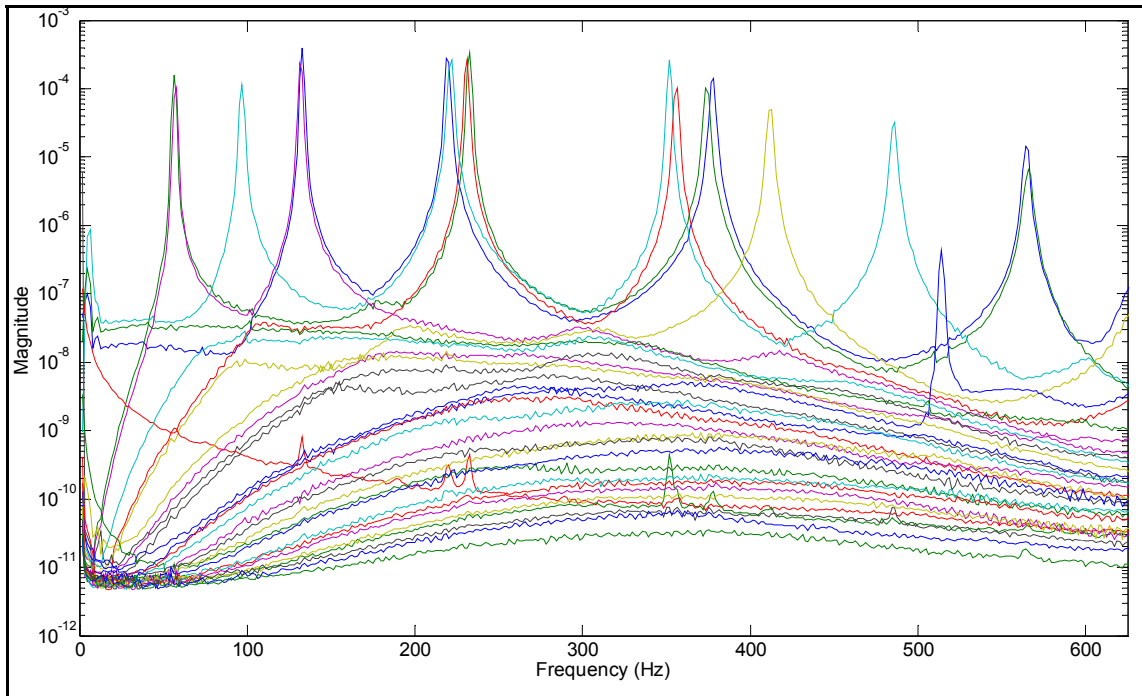


Figure 5.8 - CMIF of circular plate excited over the entire surface (Spatially well excited)

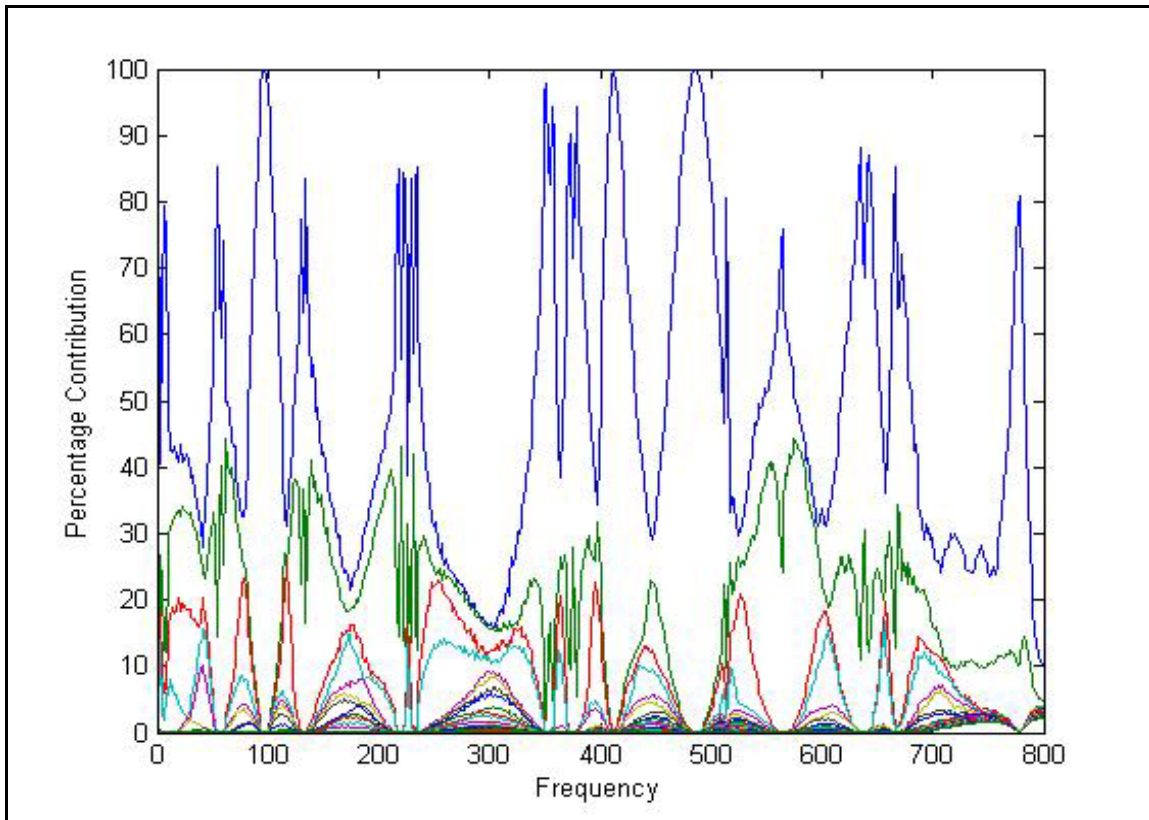


Figure 5.9 - SVPC plot for circular plate (Spatially well excited)

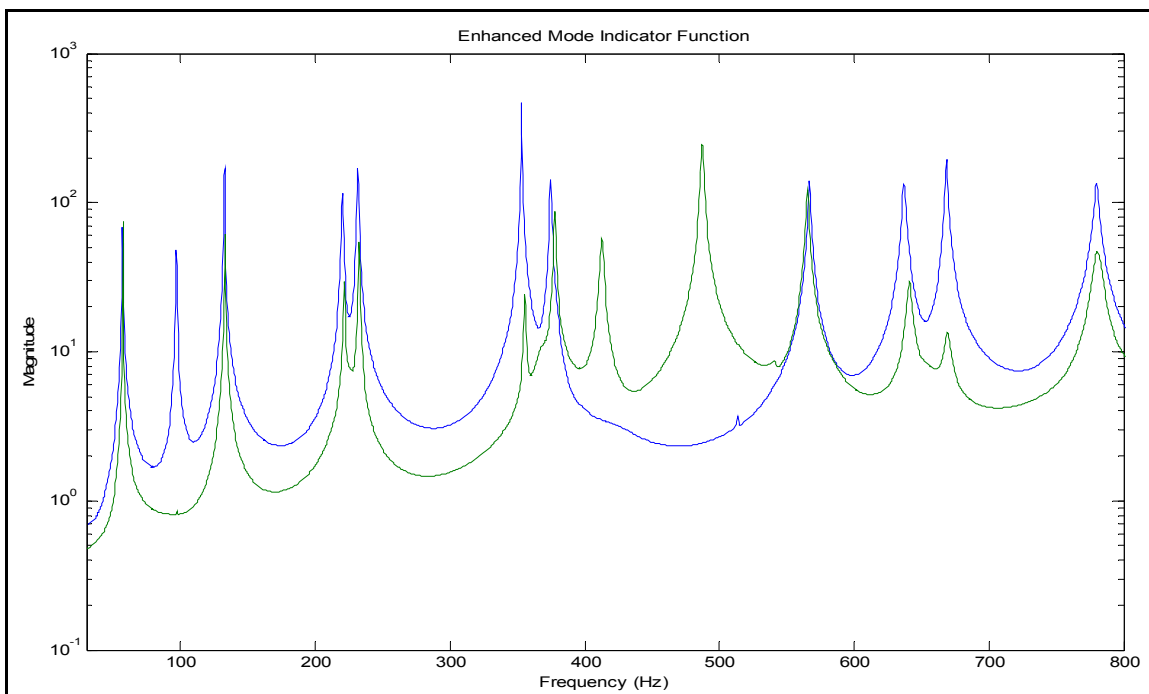


Figure 5.10 - CMIF of circular plate based on FRFs

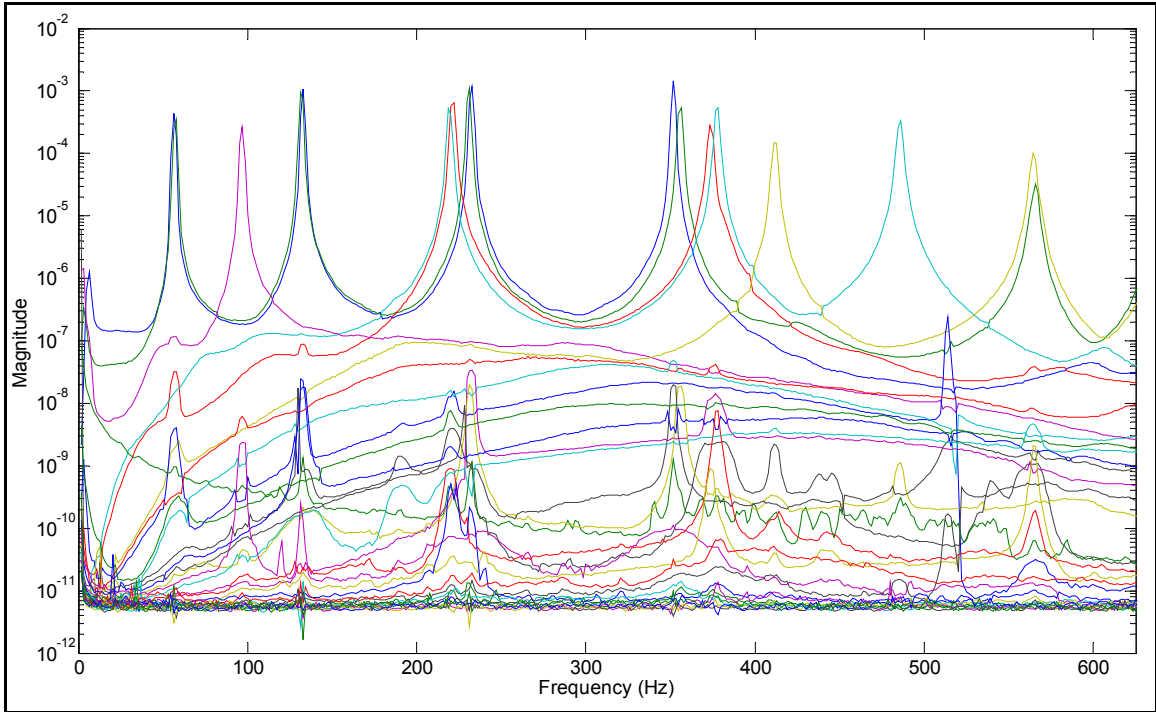


Figure 5.11 - CMIF of circular plate excited over one quarter of the surface

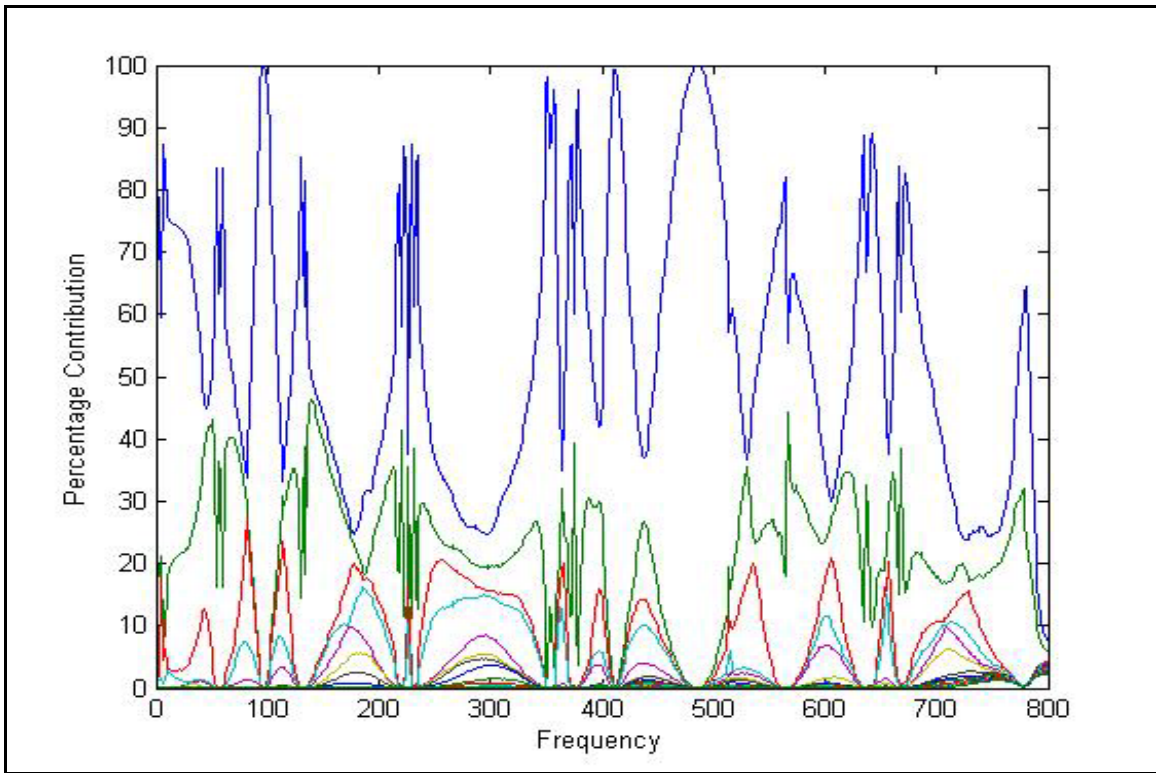


Figure 5.12 - SVPC plot for circular plate excited in one quarter

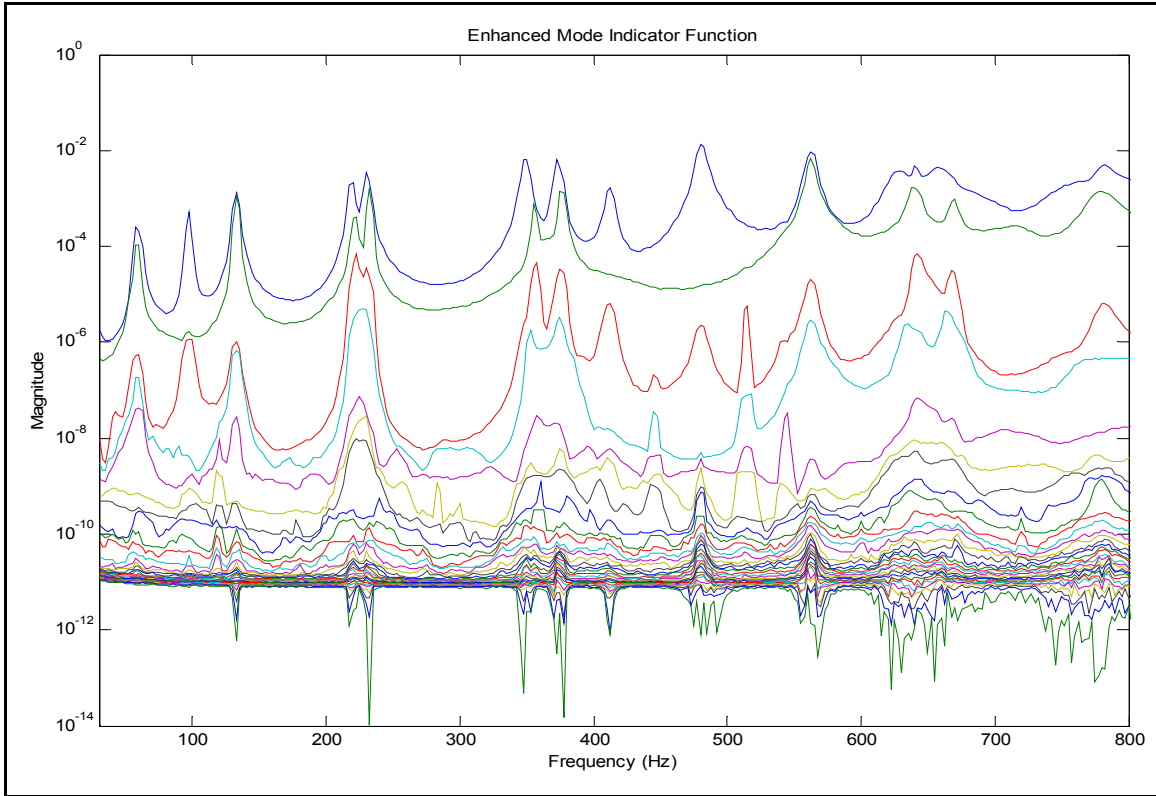


Figure 5.13 - CMIF of circular plate excited at two points

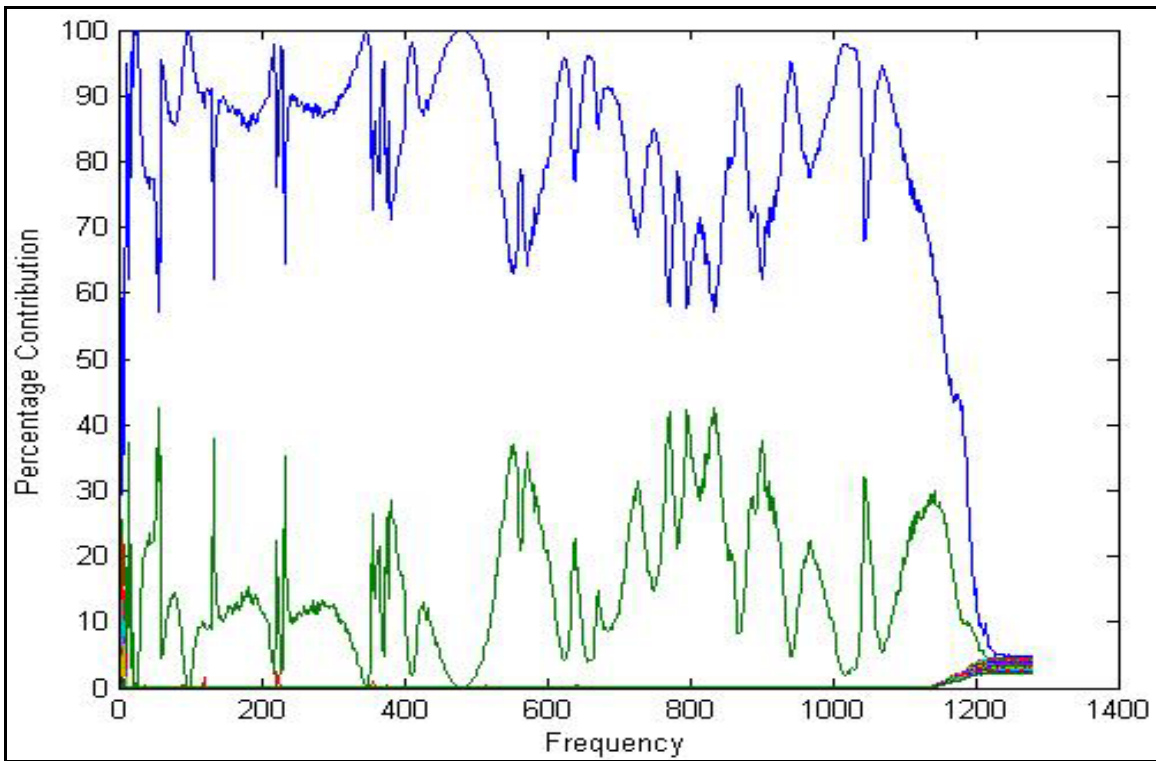


Figure 5.14 - SVPC plot for circular plate excited at two points

The results of the EMIF algorithm are shown in Table 5.3. The data used in this case corresponds to the first case where the plate is excited over its entire surface. The estimated modal parameters compare well with those obtained using the traditional FRF experimental modal analysis.

Table 5.3 - Modal parameters estimated using OMA-EMIF for lightly damped circular plate

Experimental Modal Analysis Estimation		Gxx Based EMIF Estimation	
Damp	Freq	Damp	Freq
1.427	56.496	1.365	56.43
1.094	56.946	1.368	57.29
0.713	96.542	1.112	96.69
0.466	131.882	0.699	131.79
0.44	132.709	0.652	132.75
0.377	219.543	0.481	219.33
0.445	220.92	0.532	221.38
0.371	231.224	0.423	230.87
0.287	232.126	0.416	232.45
0.224	352.433	0.265	351.65
0.242	354.893	0.344	355.79
0.265	374.492	0.371	373.92
0.285	376.813	0.335	377.51
0.443	412.487	0.363	411.75
0.269	486.16	0.322	485.39

5.4.3 H Frame Structure

The H-Shaped rectangular steel frame (H-Frame) shown in Figure 5.15 was excited first by using two electro-mechanical shakers with a band limited random excitation signal at two locations. The acceleration response at 58 locations was measured in the frequency range of 0-625Hz. The H-Frame system was then excited by impacting randomly over the entire structure. This excitation technique assured that the system was spatially well excited. Again, the response at 58 locations was measured. The cross-spectra between all output locations were calculated for both cases.

The cross-spectral matrix for the well excited case was then used to calculate the CMIF plot shown in Figure 5.16. This CMIF closely resembles the CMIF that would be calculated using a full FRF matrix for the same structure. However, when inspecting the CMIF created from the system excited at only two locations, as shown in Figure 5.18, it can be seen that it differs significantly from the previous example. The SVPC plots for the two cases (Figure 5.17, 5.19) better illustrate the spatial distribution of the excitation forces. As observed in the case of the analytical system and circular plate; the SVPC plots clearly indicate when the H-frame is being excited spatially uniformly (Figure 5.17 indicates that there are a lot of significant singular values at most frequencies) and when it is being excited locally (Figure 5.19 indicates that major contribution is from two significant singular values only).

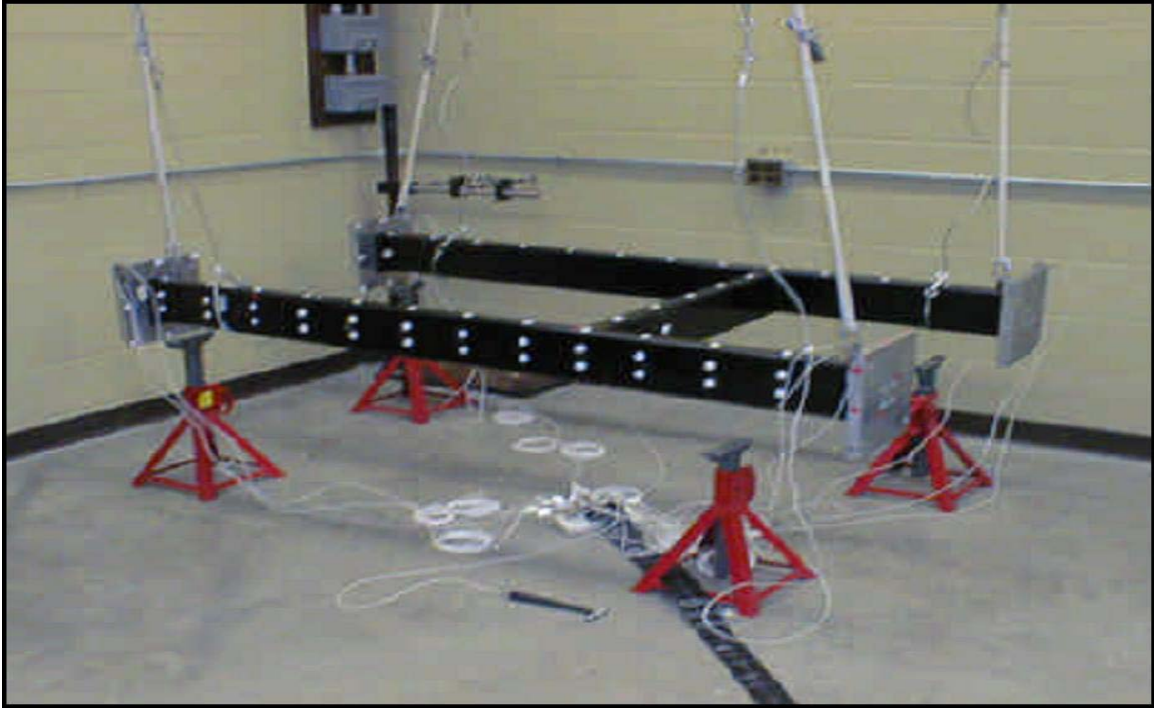


Figure 5.15 - H-Frame structure

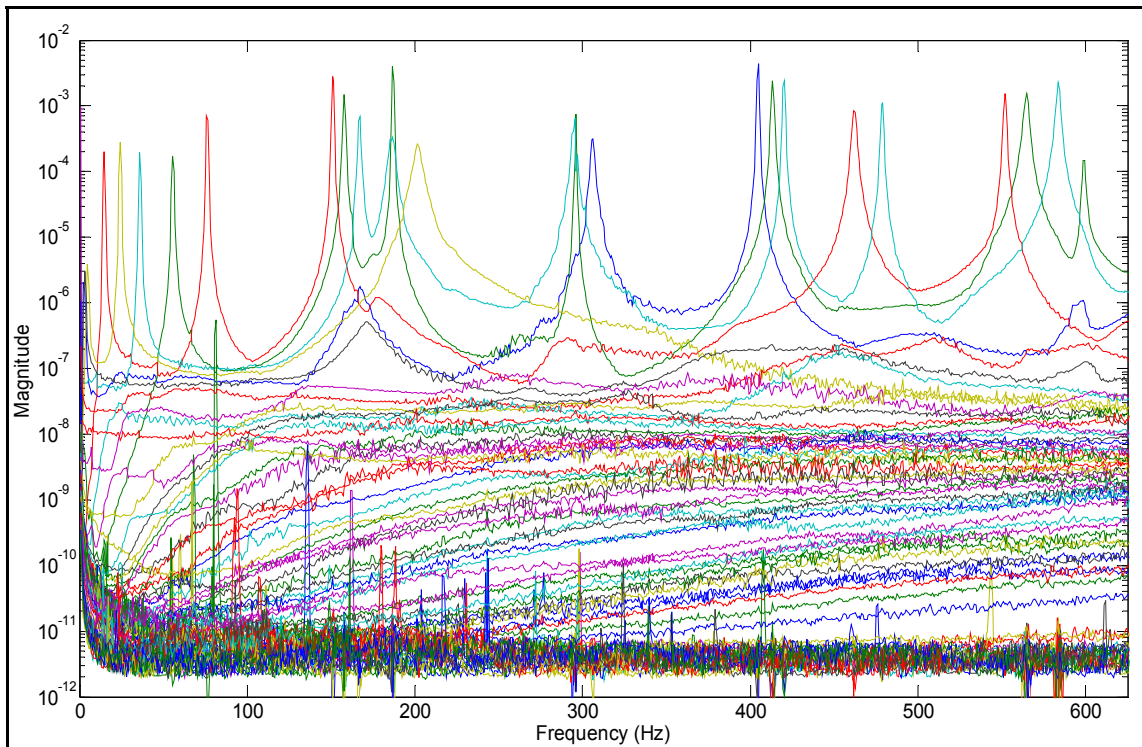


Figure 5.16 - CMIF of the spatially well excited H-Frame structure

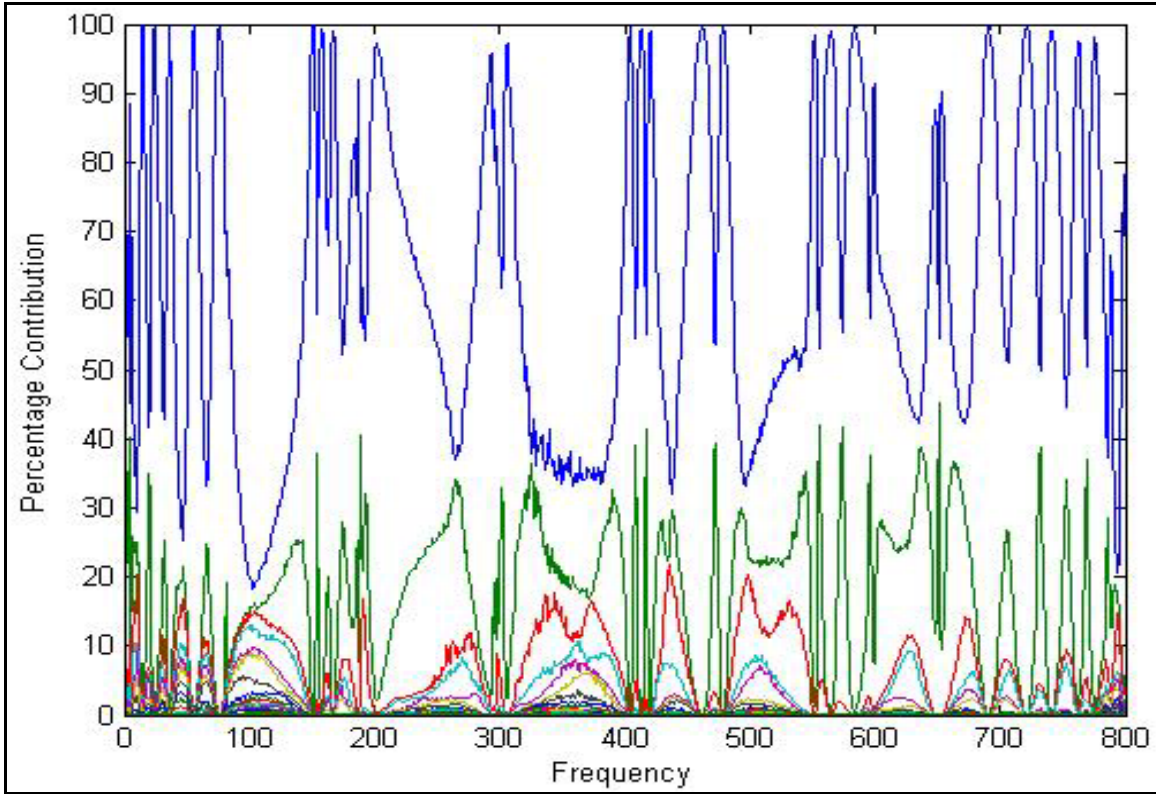


Figure 5.17 - SVPC plot for spatially well excited H-Frame

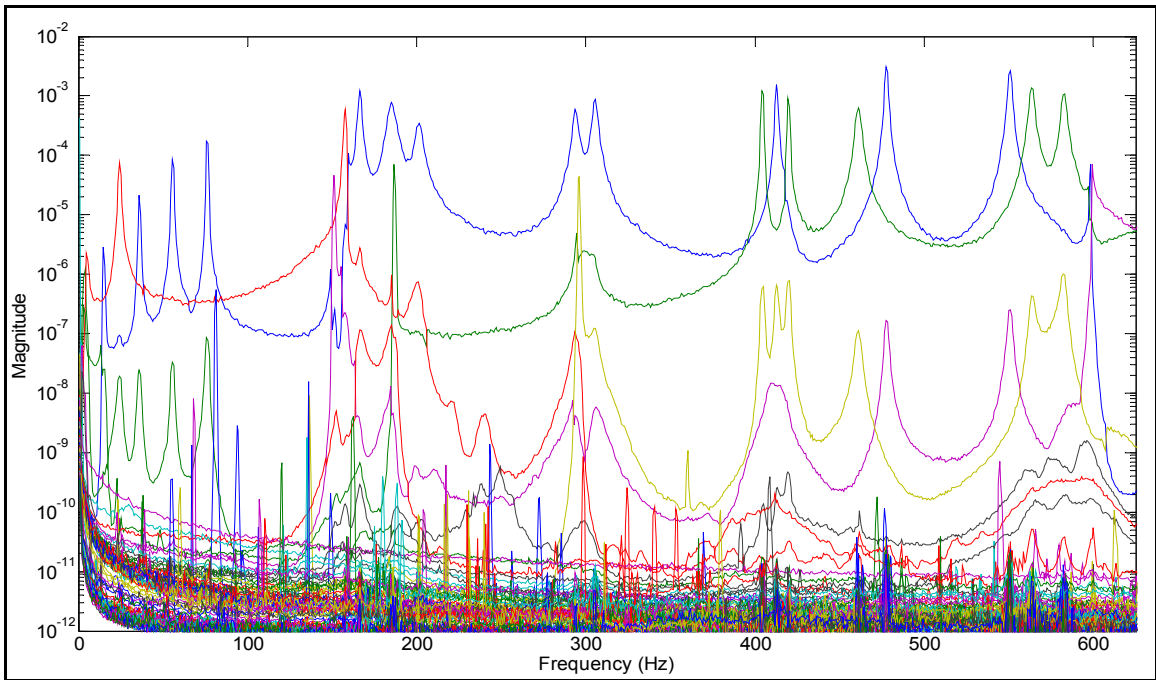


Figure 5.18 - CMIF of the H-Frame structure excited at two locations

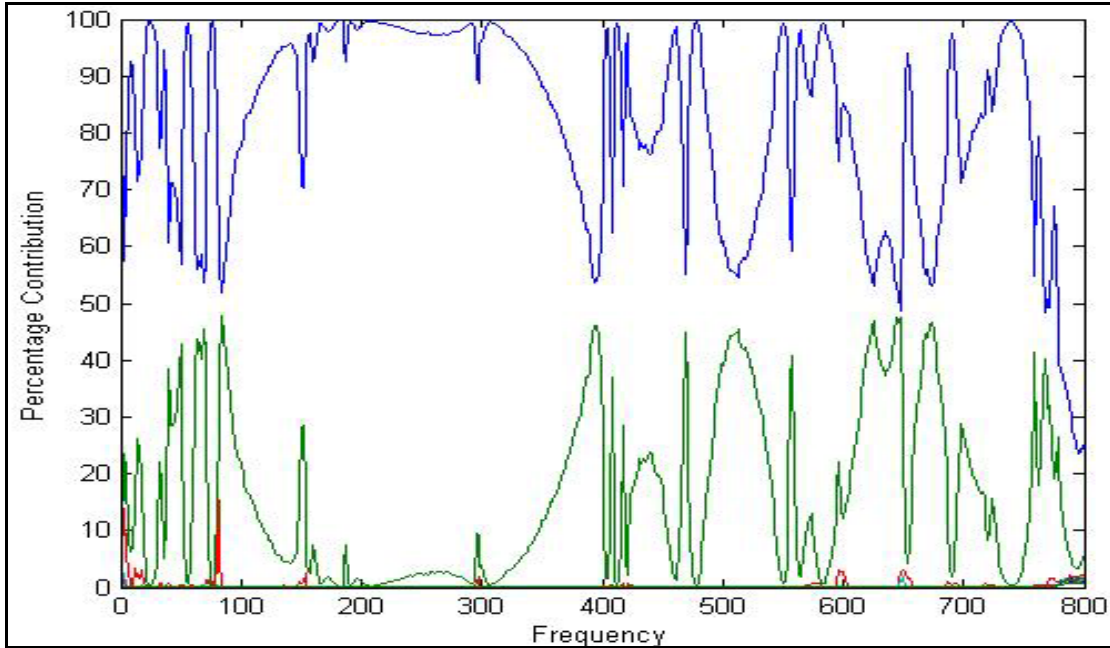


Figure 5.19 - SVPC plot for H-Frame excited at two points

Table 5.4 - Modal parameters estimated using OMA-EMIF for the H-Frame structure

Experimental Modal Analysis Estimation		Gxx Based EMIF Estimation	
Damp	Freq	Damp	Freq
1.931	15.035	3.96	15.013
1.03	24.174	4.48	24.267
0.856	36.112	0.013	35.747
0.79	55.729	1.413	55.734
0.411	76.165	1.127	75.879
0.253	151.349	0.119	150.408
0.353	157.83	0.695	157.588
0.422	166.828	0.755	166.463
1.038	185.888	1.838	184.269
0.187	186.671	0.442	186.252
1.023	201.716	1.26	201.314
0.578	294.066	0.542	293.686
0.484	305.472	0.606	305.334
0.108	404.394	0.195	404.226
0.159	413.021	0.247	412.697
0.129	419.93	0.222	419.744
0.339	461.706	0.429	461.039
0.124	478.475	0.291	477.607

The effectiveness of the proposed EMIF algorithm is demonstrated again in Table 5.4 as estimated modal parameters compare well with the corresponding EMA estimation.

5.5 Conclusions

In this chapter, a new approach for estimating modal parameters using the complex mode indicator functions based on output-only response power spectrums is developed. This technique, the *Enhanced Mode Indicator Function*, differs from the popular eFDD technique as it estimates the modal parameters in the frequency domain. One of the major advantages of estimating the modes in frequency domain is the ability to utilize residuals which helps in improving the results by taking into account the contribution of the out-of-band modes. The algorithm is shown to give good results by implementing it on analytical and experimental systems. Additionally, unlike eFDD approach, more than one mode can be estimated at a time.

Further, the second OMA assumption about the spatial distribution of the natural excitation force is explored in more detail. It is shown how the ability of CMIF based methods is limited when the system is not adequately excited spatially. Though such problems are not encountered while analyzing structures such as bridges and buildings (where forcing is uniform), in situations like automobiles on the road having narrow band point excitations (such as engine unbalance or other rotating unbalance), this can be a major problem as the resulting CMIF plot might not indicate the modes correctly. A tool based on contribution of singular values to total variance, *Singular Value Percentage Contribution* plot, is devised which helps in determining whether the system is being excited locally or spatially uniformly. This tool makes it possible to use the CMIF plot even in cases where the system is not spatially well excited.

The EMIF algorithm and SVPC plots are shown to perform very well on analytical and experimental systems, thus providing one more alternative of estimating modal parameters through Operational Modal Analysis techniques.

Chapter Six

Application of ICA/BSS Techniques to OMA

Independent Component Analysis (ICA) / Blind Source Separation (BSS) is an emerging research area in the field of signal processing. The goal of ICA / BSS techniques is to identify statistically independent and non-Gaussian sources from a linear mixture of such sources. It also extracts the unknown mixture matrix in the process. This Chapter explores the possibilities of utilizing the concept of ICA and BSS for the purpose of Operational Modal Analysis. Independent Component Analysis and other related problems such as Blind Source Separation (BSS), Blind Signal Extraction (BSE) and Multichannel Blind Deconvolution (MBD) share the same generalized blind signal processing problem where the aim is to estimate the original source signal and corresponding mixing matrix based only on the knowledge of mixed output signals. There are several good resources that explain the concept of ICA, BSS and other related problems including Cardoso, 1998; Lathauwer et al., 2000; Hyvarinen, Oja, 2000; Hyvarinen et al., 2001; and Cichocki, Amari, 2002. ICA based methods have found application in diverse areas such as biomedical signal analysis (EEG, MMG etc.), speech enhancement, image processing, wireless communication, etc. ICA based methods have also found application in structural dynamics related areas such as damage detection and fault diagnosis [Poyhonen, Jover, Hyotyniemi, 2003; Zang, Friswell, Imregun, 2004], rotating machinery vibration [Ypma, Pajunen, 1999] etc.

Recently, it was [Kerschen, Poncelet, Golinval, 2006; Poncelet, Kerschen, Golinval, 2006] shown that ICA can also be used for parameter estimation purposes.

Four different ICA algorithms namely, AMUSE [Tong, Soon et al., 1990], Second Order Blind Identification (SOBI) [Belouchrani, Abed-Meraim et al., 1993], Joint Approximate Diagonalization (JADE) [Cardoso, Souloumiac, 1996] and Fourth Order Blind Identification (FOBI) [Cardoso, 1991; Nandi, Zarzoso, 1996], are used in this study by applying them on a 15 degrees-of-freedom analytical system. These algorithms differ from each other on the basis of the optimizing techniques implemented and by utilization of second or higher order statistics. The modal parameters estimated using these methods are compared with true system parameters and also with one of the Operational Modal Analysis techniques.

6.1 Independent Component Analysis

Independent Component Analysis (ICA) or Blind Source Separation (BSS) can be seen as an extension to Principal Component Analysis (PCA) which aims at recovering the source signals from a set of observed, instantaneous linear mixtures (response data) without any *a priori* knowledge of the mixing system.

Mathematically, the ICA problem can be formulated as

$$\{x(t)\} = [A]\{s(t)\} \quad 6.1)$$

where $x(t)$ is a column vector of m output observations representing an instantaneous linear mixture of source signals $s(t)$ which is a column vector of n sources at time instant t . A is an $m \times n$ matrix referred to as “mixing system” or more commonly as the “mixing matrix”.

Although ICA and BSS techniques claim to identify both the source signals and the mixing matrices, they do so within certain indeterminacies that include arbitrary scaling, permutation and delay of estimated source signals. However, in spite of these limitations the waveform of the original signal is recovered and, in many applications, knowledge of source waveform is the most relevant information.

The task of estimating both s and A , the two unknowns in the above mentioned problem requires certain assumptions to be made about the statistical properties of the sources s_i . ICA assumes that the sources s_i are statistically independent and that they have non-Gaussian distribution. A detailed discussion of the subject of ICA is beyond the scope of this chapter; interested readers can refer to the sources mentioned previously for general introduction and details of the various aspects of ICA. In addition to these resources, readers can also refer to the special issue on ICA and BSS published by *Mechanical Systems and Signal Processing* in 2005.

6.1.1 ICA / BSS Algorithms

A wide variety of ICA algorithms are available in the literature [Hyvarinen, Oja, 2000; Hyvarinen et al., 2001; and Cichocki, Amari, 2002]. These algorithms differ from each other on the basis of the choice of objective function and selected optimization scheme. Although the assumption about statistical independence requires the sources to be non-Gaussian in order to utilize the higher-order statistics (HOS) based BSS methods, several second-order statistics (SOS) based techniques are also available. SOS methods exploit weaker conditions for separating the sources assuming that they have a temporal structure with different autocorrelation functions (or power spectra).

In this section, four ICA / BSS methodologies are briefly discussed.

Algorithm for Multiple Unknown Signals Extraction (AMUSE)

SOS based algorithms like AMUSE assume that:

1. The mixing matrix A is of full column rank.
2. Sources are spatially uncorrelated with different autocorrelation functions but are temporally correlated (colored) stochastic signals with zero-mean.
3. Sources are stationary signals and / or second order non-stationary signals i.e. their variances are time varying.

The AMUSE algorithm is outlined below:

1. Estimate the covariance (mean removed correlation) matrix of the output observations

$$\hat{R}_x(0) = \frac{1}{N} \sum_{k=1}^N x(k)x^T(k) \quad 6.2)$$

where $\hat{R}_x(0)$ is the covariance matrix at zero time lag and N is the total number of time samples taken.

2. Compute EVD (or SVD) of $\hat{R}_x(0)$

$$\hat{R}_x(0) = U_x \Sigma_x V_x^T = V_x \Lambda_x V_x^T = V_s \Lambda_s V_s^T + V_N \Lambda_N V_N^T \quad 6.3)$$

where V_s is $m \times n$ matrix of eigenvectors associated with n principal eigenvalues of $\Lambda_s = \text{diag}\{\lambda_1, \lambda_2, \dots, \lambda_n\}$ in descending order. V_N is $m \times (m-n)$ matrix containing the $(m-n)$ noise eigenvectors associated with noise eigenvalues $\Lambda_n = \text{diag}\{\lambda_{n+1}, \lambda_{n+2}, \dots, \lambda_m\}$. The number of sources n are thus estimated based on the n most significant eigenvalues (or singular values in case of SVD).

3. Perform pre-whitening transformation

$$\bar{x}(k) = \Lambda_s^{-1/2} V_s^T x(k) = Qx(k) \quad 6.4)$$

4. Estimate the covariance matrix of the vector $\bar{x}(k)$ for specific time lag other than $p=0$ (say $p=1$). Perform SVD on the estimated covariance matrix.

$$\hat{R}_{\bar{x}}(p) = \frac{1}{N} \sum_{k=1}^N \bar{x}(k) \bar{x}^T(k-p) = U_{\bar{x}} \Sigma_{\bar{x}} V_{\bar{x}}^T \quad 6.5)$$

5. The mixing matrix and source signals can now be estimated as

$$\hat{A} = Q^+ U_{\bar{x}} = V_s \Lambda_s^{1/2} U_{\bar{x}} \quad 6.6)$$

$$y(k) = \hat{s}(k) = U_{\bar{x}}^T \bar{x}(k) \quad 6.7)$$

AMUSE performs well for colored sources with different power spectra shapes which means that the eigenvalues of the time-delayed covariance matrix are distinct. The accuracy of AMUSE however deteriorates in presence of additive noise.

Fourth Order Blind Identification Algorithm (FOBI)

FOBI is an extension of the AMUSE algorithm which uses contracted quadricovariance matrices instead of covariance matrices. This technique is aimed at separating independent non-Gaussian source signals. The quadricovariance matrices are defined as

$$\begin{aligned}
C_{\bar{x}}(\mathbf{E}) &= C_{\bar{x}} \{ \bar{x}^T(k) \mathbf{E} \bar{x}(k) \bar{x}(k) \bar{x}^T(k) \} \\
&= E \{ \bar{x}^T(k) \mathbf{E} \bar{x}(k) \bar{x}(k) \bar{x}^T(k) \} - R_{\bar{x}}(0) \mathbf{E} R_{\bar{x}}(0) - \text{tr}(\mathbf{E} R_{\bar{x}}(0)) R_{\bar{x}}(0) - R_{\bar{x}}(0) \mathbf{E}^T R_{\bar{x}}(0)
\end{aligned} \tag{6.8}$$

where $R_{\bar{x}}(0) = E \{ \bar{x}(k) \bar{x}^T(k) \}$ and \mathbf{E} is an $m \times n$ freely chosen matrix called eigenmatrix (typically $\mathbf{E} = \mathbf{I}_n$ or $\mathbf{E} = \mathbf{e}_q \mathbf{e}_q^T$, where \mathbf{e}_q are vectors of some unitary matrix).

The eigenvalue decomposition of the quadricovariance matrix is of the following form

$$C_{\bar{x}}(\mathbf{E}) = U \Lambda_{\mathbf{E}} U^T \tag{6.9}$$

with $\Lambda_{\mathbf{E}} = \text{diag}(\lambda_1 u_1^T \mathbf{E} u_1, \dots, \lambda_n u_n^T \mathbf{E} u_n)$, $\lambda_i = \kappa_4(s_i) = E \{ s_i^4 \} - 3E^2 \{ s_i^2 \}$ is the kurtosis of the zero-mean i^{th} source and u_i is the i -th column of the orthogonal eigenvector matrix U .

The main advantage of the FOBI algorithm is that it is insensitive to arbitrary Gaussian noise and that it allows the mixing system to be identified when sources are i.i.d. and mutually independent. However, it should be noted that quadricovariance matrices require many more time samples for correct estimates in comparison to covariance matrices. FOBI also has a restriction that it only works for sources having different kurtosis; thus it will not give good results in cases where sources have identical distributions.

Second Order Blind Identification (SOBI)

SOBI algorithm utilizes the joint diagonalization procedure [Cichoki, Amari, 2002; Cardoso, Souloumiac, 1996; Hori, 2000] unlike AMUSE and FOBI which use EVD / SVD techniques. SOBI works well for simple colored sources with distinct power spectra (or

distinct autocorrelation functions). Like AMUSE, it operates on time delayed covariance matrices.

SOBI utilizes the pre-whitening transformation similar to that described in case of AMUSE. This is followed by estimation of set of covariance matrices for a preselected set of time lags (p_1, p_2, \dots, p_L)

$$\hat{R}_{\bar{x}}(p_i) = \frac{1}{N} \sum_{k=1}^N \bar{x}(k) \bar{x}^T(k - p_i) = Q \hat{R}_x(p_i) Q^T \quad 6.10)$$

Joint approximate diagonalization (JAD) is performed on the above matrices; $R_{\bar{x}}(p_i) = U D_i U^T$, to estimate the orthogonal matrix U that diagonalizes a set of covariance matrices. Several efficient algorithms are available for this purpose including Jacobi techniques, Alternating Least Squares, Parallel Factor Analysis etc. [Cardoso, Souloumiac, 1996; Hori, 2000]. Finally the sources and signals can be estimated using the same equations as explained earlier with AMUSE.

It should be noted that $D_i(p_i)$ is a diagonal matrix that has distinct diagonal entries. However, it is difficult to determine a priori a single time lag p at which the above criterion is satisfied. Joint diagonalization procedure avoids this difficulty by providing an optimum solution considering a number of time lags.

Joint Approximate Diagonalization of Eigenmatrices (JADE)

JADE [Cardoso, Souloumiac, 1993] can be considered as an extension of SOBI and FOBI algorithms. Like FOBI, JADE works on the contacted quadricovariance matrices but instead of employing EVD / SVD it jointly diagonalizes a set of such matrices just like SOBI. The aim of JADE is to estimate an orthogonal matrix U which diagonalizes a set of quadricovariance matrices. JADE is a mathematically intensive algorithm and the

complete explanation is beyond the scope of this chapter. Interested readers can refer the above mentioned references for more details.

6.2 ICA and BSS in Vibrations

Due to the tremendous potential of ICA / BSS techniques, it is not a surprise that the research community in the area of vibrations have also started looking at utilizing the techniques for a variety of purposes. In [Ypma, Pajunen, 1999], second order ICA techniques were utilized for rotating machinery vibration analysis. ICA of vibration signals was also used for fault diagnosis of an induction motor [Poyhonen, Jover, Hyotyniemi, 2003]. ICA was used along with Artificial Neural Network (ANN) for data reduction purposes while detecting structural damage [Zang, Friswell, Imregun, 2004]. However in spite of their tremendous potential, use of ICA and BSS techniques in vibration and related areas has been slow in comparison to some of the other areas. Antoni has discussed the issues associated with application of ICA / BSS techniques for vibration signals in detail [Antoni, 2005]. One of the major issues with the application of ICA / BSS techniques to vibrations, particularly structural identification related applications, is the fact that vibrating systems are dynamic or convolutive in nature as opposed to static (instantaneous linear) mixtures for which the ICA / BSS theory is originally designed. One obvious way to tackle the convolutive mixtures is to deal with them in the frequency domain as convolution in the time domain is equivalent to multiplication in the frequency domain. However, there are two other problems which are inherent to ICA / BSS techniques; 1) scaling of sources and 2) the order in which they are identified, often referred as 'permutation problem'. This is the same problem encountered in estimating partial coherence and/or conditioned partial coherence over 20 years ago with respect to partially dependent sources in acoustics (general MIMO problem) and in multiple input excitation problems in structural dynamics (MIMO-FRF

estimation). In the case of frequency domain ICA / BSS, these two problems become much more severe as they now become a function of each frequency bin. Frequency domain ICA / BSS is a topic of ongoing research efforts [Smaragdis, 1998; Dapena, Serviere, 2001; Rahbar, Reilly, 2001; Joho, Rahbar, 2002]. Most of these algorithms were based on the fact that convolved mixing in the time domain corresponds to instantaneous mixing in the frequency domain. The work done in this aspect deals with handling of the scaling and permutation problems. However, no significant success has been achieved so far in this aspect and research is still going on.

6.2.1 ICA / BSS Techniques for Operational Modal Analysis

Operational Modal Analysis is an emerging technique in the field of modal analysis where dynamic characteristics of a system are identified based only on the output responses. Since, by definition, ICA / BSS techniques work only on system outputs to identify either the sources or the system (mixing matrix) without any a priori (or very little) information about them, it is logical to believe that these techniques can also be used for OMA purposes. Recently, it was shown how ICA / BSS techniques can be utilized for the purpose of modal analysis [Kerschen, Poncelet, Golinval, 2006; Poncelet, Kerschen, Golinval, 2006; Randall, Holley, 2006].

The basic fundamentals behind the application of ICA / BSS techniques to modal analysis goes back to the concept of the expansion theorem [Meirovitch, 1967] and modal filters [Shelly, 1991; Shelly, Allemang, 1992; Shelly, Allemang et al., 1993]. According to the expansion theorem, the response of a distributed parameter structure can be expressed as

$$\{x(t)\} = \sum_{r=1}^{\infty} [\phi_r] \{\eta_r(t)\} \quad 6.11)$$

where Φ_r are the modal vectors weighted by the modal coordinates η_r . For real systems, however, the response of the system can be represented as a finite sum of modal vectors weighted by the modal coordinates. To obtain a particular modal coordinate η_i from response vector x , a modal filter vector ψ_i is required such that

$$\{\psi_i\}^T \{\phi_i\} = 0, \text{ for } i \neq j \quad 6.12)$$

and

$$\{\psi_i\}^T \{\phi_i\} \neq 0, \text{ for } i = j \quad 6.13)$$

so that

$$\{\psi_i\}^T \{x(t)\} = \{\psi_i\}^T \sum_{r=1}^N [\phi_r] \{\eta_r(t)\} \quad 6.14)$$

or

$$= \{\psi_i\}^T \{\phi_i\} \{\eta_i\} \quad 6.15)$$

Thus the modal filter performs a coordinate transformation from physical to modal coordinates. Multiplying the system response x with modal filter matrix ψ^T results in uncoupling of the system response into single degree of freedom (SDOF) modal coordinate responses (η).

In order for ψ_i to exist, the associated modal vector ϕ_i must be linearly independent with respect to all other modal vectors [Shelly, 1991]. This is also the reason why ICA / BSS

based techniques can be utilized for the purpose of decomposing the output system response into a product of modal vectors and corresponding modal coordinate responses. Also, a modal filter vector is unique if and only if the number of sensors used for the modal filter implementation is equal to or greater than the number of linearly independent modal vectors contributing to the system response.

In the past, SDOF modal coordinate responses have been obtained by utilizing modal filters calculated using FRF based data. The ICA / BSS based techniques differ from this approach in the sense that they directly work on output system response to obtain the modal coordinate responses (η). This approach is similar to that in [Kerschen, Poncelet, Golinval, 2006; Poncelet, Kerschen, Golinval, 2006] where modal coordinates are treated as virtual sources.

In the following section, four different ICA algorithms as described in Section 6.1.1 are applied to a 15 degrees of freedom system.

6.3 Analytical 15 Degree of Freedom System

Figure 6.1 shows the 15 degree of freedom system which was previously introduced in Chapter 4. The system is excited at all 15 degrees of freedom by means of a white random uncorrelated set of inputs. The chosen system has some closely spaced modes (around 53 Hz), some modes that are lightly damped, other modes that are moderately damped and also some local modes that are well separated from each other. This makes it a good system to investigate the various ICA / BSS algorithms described in Section 6.1.1.

Figure 6.2-6.5 show the plot of the auto-power spectrums of the modal coordinate responses (η) obtained using various algorithms. The Second Order Statistics (SOS)

based algorithms, AMUSE and SOBI, uncouple the system response into SDOF modal coordinate responses. However, both Higher Order Statistics (HOS) based methods, JADE and FOBI, fail to successfully separate the response into corresponding modal coordinate response. Possible reasons for the inferior behavior of the HOS based methods can be that quadricovariance matrices are not correctly estimated and also the fact that SOS based methods better exploit the temporal coherence (uniqueness of autopower spectra) of various modal coordinate responses.

Modal parameters obtained using the SDOF response based on AMUSE and SOBI are listed in Table 6.1 and are compared with true analytical modes of the system and also with the results obtained using OMA-EMIF algorithm which was described in Chapter 5. Though the frequency estimates using AMUSE and SOBI are close to the true modes in comparison to the OMA-EMIF algorithm, damping is overestimated for all the modes. However, overall results are satisfactory. Further, Figures 6.6-6.9 show, the modal assurance criterion (MAC) plots for comparing the modal vectors obtained using various methods. The modal vectors obtained using AMUSE and SOBI are in good agreement with each other. However the MAC values are not that high when modal vectors obtained using AMUSE are compared with true modes or OMA-EMIF results. The high MAC values for true and OMA-EMIF modal vectors indicate that the OMA-EMIF method is able to extract the modal vectors of the system better in comparison to the ICA techniques.

Note that using AMUSE or SOBI, the modes are obtained in a random order. Also, the repeated modes around 53.3 Hz have interchanged when estimated using OMA-EMIF algorithm.

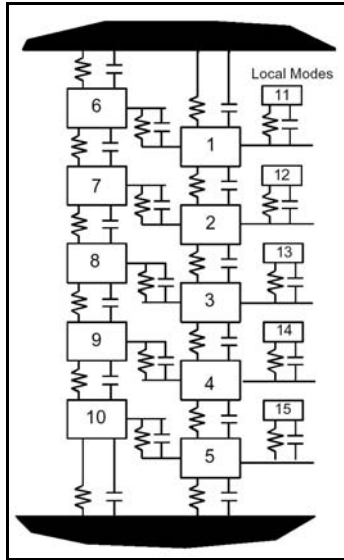


Figure 6.1: Analytical 15 degree of freedom system

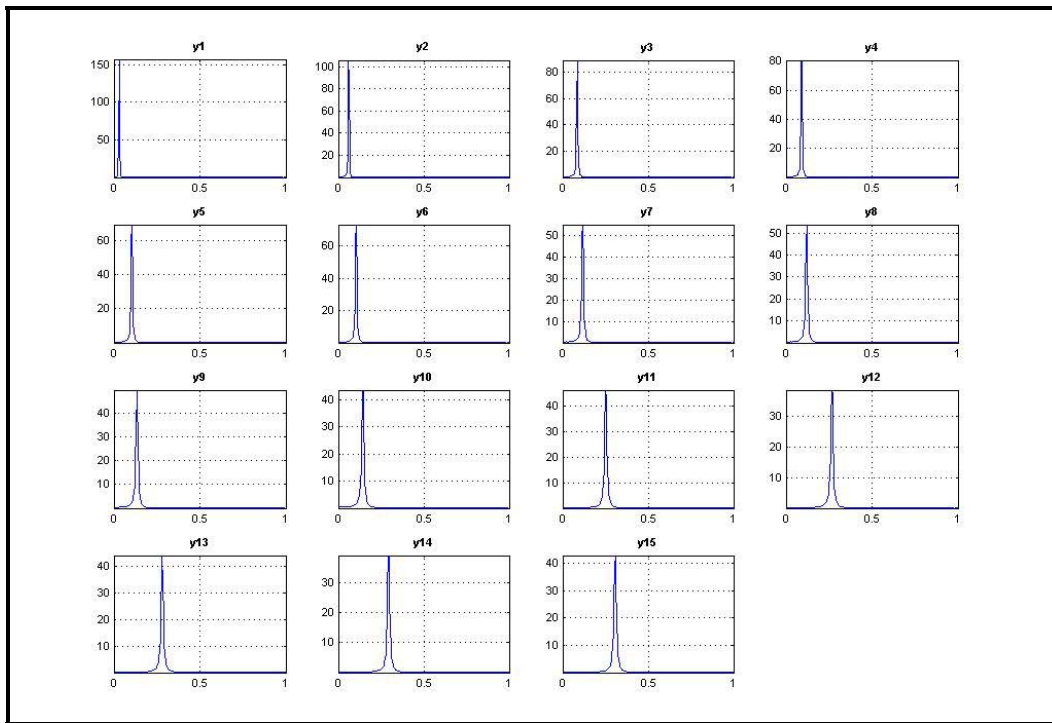


Figure 6.2: Power spectrum of modal coordinate responses obtained using AMUSE

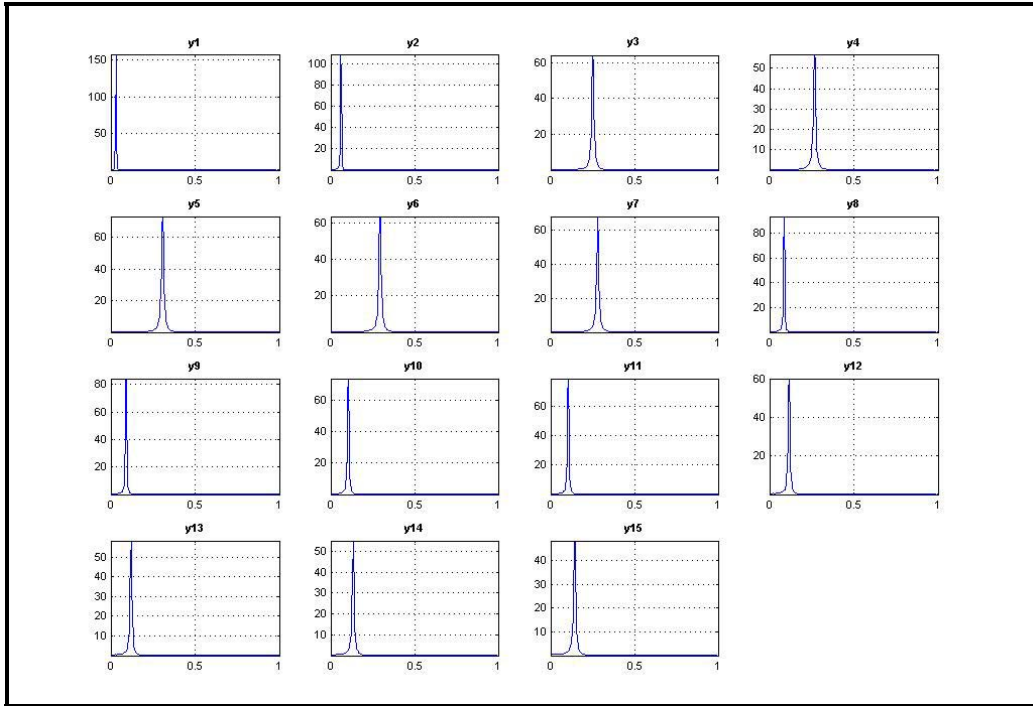


Figure 6.3: Power spectrum of modal coordinate responses obtained using SOBI

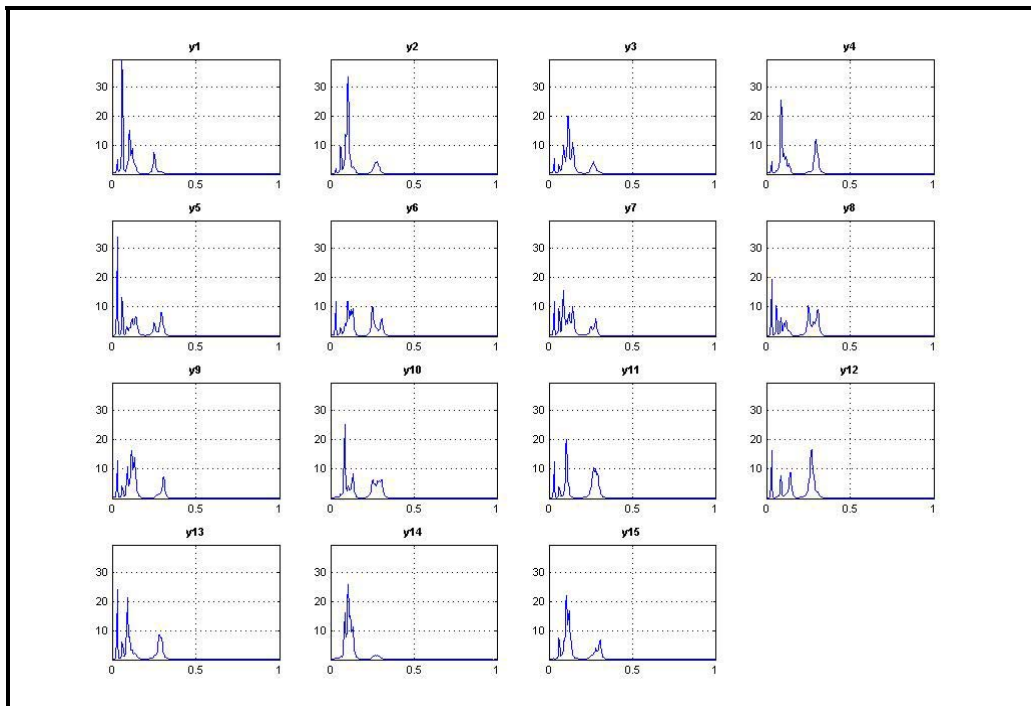


Figure 6.4: Power spectrum of modal coordinate responses obtained using FOBI

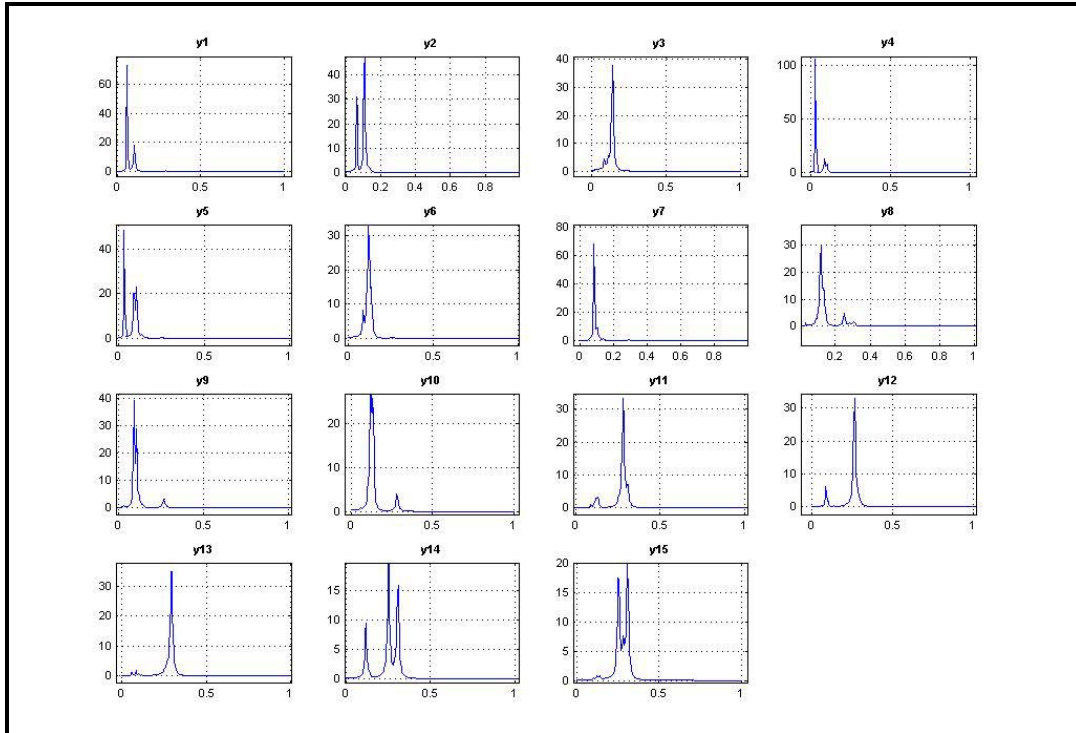


Figure 6.5: Power spectrum of modal coordinate responses obtained using JADE

Table 6.1: Comparison of modal parameter estimates using ICA techniques and OMA-EMIF

True Modes		OMA-EMIF		ICA - AMUSE		ICA - SOBI	
Damp	Freq	Damp	Freq	Damp	Freq	Damp	Freq
1.0042	15.985	3.3289	15.9857	2.1133	15.9774	2.2314	15.9806
1.9372	30.858	2.8564	30.8619	2.4042	30.8709	2.4123	30.8725
2.7347	43.6	3.2718	43.6932	3.1196	43.6511	3.1441	43.6543
2.9122	46.444	3.6481	46.5883	3.4458	46.4035	3.4787	46.4059
3.3375	53.317	4.0763	53.7487	3.7103	53.3869	3.8181	53.4067
3.3454	53.391	4.7860	53.7683	3.5785	53.4237	3.6199	53.4271
3.7145	59.413	3.6833	59.1164	4.1244	59.4877	4.2735	59.5196
3.858	61.624	3.6157	61.3713	4.3618	61.6476	4.4495	61.6577
4.2978	68.811	4.1523	68.2375	4.5887	68.9075	4.7218	68.9299
4.5925	73.63	4.4249	73.1519	4.8149	73.7923	4.9619	73.8233
2.6093	128.84	2.6146	128.5604	2.710	128.9026	2.7803	128.9105
2.4548	136.55	2.6030	136.4652	2.5743	136.6159	2.6264	136.6253
2.3288	143.86	2.4513	143.8957	2.4323	143.9370	2.4734	143.9487
2.221	150.83	2.3207	150.8782	2.3162	150.9051	2.3589	150.9175
2.122	157.47	2.0669	157.7820	2.2087	157.54	2.2391	157.5533

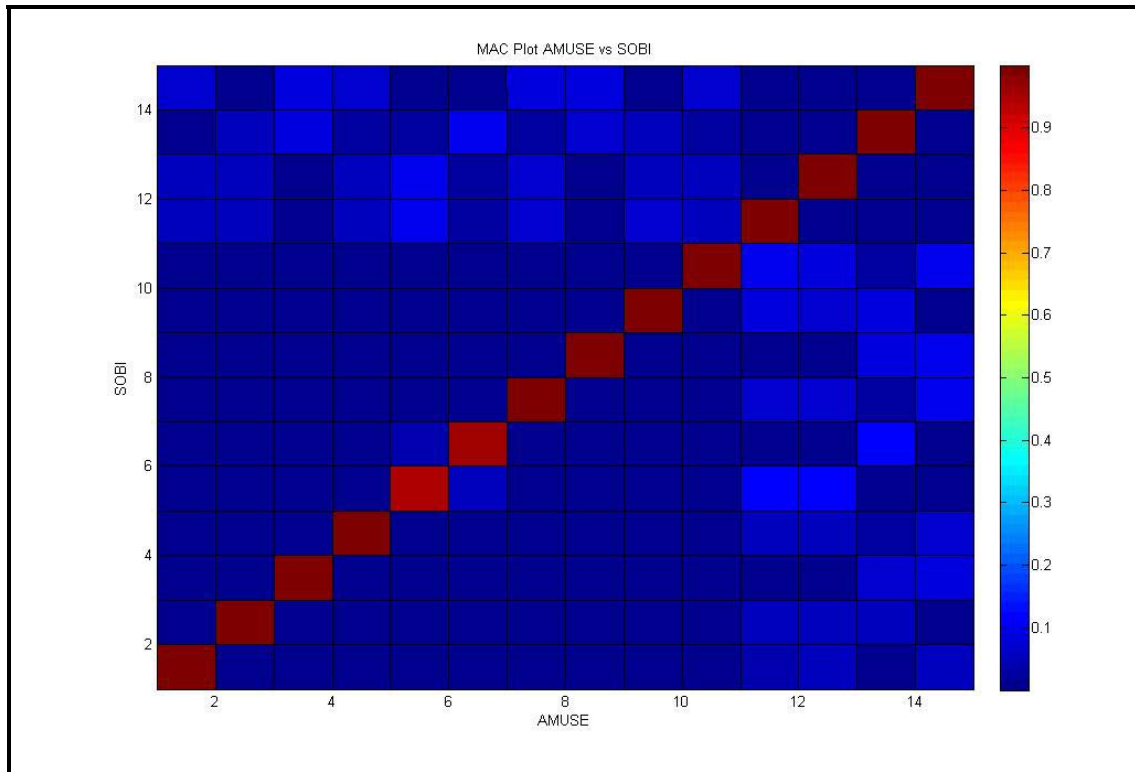


Figure 6.6: MAC comparison plot - AMUSE / SOBI

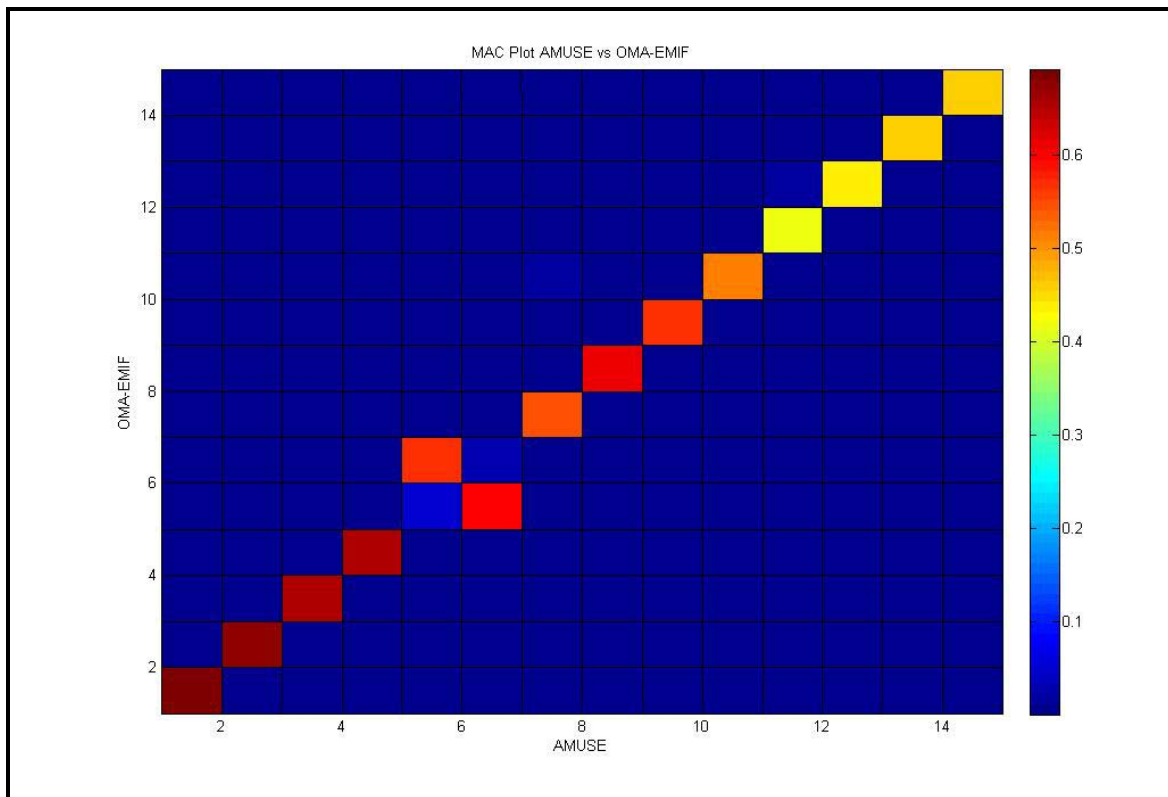


Figure 6.7: MAC comparison plot - AMUSE / OMA-EMIF

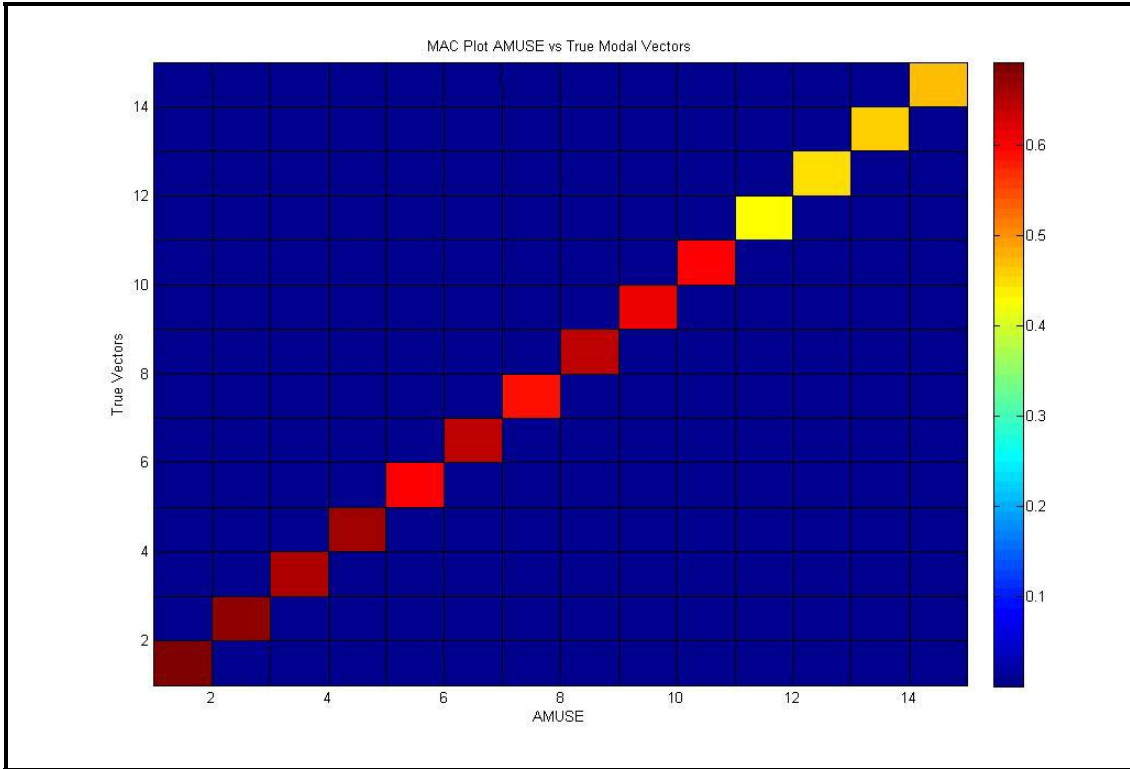


Figure 6.8: MAC comparison plot - AMUSE / True Modes

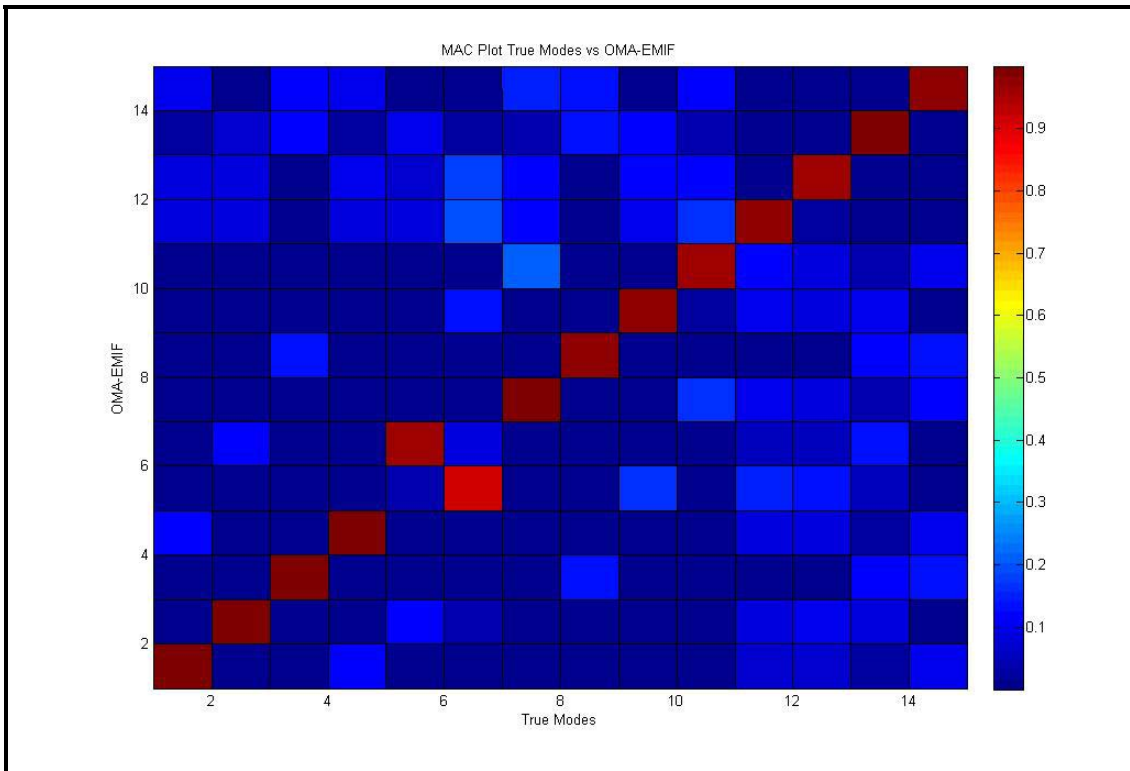


Figure 6.9: MAC comparison plot - True Modes / OMA-EMIF

6.4 Conclusions

Four popular ICA / BSS techniques are discussed along with an introduction to the general concept of independent component analysis (ICA) and blind source separation (BSS). These techniques can be related to the concept of modal filtering and the modal expansion theorem in order to utilize them for output-only modal parameter estimation. The studies conducted on an analytical system reveal that second order statistics based ICA / BSS algorithms give better results in comparison to the higher order statistics based algorithms. Though ICA / BSS based results are not as good as general OMA algorithms based results, it is still an interesting area to explore considering the simplicity of the method and its ability to extract all modal parameters (modal frequencies and mode shapes) in one step. These algorithms are comparatively less time consuming and do not require use of such tools as consistency diagrams.

Chapter Seven

Damping Estimation Using OMA Techniques

Due to the unavailability of input force information in OMA, certain assumptions are made when applying these techniques for modal parameter estimation. These assumptions are primarily about the nature of the input forces which are considered to be random and uncorrelated. Further, the forcing functions are assumed to be uniformly distributed in a spatial sense. For accurate estimates of the modal parameters, it is crucial that these assumptions be as true as possible. Further, the power spectra (analogous to FRFs in EMA) should be estimated accurately and free from random and bias errors for accurate modal parameter estimation. Several signal processing techniques such as the Welch periodogram, correlogram etc. [Kay, 1988; Oppenheim, Schafer, 1989; Stoica, Moses, 1997] are available that are commonly used for computing the power spectra.

This Chapter focuses on the damping estimation from OMA techniques, which has been a contentious issue with no accepted rationale. It has been observed that even though modal frequencies are well estimated using Operational Modal Analysis (OMA) techniques, damping estimation is not as accurate and often the errors are significant [Avitable, 2006]. This Chapter attempts to identify the causes for the damping inaccuracy and assess the currently available signal processing techniques for correcting this

problem. Thus, emphasis is laid on studying the OMA procedure, data processing and modal parameter estimation with respect to proper damping estimation.

An analytical 5 Degree of Freedom system used for this study is described in the next section. This is followed by the theoretical background on Cyclic Averaging as this signal processing is shown to reduce leakage errors resulting in better estimates for damping in FRF applications. Finally, the effects of Cyclic Averaging and partially correlated forces on damping estimation are discussed by means of observed results.

7.1 Analytical 5 DOF System

A simple 5 degree of freedom with following [M], [C] and [K] matrices is used in this study.

$$M = \begin{bmatrix} 250 & 0 & 0 & 0 & 0 \\ 0 & 350 & 0 & 0 & 0 \\ 0 & 0 & 30 & 0 & 0 \\ 0 & 0 & 0 & 450 & 0 \\ 0 & 0 & 0 & 0 & 50 \end{bmatrix} \quad C = \begin{bmatrix} 3250 & -250 & 0 & 0 & 0 \\ -250 & 450 & -200 & 0 & 0 \\ 0 & -200 & 320 & -120 & 0 \\ 0 & 0 & -120 & 190 & -70 \\ 0 & 0 & 0 & -70 & 270 \end{bmatrix}$$

$$K = 1000 \times \begin{bmatrix} 9000 & -5000 & 0 & 0 & 0 \\ -5000 & 11000 & -6000 & 0 & 0 \\ 0 & -6000 & 12500 & -6500 & 0 \\ 0 & 0 & -6500 & 14500 & -8000 \\ 0 & 0 & 0 & 0 & 15000 \end{bmatrix}$$

Table 7.1 and 7.2 show the frequency, damping and modal matrix of the system

Table 7.1: Modal frequencies and damping of the 15 DOF analytical system

Frequency	Damping (% Critical)
12.5263	1.1486
22.083	1.0589
34.8635	2.172
88.5238	0.4872
104.7787	0.8473

Table 7.2: Modal Matrix of the 15 DOF analytical system

Freq/DOF	12.52 Hz	22.08 Hz	34.86 Hz	88.52 Hz	104.77 Hz
1	1 + 0i	1 + 0i	1 + 0i	1 + 0i	1 + 0i
2	1.489 + 0.038i	0.837 + 0.064i	-0.601 + 0.045i	-13.655 + 0.591i	-19.855 + 0.717i
3	1.360 + 0.046i	-0.238 + 0.029i	-0.249 + 0.013i	220.441 - 11.856i	464.647 - 19.555i
4	1.201 + 0.051i	-1.209 - 0.006i	0.132 - 0.016i	121.877 - 4.464i	-17.659 + 0.872i
5	0.654 + 0.027i	-0.689 - 0.004i	0.084 - 0.010i	-2079.587 + 68.451i	21.140 - 1.517i

The system is excited by means of a white random uncorrelated set of inputs at all 5 degrees of freedom. Figure 7.1 shows typical auto-power (1-1) and cross-power (1-2) spectra of the input forces. It can be observed that the forces are not entirely uncorrelated as the cross-power spectrum is only one order less in magnitude in comparison to the auto-power spectrum. That the forces are uncorrelated is also shown by means of the virtual forces (or the principal components of the force power spectra matrix) in Figure 7.2.

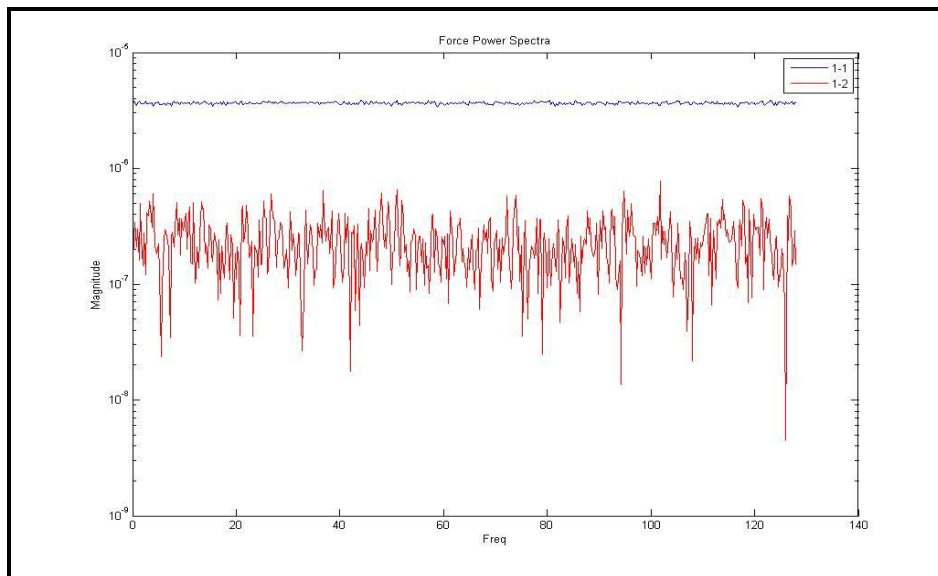


Figure 7.1: Input force power spectra comparison (5 DOF analytical system)

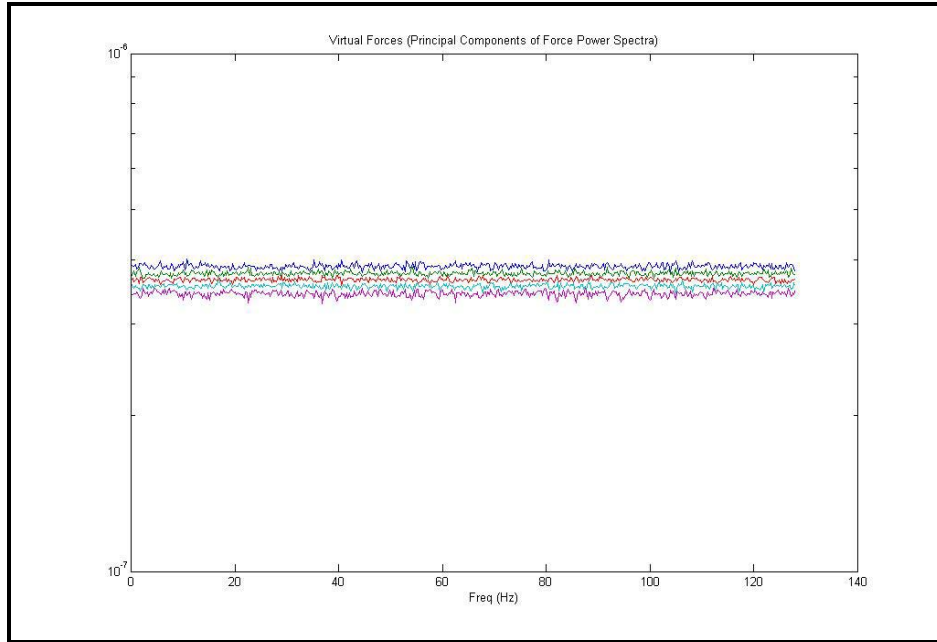


Figure 7.2: Virtual forces

The magnitude of the theoretical driving point frequency response functions are shown in Figure 7.3. It can be seen from the FRFs that, from an observability point of view, some of the system degrees of freedom are on the node lines of some of the modes and thus all the modes cannot be observed from any single reference degree of freedom.

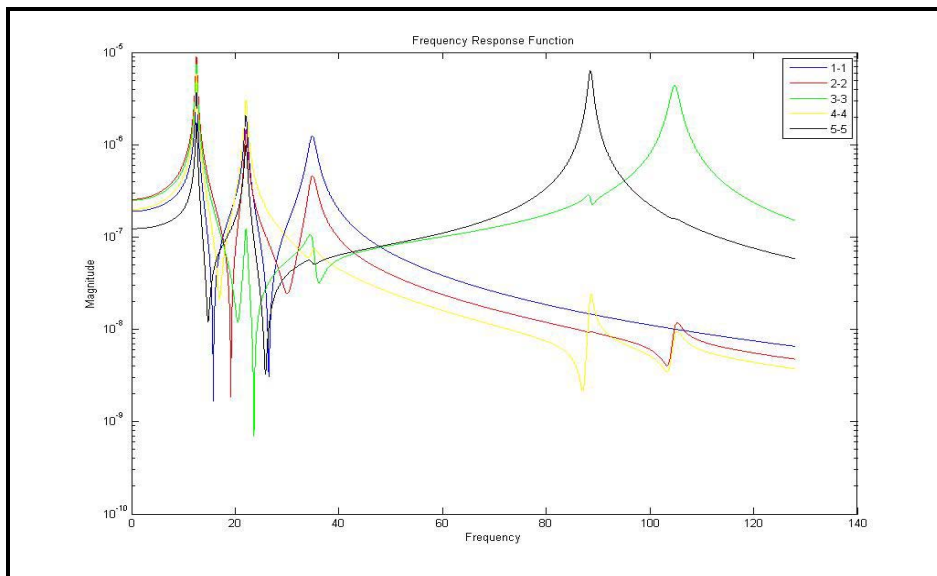


Figure 7.3: Theoretical frequency response functions (5 DOF analytical system)

The next section discusses the Cyclic Averaging signal processing technique and how its application to the observed time responses results in power spectra with reduced leakage. In subsequent sections, it is shown how this approach gives more accurate estimates of modal frequency and damping, in comparison to other more commonly used signal processing approaches.

7.2 Cyclic Averaging

One major difference between EMA and OMA is that, whereas frequency response functions (FRFs) are the primary data in EMA, in OMA the primary data is output power spectra. For estimating FRFs, input/output auto and cross spectra are required (depending on the estimation algorithm). It is worth noting that the FRF is assumed to be unique but the same is not true for the power spectra unless the input is stationary and a sufficiently large number of averages is taken. This is not a cause of concern in EMA as the desired data is FRF, not the power spectra used to estimate the FRF. However, in OMA, it can lead to several issues resulting in estimated power spectra being contaminated by noise due to random and bias errors.

For the above stated reasons, in general, better estimation of the power spectra require longer time histories in comparison (so as to have a greater number of averages to reduce the random errors). The bias errors, such as leakage, are however not reduced by averaging. Use of overlapping weighting functions (windowing) along with averaging is one of the most common methods of reducing leakage error.

The use of cyclic averaging, along with asynchronous or synchronous averaging [Allemang, 1999], is a powerful technique for reducing the leakage, as well as, random errors. Cyclic averaging reduces the leakage bias error by digitally filtering the data to eliminate the frequency information that cannot be described by the FFT (only integer multiples of Δf are retained) completely prior to the application of FFT.

7.2.1 Cyclic Averaging Theory

The cyclic averaging [Allemang, 1980; Allemang, Phillips, 1996; Phillips, Allemang et al., 1998; Fladung, Zucker et al., 1999; Phillips, Zucker et al., 1999] is a special case of linear averaging where the digitization is coherent between cyclic averages. In the frequency domain, this is equivalent to a digital comb filter with passbands at frequency increments that are integer multiples of the Δf ; thus resulting in attenuation between the passbands.

The Fourier transform of an output time history $x(t)$ is given by

$$X(\omega) = \int_{-\infty}^{+\infty} x(t) e^{-j\omega t} dt \quad (7.1)$$

Fourier transform of the same time history shifted by amount t_0 is

$$X(\omega) e^{-j\omega t_0} = \int_{-\infty}^{+\infty} x(t+t_0) e^{-j\omega t} dt \quad (7.2)$$

or

$$X(\omega) e^{-j n \frac{2\pi}{T} t_0} = \int_{-\infty}^{+\infty} x(t+t_0) e^{-j\omega t} dt \quad (7.3)$$

where $\omega = n \frac{2\pi}{T}$ with n as an integer, since each frequency in the spectra is assumed to be an integer multiple of the fundamental frequency $\Delta f = 1/T$. In Eqn. (7.3) it is worth noting that the correction for the cases where $t_0 = N T$ where N is an integer, will be a unit magnitude with zero phase. Thus, if the time histories that are being averaged occur

at a time shift that is an integer multiple of the observation period T , then the correction due to the time shift does not affect the frequency domain characteristics of the averaged result. The averaged time history is given by

$$\bar{x}(t) = \frac{1}{N_C} \sum_{i=0}^{N_C-1} x_i(t) \quad 7.4)$$

where N_C is number of cyclic averages. When $x(t)$ is continuous over the time period $N_C T$, the Fourier coefficients of the averaged time history are

$$C_k = \frac{1}{T} \int_0^T \bar{x}(t) e^{-j\omega_k t} dt \quad 7.5)$$

or

$$C_k = \frac{1}{N_C T} \int_0^{N_C T} \sum_{i=0}^{N_C-1} x_i(t) e^{-j\omega_k t} dt \quad 7.6)$$

and finally

$$C_k = \frac{1}{N_C T} \int_0^{N_C T} x(t) e^{-j\omega_k t} dt \quad 7.7)$$

It is clear from the above equation that the Fourier coefficients of the cyclic averaged history, spaced at $\Delta f = 1/T$, are the same Fourier coefficients as those from the original time history, spaced at $\Delta f = 1/N_C T$. The Fourier coefficients of a cyclic averaged time history are $1/N_C$ times those of original history. Note that the conditions of the Parseval's

theorem are not preserved by cyclic averaging since the frequency information, not related to the harmonics of $\Delta f = 1/T$, is removed [Hsu, 1970].

7.2.2 Effect of Cyclic Averaging

Three cases of different signal processing (**No** Cyclic Averages, **5** Cyclic Averages and **10** Cyclic Averages) are considered here. All these cases differ in terms of the number of cyclic averaging but the total measured time is constant (Total measured time is approximately equal to $N_c \times \text{Block Size} \times (1 - \text{Fractional Overlap}) \times N_{rms}$). Other parameters such as block size, type of window, etc are same in all the cases. These constant parameters are as follows

Block Size: 1024

Window: Hanning

Overlap: 75%

Typical auto and cross power spectra plots obtained using the three signal processing approaches are shown in Figures 7.4 and 7.5. When the cyclic averaging is not used the power spectrums seem clearer in comparison to the cases where the cyclic averaging is used. This is because of the fact that, since the same total time history is processed using the three approaches, the number of RMS averages is greater for the case where cyclic averaging is not used than the ones where it is.

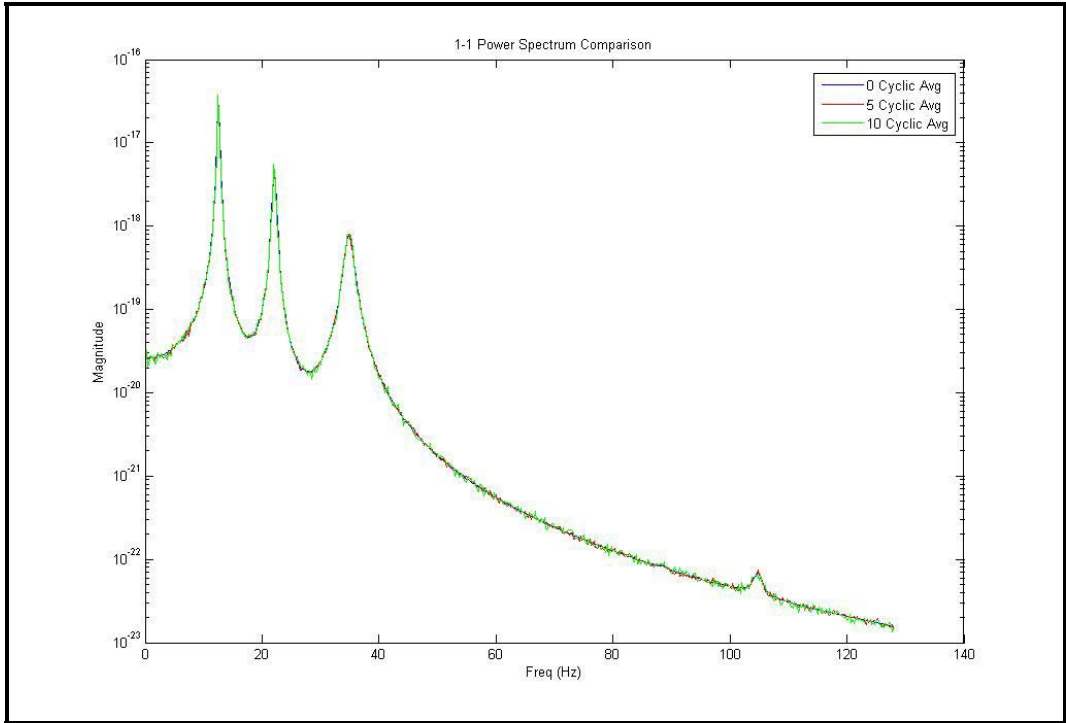


Figure 7.4: Effect of cyclic averaging (Power spectrum comparison 1-1)

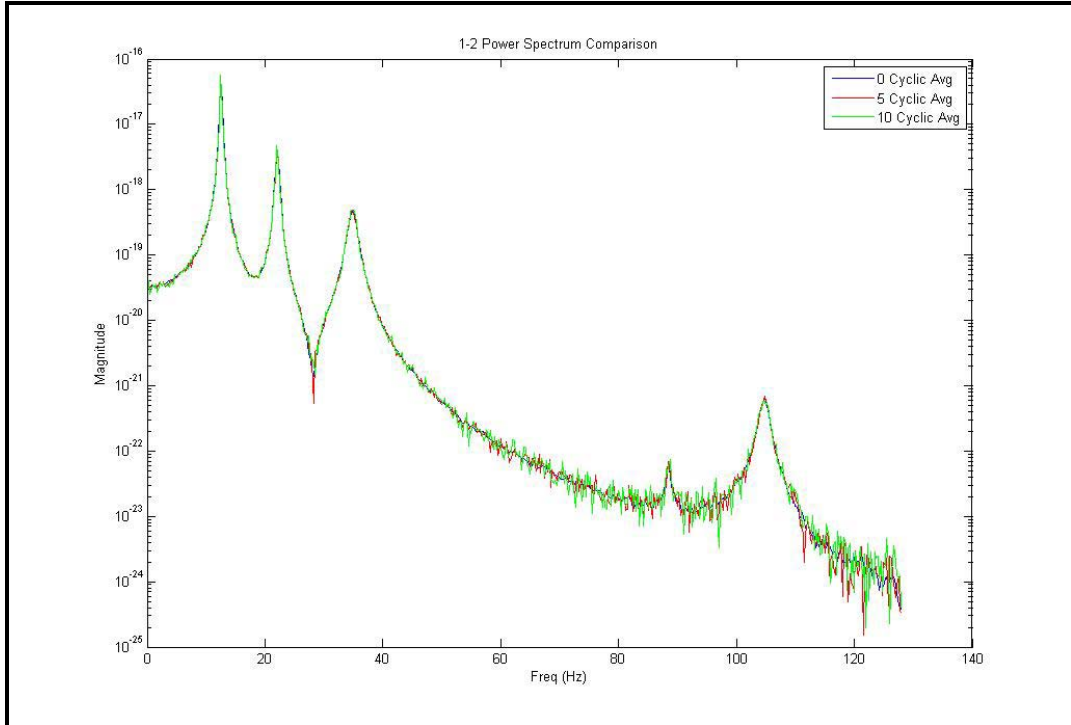


Figure 7.5: Effect of cyclic averaging (Power spectrum comparison 1-2)

Table 7.3: Effect of cyclic averaging ($N_c = 0$, RMS Averages = 3997)

Frequency	% Error	Damping (% Critical)	% Error
12.5276	0.0104	1.5377	33.8760
22.0843	0.0059	1.2344	16.5738
34.8662	0.0077	2.2036	1.4549
88.5231	-0.0008	0.5117	5.0287
104.7830	0.0041	0.8457	-0.1888

Table 7.4: Effect of cyclic averaging ($N_c = 5$, RMS Averages = 797)

Frequency	% Error	Damping (% Critical)	% Error
12.5074	-0.1509	1.0523	-8.3841
22.0709	-0.0548	1.0978	3.6736
34.8606	-0.0083	2.1464	-1.1786
88.5253	0.0017	0.4872	0.0000
104.7815	0.0027	0.8322	-1.7821

Table 7.5: Effect of cyclic averaging ($N_c = 10$, RMS Averages = 397)

Frequency	% Error	Damping (% Critical)	% Error
12.5122	-0.1126	1.0257	-10.7000
22.0746	-0.0380	1.1150	5.2980
34.8624	-0.0032	2.1071	-2.9880
88.5269	0.0035	0.4846	-0.5337
104.7805	0.0017	0.8316	-1.8529

As indicated in Tables 7.3-7.5 and Figure 7.6, the error in modal frequency estimates with or without the use of cyclic averages is not very significant and for all the five modes the frequency is estimated fairly well. However, the same is not true for the damping estimates.

With no cyclic averaging, the error in damping estimates is significantly higher, especially for the first and second modes (indicated by the grayed cells). Further, the damping is over-estimated in most cases. This error drops down with the use of cyclic averaging. With 5 cyclic averages, except for the first mode, the error drops down below

5% and even for the first mode it is -8% which is significantly lower than the 33% when no cyclic averaging is done. The effect is considerable in other modes as well.

Increasing the number of cyclic averages to 10 doesn't improve the overall results. In fact, it either gives as good or comparatively inferior results to the case where 5 cyclic averages are used. This can be attributed to the reduced number of RMS averages in the case of 10 cyclic averages in comparison to the 5 cyclic averaging case. One additional thing to note is that cyclic averaging tends to underestimate the damping values in contrast to the case with no cyclic averages where the values were significantly overestimated. In this study, the total time is limited to yield a representative measurement comparison. Increasing the number of RMS averages should improve the results in Tables 7.4 and 7.5. This is explained in the next case.

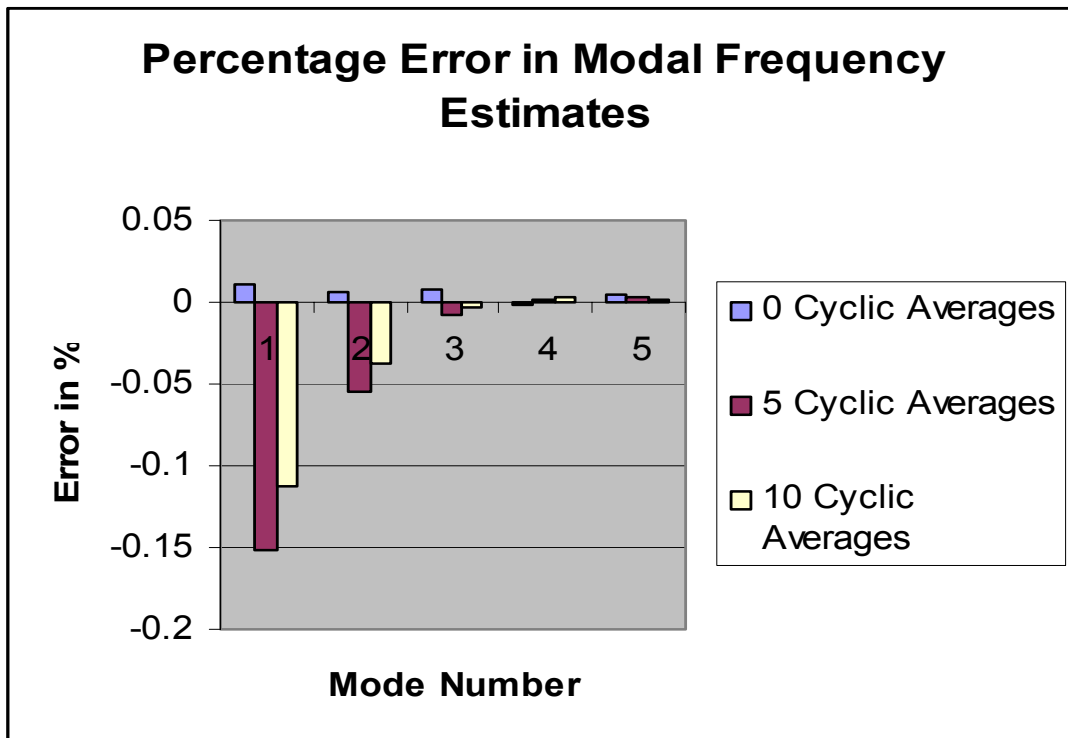


Figure 7.6: Effect of cyclic averaging (Percentage error in modal frequency estimates)

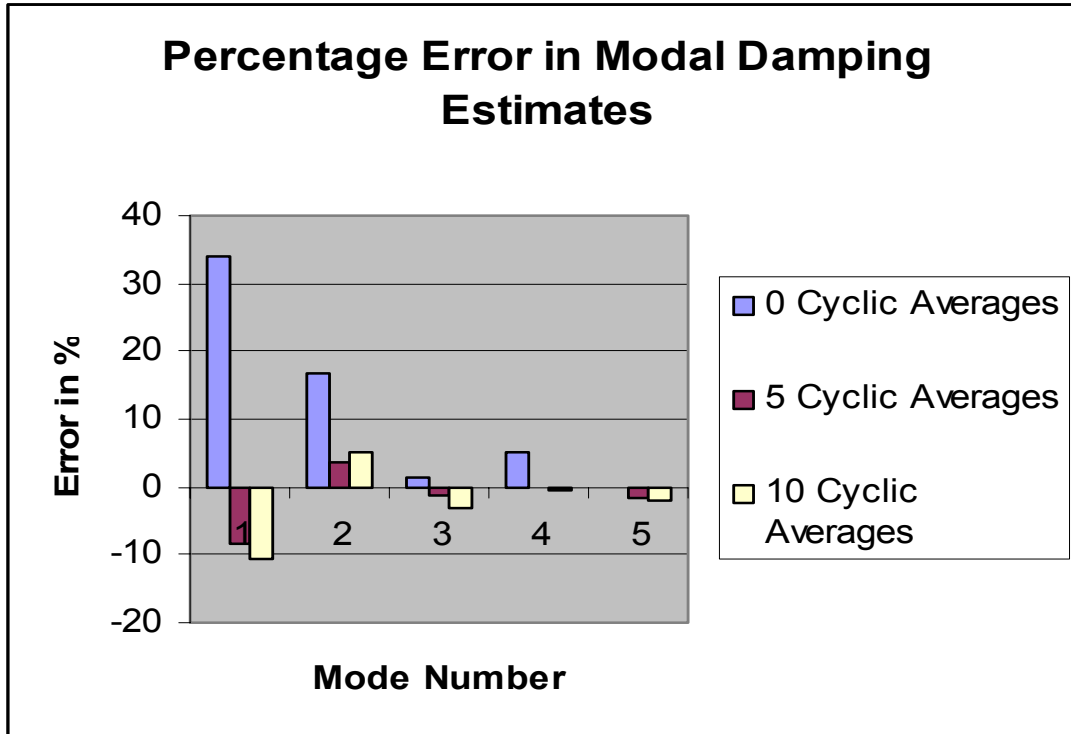


Figure 7.7: Effect of cyclic averaging (Percentage error in modal damping estimates)

7.2.3 Effect of More RMS Averages (Use of Longer Time Histories)

This study tries to determine if an increased number of RMS averages is collected using the same number of cyclic averages results in improving the modal parameter estimates or not. Two cases, 5 cyclic averages and 10 cyclic averages are considered and in each case three time histories of different lengths (having different numbers of time sample points) are processed using the same signal processing parameters which are as follows

Case A

Block Size: 1024
 Window: Hanning
 Overlap: 75%
 Cyclic Averages: 5

Table 7.6: Effect of longer time histories ($N_c = 5$, Time points = 102400, RMS Averages = 77)

Frequency	% Error	Damping (% Critical)	% Error
12.5158	-0.0838	0.9918	-13.6514
22.0887	0.0258	1.1360	7.2811
34.8606	-0.0083	2.1915	0.8978
88.5225	-0.0015	0.4867	-0.1026
104.7702	-0.0081	0.8386	-1.0268

Table 7.7: Effect of longer time histories ($N_c = 5$, Time points = 1024000, RMS Averages = 797)

Frequency	% Error	Damping (% Critical)	% Error
12.5074	-0.1509	1.0523	-8.3841
22.0709	-0.0548	1.0978	3.6736
34.8606	-0.0083	2.1464	-1.1786
88.5253	0.0017	0.4872	0.0000
104.7815	0.0027	0.8322	-1.7821

Table 7.8: Effect of longer time histories ($N_c = 5$, Time points = 1536000, RMS Averages = 1197)

Frequency	% Error	Damping (% Critical)	% Error
12.5159	-0.0830	0.9834	-14.3827
22.0733	-0.0439	1.0482	-1.0105
34.8590	-0.0129	2.1842	0.5617
88.5241	0.0003	0.4866	-0.1232
104.7826	0.0037	0.8372	-1.1920

As seen earlier, in this study as well, the frequencies are fairly well estimated. The error in estimation is within $\pm 0.1\%$ in all cases. The damping estimates are still not this accurate and there isn't a definite trend when a longer time history (more overall averages) is used. Though overall the results do improve as longer time histories are used, unexpectedly the damping estimate for the first mode, or the first two modes, deteriorates.

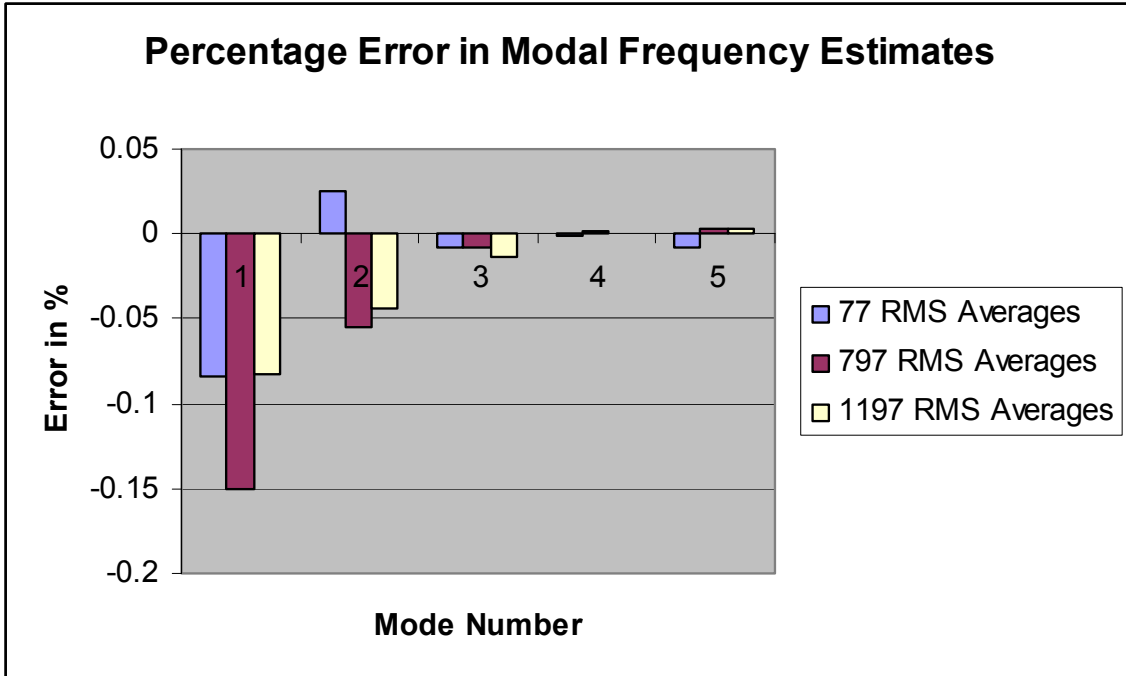


Figure 7.8: Effect of longer time histories $N_c = 5$ (Percentage error in modal frequency estimates)

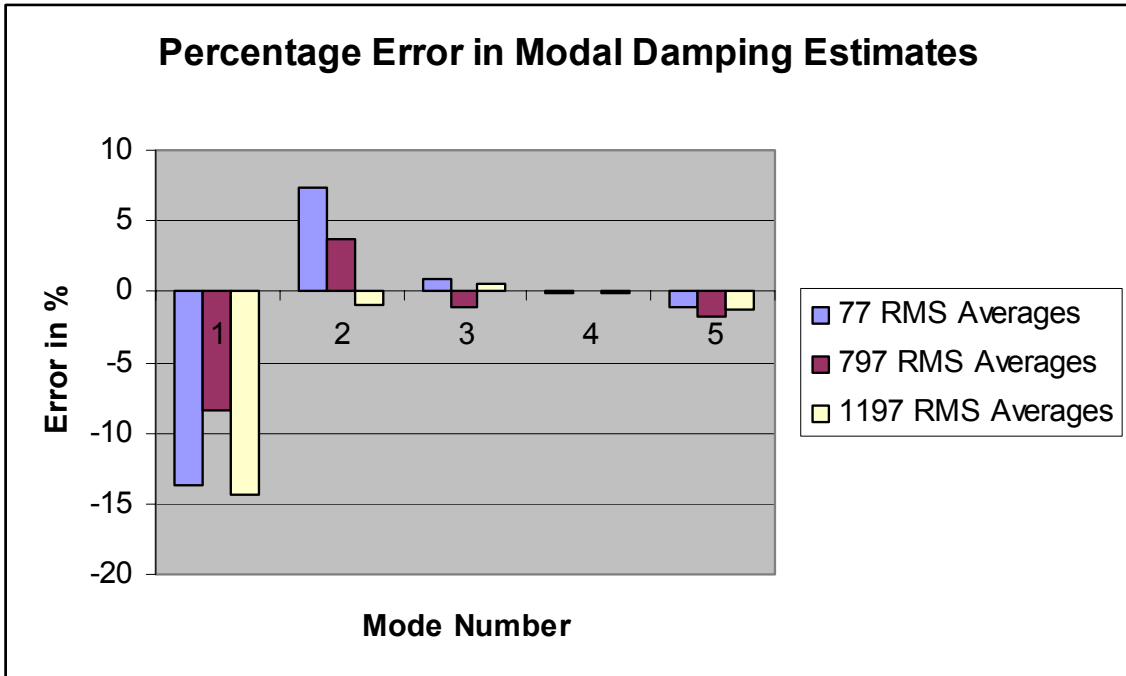


Figure 7.9: Effect of longer time histories $N_c = 5$ (Percentage error in modal damping estimates)

Case B

Block Size: 1024

Window: Hanning

Overlap: 75%

Cyclic Averages: 10

Table 7.9: Effect of longer time histories ($N_C = 10$, Time points = 102400, RMS Averages = 37)

Frequency	% Error	Damping (% Critical)	% Error
12.5165	-0.0782	1.0064	-12.3803
22.0855	0.0113	1.0599	0.0944
34.8015	-0.1778	2.2803	4.9862
88.5226	-0.0014	0.4763	-2.2373
104.7938	0.0144	0.8103	-4.3668

Table 7.10: Effect of longer time histories ($N_C = 10$, Time points = 1024000, RMS Averages = 397)

Frequency	% Error	Damping (% Critical)	% Error
12.5122	-0.1126	1.0257	-10.7000
22.0746	-0.0380	1.1150	5.2980
34.8624	-0.0032	2.1071	-2.9880
88.5269	0.0035	0.4846	-0.5337
104.7805	0.0017	0.8316	-1.8529

Table 7.11: Effect of longer time histories ($N_C = 10$, Time points = 1536000, RMS Averages = 597)

Frequency	% Error	Damping (% Critical)	% Error
12.5149	-0.0910	0.9834	-14.3827
22.0722	-0.0489	1.0458	-1.2371
34.8685	0.0143	2.1748	0.1289
88.5241	0.0003	0.4858	-0.2874
104.7838	0.0049	0.8363	-1.2982

Tables 7.9-7.11 indicate the error in frequency and damping estimates for 10 cyclic averaging case. Except for the first mode, longer time histories when processed using

10 cyclic averages tend to reduce errors in damping estimates (Figure 7.11). When only 37 RMS averages are taken, the damping estimates are more erroneous (highlighted in orange in Table 7.9). The error is reduced subsequently when more RMS averages are taken due to longer time histories. The damping estimate for the second mode does deteriorate in one dataset (Table 7.10) but it also starts to approach the true value for 597 RMS averages dataset (Table 7.11), for which damping is correctly estimated for most modes. Modal frequencies are fairly well estimated in all datasets (Figure 7.10).

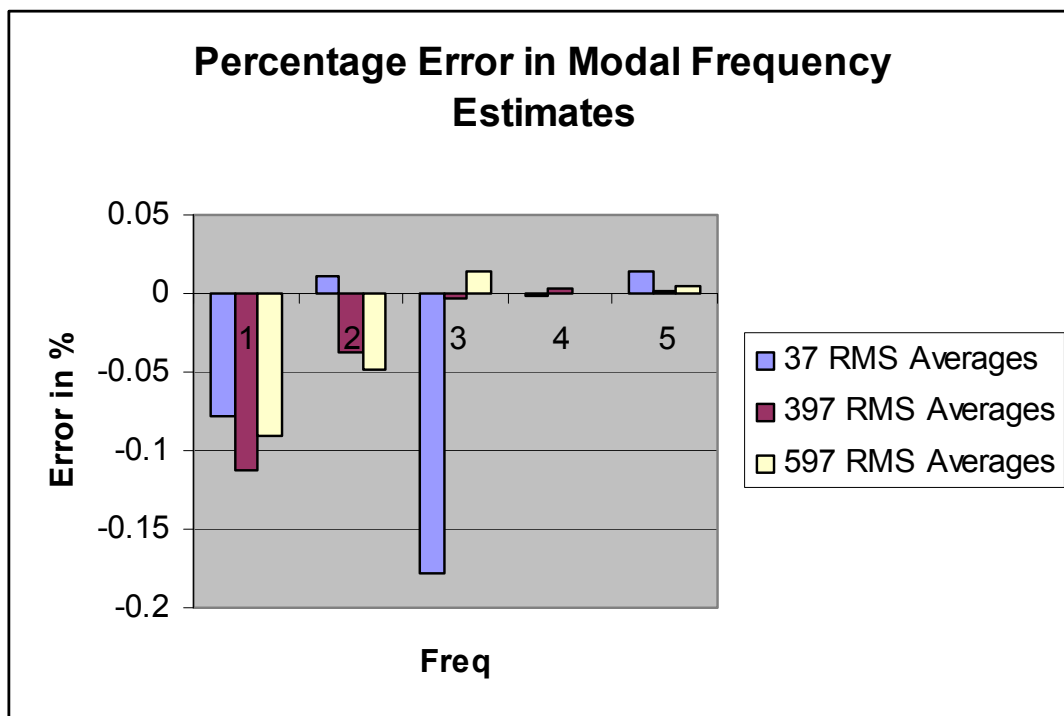


Figure 7.10: Effect of longer time histories $N_c = 10$ (Percentage error in modal frequency estimates)

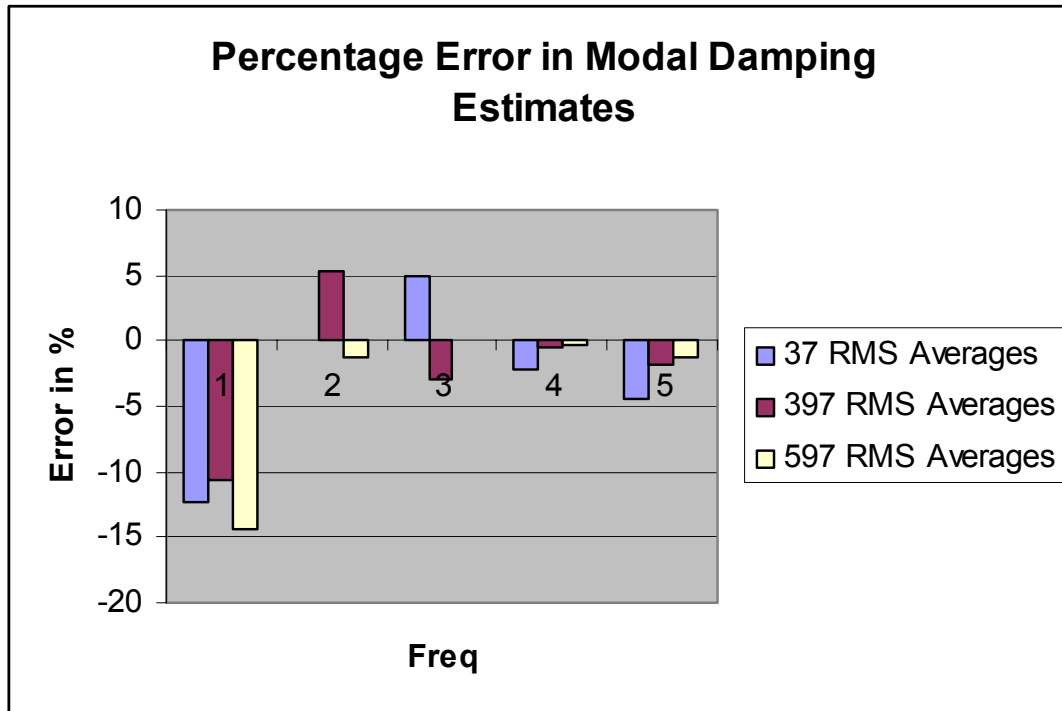


Figure 7.11: Effect of longer time histories $N_c = 10$ (Percentage error in modal damping estimates)

It should be noted that in these studies PTD, a time domain algorithm, is used for parameter identification purposes. Similar results are obtained if frequency domain algorithms, which operate on the positive power spectra (PPS), are used. This is shown in Tables 7.12 and 7.13 which indicate similar results as those obtained in Tables 7.4 and 7.5.

Table 7.12: Damping estimation by frequency domain OMA algorithms utilizing PPS ($N_c = 5$, RMS Averages = 797)

Frequency	% Error	Damping (% Critical)	% Error
12.5216	-0.0375	1.0560	-8.0620
22.0709	-0.0548	1.0890	2.8426
34.8603	-0.0092	2.1411	-1.4227
88.5253	0.0017	0.4867	-0.1026
104.7805	0.0017	0.8370	-1.2156

Table 7.13: Damping estimation by frequency domain OMA algorithms utilizing PPS ($N_c = 10$, RMS Averages = 397)

Frequency	% Error	Damping (% Critical)	% Error
12.5111	-0.1213	0.9909	-13.7298
22.0727	-0.0466	1.1126	5.0713
34.8622	-0.0037	2.1077	-2.9604
88.5261	0.0026	0.4850	-0.4516
104.7821	0.0032	0.8366	-1.2628

The RFP-z frequency domain algorithm is used for this study and PPS are obtained from the 1,024,000 sample points of time history using 1024 block size, Hanning window and 75% overlap as signal processing parameters, i.e. same as those used for the time domain algorithms. It should be noted that the frequency resolution is reduced by half while calculating the PPS. This is because of the fact that the negative lag portion of the correlation is removed and only positive lags are considered. Thus the Fourier transform is applied only to the number of points equal to half the initial block size while converting positive lags portion of the correlation to PPS. This results in doubling Δf or reducing the frequency resolution.

7.3 Correlated Input Forces and OMA Parameter Estimation

Intrinsic to operational modal analysis are the two assumptions concerning the nature of input forces acting on the system. These assumptions are [17]

1. Input forces acting on the system are random, uncorrelated and broadband in nature, and
2. Input forces are uniformly distributed in a spatial sense.

$$[G_{XX}(\omega)] = [H(\omega)] [G_{FF}(\omega)] [H(\omega)]^H \quad 7.8)$$

Equation 7.8 forms the key to all OMA related parameter estimation. As per the first assumption, the output response power spectra $[G_{xx}(\omega)]$ is proportional to the product $[H(\omega)][H(\omega)]^H$ if and only if the input force power spectra matrix $[G_{FF}(\omega)]$ is diagonal or in other words, the input forces acting on the system are uncorrelated and uncoupled.

In this section, the efforts are concentrated on exploring this assumption of uncorrelation by means of the 5 degree of freedom system explained earlier and how it affects the modal parameters, specially damping.

As is earlier shown in Figure 7.1, the input forces that excite the system are not entirely uncorrelated. The methodology used for this purpose involves performing modal parameter estimation on various kinds of data utilizing the same time history. These different datasets are

1. Generated Frequency Response Functions (H_{Gen}),
2. Generated FRF multiplied by its Hermitian ($G_{FF} = [I]$) (H^*H^H) $_{Gen}$,
3. ($H^*G_{FF}^{diag}H^H$) $_{Gen}$ This dataset represents output response power spectra formulated as per Equation 7.8 with the condition that G_{FF} is diagonal i.e. it only contains auto power terms and cross power terms are zero. This is the ideal case where assumption 1 is completely true.
4. ($H^*G_{FF}H^H$) $_{Gen}$ This dataset represents output response power spectra formulated as per Equation 7.8 with the complete G_{FF} matrix i.e. containing both the diagonal and off-diagonal terms (both auto and cross-power terms).
5. G_{xx} The output response power spectrum computed from the response time histories. This is theoretically similar to the ($H^*G_{FF}H^H$) $_{Gen}$.

These datasets for the following case are analyzed first

Case A

Block Size: 1024

Window: Hanning

Overlap: 50%

Cyclic Averages: 10

Table 7.14: H_{Gen} - Effect of Correlated Forces (Case A)

Frequency	% Error	Damping (% Critical)	% Error
12.5235	-0.0224	1.1494	0.0697
22.0834	0.0018	1.0700	1.0483
34.8632	-0.0009	2.1718	-0.0092
88.5238	0.0000	0.4886	0.2874
104.7823	0.0034	0.8415	-0.6845

Table 7.15: $(H^*H^H)_{Gen}$ - Effect of Correlated Forces (Case A)

Frequency	% Error	Damping (% Critical)	% Error
12.5189	-0.0591	1.1470	-0.1393
22.0735	-0.0430	1.0441	-1.3977
34.8849	0.0614	2.1643	-0.3545
88.5254	0.0018	0.4869	-0.0616
104.7797	0.0010	0.8394	-0.9324

Table 7.16: $(H^*GFF_{diag}^*H^H)_{Gen}$ - Effect of Correlated Forces (Case A)

Frequency	% Error	Damping (% Critical)	% Error
12.5144	-0.0950	1.1427	-0.5137
22.0789	-0.0186	1.0768	1.6904
34.8717	0.0235	2.1841	0.5571
88.5402	0.0185	0.4882	0.2053
104.7853	0.0063	0.8400	-0.8616

Table 7.17: $(H^*G_{FF_{comp}}*H^H)_{Gen}$ - Effect of Correlated Forces (Case A)

Frequency	% Error	Damping (% Critical)	% Error
12.5174	-0.0711	1.0739	-6.5036
22.0905	0.0340	1.0497	-0.8688
34.8420	-0.0617	2.4006	10.5249
88.5232	-0.0007	0.4956	1.7241
104.7852	0.0062	0.8395	-0.9206

Table 7.18: G_{XX} - Effect of Correlated Forces (Case A)

Frequency	% Error	Damping (% Critical)	% Error
12.5157	-0.0846	1.0090	-12.1539
22.0913	0.0376	1.0825	2.2287
34.8580	-0.0158	2.3750	9.3462
88.5315	0.0087	0.4877	0.1026
104.7711	-0.0073	0.8167	-3.6115

This study produces some very interesting results. The frequency is well estimated in all the datasets (Figure 7.12) and does not seem to be affected by the presence of cross power force spectra terms (off-diagonal terms due to the partially correlated nature of the forces). The damping estimates, as indicated in Tables 7.17, 7.18, and Figure 7.13, are however severely affected, especially the first and the third mode. Dataset 1 (Generated FRFs) expectedly gives good results. Dataset 2 is the ideal OMA case, where the first assumption is completely valid and the G_{FF} matrix is an identity. For this dataset as well as Dataset 3, where G_{FF} is not an identity but is uncoupled, the estimates are still good and fairly accurate within the error limits. But as more realistic datasets are considered, like those in Datasets 4 and 5, where the input forces are more likely to be correlated to a certain degree and the OMA assumptions are not strictly met, it is observed that some damping estimates are seriously affected and are not as accurate as the other three datasets.

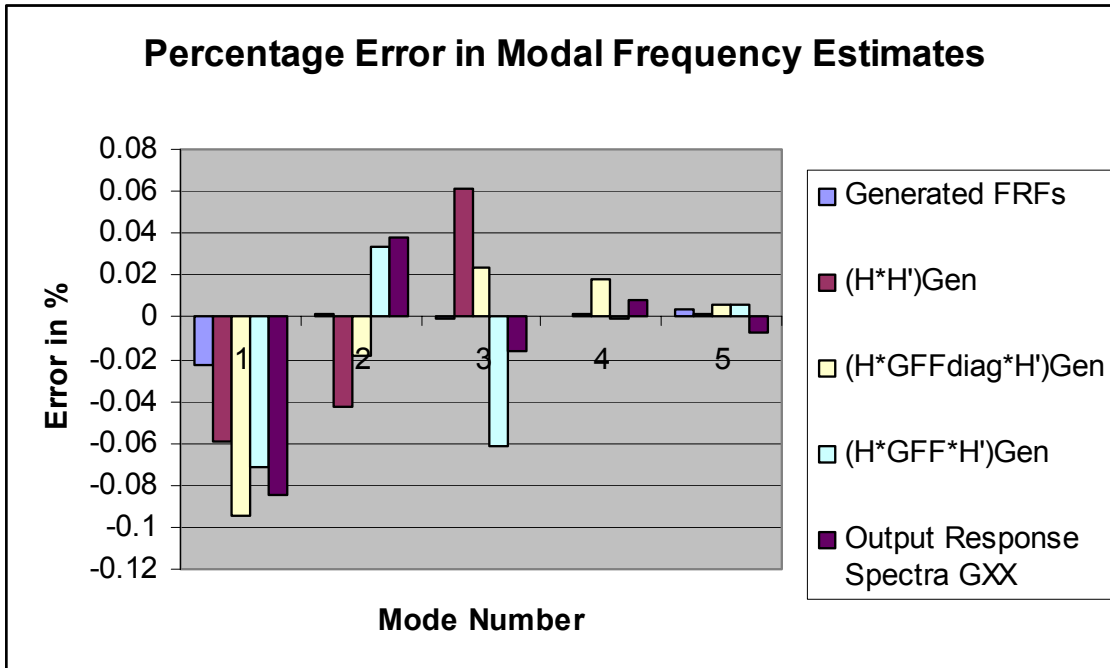


Figure 7.12: Effect of correlated input forces Case A (Percentage error in modal frequency estimates)

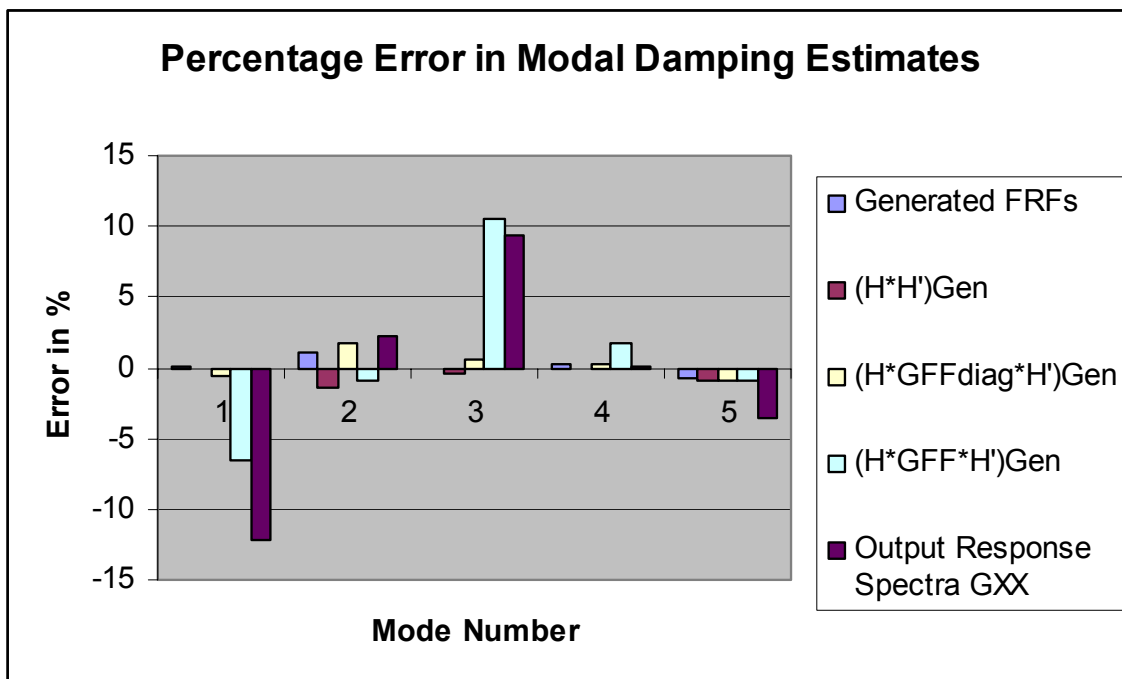


Figure 7.13: Effect of correlated input forces Case A (Percentage error in modal damping estimates)

Case B

To investigate this further, the system is now excited by means of partially correlated forces. The forces used to excite the system in Case A are mixed in the following manner to make them partially correlated.

$$F_1 = F_A + .1F_B + .1F_C + .1F_D + .1F_E$$

$$F_2 = .1F_A + F_B + .1F_C + .1F_D + .1F_E$$

$$F_3 = .1F_A + .1F_B + F_C + .1F_D + .1F_E$$

$$F_4 = .1F_A + .1F_B + .1F_C + F_D + .1F_E$$

$$F_5 = .1F_A + .1F_B + .1F_C + .1F_D + F_E$$

Figure 7.14 and Figure 7.15 shows that unlike the previous case, due to the correlated nature of the input forces, the auto (1-1) and cross (1-2) power terms of the input force power spectrum matrix are of the same order and that there are only two principal virtual forces. The signal processing in this case is similar to that used previously.

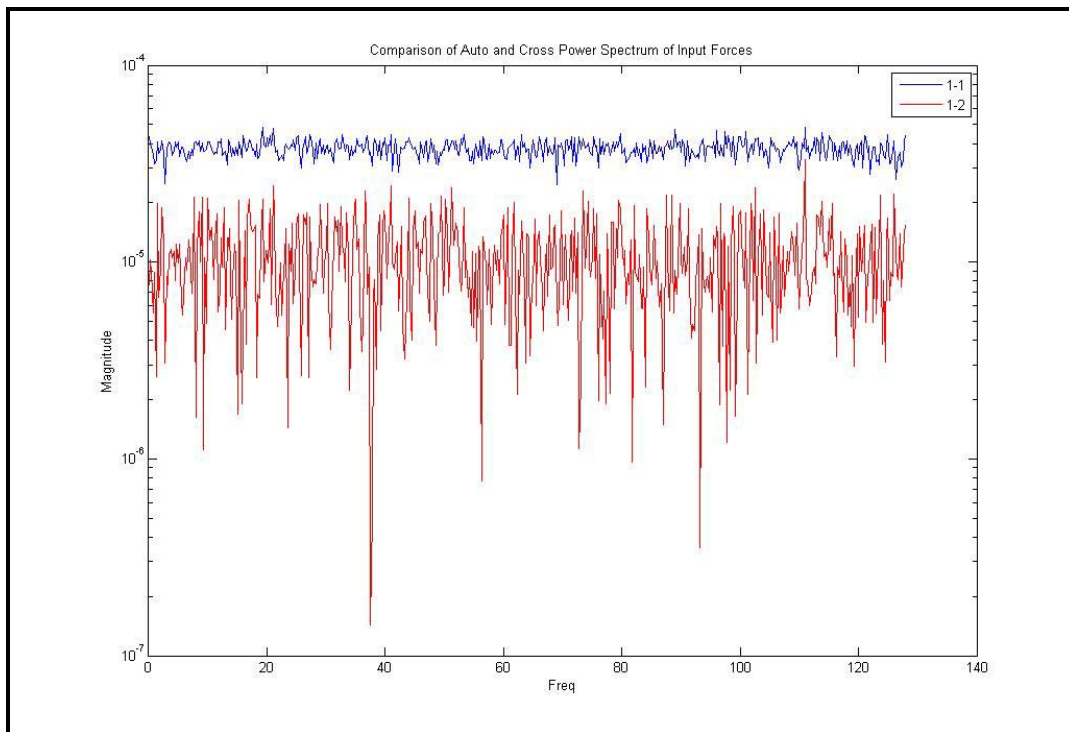


Figure 7.14: Comparison of auto and cross power spectrum of input forces (Case B)

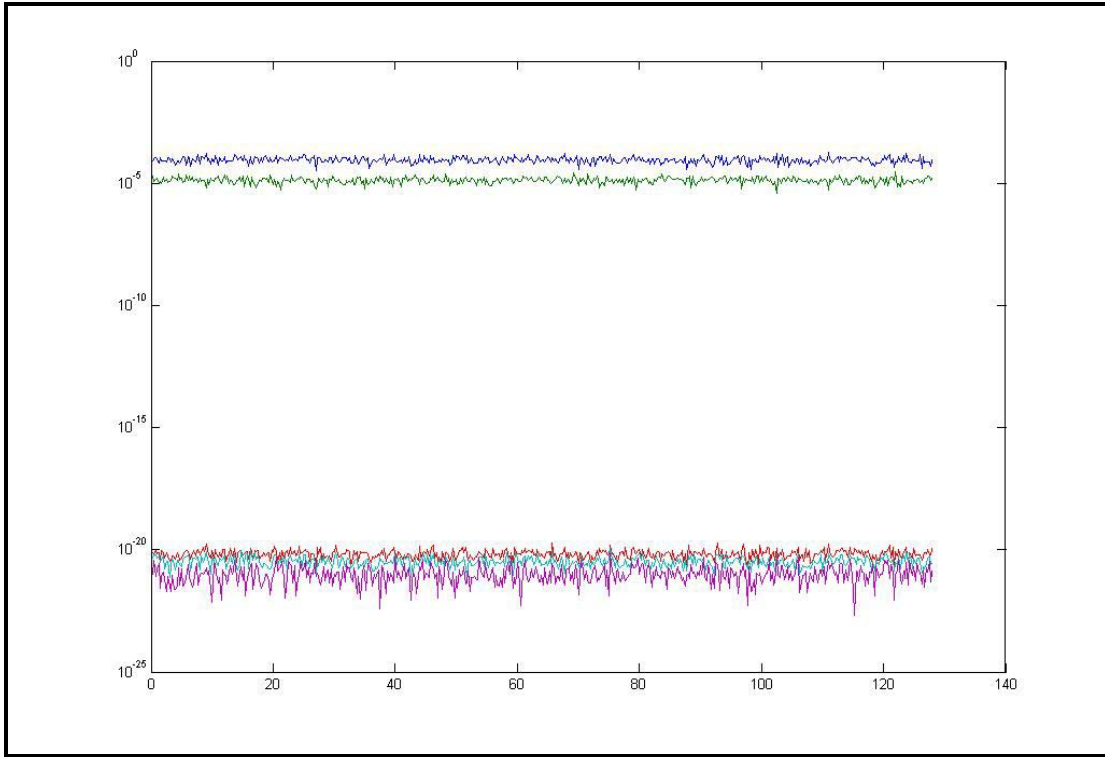


Figure 7.15: Virtual forces (Case B)

Table 7.19: $(H \cdot GFF_{diag} \cdot H^H)_{Gen}$ - Effect of Correlated Forces (Case B)

Frequency	% Error	Damping (% Critical)	% Error
12.5037	-0.1804	1.1325	-1.4017
22.0817	-0.0059	1.0896	2.8992
34.8862	0.0651	2.1611	-0.5018
88.5358	0.0136	0.4882	0.2053
104.8028	0.0230	0.8182	-3.4344

Table 7.20: $(H \cdot GFF_{comp} \cdot H^H)_{Gen}$ - Effect of Correlated Forces (Case B)

Frequency	% Error	Damping (% Critical)	% Error
12.5221	-0.0335	1.0759	-6.3294
22.0867	0.0168	1.0492	-0.9160
34.8439	-0.0562	2.4063	10.7873
88.5399	0.0182	0.4895	0.4721
104.7890	0.0098	0.8243	-2.7145

Table 7.21: G_{xx} - Effect of Correlated Forces (Case B)

Frequency	% Error	Damping (% Critical)	% Error
12.5113	-0.1197	1.0355	-9.8468
22.0896	0.0299	1.0744	1.4638
34.8272	-0.1041	2.3749	9.3416
88.5261	0.0026	0.4815	-1.1700
104.7860	0.0070	0.8287	-2.1952

As was noted in Case A, the damping estimates suffer significantly as the conditions deviate from those listed in the first assumption, i.e. as the forces become correlated, the damping estimates become more error prone. This is shown in Figure 7.17 (and Tables 7.19-7.21). Dataset 1, in which only the diagonal terms of the input force power spectrum matrix are considered, results in accurate frequency and damping estimates but when the off-diagonal terms accounting for the potential correlation between the forces are included (as in Datasets 2 and 3), the damping estimates deteriorate though the frequency estimates are still good.

These two cases suggest that the violation of the assumption that the forces are random and uncorrelated results in affecting the damping estimation adversely and errors can be significant depending on the extent to which the forces are correlated.

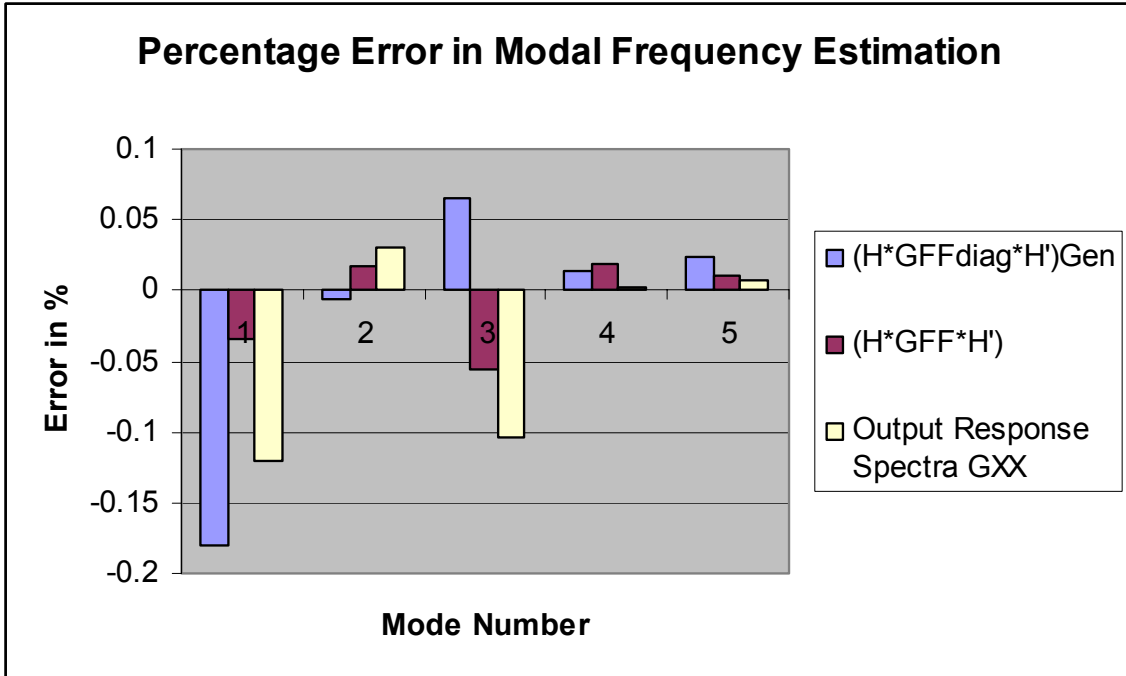


Figure 7.16: Effect of correlated input forces Case B (Percentage error in modal frequency estimates)

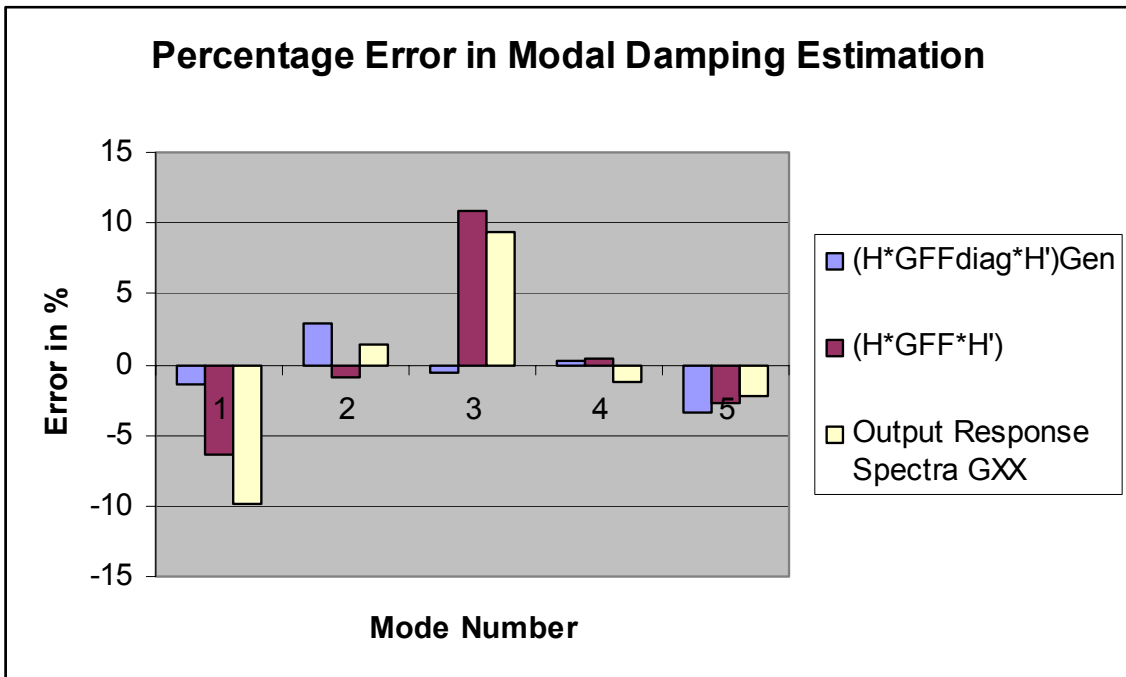


Figure 7.17: Effect of correlated input forces Case B (Percentage error in modal damping estimates)

Finally, one more test case is considered to verify that damping estimates are affected not only by the degree of correlation among input forces but also due to the leakage error which can be reduced by cyclic averaging based signal processing.

Case C

In this scenario, the datasets as described before are generated for the case where no cyclic averaging is done. Note that the output time histories used for this purpose are the same as those considered for Case A. The signal processing parameters in this case are as follows

Block Size: 1024
 Window: Hanning
 Overlap: 50%
 Cyclic Averages: None

Table 7.22: H_{Gen} - Effect of Correlated Forces (Case C)

Frequency	% Error	Damping (% Critical)	% Error
12.4988	-0.2195	1.1999	4.4663
22.0828	-0.0009	1.2311	16.2622
34.8691	0.0161	2.2081	1.6621
88.5232	-0.0007	0.4962	1.8473
104.7866	0.0075	0.8776	3.5761

Table 7.23: $(H^*H^H)_{Gen}$ - Effect of Correlated Forces (Case C)

Frequency	% Error	Damping (% Critical)	% Error
12.5315	0.0415	1.7204	49.7823
22.0780	-0.0226	1.3046	23.2033
34.8658	0.0066	2.2378	3.0295
88.5148	-0.0102	0.5325	9.2980
104.7896	0.0104	0.8654	2.1362

Table 7.24: $(H^*GFF_{diag}^*H^H)_{Gen}$ - Effect of Correlated Forces (Case C)

Frequency	% Error	Damping (% Critical)	% Error
12.5307	0.0351	1.7207	49.8085
22.0792	-0.0172	1.2765	20.5496
34.8602	-0.0095	2.2363	2.9604
88.5216	-0.0025	0.5304	8.8670
104.7893	0.0101	0.8735	3.0922

Table 7.25: $(H^*GFF_{comp}^*H^H)_{Gen}$ - Effect of Correlated Forces (Case C)

Frequency	% Error	Damping (% Critical)	% Error
12.5320	0.0455	1.7651	53.6740
22.0889	0.0267	1.3253	25.1582
34.8683	0.0138	2.2297	2.6565
88.4946	-0.0330	0.4791	-1.6626
104.7894	0.0102	0.8717	2.8797

Table 7.26: G_{XX} - Effect of Correlated Forces (Case C)

Frequency	% Error	Damping (% Critical)	% Error
12.5341	0.0623	1.5241	32.6920
22.0986	0.0706	1.2697	19.9075
34.8583	-0.0149	2.1987	1.2293
88.5182	-0.0063	0.5180	6.3218
104.7836	0.0047	0.8604	1.5461

Green cells in Tables 7.22-7.26 indicate the instances where the error in damping estimate is more than 5%. Figure 7.18 shows that this error is very high (above 20% for some modes) and is present even in datasets where the assumption of uncorrelated forces is completely observed (Datasets 2 and 3). On the other hand frequency estimates are accurate as seen in previous cases. Thus, it can be inferred that damping estimation is affected mainly by leakage and correlation between the input forces. Whereas the first can be reduced, to some extent, by proper signal processing, having a control on the second factor is not so easy. This is true particularly for typical OMA

situations like bridges, buildings, vehicle on road, etc where test engineers have no control over the forcing conditions which are usually ambient in nature.

In relation to the leakage related issues, it has been shown that the use of cyclic averaging results in a more leakage free estimation of the power spectrums that in comparison help produce more reliable damping estimates.

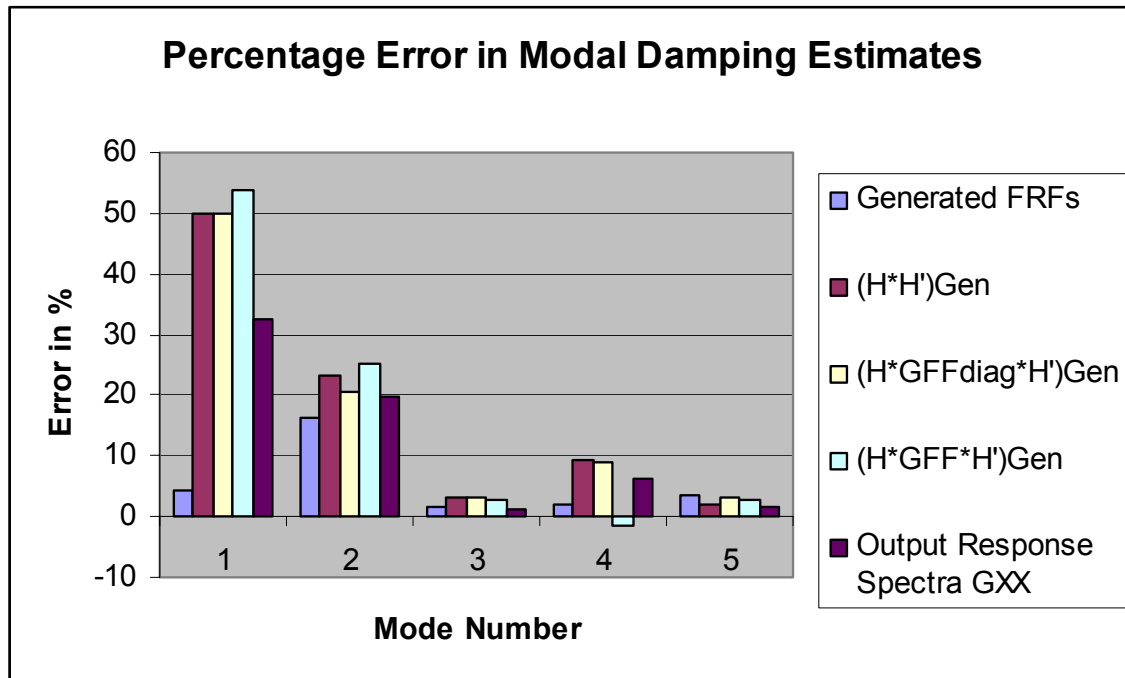


Figure 7.18: Effect of correlated input forces Case C (Percentage error in modal damping estimates)

7.4 Conclusions

This Chapter emphasizes the need to understand the OMA process by conducting more intensive studies regarding the factors that influence the estimated modal parameters including damping. This makes it important to understand the signal processing techniques for the correct estimation of modal parameters. Further, the situations where OMA assumptions do not hold true should also be explored for complete understanding

of the limitations of OMA. The work presented in this Chapter is inspired by the above need.

This Chapter shows how it is very difficult to get good leakage free estimates of the power spectrums in comparison to the FRFs and how cyclic averaging together with RMS averaging, windowing and overlapping is an effective way of dealing with leakage in comparison to more common RMS signal processing that involves only windowing and overlapping. The cyclic averaging technique is not always used in the estimation of FRFs, partially because one is often able to attain good estimate of FRFs even without its use. However, its use in OMA results in considerable improvement and thus this methods need to be explored more with respect to OMA related applications.

Yet another interesting observation made in this Chapter regards the effect of the violation of the basic OMA assumption (input forces being random and uncorrelated) on the modal parameters. It is shown how, in such situations, the error in damping estimates is considerably increased. It is also important to point out that the frequency estimates are well estimated in most cases, even when the power spectrums suffer from bias errors and when input forces are not completely uncorrelated.

As per this study it will be a fair conclusion to say that for accurate estimation of damping, it is necessary to have good estimates (leakage free) of the output response power spectrum and that the input forces be as uncorrelated as possible. Importantly, while the first issue can be improved by using signal processing techniques like cyclic averaging, the second factor is often beyond one's control, especially in real-life scenarios.

The interesting results shown by this study makes it even more important to conduct similar studies on more practical and experimental systems and also explore various other cases such as the effect of uneven forcing functions, better estimation of positive power spectrum for the application of frequency domain OMA algorithms, etc. for a more

through understanding of Operational Modal Analysis. This is essential to develop a better understanding of the OMA procedure which will help immensely when applying these techniques to practical real-life situations.

Chapter Eight

Application to Civil Structures

Civil Structures, especially bridges, are one of the major OMA application areas including dynamic characterization, damage detection, condition assessment, etc [Peeters, Ventura, 2003; Cunha, Caetano, 2005]. This Chapter presents the OMA related studies carried out on two cable stayed bridges in the State of Ohio, USA. The two bridges, the US Grant Cable-stayed Bridge in Portsmouth and the Maumee River Crossing Bridge in Toledo, are recently built bridges and the Chapter discusses the results of the OMA techniques applied to data collected on these bridges. This Chapter focuses on various aspects of operational modal tests that were conducted on the bridges; design of the tests, collection of ambient deck vibration data, parameter estimation techniques used, validation of results and the comparison with the finite element model based predictions.

8.1 US Grant Cable-Stayed Bridge

The US Grant Bridge is one of three cable-stayed bridges being proposed to be built in the State of Ohio, and is constructed across the Ohio River at Portsmouth, OH. The bridge was completed and opened to public in October, 2006. It is a three-span cable-stayed bridge with main span of 875 ft and side spans of 350 ft and 457.1 ft at the Kentucky and Ohio ends respectively (Figure 8.1). The typical elevation and plan of the bridge is shown in Figure 8.2. The bridge deck has a total width of 70.25 ft, with center to

center spacing of 65 ft between the longitudinal girders. This bridge has a modified-fan system, and the deck system consists of precast post-tensioned concrete deck slab supported on two longitudinal steel girders, interconnected by an array of cross-beams and steel stringer beams. The bridge has a pair of single towers from which the inclined cables are stretched out to support the longitudinal girders. The cross beams are uniformly spaced along the length of the bridge at a typical distance of 25 ft, with the cables attached at each alternate cross-beam location. The cables are tensioned such that sag effects are minimal and the cables behave more or less like a taut piano string. Additionally, the cables are connected together by intermittent ties to prevent excessive vibrations during operating conditions, as shown in Figure 8.2.



Figure 8.1 – US Grant Cable-Stayed Bridge

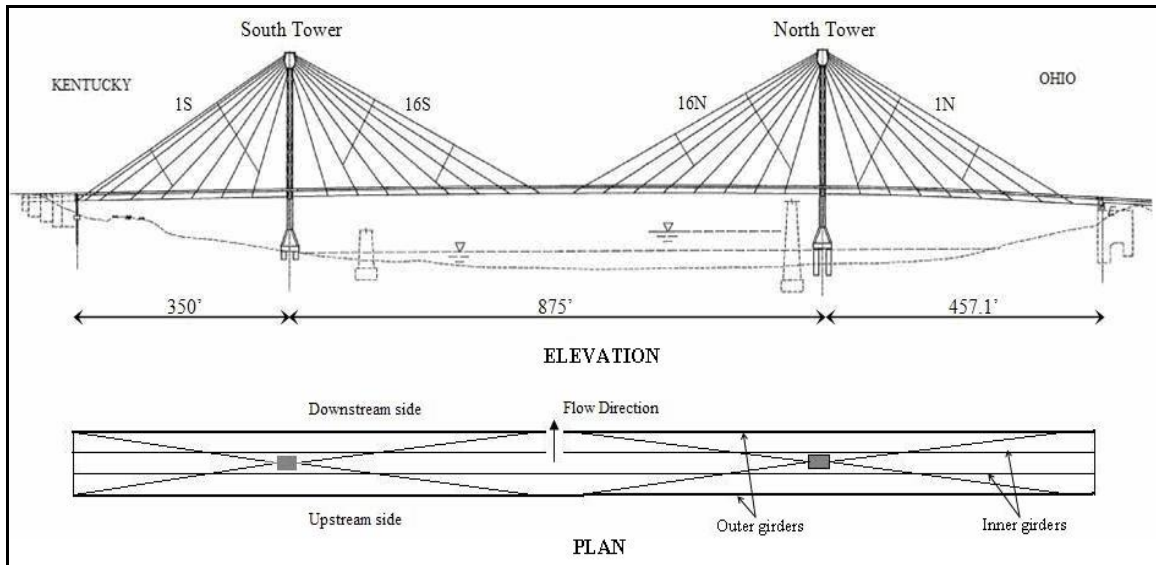


Figure 8.2 - Typical plan and elevation of the US Grant Bridge

8.1.1 Design of Experiments

A finite element model of the bridge was made and predictions of the modal frequencies and mode shapes along with the mass (modal) participation factor were made from this model. The results of this FEM study are used to design the OMA experiments. Details of this study are discussed in [Saini, 2007; Chauhan, Saini et al., 2007].

Table 8.1 lists the computed frequencies of vibration from the finite element analysis for the first 19 modes along-with their mode description and modal participation factors. Looking at the relative modal participation factors, it can be observed that the bending modes are more significant than torsion modes in terms of their effect on the overall response. Therefore, the bending modes were used to design the operational modal analysis tests and for detailed comparison as is explained in the later sections.

Table 8.1: Results of the finite element analysis of the US Grant Bridge

Frequency (Hz.)	Mode Description	Modal Participation Factors (%)					
		UX	UY	UZ	RX	RY	RZ
0.2936	Bending-1	0.297	0.000	1.427	0.000	0.025	0.000
0.3443	Tower Sway	0.000	13.22	0.000	63.59	0.000	14.33
0.3842	Tower AntiSway	0.000	4.040	0.000	15.89	0.000	0.066
0.4827	Bending-2	0.318	0.000	5.586	0.000	10.14	0.000
0.6786	Torsion-1	0.000	0.025	0.000	1.678	0.000	0.017
0.7052	Bending-3	0.076	0.000	21.67	0.000	31.35	0.000
0.7971	Torsion-2	0.000	0.806	0.000	0.054	0.000	0.822
0.8150	Bending-4	0.182	0.000	4.624	0.000	0.448	0.000
0.8391	Torsion-3	0.000	0.703	0.000	0.001	0.000	2.593
0.9230	Bending-5	0.160	0.000	12.97	0.000	6.900	0.000
0.9511	Torsion-4	0.000	0.131	0.000	0.002	0.000	0.059
1.0201	Torsion-5	0.000	1.385	0.000	0.031	0.000	0.811
1.0855	Bending-6	0.369	0.000	1.771	0.000	1.141	0.000
1.1678	Torsion-6	0.000	0.321	0.000	0.043	0.000	0.410
1.1749	Bending-7	0.194	0.000	0.015	0.000	1.196	0.000
1.2571	Torsion-7	0.000	0.049	0.000	0.008	0.000	0.397
1.4233	Bending-8	1.247	0.000	0.902	0.000	0.583	0.000
1.5113	Torsion-8	0.011	0.023	0.000	0.031	0.000	0.021
1.5122	Bending-9	44.36	0.000	0.000	0.000	0.042	0.000

Before carrying out the final superstructure test, a series of smaller tests were conducted with an aim to establish a certain degree of confidence in the testing procedure, data acquisition and subsequent data processing methodologies.

The initial tests focused on ascertaining the accuracy of one type of sensors (piezoelectric accelerometers) with respect to another type of sensors (capacitive accelerometers). The capacitive accelerometers as per specifications behaved better in the low frequency range (below 2 Hz) in comparison to piezoelectric accelerometers. Since the number of capacitive accelerometers was limited, in order to conduct a superstructure test that will yield satisfactory results, it was imperative to use the piezoelectric sensors and thus it was also necessary to establish their behavior and consistency in the low frequency range. The tests revealed that both the piezoelectric and capacitive accelerometers behaved comparably except for extremely low

frequencies below 1 Hz (Figure 8.3). This was confirmed based on analyzing the data collected over various sensor locations and also at different times.

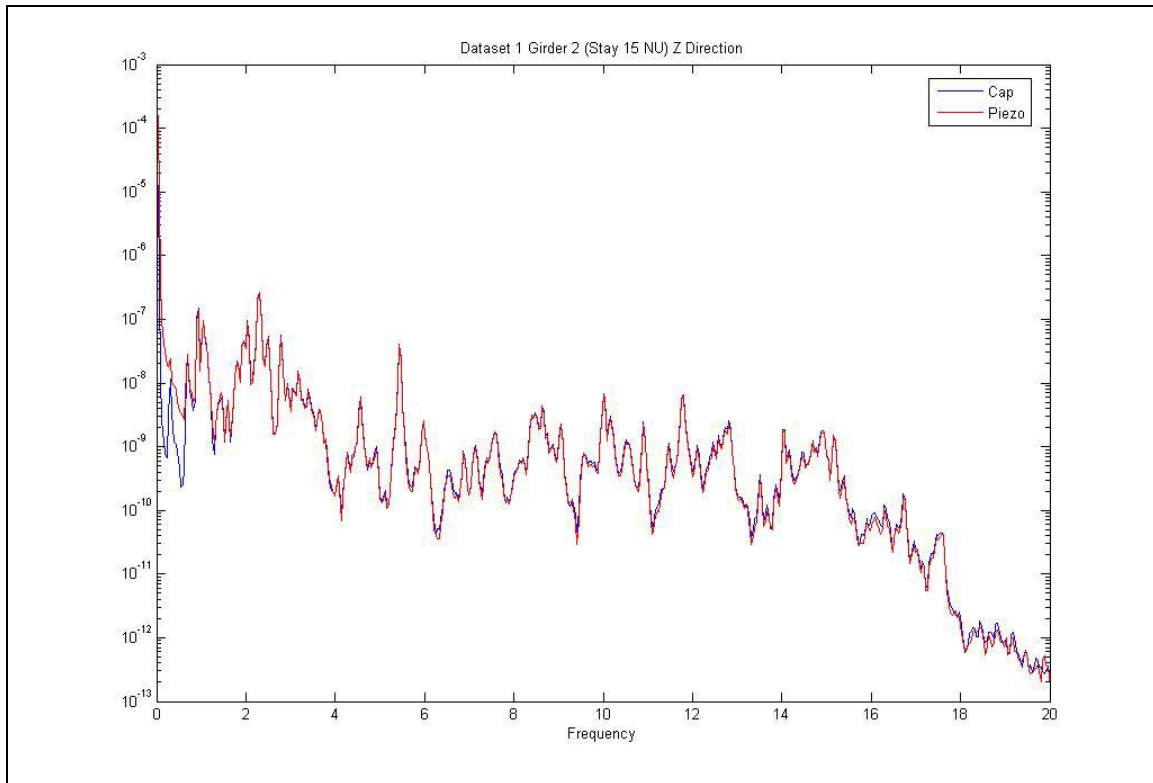


Figure 8.3 – Response comparison measured using a capacitive and a piezoelectric accelerometer

Based on the studies conducted using the finite element model, it was observed that the bridge movement is significant in vertical direction (Z direction) (refer to Figure 8.5). Further, the FE model based studies also revealed that the only significant motion across the bridge (Y direction) was predominantly the tower motion and the deck's dominant motion was mainly in the vertical direction. This was also validated by means of the preliminary small scale modal tests where accelerometers were placed in all three directions; vertical (Z direction), along the length of the bridge (X direction) and across the bridge (Y direction). Figure 8.4 shows that the signal in Z direction is indeed much higher in comparison to that in X and Y directions. This was verified for various sensor locations and, though the bridge movement is always subject to weather conditions and

specific location, it can still be noted, based on FE model and preliminary experimentation, that, from the modal analysis point of view, Z direction modes are most important.

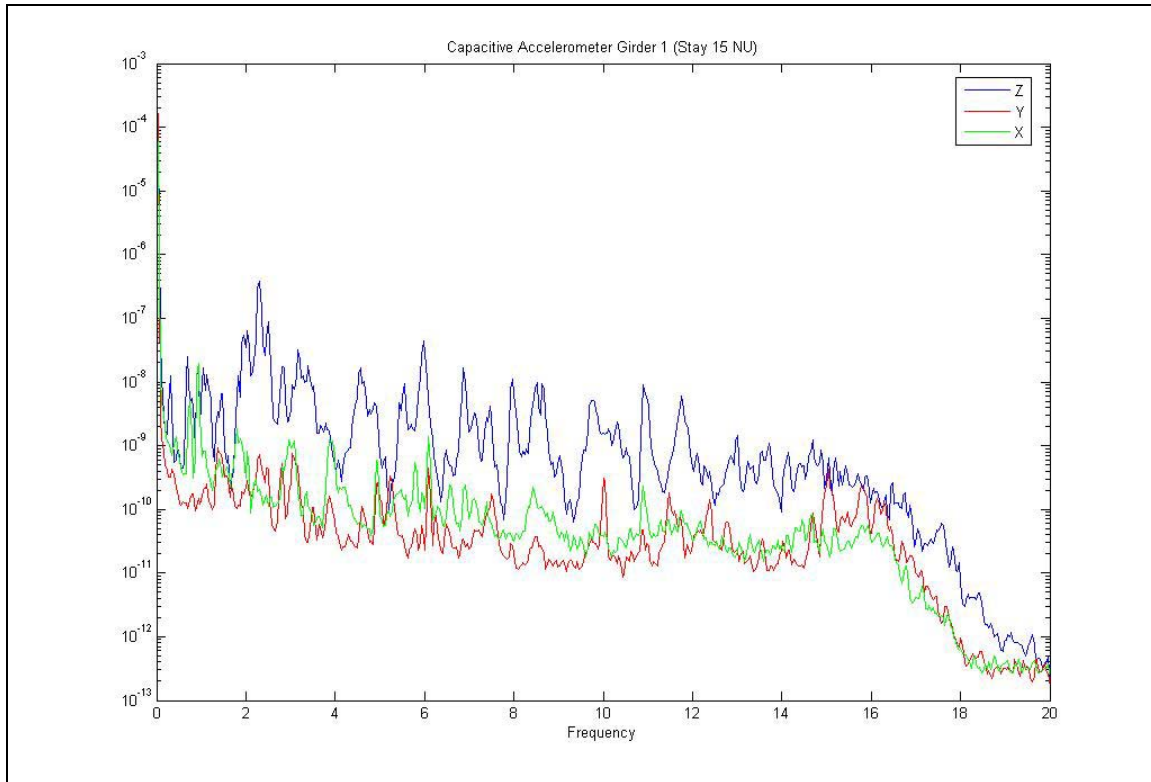


Figure 8.4 – Comparative bridge response in X, Y and Z directions (US Grant Bridge)

Apart from the above mentioned objectives, these tests were also utilized for finalizing the test set up and data acquisition requirements for the final OMA test. The first preliminary test that was conducted had sensors placed at eight locations (Figure 8.5) on the upstream side of the bridge in the mid span around the centre of the bridge. The two sensor lines along the length of the bridge were chosen to correspond with the inner and outer girder lines on the upstream side. Note that location 12 in Figure 8.5 is at stay cable 15 SUI (South, Upstream, Inner girder) and the distance between the individual sensors along the length of the bridge is 50 feet. On analyzing the data collected in this test, it was observed that due to lack of spatial resolution (only a subsection of the bridge

is instrumented and at a very few locations), very few modes are clearly identified. Not many torsional modes were identified due to the fact that only one side of the bridge was instrumented and due to selecting locations where torsional modes don't show much activity.

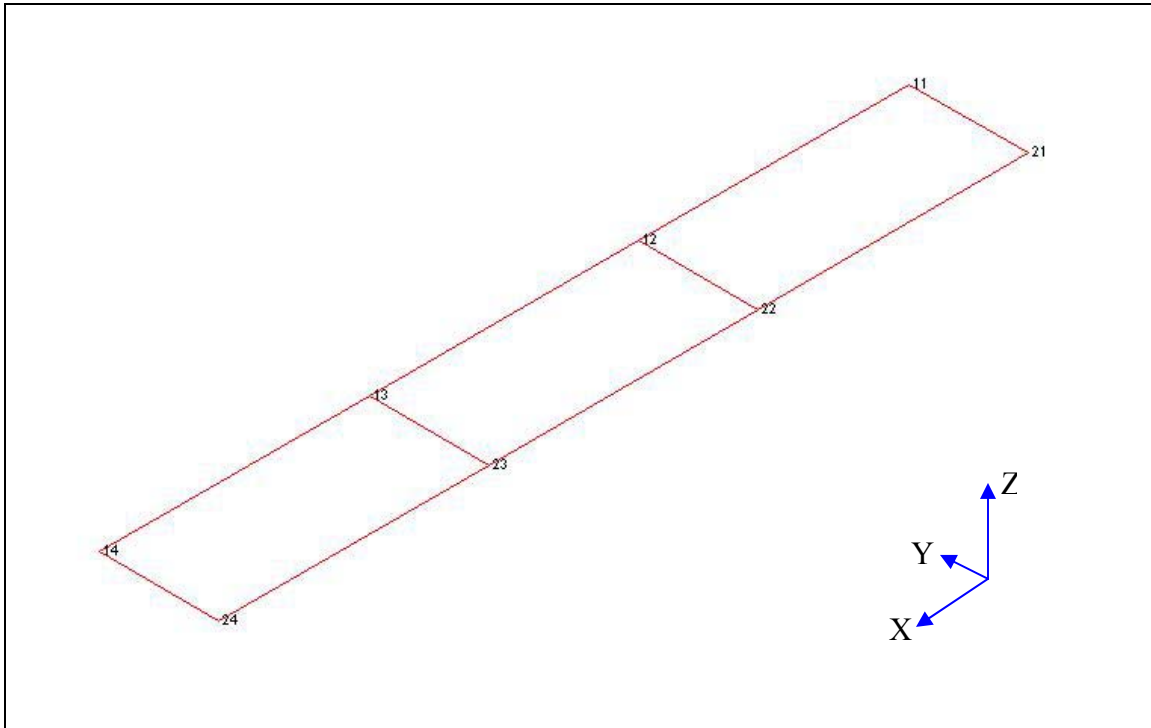


Figure 8.5 – Sensor layout for first preliminary test (US Grant Bridge)

The first preliminary test was followed by a second preliminary test which was designed in view of the findings of the first test. Figure 8.6 shows the layout of the sensors for this test. The test was again restricted to the upstream side of the bridge but sensors were placed at 18 locations and the bridge length instrumented in this case was more than the previous case. Table 8.2 lists down the bridge locations corresponding to the labels in Figure 8.6. This test revealed a much clear picture and better estimation of modes in comparison to the previous preliminary test. However, there were still certain uncertainties regarding the validity of the modes chosen. Though this set up helped in identifying some of the torsional modes, their identification was still not as obvious as the

bending modes. Further, since the bridge excitation depended solely on ambient sources, some of the modes which were clearly visible in the previous test were not that dominant in this case and vice versa.

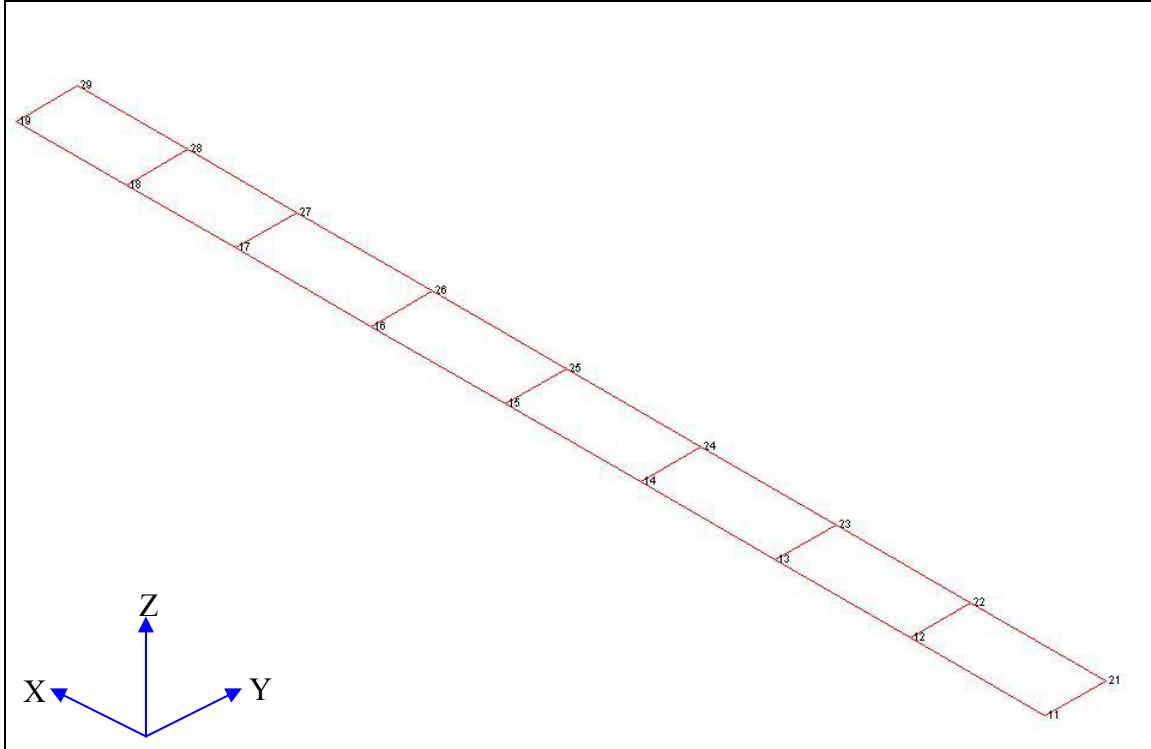


Figure 8.6 – Sensor layout for second preliminary test (US Grant Bridge)

Table 8.2 – Sensor locations on the US Grant Bridge (Second Preliminary Test) (NU – North, Upstream, SU – South Upstream)

Sensor Label	Location on Bridge	Sensor Label	Location on Bridge
11	Cable 10 NU Outer Girder	21	Cable 10 NU Inner Girder
12	Cable 11 NU Outer Girder	22	Cable 11 NU Inner Girder
13	Cable 12 NU Outer Girder	23	Cable 12 NU Inner Girder
14	Cable 13 NU Outer Girder	24	Cable 13 NU Inner Girder
15	Cable 14 NU Outer Girder	25	Cable 14 NU Inner Girder
16	Cable 15 NU Outer Girder	26	Cable 15 NU Inner Girder
17	Cable 16 NU Outer Girder	27	Cable 16 NU Inner Girder
18	Central Span Outer Girder	28	Central Span Inner Girder
19	Cable 16 SU Outer Girder	29	Cable 16 SU Inner Girder

8.1.2 Final Superstructure Test: Test Set-Up and Data Acquisition

The main purpose that the two preliminary tests served was to help in designing the final superstructure test. While doing the set up for the final test, the findings from the previous tests were considered and it was decided to instrument both the upstream and downstream sides of the bridge. Thus, there were three lines of sensors running along the length of the bridge; along the outer and inner girder on the upstream side (as in the preliminary tests) and along the outer girder on the downstream side. As in the case of the second mini test, the sensors were placed at cable locations starting from 10 S to 16 N including the sensor at the central span (thus 9 sensors per sensor line along the length of the bridge). Further in addition to these 27 sensors, 4 more sensors were placed at the locations corresponding to cable stays 5 N and 5 S at the outer girders on the upstream and downstream side, at the side spans. The purpose of putting these extra sensors was to help in distinguishing the modes which might have appeared similar in the central span with the difference being more apparent in the side spans. Figure 8.9 shows the layout of the sensors and their corresponding locations are explained in Table 8.3.

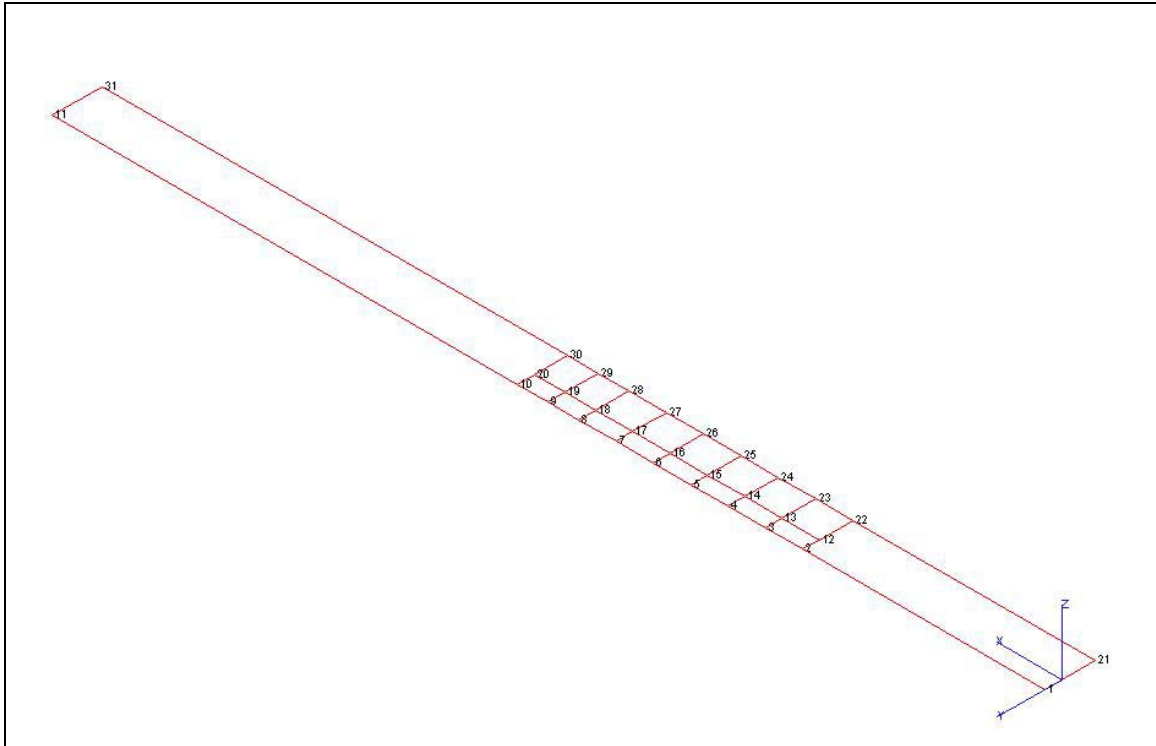


Figure 8.7 – Sensor layout for final superstructure test (US Grant Bridge)

Table 8.3 - Sensor locations on the US Grant Bridge (Final Superstructure Test)

Sensor Label	Location on Bridge	Sensor Label	Location on Bridge	Sensor Label	Location on Bridge
1	Cable 5 NU Outer Girder			21	Cable 5 ND Outer Girder
2	Cable 10 NU Outer Girder	12	Cable 10 NU Inner Girder	22	Cable 10 ND Outer Girder
3	Cable 11 NU Outer Girder	13	Cable 11 NU Inner Girder	23	Cable 11 ND Outer Girder
4	Cable 12 NU Outer Girder	14	Cable 12 NU Inner Girder	24	Cable 12 ND Outer Girder
5	Cable 13 NU Outer Girder	15	Cable 13 NU Inner Girder	25	Cable 13 ND Outer Girder
6	Cable 14 NU Outer Girder	16	Cable 14 NU Inner Girder	26	Cable 14 ND Outer Girder
7	Cable 15 NU Outer Girder	17	Cable 15 NU Inner Girder	27	Cable 15 ND Outer Girder

8.1.3 Operational Modal Analysis

The data collected was processed to obtain the power spectrums using the Cyclic Averaging approach as explained in Chapter Seven, a block size of 4096 was used along with Hanning window, thus a frequency resolution of 0.0098 Hz was obtained. The number of cyclic averages and overlap were chosen as 3 and 75% respectively. A typical auto-power spectrum is shown in Figure 8.11. Before carrying out the modal parameter estimation process, Short Time Fourier Transform (STFT) [Qian, 2002] plots were used to check the consistency of the data collected from the various sensors. A typical STFT plot is shown in Figure 8.12. Data collected from various sensors was observed to be consistent except for a few channels where either the data has to be multiplied by a calibration factor or certain portions of the data were inconsistent needed to be cleared. Further while analyzing the two datasets, it was observed that driving the van over the bridge resulted in better signal-to-noise ratio in comparison to the case when bridge is excited only by means of natural sources (wind) only.

The Complex Mode Indicator Plot (CMIF) plot based on power spectrum data for the second dataset is shown in Figure 8.13. CMIF is an excellent tool that gives an idea about the number of modes present in the frequency range of interest (which in this case is 0-3 Hz).

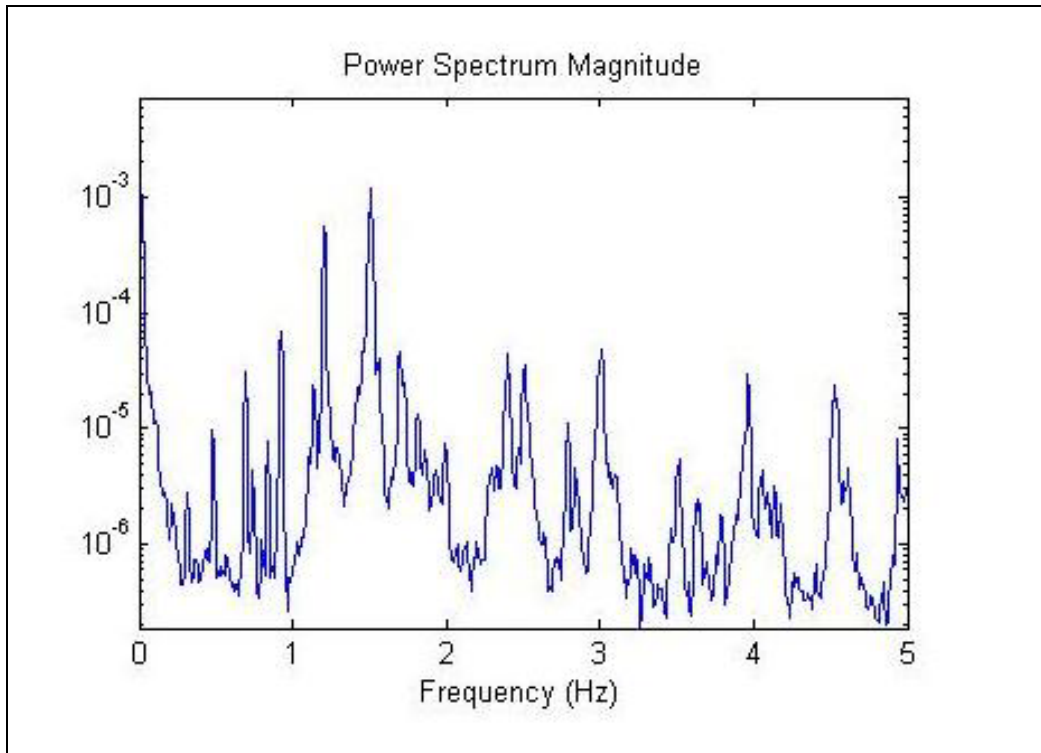


Figure 8.9 – Typical auto-power spectrum of a measured response

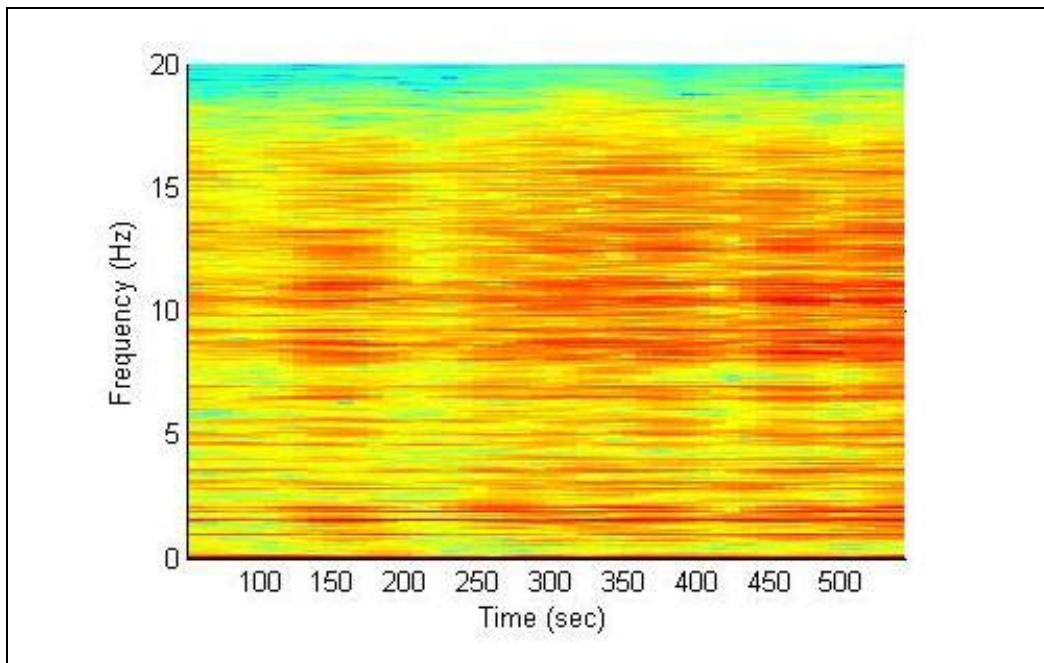


Figure 8.10 – Typical Short Time Fourier Transform (STFT) plot of response data for a chosen location

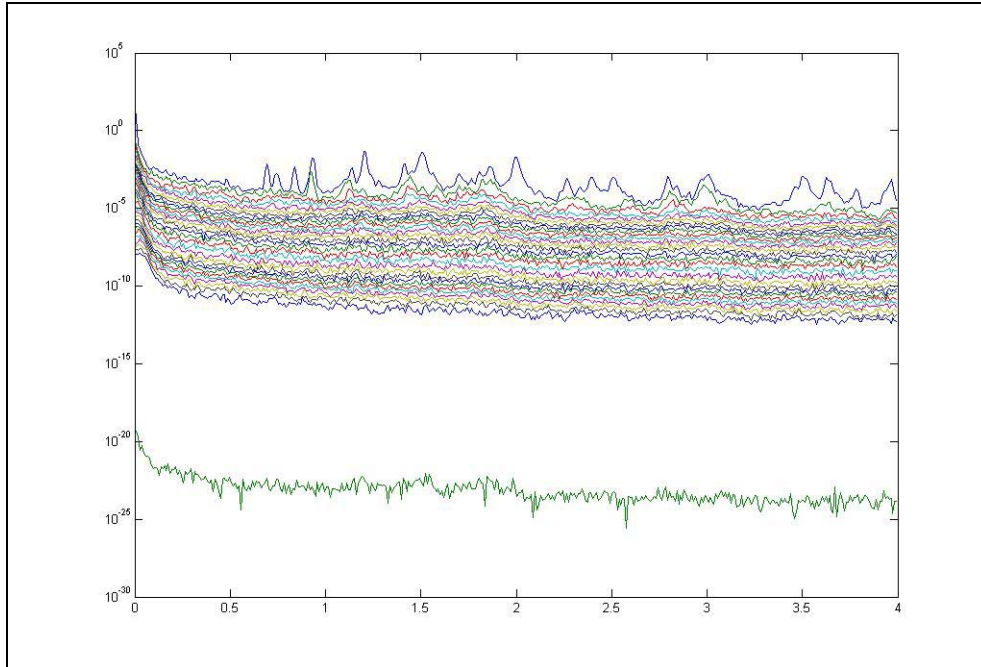


Figure 8.13 – CMIF plot of second dataset (Final superstructure test of the US Grant Bridge)

The parameter estimation process was carried out using the OMA-EMIF algorithm explained in Chapter 5. The estimated parameters are listed in Table 8.4 and some of the mode shapes and the corresponding finite element mode shapes are shown in Figure 8.14.

Table 8.4 - Estimated modal parameters for the US Grant Bridge using OMA-EMIF

Frequency (Hz)	Damping (% Critical)	Description
0.4966	1.3182	Vertical
0.6982	1.8078	Vertical
0.7418	1.8808	Torsion
0.8424	2.1355	Vertical
0.8995	1.1372	Vertical
0.9296	1.2494	Torsion
1.1259	1.2018	Torsion
1.1414	0.8501	Vertical
1.2068	1.0884	Vertical
1.4107	0.9113	Torsion
1.4444	0.9153	Torsional (Probably KY Sidespan)
1.5177	1.4354	Vertical

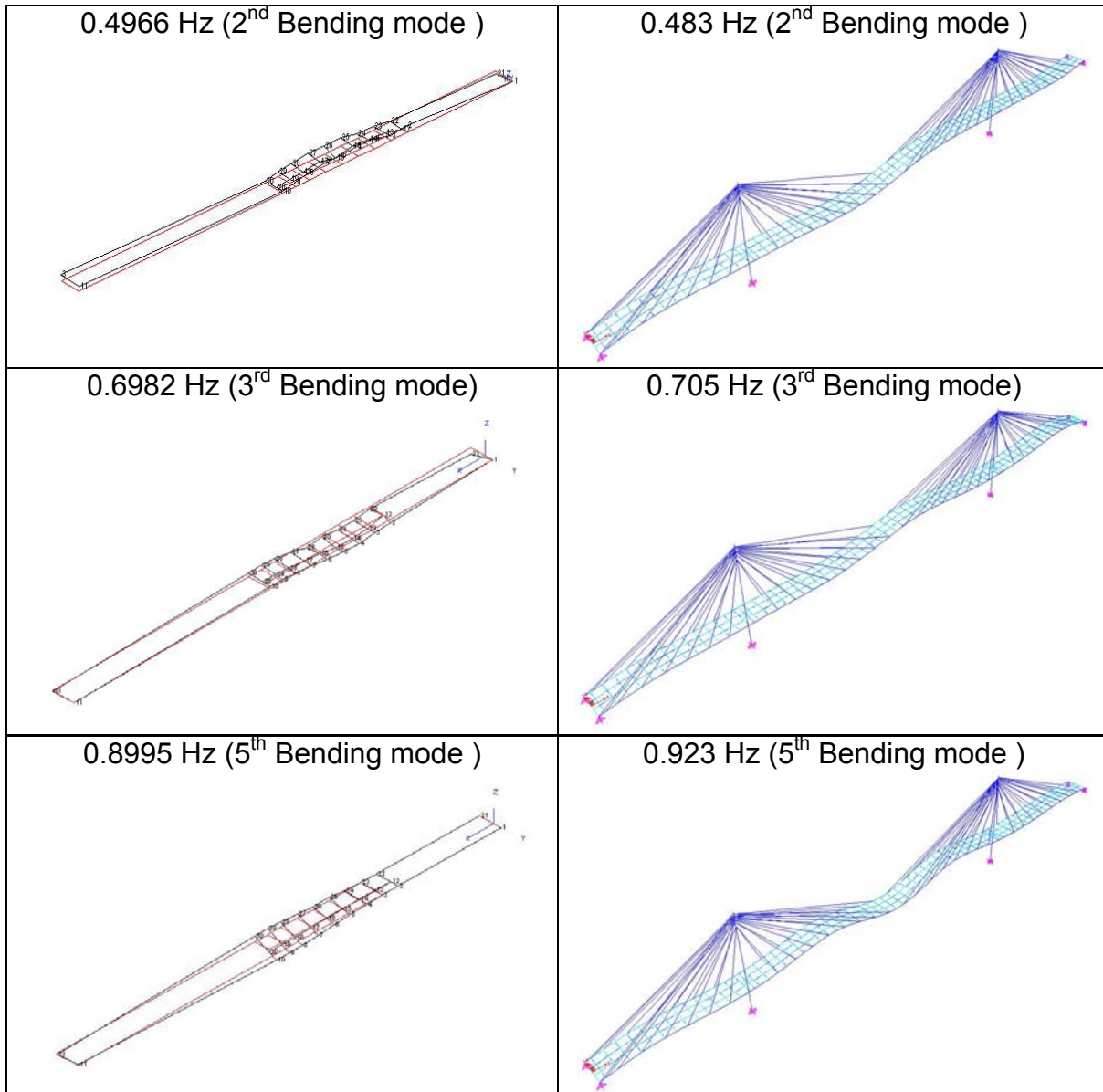


Figure 8.12 – Mode shapes (OMA vs. FEM) (US Grant Bridge)

A comparison of the selected modes among themselves is also done using the Modal Assurance Criterion and the MAC plot is shown in Figure 8.15. The MAC plot shows that most modes are fairly independent of each other, however as per the MAC plot modes at 1.1414 and 1.2068 Hz and the torsion modes at 0.742 and 0.929 Hz (shown in green and orange in Table 3) appear to be similar though these are well separated in frequency. One of the reasons for this is likely to be an observability problem. These

modes are similar in mid span, where most of the sensors were instrumented, but the mode shapes are likely to be different in the side spans. But since only mid span is instrumented sufficiently in a spatial sense, it might not be possible to differentiate between these modes.

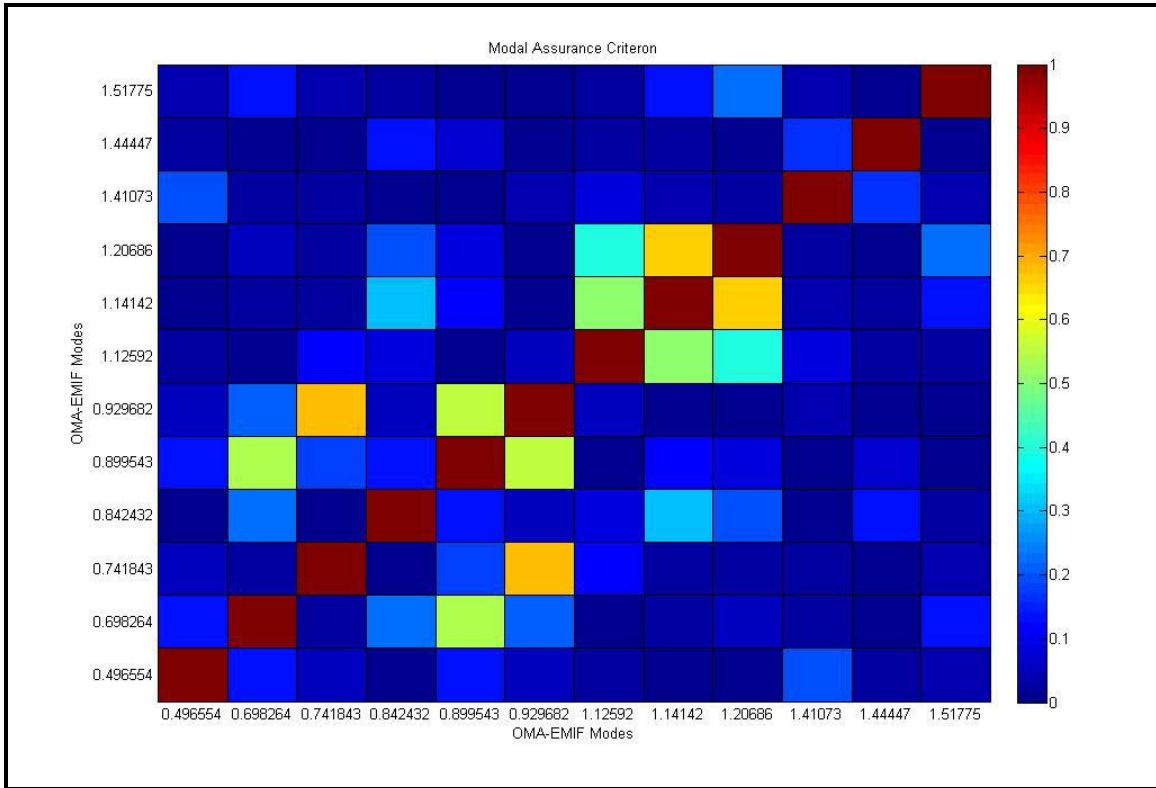


Figure 8.13 – MAC plot between the various modes obtained using OMA of the US Grant Bridge

Table 8.5 shows the comparison of the FE model based prediction of bridge modes with the experimentally obtained modes. Table 8.6 shows the MAC values for these modes obtained using the FE model and experimentally. Only the modes having large modal participation factor based on finite element analysis (as indicated in Table 8.5) are considered for MAC comparison. Table 8.5 shows that most of the bending modes are comparing well with the finite element prediction within error limits. The torsional response of the bridge didn't match well as compared to the bending response. This is

due to the fact that the girder stiffness correction in the finite element model was directed at correcting the flexural response due to the relative importance of bending modes compared to torsion modes. This stiffness correction is accurate for minimizing the differences in the bridge bending modes, but since the girders and deck are still modeled at the same horizontal plane, the differences in the torsion behavior are not corrected. Note that the experimentally obtained 1st bending mode, as indicated in the table, is obtained from the second preliminary test. This mode was not observed in the final superstructure test perhaps because of the low signal-to-noise ratio. This can be considered as one of the shortcomings of the operational modal analysis as mode observability depends considerably on favorable ambient conditions.

Table 8.5 - Comparison of FEM and OMA modes for the US Grant Bridge

FEM Modes				OMA Modes	
Description	Remarks	Freq	Modal participation Factor (Z Dir.)	Freq	Descr.
Bending-1	Center span + OH span	0.2936	1.4270	0.31	B
Tower Sway		0.3443	0.0000	-	-
Tower Anti Sway		0.3842	0.0000	-	-
Bending-2	All spans	0.4827	5.5860	0.4966	B
Deck Lateral	Center span	0.5942	0.0000	-	-
Torsion-1	Center span + small torsion in end spans	0.6786	0.0000	0.7418	T
Bending-3	All spans	0.7052	21.6690	0.6982	B
Torsion-2	Center span + OH span + small torsion in KY span	0.7971	0.0000	-	-
Bending-4	KY span + Center span + small bending in OH span	0.8150	4.6240	0.8424	B
Torsion-3	Center span + small torsion in end spans	0.8391	0.0000	-	-
Bending-5	Center span + small bending in end spans	0.9230	12.9690	0.8995	B
				0.9296	T
Torsion-4	KY span + Center span + small torsion in OH span	0.9511	0.0000		
Torsion-5	Center span + KY span + small torsion in OH span	1.0201	0.0000		
				1.1259	T
Bending-6	OH span + Center span + small bending in KY span	1.0855	1.7710	1.1414	B
Torsion-6	OH span + small torsion in center span and KY span	1.1678	0.0000		
Bending-7	All spans	1.1749	0.0150	1.2068	B
Torsion-7	All spans	1.2571	0.0000		
				1.4107	T
				1.4444	T
Bending-8	All spans	1.4233	0.9020	1.5177	B

Table 8.6: Cross MAC between OMA and FEM Bending Modes for the US Grant Bridge

FEM (Hz)	OMA (Hz)	MAC
0.483	0.497	0.88
0.704	0.698	0.91
0.815	0.842	0.60
0.924	0.899	0.84
1.087	1.141	0.69
1.178	1.207	0.89

Additionally, a time domain (PTD) and a frequency domain (RFP-z) OMA algorithm are also applied to the collected data, in order to compare their performance with the OMA-EMIF algorithm. As mentioned in Chapter 3, Polyreference Time Domain (PTD) and Rational Fraction Polynomial in z Domain (RFP-z) algorithms are high order algorithms, PTD being a time domain where RFP-z being a frequency domain algorithm. RFP-z is similar to the POLYMAX algorithm. Details of these algorithms are discussed in Chapter 3. Table 8.7 lists frequency and damping estimates obtained using the two algorithms along with the estimates of OMA-EMIF algorithm.

Table 8.7 – Comparison between RFP-z, PTD and OMA-EMIF estimates for the US Grant Bridge

RFP-z		PTD		OMA-EMIF	
Frequency	Damping	Frequency	Damping	Frequency	Damping
0.315	3.940	0.322	4.156	-	-
-	-	-	-	0.4966	1.3182
0.697	1.617	0.694	1.468	0.6982	1.8078
0.741	1.242	0.736	1.238	0.7418	1.8808
0.841	2.147	0.834	1.425	0.8424	2.1355
0.917	1.860	-	-	0.8995	1.1372
0.932	1.219	0.925	0.997	0.9296	1.2494
1.098	1.410	-	-	1.1259	1.2018
1.140	1.504	1.127	1.211	1.1414	0.8501
1.207	0.983	1.198	0.687	1.2068	1.0884
1.413	0.780	1.402	0.868	1.4107	0.9113
1.447	0.897	1.435	0.855	1.4444	0.9153
1.516	1.386	1.502	1.341	1.5177	1.4354

Both algorithms were able to estimate the mode around 0.315 Hz which was not estimated by OMA-EMIF algorithm. Further, PTD was not able to identify two modes (highlighted in the table) which were estimated by RFP-z and OMA-EMIF algorithms. The 0.49 Hz mode that was estimated by OMA-EMIF algorithm is not estimated by either PTD or RFP-z.

The MAC plots for PTD and RFP-z are shown in Figures 8.16, 8.17. As seen earlier with OMA-EMIF MAC, some modes do appear to be similar, however most of the estimated

modes are independent.

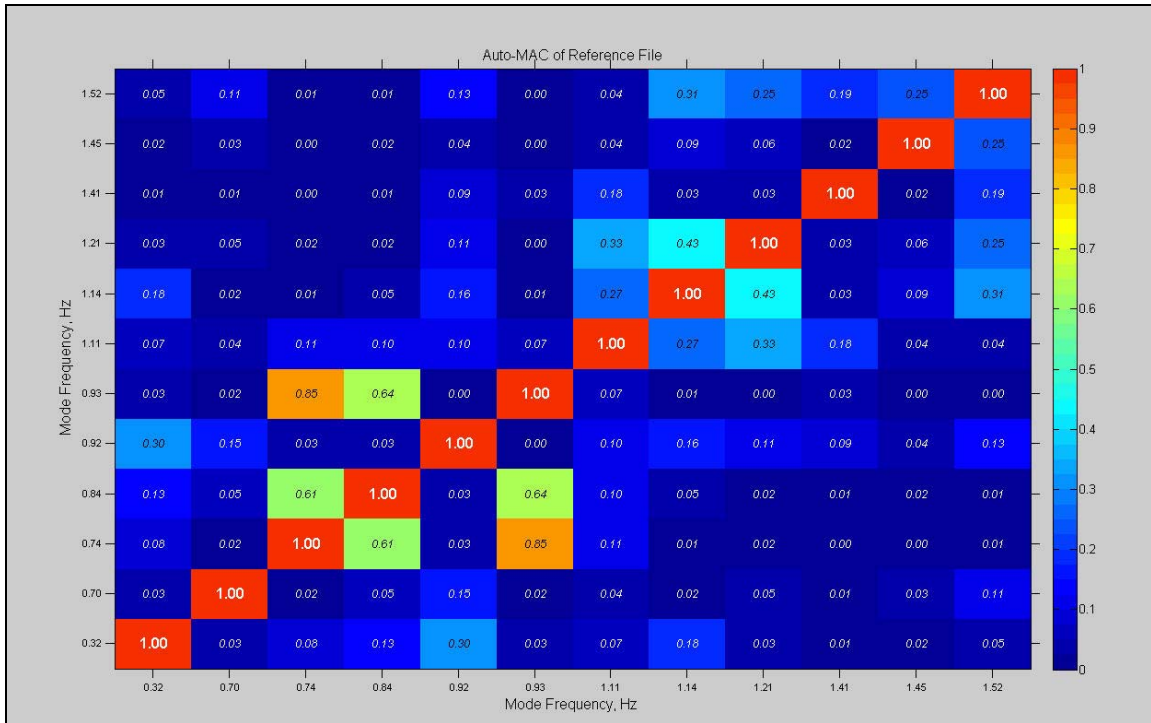


Figure 8.14: MAC for RFP-z estimates (US Grant Bridge)

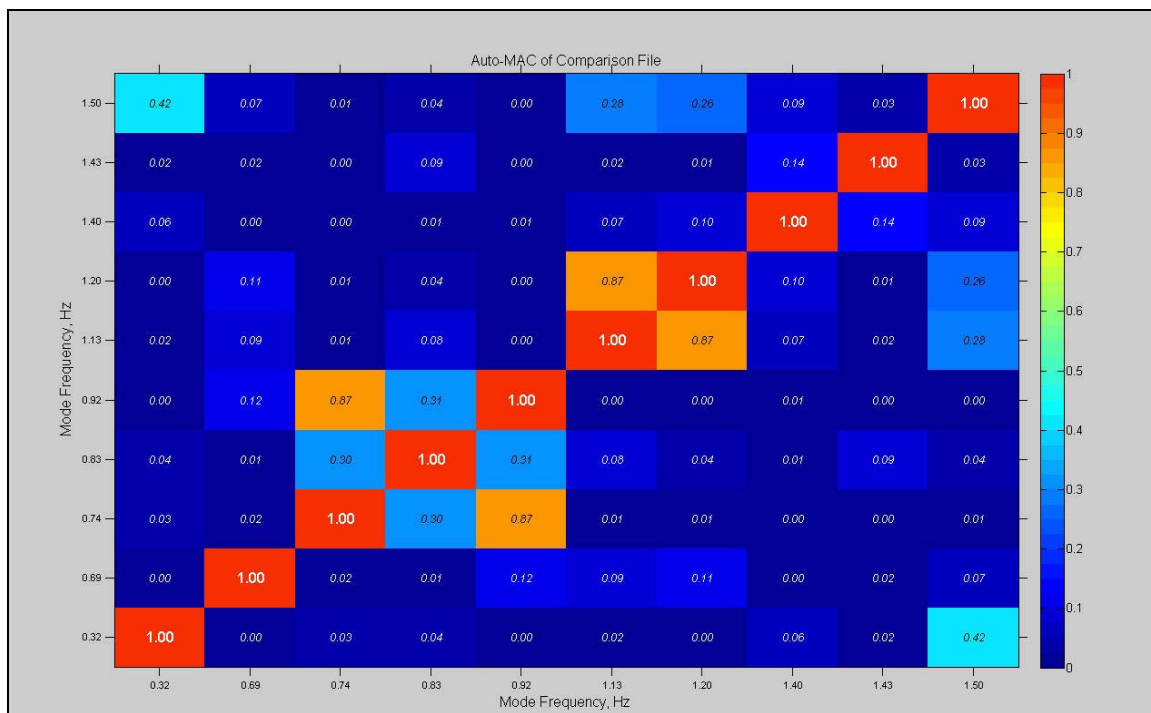


Figure 8.15: MAC for PTD estimates (US Grant Bridge)

In Table 8.8, the Cross MAC values between the various modes estimated by the three algorithms are presented. Some modes (highlighted in the table) have low Cross MAC values or are not identified by some algorithms, indicating that the estimation of these modes is not consistent through the various algorithms. However, most of the bending modes (except for the 0.89 Hz mode) were identified satisfactorily. It should again be noted that emphasis was placed, while designing the OMA experiment to observe these modes which were found to have high mass participation factor as per the finite element study.

Table 8.8 - Cross MAC comparison between various OMA algorithms for the US Grant Bridge

Frequency	OMA-EMIF/RFP-z	OMA-EMIF/PTD	RFP-z/PTD
0.31	-	-	0.169
0.49	-	-	-
0.69	0.756	0.686	0.903
0.74	0.644	0.789	0.850
0.84	0.117	0.279	0.816
0.89	0.012	-	-
0.93	0.988	0.985	.0979
1.12	0.324	-	-
1.14	0.645	0.876	0.687
1.20	0.999	0.998	0.999
1.41	0.486	0.606	0.756
1.44	0.597	0.732	0.841
1.51	0.980	0.986	0.997

8.2 Maumee River Crossing Cable-Stayed Bridge

The MRC Bridge or the Veterans' Glass City Skyway Bridge (Figure 8.18), as it is now called, is a single pylon cable-stayed bridge in Toledo, Ohio over the Maumee river on Interstate 280 on the eastern edge of Toledo downtown. The bridge replaces the Craig Memorial Bridge which was one of the last remaining drawbridges on the US interstate highways. The bridge opened to public in June, 2007.

The bridge has symmetric spans of length 612.5 ft (Figure 8.19) and the decking system consists of concrete box segments. The pylon consists of a unique cradle system which allows the cable to pass through the pylon continuously and terminating at the deck level. Thus instead of having 20 cables each on both sides of the pylon, there are only 20 cables in total which pass from one side of the bridge to the other through the pylon. The cables consist of 6 inch steel strands which are epoxy coated. Additionally, the stays are supported by mechanical dampers near the anchorage to take care of any wind or traffic induced vibrations.



Figure 8.16: Maumee River Crossing Bridge, Toledo, OH

8.2.1 OMA Test Set-Up

Figure 8.19 shows the test set-up layout. The sensor grid used for the test is much coarser in comparison to the one used for the US Grant Bridge and thus it is expected that some of the modes might appear to be similar (poor observability). A total of 10 sensors are used, 5 on each side of the parapet. The sensor lines extend from the back span side to the front span side with 8 sensors on one side of the pylon and 2 on the other as indicated in Figure 8.19. The sensor line extends 500m from Cable 14B on the back span to 6A on the front span. Note that notations *A* and *B* are for front and back spans respectively. Figure 8.20 shows one of the accelerometers glued on the bridge superstructure.

The data acquisition parameters for the test were set as following

Sampling rate	40 Hz
Frequency Range	0 – 15 Hz
Test Duration	20 Min

The bridge was partially opened to public and one lane of traffic was open during the test.

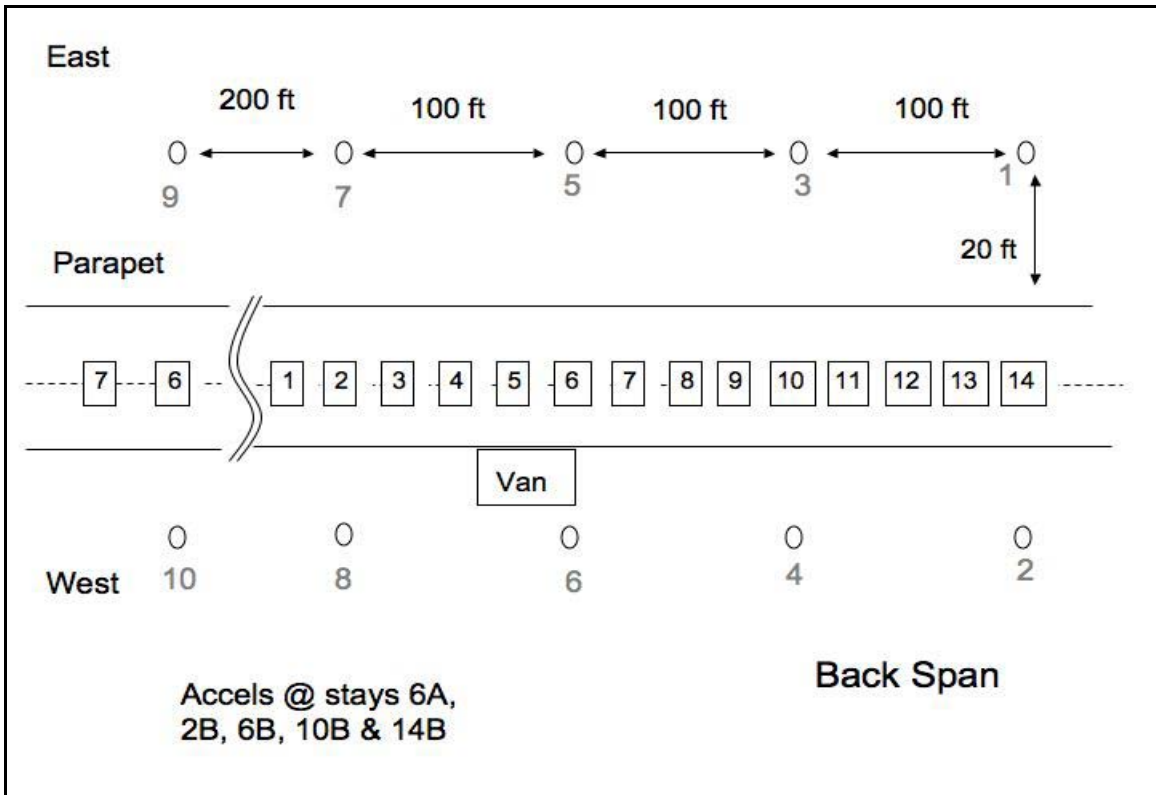


Figure 8.17: OMA Test Set-Up Layout for the MRC Bridge



Figure 8.18: Typical accelerometer set up for the MRC Bridge OMA test

8.2.2 Operational Modal Analysis

The data was processed using the Cyclic Averaging approach to obtain the power spectrums. A block size of 2048 was used along with 3 cyclic averages, Hanning window, and 90% overlap. The autopower plot of individual channels is shown in Figure 8.21. The plot indicates the presence of at least 6 modes below 1.4 Hz frequency range.

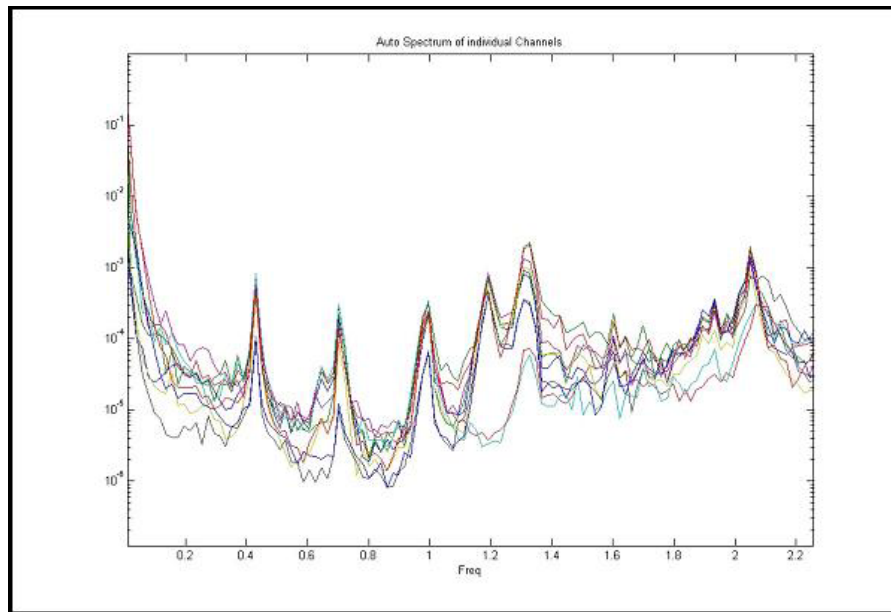


Figure 8.19: Autopower spectrum of individual channels (MRC Bridge)

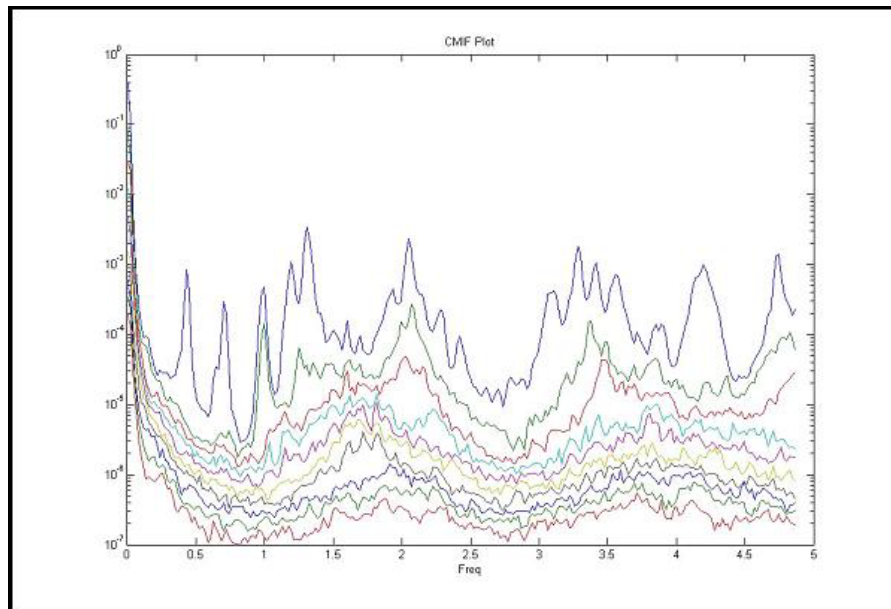


Figure 8.20: Complex Mode Indicator Function Plot (MRC Bridge)

The CMIF plot (Figure 8.22) indicates the presence of two close modes around 1 Hz in addition to the modes indicated by the Autopower plot.

The results of the OMA-EMIF algorithm based modal parameter estimation are listed in Table 8.9. The MAC plot (Figure 8.23) confirms that due to lack of sufficient spatial resolution (coarse sensor grid) some of the mode shapes appear to be similar even though they are well separated in terms of modal frequency. This is likely due to the fact that sensor layout doesn't account for lateral modes and cable vibration modes.

Table 8.9 - Estimated modal parameters for MRC Bridge using OMA-EMIF

Frequency (Hz)	Damping (% Critical)	Description
0.4332	2.6295	Vertical
0.6442	3.5498	Vertical
0.7083	1.8311	Vertical
0.9849	1.4854	Torsional
0.9919	1.5223	Torsional
1.1915	1.7819	Vertical
1.3116	1.7276	Vertical
1.5147	1.9206	Vertical
1.6041	1.3371	Vertical
1.6984	1.2087	Vertical
1.8439	1.1041	Torsional
1.9508	1.8700	Torsional
2.0530	1.3031	Torsional
2.0873	0.6938	Vertical + Torsional
2.2991	1.6992	Vertical
2.4198	1.6646	Vertical

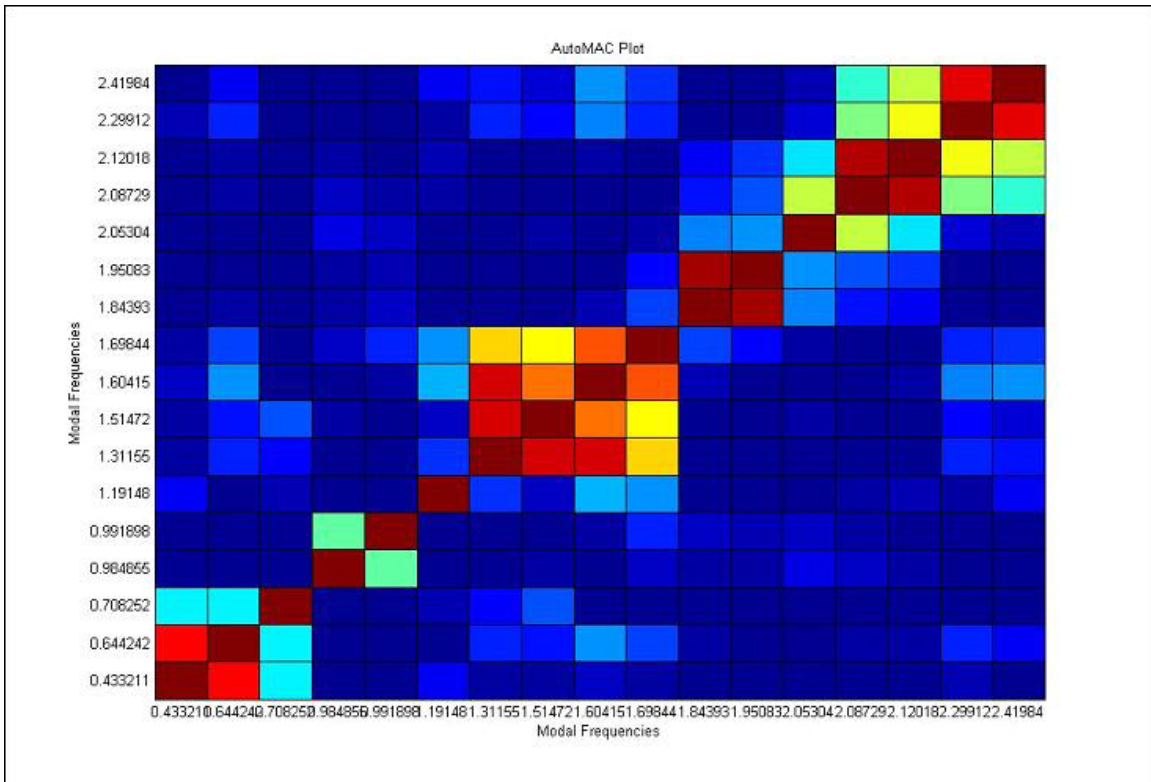


Figure 8.21: AutoMAC plot for the various modes obtained by OMA of the MRC Bridge

The green cells in Table 8.9 indicate the modes which are not well observed. These modes also appear to be similar to other modes as indicated by the MAC plot. The fact that these modes do not show up when other OMA parameter estimation algorithms are applied to the same data also provide little confidence in these modes. However this limitation is not on part of the algorithm but the test set up and resulting data and this problem can be attributed to several factors including instrumenting only a section of the bridge resulting in insufficient spatial resolution, a limited sensor grid, mounting the sensors in only the vertical direction thus not accounting for lateral motion of the bridge, tower sway and cable vibrations. Thus just like EMA, the need for proper test design is utmost for getting good estimates of the modal parameters.

Since the results of the FE analysis for this bridge were not available, a comparison on the lines of US Grant bridge was not possible. However, a preliminary test with a smaller sensor layout (only 5 sensors) was conducted and the result of the final test matched well with that test. The mode shapes of the few selected modes are shown in Figure 8.24. Most of the modes are fairly real normal modes.

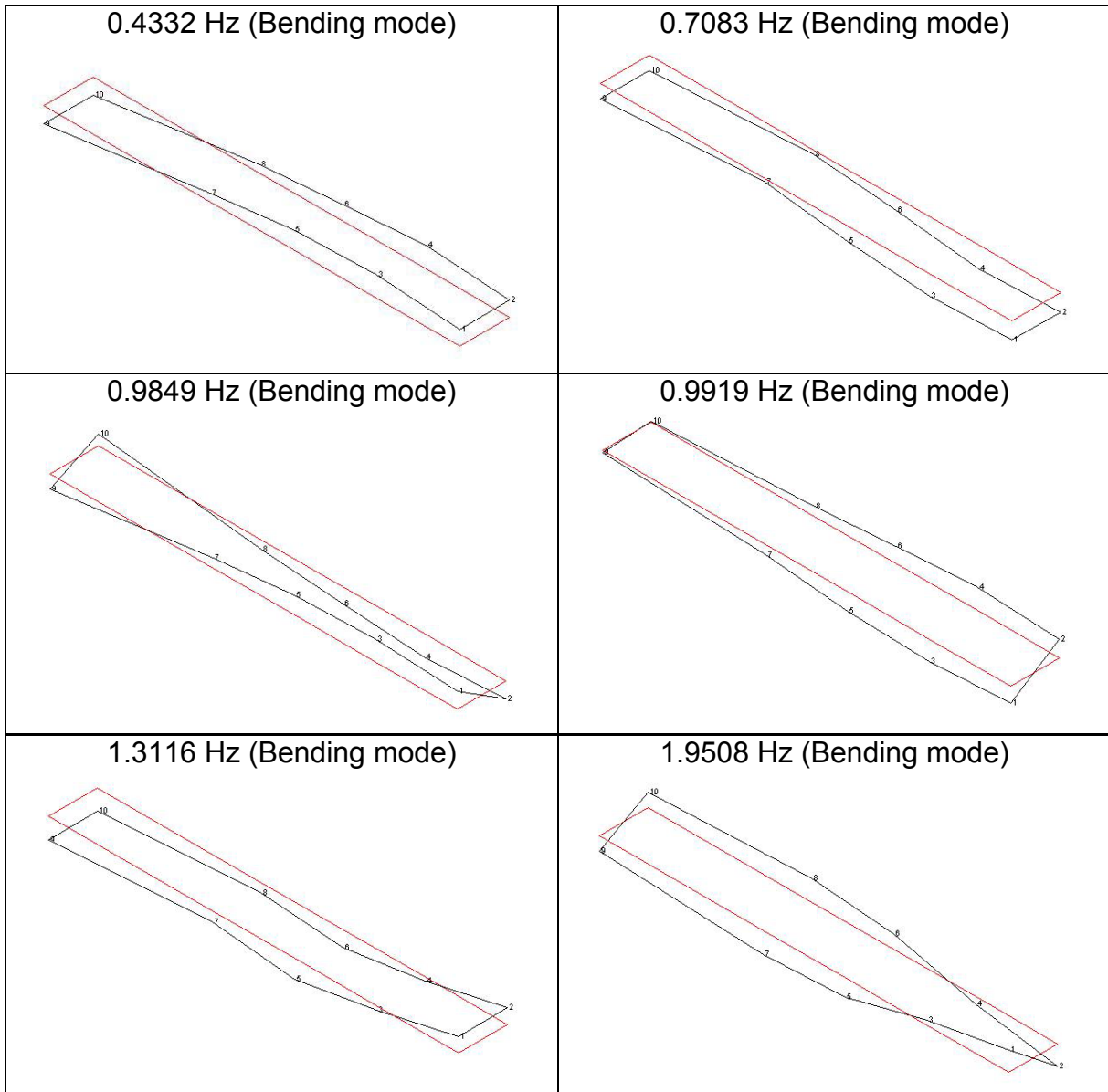


Figure 8.22 – Mode shapes (MRC Bridge)

8.3 Conclusions

The OMA-EMIF algorithm developed in Chapter 5 is applied to two cable-stayed bridges and is shown to work satisfactorily in both the cases. In the case of the US Grant Bridge, the results of the OMA-EMIF algorithm are found to be similar to those obtained using other OMA algorithms like PTD and RFP-z as well as the finite element model based study.

It is observed that an important aspect of applying these techniques to real-life structures is careful planning and design of the tests. This is also an important step in traditional experimental modal analysis. Finite element models and smaller preliminary tests are of considerable use in this regard. They provide useful a priori information that can be of much help while testing such large structures, especially in view of limitations on sensors and cabling. As is shown in the case of the US Grant Bridge, the importance of designing the final test in this manner comes from the fact that the chosen set up is optimum for the intended purpose which helps in reducing set up time, instrumentation and sensor requirement etc.

In the future, the estimated modal parameters can be used for a variety of purposes. FE model updating is one such area where based on the experimentally observed modal parameters, the FE model is updated to correctly simulate the dynamic behavior of the structure. The modal parameters can also be used for damage detection and structural health monitoring purposes. Since the tests are conducted before the bridge is opened for service, the attained modal parameters can act as base line and similar modal tests can be conducted in the future. The modal parameters can be compared with these base line parameters to determine if the bridge dynamics have changed or not.

Chapter Nine

Conclusions and Recommendations for Future Work

9.1 Summary and Conclusions

Despite being a relatively new field, Operational Modal Analysis has shown a lot of promise especially in situations difficult handle using traditional Experimental Modal Analysis techniques. Due to this, OMA techniques have generated a growing interest in the research community and are gaining popularity with time. However, the field is still in its developmental stage and efforts are needed towards understanding its advantages and limitations in more detail.

The main focus of this dissertation was the modal parameter estimation for OMA and the signal processing techniques needed for the same. The work presented in this dissertation contributes to the field of OMA in two aspects;

1. development of new and illustration of existing, parameter estimation techniques for OMA together with associated signal processing techniques,
2. assessment of conditions where the OMA parameter estimation process will work satisfactorily and where it will struggle, thus providing useful insights to the application of OMA techniques.

It can be concluded, on the basis of the research work carried out in this dissertation, that:

- The Unified Matrix Polynomial Approach (UMPA) is a powerful concept for formulating various OMA algorithms like SSI, PolyMAX, etc. which have otherwise been developed in isolation. UMPA provides a common mathematical framework which aids in better understanding of the various algorithms, their similarities and differences, advantages and limitations. The concept can further be utilized for developing other algorithms such as low order frequency and Z domain variants as presented in Chapter Four.
- The Positive Power Spectrum (PPS) is an effective signal processing technique for dealing with the numerical conditioning problems emerging due to the fact that the power spectrum has twice the order of frequency response functions and contains the same modal parameters related information twice. In this regard PPS helps great deal in making parameter estimation OMA frequency domain algorithms a reality.
- The UMPA-LOFD and its variant that uses complex Z mapping are useful additions to the existing OMA algorithms. These algorithms are frequency domain OMA algorithms based on the PPS. These algorithms utilize low model order thus avoiding numerical conditioning issues associated with higher order algorithms such as the RFP. The parameter estimation results of these algorithms are comparable to the existing OMA algorithms.
- By utilizing the OMA-EMIF, a spatial domain algorithm developed as a part of this research, it is possible to estimate multiple modes at a time, unlike the FDD/eFDD approach that estimates one mode at a time. It is also possible to utilize the residual terms to account for the effect of out-of-band modes while using the OMA-EMIF, as this algorithm works in frequency domain.

- The performance of any and all OMA algorithms, including the FDD, deteriorates if the assumption of complete uniform spatial excitation is violated. In such situations, the power spectrum based CMIF (or FDD) plots contain spurious peaks which can be confused as the system modes especially in case of poor signal-to-noise ratio; conditions that are very common in real life. A simple but useful tool, *Singular value Percentage Contribution (SVPC)* plot, can deal with such situations by providing means to interpret the CMIF plots in situations of insufficient spatial excitation.
- New signal processing approaches like Independent Component Analysis and Blind Source Separation (ICA/BSS) can be exploited to obtain modal parameters without requiring the knowledge of the excitation forces by utilizing the concepts of modal filters and modal expansion. The fact that these techniques do not require the use of consistency or stabilization diagrams, makes them an interesting option for OMA purposes.
- Though modal frequency estimation remains unaffected, estimation of the modal damping is affected greatly if leakage errors are present in the computed output response power spectra, which are comparatively more difficult to estimate than the frequency response functions. Cyclic Averaging is a powerful signal processing technique which should be used along with RMS averaging, windowing and overlapping for reducing the effects of leakage and hence improving the accuracy of damping estimates.
- The accuracy of damping estimates is also affected in situations where the basic OMA assumption that excitation forces should be random, uncorrelated and broadband in spectrum is violated. Unlike the leakage related problems that can be dealt with, up to a certain extent, by using techniques like Cyclic Averaging,

the nature of natural excitation is beyond one's control and thus difficult to deal with in real life situations.

- The OMA-EMIF algorithm works satisfactorily when applied to complex, real-life structures such as the two cable-stayed bridges, the US Grant Bridge and the Maumee River Crossing Bridge, tested as a part of this research. The study also underlines the importance of proper designing of the OMA tests before carrying out the final superstructure test. The FE modeling and series of smaller preliminary tests vastly help in this regard by optimizing the final tests.

9.2 Recommendations for Future Work

As a researcher, one constantly seeks to push the boundaries in order to solve problems that are complex and difficult to solve by using existing methodologies. Operational Modal Analysis, as an application technique, developed due to researchers pushing beyond the known realms of Experimental Modal Analysis. The aim was to understand the dynamics of complex structures which do not lend themselves readily to EMA techniques. In the past ten years, the field of OMA has progressed from being an interesting concept on a researcher's table to a commercially available technique. In this current scenario, the challenges for the future are governed by the need to strengthen the field of OMA by having a sound and deep understanding necessary for its correct implementation and at the same time also aimed at widening of its scope. This means future research has to focus on both the deeper and finer issues such as accurate damping estimation, as well as the broader issues for e.g. utilizing OMA techniques for related application such as active vibration control etc.

The damping issue explored in Chapter Seven of the dissertation is one area which needs to be explored further to understand completely the reasons why damping

estimation is with OMA techniques is not as accurate. In Chapter Seven, cyclic averaging was suggested as one of the methods to overcome leakage related errors that affect the damping estimates. Future research should concentrate on finding signal processing techniques that should aid in more accurate estimation of damping. BSS / ICA based techniques might be one such option as these techniques differ from the more common parameter estimation approaches. In this dissertation, mostly power spectrum data was obtained using the Welch Periodogram approach and occasionally with Cyclic Averaging. It will be interesting to see how damping estimates are affected if correlogram approach is used instead. The Cyclic Averaging approach needs to be explored further in more details. It will also be insightful to understand how various kinds of windows, overlapping and zero padding, etc. affect the damping estimation.

Structural health monitoring and damage detection are two important fields in the area of structural dynamics and future research should involve the exploitation of the OMA algorithms presented in this research for these purposes. These techniques can be used for continuous monitoring of big civil structures such as bridges, buildings etc. as they utilize natural excitation which is not required to be measured. OMA techniques lend themselves more easily for continuous monitoring purposes in comparison to Experimental Modal Analysis which requires the measurement of the force exciting the structure. Thus, the OMA based approach could not only be a more feasible but also a comparatively less costly option. An ICA/BSS based approach as documented in Chapter Six could be very effective as this method yields mode shapes and modal frequencies in one step. This needs to be explored further to find out how sensitive this approach is to small local damages in the structure.

OMA is still a developing area and scope of improved parameter estimation algorithms continue to exist. In this regard, the idea of frequency domain ICA algorithm for OMA, as introduced in Chapter Six, needs to be explored in more detail. An OMA model is similar

to a BSS/ICA model in frequency domain. However, such a model exists for each frequency bin and the order of the identified sources isn't same in various frequency bins. Thus a permutation error is introduced which is difficult to overcome, thus making frequency domain BSS/ICA based OMA algorithm much more challenging to develop. Future research in application of BSS/ICA techniques to OMA should involve development of the frequency domain approach as well as application of these algorithms to practical real life structures.

The concept of modal filters in the past has been used for applications involving active vibration control of structures, flight flutter testing, etc. BSS/ICA techniques are based on the concept of modal filters and directly uncouple the system responses into SDOF modal coordinate responses. Thus these techniques lend themselves naturally to these applications and this very aspect of these techniques makes them very attractive future research area.

Similarly, researchers across the globe are working on utilizing signal processing techniques other than computing power spectra or correlation functions for the purpose of OMA. Some of these attempts include utilization of transmissibility functions [Devriendt, Guillaume et al., 2007], cyclostationarity and cepstrum analysis [Hanson, Randall, et al., 2007] etc. Most of these methods are still in primitive stages and it will be interesting to how they compare with more established OMA algorithms while testing real structures. It will also be important to note whether these methods yield more accurate damping estimates as they utilize different signal processing approach.

Finally, the ultimate challenges for Operational Modal Analysis are those very ones that are associated with Experimental Modal Analysis as well. Having achieved a level of comfort while dealing with the problems that categorizes as linear, time-invariant systems; the future research needs to push further and explore systems that are

nonlinear and time variant; systems that are often so complex that behavior cannot be sufficiently explained with the range of EMA/OMA assumptions.

Just like EMA, most of the OMA algorithms use stabilization diagrams as a part of modal parameter estimation process to find out true modes of the system from the mathematical modes. Often the user chooses one of the estimates amongst the stabilized modes as the system mode and this makes the whole selection process based very much on the user judgment. A statistical tool based on minimum distance (such as Euclidian or Mahalanobis distance from the target) can be developed to aid this selection process. This process can involve algorithms such as k-nearest neighbor (for example, to the mean) etc. in order to identify the parameter closet to the mean of its various estimates. The same process can also be applied to EMA algorithms.

References

1. Aenlle, M.A., Brincker, R., Canteli, A.F. (2005), "Some Methods to Determine Scaled Mode Shapes in Natural Input Modal Analysis", Proceedings of the 23rd IMAC, Orlando, FL.
2. Agneni, A., Brincker, R., Coppotelli, G. (2004), "On Modal Parameter Estimation from Ambient Vibration Tests", Proceedings of ISMA International Conference on Noise and Vibration Engineering, Katholieke Universiteit Leuven, Belgium.
3. Agneni, A., Coppotelli, G. (2006), "Modal Parameter Identification from Operative Responses", Proceedings of ISMA International Conference on Noise and Vibration Engineering, Katholieke Universiteit Leuven, Belgium.
4. Akaike, H. (1974) "Stochastic Theory of Minimal Realization", IEEE Transaction on Automatic Control, 19, 667-674.
5. Allemang, R.J. (1980); "Investigation of some multiple input/output frequency response function experimental modal analysis techniques", PhD Dissertation, University of Cincinnati, Mechanical Engineering Department.
6. Allemang, R.J. (1999), "Vibrations: Experimental Modal Analysis", Structural Dynamics Research Laboratory, Department of Mechanical, Industrial and Nuclear Engineering, University of Cincinnati,
http://www.sdrl.uc.edu/sdrl_jscript_homepage.html
7. Allemang, R. J., Brown, D. L., Fladung, W.A. (1994), "Modal Parameter Estimation: A Unified Matrix Polynomial Approach", Proceedings of the 12th IMAC, Honolulu, Hawaii.

8. Allemang, R. J., Brown, D. L. (1998), "A Unified Matrix Polynomial Approach to Modal Identification", *Journal of Sound and Vibration*, Volume 211, Number 3, pp. 301-322.
9. Allemang, R.J., Brown, D.L. (2006), "A Complete Review of the Complex Mode Indicator Function (CMIF) with Applications", *Proceedings of ISMA International Conference on Noise and Vibration Engineering*, Katholieke Universiteit Leuven, Belgium.
10. Allemang, R.J., Phillips, A.W. (1996); "Cyclic averaging for frequency response function estimation", *Proceedings of 14th International Modal Analysis Conference*.
11. Allemang, R. J., Phillips, A.W. (2004), "The Unified Matrix Polynomial Approach to Understanding Modal Parameter Estimation: An Update", *Proceedings of ISMA International Conference on Noise and Vibration Engineering*, Katholieke Universiteit Leuven, Belgium.
12. Andersen, P. (1997), *Identification of Civil Engineering Structures using Vector ARMAR Model*, Ph.D. Thesis, Aalborg University, Denmark.
13. Andersen, P., Brincker, R., Peeters, B., De Roeck, G., Hermans, L., Kramer, C. (1999), "Comparison of systems identification methods using ambient bridge test data", *Proceedings of the 17th IMAC*, Kissimmee, FL.
14. Antoni, J. (2005); "Blind separation of vibration components: principles and demonstrations", *Mechanical Systems and Signal Processing*, Vol. 19 (6), pp. 1166-1180.
15. Aoki, M. (1987), *State Space Modeling of Time Series*, Springer-Verlag, Berlin, Germany.

16. Arun, K.S., Kung, S.Y. (1990), "Balanced Approximation of Stochastic System", *SIAM Journal of Matrix Analysis Application*, 11(1).
17. Avitable, P. (2006), "Someone told me that operating modal analysis produces better results", *Modal Space – Back to Basics, Experimental Techniques*.
18. Belouchrani, A., Abed-Meraim, K.K., Cardoso, J.F., Moulines, E. (1993); "Second order blind separation of correlated sources", *Proceedings of International Conference on Digital Signal Processing*, pp. 346-351.
19. Bendat, J., Piersol, A. (1986), *Random Data: Analysis and Measurement Procedures*, 2nd edition, Wiley, New York.
20. Bendat, J., Piersol, A. (1993), *Engineering Applications of Correlation and Spectral Analysis*, 2nd edition, Wiley, New York.
21. Benveniste, A., Fuchs, J.J. (1985), "Single Sample Modal Identification of a Nonstationary Stochastic Process", *IEEE Transactions on Automatic Control*, 30, 66-74.
22. Brincker, R., Andersen, P. (2003), "A Way of Getting Scaled Mode Shapes in Output Only Modal Testing", *Proceedings of the 21st IMAC, Kissimmee, FL*.
23. Brincker, R., Andersen, P., Moller, N. (2000), "An Indicator for Separation of Structural and Harmonic Modes in Output-Only Modal Testing", *Proceedings of the 18th IMAC, San Antonio, TX*.
24. Brincker, R., Andersen, P., Moller, N. (2000), "Output Only Modal testing of a Car Body Subject to Engine Excitation", *Proceedings of the 18th IMAC, San Antonio, TX*.
25. Brincker, R., Ventura, C., Andersen, P. (2000), "Damping Estimation by Frequency Domain Decomposition", *Proceedings of the 18th IMAC, San Antonio (TX), USA*.

26. Brincker, R., Zhang, L., Andersen, P. (2000), "Modal Identification from Ambient Responses Using Frequency Domain Decomposition", Proceedings of the 18th IMAC, San Antonio (TX), USA.
27. Brown, D.L., Allemang, R.J., Zimmerman, R.J., Mergeay, M. (1979), "Parameter Estimation Techniques for Modal Analysis", SAE Paper 790221.
28. Cardoso, J.F. (1991); "Super-symmetric decomposition of the fourth order cumulant tensor. Blind identification of more sources than sensors", Proceedings of IEEE ISCAS, pp. 3109-3112, Vol. 5, Toronto.
29. Cardoso, J.F. (1998); "Blind signal separation: statistical principles", Proceedings of the IEEE, Vol. 86, Number 10, pp. 2009-2025.
30. Cardoso, J.F., Souloumiac, A. (1993); "Blind beamforming for non Gaussian signals", Proceedings of IEE Radar and Signal Processing, Vol. 140 (6), pp. 362-370.
31. Cardoso, J.F., Souloumiac, A. (1996); "Jacobi angles for simultaneous diagonalization", SIAM Journal of Matrix Analysis and Applications, Vol. 17, Number 1, pp. 161-164.
32. Chauhan, S., Martell, R., Allemang, R. J. and Brown, D. L. (2006), "Utilization of traditional modal analysis algorithms for ambient testing", Proceedings of the 23rd IMAC, Orlando (FL), USA.
33. Chauhan, S., Martell, R., Allemang, R. J. and Brown, D. L. (2006), "A Low Order Frequency Domain Algorithm for Operational Modal Analysis", Proceedings of ISMA International Conference on Noise and Vibration Engineering, Katholieke Universiteit Leuven, Belgium.
34. Chauhan, S., Martell, R., Allemang, R. J. and Brown, D. L. (2006), "Considerations in the Application of Spatial Domain Algorithms to Operational

- Modal Analysis”, Proceedings of ISMA International Conference on Noise and Vibration Engineering, Katholieke Universiteit Leuven, Belgium.
35. Chauhan, S., Martell, R., Allemang, R. J. and Brown, D. L. (2007), “A Unified Matrix Polynomial Approach for Operational Modal Analysis”, Proceedings of the 25th IMAC, Orlando (FL), USA.
 36. Chauhan, S., Martell, R., Allemang, R. J. and Brown, D. L. (2007), “Application of Independent Component Analysis and Blind Source Separation techniques to Operational Modal Analysis”, Proceedings of the 25th IMAC, Orlando (FL), USA.
 37. Chauhan, S., Phillips, A.W., Allemang, R.J. (2008), “Damping Estimation Using Operational Modal Analysis”, Proceedings of the 26th IMAC, Orlando (FL), USA.
 38. Chauhan, S., Saini, J.S., Helmicki, A.J., Hunt, V.J., Swanson, J.A., Allemang, R.J. (2007), “Operational Modal Analysis of the US Grant Bridge at Portsmouth, Ohio”, Proceedings of the SEM Annual Conference, Springfield, MA.
 39. Chauhan, S., Saini, J.S., Kangas, S., Helmicki, A.J., Hunt, V.J., Allemang, R.J. (2008), “Application of OMA Algorithms to US Grant Bridge at Portsmouth, Ohio”, Proceedings of the 26th IMAC, Orlando (FL), USA.
 40. Cichocki, A., Amari, S. (2002), *Adaptive Blind Signal and Image Processing*, John Wiley and Sons, New York.
 41. Cunha, A., Caetano, E. (2005), “From Input-Output to Output Only Modal Identification of Civil Engineering Structures”, Proceedings of the 1st IOMAC, Copenhagen, Denmark.
 42. Dapena, A., Servière, C. (2001); “A simplified frequency domain approach for blind separation of convolutive mixtures”, Proceedings of ICA, San Diego, USA, pp. 569–574.

43. Devriendt, C., Guillaume, P., Reynders, E., De Roeck, G. (2007), "Operational Modal Analysis of a Bridge Using Transmissibility Measurements", Proceedings of the 25th IMAC, Orlando (FL), USA.
44. Ewins, D.J. (2000), *Modal testing: Theory, Practice and Applications*, 2nd edition, Research Studies Press Limited, Hertfordshire, England.
45. Felber, A.J. (1993), *Development of a Hybrid Bridge Evaluation System*, PhD Thesis, Dept. of Civil Engineering, University of British Columbia, Vancouver, Canada.
46. Fladung, W.A (2001), *A Generalized Residuals Model for the Unified Matrix Polynomial Approach to Frequency Domain Modal Parameter Estimation*, PhD Dissertation, Department of Mechanical, Industrial and Nuclear Engineering, University of Cincinnati, USA.
47. Fladung, W.A, Phillips, A.W, Brown, D.L. (1997), "Specialized Parameter Estimation Algorithms for Multiple Reference Testing", Proceedings of the 15th IMAC, Orlando, FL, USA.
48. Fladung, W.A., Zucker, A.T., Phillips, A.W., Allemang, R.J. (1999); "Using cyclic averaging with impact testing", Proceedings of 17th International Modal Analysis Conference.
49. Fukuzono, K. (1986), *Investigation of the Multiple Reference Ibrahim Time Domain Modal Parameter Estimation Technique*, M.S. Thesis, Dept. of MINE, University of Cincinnati.
50. Gade, S., Moller, N., Herlufsen, H., Hansen, H. (2005), "Frequency Domain Techniques for Operational Modal Analysis", Proceedings of the 23rd IMAC, St. Louis (MO), USA.

51. Gersch, W., Fouth, D.A. (1974), "Least Squares Estimates of Structural System Parameters Using Covariance Function Data", IEEE Transactions on Automatic Control, Vol. AC-19 (6), pp. 898-903.
52. Gersch, W., Luo, S. (1972), "Discrete Time Series Synthesis of Randomly Excited Structural System Responses", Journal of the Acoustical Society of America, Vol. 51 (1), pp. 402-408.
53. Goursat, G., Basseville, M., Benveniste, A., Mevel, L. (2001), "Output-Only Modal Analysis of Ariane 5 Launcher", Proceedings of the 19th IMAC, Kissimmee (FL), USA.
54. Guillaume, P., Verboven, P., Vanlanduit, S. (1998), "Frequency-Domain Maximum Likelihood Identification of Modal Parameters with Confidence Intervals", ", Proceedings of ISMA International Conference on Noise and Vibration Engineering, Katholieke Universiteit Leuven, Belgium.
55. Guillaume, P., Verboven, P., Vanlanduit, S., H. Van Der Auweraer, Peeters, B. (2003), "A Poly-Reference Implementation of the Least-Squares Complex Frequency-Domain Estimator", Proceedings of the 21st IMAC, Kissimmee (FL), USA.
56. Hanson, D., Randall, R.B., Antoni, J., Thompson, D.J., Waters, T.P., Ford, R.A.J. (2007), "Cyclostationary and the Cepstrum for Operational Modal Analysis of MIMO Systems- Part I: Modal Parameter Identification", Mechanical Systems and Signal Processing, 21, 2441-2458.
57. He, J., Fu, Z. (2001), *Modal Analysis*, Butterworth-Heinemann, Oxford.
58. Herlufsen, H., Gade, S., Moller, N. (2005), "Identification Techniques for Operational Modal Analysis – An Overview and Practical Experiences", Proceedings of the 23rd IMAC, St. Louis (MO), USA.

59. Hermans, L., Van der Auweraer, H. (1999), "Modal Testing and Analysis of Structures Under Operational Conditions: Industrial Applications", *Mechanical Systems and Signal Processing*, 13, 193-216.
60. Hermans, L., Van der Auweraer, H., Guillaume, P. (1998), "A Frequency-Domain Maximum Likelihood Approach for the Extraction of Modal Parameters from Output-Only Data", ", Proceedings of ISMA International Conference on Noise and Vibration Engineering, Katholieke Universiteit Leuven, Belgium.
61. Heylen, W., Lammens, S., Sas, P. (1995), *Modal Analysis Testing and Theory*, PMA-K.U. Leuven, Belgium.
62. Ho, B., Kalman, R.E. (1966), "Efficient Construction of Linear State Variable Models from Input/Output Functions", *Regelungstechnik* 14.
63. Hori, G. (2000); "A new approach to joint diagonalization", Proceedings of 2nd International Workshop on ICA and BSS, ICA' 2000, pp. 151-155, Helsinki, Finland.
64. Horyna, T., Ventura, C. (2000), "Summary of HCT Building Ambient Vibration Data Analysis", Proceedings of the 18th IMAC, San Antonio (TX), USA.
65. Hsu, H.P. (1970); *Fourier Analysis*, Simon and Schuster.
66. Hyvarinen, A., Karhunen, J., Oja, E. (2001), *Independent Component Analysis*, John Wiley and Sons, New York.
67. Hyvarinen, A., Oja, E. (2000); "Independent component analysis: Algorithms and applications", *Neural Networks*, Vol. 13, p. 411-430.
68. Ibrahim, S.R., Mikulcik, E.C. (1977), "A Method for Direct Identification of Vibration Parameters from the Free Response", *Shock and Vibration Bulletin* 47 (4), 183-198.

69. James, G.H., Carne, T.G., Lauffer, J.P. (1995), "The Natural Excitation Technique (NExT) for Modal Parameter Extraction from Operating Structures", *Modal analysis: The International Journal of Analytical and Experimental Modal Analysis* 10, 260-277.
70. Jacobsen, N.J. (2006), "Separating Structural Modes and Harmonic Components in Operational Modal Analysis", *Proceedings of the 24th IMAC, St. Louis, MO, USA*.
71. Joho, M., Rahbar, K. (2002); "Joint diagonalization of correlation matrices by using Newton methods with application to blind signal separation", *Proceedings Of IEEE Sensor Array and Multichannel Signal Processing Workshop SAM*.
72. Juang, R.N. (1994), *Applied System Identification*, Prentice Hall, Englewood Cliffs, NJ, USA.
73. Juang, J.N., Pappa, R.S. (1985), "An Eigensystem Realization Algorithm for modal parameter identification and model reduction", *AIAA Journal of Guidance, Control and Dynamics* 8 (4) 620-627.
74. Kay, S.M. (1988), *Modern Spectral Estimation*, Englewood Cliffs, NJ: Prentice Hall.
75. Kerschen, G., Poncelet, F., Golinval, J.C. (2006); "Physical interpretation of independent component analysis in structural dynamics", *Mechanical Systems and Signal Processing*, doi: 10.1016/j.ymsp.2006.07.009.
76. Kung, S. (1978), "New Identification and Model Reduction Algorithm via Singular Value Decomposition", *Proceedings of the 12th Asilomar Conference on Circuits, System and Computers*.

77. Lathauwer, L.D., De Moor, B., Vandewalle, J. (2000); "An introduction to independent component analysis", *Journal of Chemometrics*, Vol. 14, pp. 123-149.
78. Lembregts, F., Leuridan, J.L., Zhang, L., Kanda, H. (1986), "Multiple Input Modal Analysis of Frequency Response Functions Based on Direct Parameter Identification", *Proceedings of the 4th IMAC*, Los Angeles, CA.
79. Lembregts, F., Leuridan, J.L., H. Van Brussel (1989), "Frequency Domain Direct Parameter Identification for Modal Analysis: State Space Formulation", *Mechanical Systems and Signal Processing*, 4 (1) 65-76.
80. Ljung, L. (1999), *System Identification: Theory for the User*, Second edition. Prentice-Hall, Upper Saddle River, NJ.
81. Longman, R.W., Juang, J.N. (1989), "Recursive Form of the Eigensystem Realization Algorithm for System Identification", *AIAA Journal of Guidance, Control and Dynamics* 12 (5), 647-652.
82. Maia, J.M., Silva, J.M. (1997), *Theoretical and Experimental Modal Analysis*, Research Studies Press Limited, Hertfordshire, England.
83. Meirovitch, L. (1967); *Analytical methods in vibrations*, The Macmillan Company, New York.
84. Mohanty, P., Rixen, D.J. (2004), "A Modified Ibrahim Time Domain Algorithm for Operational Modal Analysis Including Harmonic Excitation", 275, 375-390.
85. Moller, N., Brincker, R., Andersen, P. (2000), "Modal Extraction on a Diesel Engine in Operation", *Proceedings of the 18th IMAC*, San Antonio, TX.
86. Nandi, A.K., Zarzoso, A. (1996); "Fourth-order cumulant based blind source separation", *IEEE Signal Processing Letters*, Vol. 3 Number 12, pp. 312-314.

87. Oppenheim, A.V., Schafer, R.W. (1989), *Discrete-Time Signal Processing*, Prentice-Hall.
88. Pandit, S.M. (1977), "Analysis of Vibration Records by Data Dependent Systems", *Shock and Vibration Bulletin*, Number 47, pp. 161-174.
89. Pandit, S.M., Suzuki, H. (1979), "Application of Data Dependent Systems to Diagnostic Vibration Analysis", ASME Paper No. 79-DET-7, 9 pp.
90. Pappa, R.S. (1982), "Some Statistical Performance Characteristics of the ITD Modal Identification Algorithm", AIAA Paper Number 82-0768, pp. 19.
91. Parloo, E., Verboven, P., Guillaume, P., Van Overmeire, M. (2002), "Sensitivity-Based Operational Mode Shape Normalization", *Mechanical Systems and Signal Processing*, 16 (5), 757-767.
92. Peeters, B. (2000), *System Identification and Damage Detection in Civil Engineering*, PhD Thesis, Dept. of Civil Engineering, Katholieke Universiteit leuven, Belgium.
93. Peeters, B., De Roeck, G (1999), "Reference Based Stochastic Subspace Identification for Output-Only Modal Analysis", *Mechanical Systems and Signal Processing*, 13 (6), 855-878.
94. Peeters, B., De Roeck, G. (2001), "Stochastic System Identification for Operational Modal Analysis: A Review", *ASME Journal of Dynamic Systems, Measurement, and Control* 123.
95. Peeters, B., H. Van der Auweraer (2005), "POLYMAX: A Revolution in Operational Modal Analysis", *Proceedings of the 1st International Operational Modal Analysis Conference*, Copenhagen, Denmark.

96. Peeters, B., Van der Auweraer, H., Guillaume, P., Leuridan, J. (2004), "The PolyMAX Frequency-Domain Method: A New Standard for Modal Parameter Estimation", *Shock and Vibration*, 11, 395-409.
97. Peeters, P., Ventura, B. (2003), "Comparative Study of Modal Analysis Techniques, for Bridge Dynamic Characteristics", *Mechanical Systems and Signal Processing*, 17(5), 965-988.
98. Phillips, A.W., Allemang, R.J. (1996), "Single Degree-of-Freedom Modal Parameter Estimation Methods", *Proceedings of the 14th IMAC*, Dearborn, MI, USA.
99. Phillips, A.W., Allemang, R.J. (2004), "A Low Order Implementation of the Polyreference Least Squares Complex Frequency (LSCF) Algorithm", *Proceedings of ISMA International Conference on Noise and Vibration Engineering*, Katholieke Universiteit Leuven, Belgium.
100. Phillips, A.W., Allemang, R.J., Fladung, W.A. (1998), "The Complex Mode Indicator Function (CMIF) as a Parameter Estimation Method", *Proceedings of the 16th IMAC*, Santa Barbara (CA), USA.
101. Phillips, A.W., Allemang, R.J., Zucker, A.T. (1998); "An overview of MIMO-FRF excitation/averaging techniques", *Proceedings of ISMA International Conference on Noise and Vibration Engineering*, Katholieke Universiteit Leuven, Belgium.
102. Phillips, A.W., Zucker, A.T., Allemang, R.J. (1999); "Frequency resolution effects on FRF estimation: Cyclic averaging vs. large block size", *Proceedings of 17th International Modal Analysis Conference*.
103. Pintelon, R., Guillaume, P., Rolain, Y., Schoukens, J., Van Hamme, H., "Parametric Identification of Transfer Functions in the Frequency Domain – A Survey", *IEEE Transaction on Automatic Control*, AC-39 (11), 1994, 2245-2260.

104. Poncelet, F., Kerschen, G., Golinval, J.C. (2006); "Experimental modal analysis using blind source separation techniques"; Proceedings of ISMA International Conference on Noise and Vibration Engineering, Katholieke Universiteit Leuven, Belgium.
105. Poyhonen, S., Jover, S., Hyotyniemi, H. (2003); "Independent component Analysis of vibrations for fault diagnosis of an induction motor", Proceedings of the IASTED International conference on Circuits, Signals and Systems, Cancun, Mexico, Vol. 1, pp. 203-208.
106. Qian, S. (2002), *Introduction to Time-Frequency and Wavelet Transforms*, Prentice Hall, New Jersey.
107. Rahbar, K., Reilly, J. (2001); "Blind source separation algorithm for MIMO convolutive mixtures", Proceedings of International Workshop on Independent Component Analysis and Signal Separation, pp. 242-247.
108. Richardson, M., Formenti, D. (1982), "Parameter Estimation from Frequency Response Measurements Using Rational Fraction Polynomials", Proceedings of the 1st IMAC, Orlando (FL), USA.
109. Saini, J.S. (2007), "Effect of Nonlinearities due to Geometry, Cables and Tuned Mass Dampers on The Analysis of Cable-Stayed Bridges", MS Thesis, Department of Civil Engineering, University of Cincinnati.
110. Schoukens, J., Pintelon, R. (1991), *Identification of Linear Systems: A Practical Guideline to Accurate Modelling*, Pergamon Press, London, UK.
111. Shelly, S.J. (1991); "Investigation of discrete modal filters for structural dynamic applications", PhD Dissertation, Department of Mechanical, Industrial and Nuclear Engineering, University of Cincinnati.

112. Shelley, S.J., Allemang, R.J. (1992), "Calculation of Discrete Modal Filters Using the Modified Reciprocal Modal Vector Method", Proceedings of the 10th IMAC, San Diego, CA.
113. Shelley, S.J., Allemang, R.J., Slater, G.L., Schultze, J.F. (1993), "Active Vibration Control Utilizing an Adaptive Modal Filter Based Modal Control Method", Proceedings of the 11th IMAC, Kissimmee, FL.
114. Shih, C.Y. (1989), *Investigation of Numerical Conditioning in the Frequency Domain Modal Parameter Estimation Methods*, Ph.D. Thesis, University of Cincinnati, Cincinnati, USA.
115. Shih, C.Y., Tsuei, Y.G., Allemang, R.J., Brown, D.L. (1989), "Complex Mode Indicator Function and its Applications to Spatial Domain Parameter Estimation", Proceedings of the 7th IMAC, Las Vegas (NV), USA.
116. Smaragdakis, P. (1998); "Blind separation of convolved mixtures in the frequency domain", *Neurocomputing*, Vol. 22, pp. 21-34.
117. Spitznogle, F.R., et. al (1971), "Representation and Analysis of Sonar Signals, Volume 1: Improvements in the Complex Exponential Signal Analysis Computational Algorithm", Texas Instruments, Inc. Report Number U1-829405-5, Office of Naval Research Contract Number N00014-69-C-0315, pp. 33.
118. Stoica, P., Moses, R.L. (1997), *Introduction to Spectral Analysis*, Prentice-Hall.
119. Tong, L., Soon, V.C., Huang, Y., Liu, R. (1990); "AMUSE: a new blind identification algorithm", Proceedings of IEEE ISCAS, pp. 1784-1787, Vol. 3, New Orleans, LA.
120. Van Overschee, P., De Moor, B. (1996), *Subspace Identification for Linear Systems: Theory-Implementations-Applications*, Kluwer Academic Publishers, Dordrecht, Netherlands.

121. Vecchio, A., Peeters, B., H. Van der Auweraer (2002), "Application of Advanced Parameter Estimators to the Analysis of In-Flight Measured Data", Proceedings of the 20th IMAC, Los Angeles (CA), USA.
122. Verboven, P. (2002), *Frequency Domain System Identification for Modal Analysis*, Ph.D. Thesis, Vrije Universiteit, Brussels, Belgium.
123. Vold, H. (1986), "Orthogonal Polynomials in the Polyreference Methods", Proceedings of ISMA International Conference on Noise and Vibration Engineering, Katholieke Universiteit Leuven, Belgium.
124. Vold, H., Kundrat, J., Rocklin, T., Russell, R. (1982), "A Multi-Input Modal Estimation Algorithm for Mini-Computers", SAE Transactions, Volume 91, Number 1, pp. 815-821.
125. Vold, H., Rocklin, T. (1982), "The Numerical Implementation of a Multi-Input Modal Estimation Algorithm for Mini-Computers", Proceedings of the 1st IMAC, Orlando, FL.
126. Ypma, A., Pajunen, P. (1999); "Rotating machine vibration analysis with second-order independent component analysis", Proceedings of the workshop on ICA and Signal Separation, Aussois, France, pp. 37-42.
127. Zang, C., Friswell, M.I., Imregun, M. (2004); "Structural damage detection using independent component analysis"; Structural Health Monitoring, Vol. 3, Number 1, pp 69-83.
128. Zeiger, H., McEwen, A.J. (1974), "Approximate Linear Realizations of Given Dimension via Ho's Algorithm", IEEE Transactions on Automatic Control.
129. Zhang, L., Brincker, R., Andersen, P. (2005), "An Overview of Operational Modal Analysis: Major Development and Issues", Proceedings of The 1st International Operational Modal Analysis Conference (IOMAC), Copenhagen, Denmark.

130. Zhang, L., Kanda, H., Brown, D.L., Allemang, R.J. (1984), "A Polyreference Frequency Domain Method for Modal Parameter Identification", American Society of Mechanical Engineers, Paper No. 85-DET-106.